OCEAN CIRCULATION AND GEOMAGNETIC INFLUENCES ON THE ATMOSPHERIC ^{14}C RECORD SPANNING THE PAST 50,000 YEARS FROM U-TH AND ^{14}C DATED FOSSIL CORALS

by

RICHARD ANDREW MORTLOCK

A Dissertation submitted to the

Graduate School – New Brunswick

Rutgers, The State University of New Jersey

In partial fulfillment of the requirements

for the degree of

Doctor of Philosophy

Graduate Program in Geological Sciences

Written under the direction of

James D. Wright

And approved by

_____

_____

_____

_____

New Brunswick, New Jersey

May, 2017

ABSTRACT OF THE DISSERTATION

OCEAN CIRCULATION AND GEOMAGNETIC INFLUENCES ON THE ATMOSPHERIC ^{14}C RECORD SPANNING THE PAST 50,000 YEARS FROM U-TH AND ^{14}C DATED FOSSIL CORALS

by

RICHARD ANDREW MORTLOCK

Dissertation Director

Dr. James Wright

The radiocarbon content (^{14}C) of the atmosphere is primarily controlled by changes in production, regulated by solar output and shielding in the earth's magnetic field, further influenced by changes in ocean circulation. Fossil corals provide an excellent archive for reconstructing past changes in the $^{14}C/^{12}C$ atmospheric ratio ($\Delta^{14}C$) because both the ^{14}C age and the calendar age, determined by U-series dating methods, can be obtained from the same sample. This is a requirement for computing accurate estimates of $\Delta^{14}C$.

Accuracy in coral $\Delta^{14}C$ records, however, requires that corrections be made for the age offset between the surface water in which the coral grew and the contemporaneous atmosphere, called the marine reservoir age correction. In this study

the marine reservoir correction is calculated for tropical Atlantic (Barbados) and Pacific (Kiritimati Atoll and Araki Island) corals to generate a record of $\Delta^{14}C$ from 50 to 7 thousand years before present (kyr BP).

Atlantic and Pacific coral $\Delta^{14}C$ data precisely match the timing and amplitude changes predicted in ocean-atmosphere coupled models demonstrating shutdown of North Atlantic Deep Water (NADW) at the start of the Younger Dryas cold interval (12.9 kyr BP) lowers the ^{14}C age of Atlantic surface water. A sharp decline in coral $\Delta^{14}C$ at 14.7 kyr BP coincides with proxy evidence for switch on of NADW. Taken together, these records provide credible evidence linking changes in NADW production to changes in the ^{14}C content of the atmosphere.

In contrast to 15 to 7 kyr BP when changes in $\Delta^{14}C$ largely reflect production changes in North Atlantic Deep Water, prominent features in $\Delta^{14}C$ from 50 to 15 kyr BP are due to the long-term effects of increased production of atmospheric ^{14}C during a weakened geomagnetic field at the time of the Laschamp (41 kyr BP) and Mono Lake (31.5 kyr BP) excursions. Removing the excess ^{14}C produced in the atmosphere during excursion events from the $\Delta^{14}C$ record effectively removes the rapid $\Delta^{14}C$ decline during the "Mystery Interval" (17.5 to 14.5 kyr BP) that has been widely attributed to release of ^{14}C-depleted CO_2 during ventilation of the deep ocean.

DEDICATION

To my parents, Ed and Betty, and my wife Lauren who have continuously provided support and encouragement

Acknowledgements

I first wish to thank my committee members, Dr. Richard Fairbanks, Dr. Kenneth Miller, Dr. Niall Slowey, Dr. Brent Turrin, and Dr. James Wright for their comments and contributions that greatly improved the science writing and interpretations. And particular thanks to Jim Wright and Rick Fairbanks, who have and continue to serve as mentors, advisors, co-workers, collaborators, and friends.

This work represents research conducted over two decades and it would not have been completed without the contributions of many. Thanks to the Department of Earth and Planetary Sciences and the School of Arts and Sciences who provided financial support and presented the opportunity to relocate samples, instruments, and self to Rutgers University. New laboratory space was provided for the Plasma54 and Neptune Plus instruments and was critical in establishing the U-Th dating facility. Linda Godfrey shared her technical expertise and has provided oversight and maintenance of the plasma lab. The administrative and technical staff in the front office has always cheerfully taken care of my requests, no matter which hat I was wearing.

I am also extremely grateful to have had graduate students with whom I have shared my expertise and experience, and in return they themselves made important contributions to the field and to this dissertation. It was a pleasure to have shared in this process with Dr. Nicole Abdul. I am extremely appreciative of her generous offer of time and her sharing in the multitude of responsibilities associated with accommodating the research needs of other students and PI's.

C. Chiu, L. Cao, L. Teneva, and J. May participated in the offshore drilling expeditions that returned the samples used in this dissertation and many dedicated undergraduates assisted in preparing samples and took care of the less glamorous chores and duties, keeping the lab operating both efficiently and productively.

Finally, to my wife, parents, family members, and friends. The path to accomplishing my Ph.D. degree has been somewhat circuitous, but it has been my life's goal and it could only have been made possible with the loving support of Lauren, who in shared sacrifice allowed me to pursue my passion.

Table of Contents

Mortlock, R.A., Abdul, N.A., Wright, J.D., and Fairbanks, R.G., 2016, Reply to comment by E. Bard et al. on "Younger Dryas sea level and meltwater pulse 1B recorded in Barbados reef crest coral Acropora palmata" by N.A. Abdul et al: *Paleoceanography, 31, 1609–1616, DOI: 10.1002/2016PA003047.*

List of Figures

List of Tables

Chapter One

1.1 Dissertation Introduction

Radiocarbon (^{14}C) dating is of practical importance to a wide range of scientific disciplines and is essential for measuring time and rates of change. ^{14}C dating provides the means to date artifacts related to the emergence and migration patterns associated with early human civilization and is widely applied in studies of ocean processes and climate change. Produced in the upper atmosphere by the interaction of cosmic ray neutrons with nitrogen atoms, ^{14}C is rapidly oxidized to CO_2 and mixes throughout the troposphere and exchanges with the reactive carbon reservoirs of the oceans and biosphere where it decays with a half-life of 5730 years [*Godwin*, 1962]. The production of ^{14}C is not constant and is largely controlled by changes in the Earth's magnetic field intensity which shields the earth from incoming cosmic rays, thereby increasing the $^{14}C/^{12}C$ ratio of the atmosphere ($\Delta^{14}C$) during intervals of weaker field and reducing the $^{14}C/^{12}C$ ratio during intervals of stronger field strength [*Bard et al.*, 1990; *Elsasser et al.*, 1956; *Lal*, 1988]. For the past 11,000 years before present (BP), small fluctuations in atmospheric ^{14}C have been produced by changes in the solar magnetic field, as evidenced by $\Delta^{14}C$ recorded in tree rings during sun spot events [*Stuiver and Quay*, 1980]. Changes in the carbon cycle, presumably tied to changes in deep ocean circulation are believed to contribute to atmospheric ^{14}C fluctuations as observed in deep-sea sediment records, cave deposits, and fossil corals [*Adkins and Boyle*, 1997; *Edwards et al.*, 1993; *Hughen et al.*, 1998].

Since the $^{14}CO_2$ content of the atmosphere has not been constant, calibration of the radiocarbon time scale is needed in order to convert radiocarbon years to calendar years. Calibration of the ^{14}C time scale is most commonly achieved by means of a calibration curve generated using a number of ^{14}C dated archives such as tree rings, corals, and speleothems. In each of these archives calendar ages are either known (e.g., tree rings of known age) or can be directly measured with an independent radiometric dating methods such as the Uranium-series disequilibrium method [*Bard et al.*, 1990; *Fairbanks et al.*, 2005; *Reimer et al.*, 2009; *Reimer et al.*, 2013] (Figures 1.1 and 1.2). ^{14}C dated deep-sea sediments are also widely accepted by the radiocarbon community for calibration but a disadvantage to these archives is that they have no directly measured calendar age. Instead, they must rely on assigned calendar ages that are based on visual correlations of sediment proxy or color variability to distant atmospheric climate proxy records in layer counted ice cores and U-series dated speleothems (e.g., stalactites, stalagmites). The important and underlying assumption in such tied chronologies is that the transfer of one climate signal in one record to another one is instantaneous.

Accuracy in calibration data is also limited by ^{14}C and calendar age corrections that may be applied to the raw data. For example, marine achives such as corals and planktonic foraminifera must have the their measured ^{14}C ages corrected for the age of the surface water in which they grew (the marine reservoir age correction). Speleothem ^{14}C ages must be corrected for the fraction of ^{14}C-free or "dead" carbon leached from the host bedrock by carbonic acid, prior to being precipitated as calcite. Speleothem U-Th ages also may require corrections for a contribution from detrital or initial ^{230}Th present in the percolating ground water. Another complication to using speleothems for

calibration is that their slow growth rates and relatively low U content do not permit ^{14}C and U-Th ages to be obtained from the same sub-sample and calendar ages must generated via interpolation of adjacent U-Th dates. Both sampling and age-depth corrections can therefore introduce artifacts in calibration data in specimens that display irregular growth patterns.

Regardless of the fossil archive, combining the ^{14}C age with the calendar age in the same sample provides an independent and discrete calibration and $\Delta^{14}C$ data point. During the past two decades advancements in accelerator mass spectrometry (AMS) have resulted in reduced sample size and instrument blanks thereby routinely extending the limits of ^{14}C dating in most laboratories to 55,000 ^{14}C-years BP. Today, progress in radiocarbon calibration and reconstruction of past changes in atmospheric ^{14}C appears to be limited only by the availability of high quality samples.

1.2 Background and Overview

Radiocarbon-dated tree rings of known calendar year make up the calibration curve from the present to 13.9 kyr BP. Tree rings are preferred for calibration since they are "bona fide" recorders of the atmospheric ^{14}C reservoir and provide annual layers that yield an independent calendar years time scale. Tree rings from Northern Europe provide an accurate calibration data set for 12.55 to 0 kyr BP [*Reimer et al.*, 2013]. Prior to 12.55 kyr BP the "continuous " tree ring sequence is anchored to a "floating" European Late Glacial Pine record [*Kromer et al.*, 2004] via correlation to a Huon Pine (Tasmania) ^{14}C record which spans both European tree ring records [*Friedrich et al.*, 2004; *Schaub et al.*, 2008], thereby extending the tree ring calibration series to 13.9 kyr BP [*Hua et al.*, 2009].

Prior to 13.9 kyr BP, tree ring records are largely absent and so alternative archives, both terrestrial and marine, must be exploited to extend calibration and records of $\Delta^{14}C$ back in time. Corals present an excellent opportunity for radiocarbon calibration because Uranium-series disequilibrium dating methods permit precise and accurate determination of a samples age [*R. L. Edwards et al.*, 1987]. The U-series dating method (U-Th) makes use of the decay of ^{238}U to its intermediate daughter ^{234}U (half-life of 245,250 years) and its subsequent decay to ^{230}Th (half-life 75,690 years) [*Cheng et al.*, 2000]. The relatively high U content of corals (3 ppm) make them ideal for this dating technique and development in multi-collector mass spectrometry, specifically using Inductively Coupled Plasma (ICP) sources permits dating of corals ranging in age from a few decades to 700,000 years with reported precisions of better than ± 0.5% at 2 s.d.

Unlike trees, corals do not directly sample the atmosphere but remove CO_2 as HCO_3^{-1} from the surface water reservoir. Furthermore, the ^{14}C content of the surface water in which a coral grows is not the same as the atmosphere. The offset in the ^{14}C content, and hence age, between surface water and the atmosphere is in part due to partial equilibrium between *p*CO2 and HCO_3^{-1} and the fraction of deeper and older water that is upwelled into the mixed surface layer. Therefore, all coral ^{14}C ages must be corrected for the age offset, commonly referred to as the marine reservoir age (MRA). Today, the marine reservoir age in tropical regions (25°N to 25°S) and the study area presented here ranges between 300 and 500 years [*Butzin et al.*, 2005; *Key et al.*, 2004] (Figure 1.3). However, a number of physical and chemical processes may have led to variable surface water ^{14}C age in the past and therefore the accuracy of any ^{14}C age obtained from a

marine archive (e.g., corals, foraminifera) depends on the accuracy of both the magnitude and uncertainty in MRA corrections.

This dissertation builds on prior research using fossil corals to extend radiocarbon calibration and records of $\Delta^{14}C$ [*Bard et al.*, 1990; *Cao*, 2010; *Chiu et al.*, 2007; *Chiu et al.*, 2005; *Chiu et al.*, 2006]. Since the publication of previous coral calibration data [*Fairbanks et al.*, 2005], IntCal09 and IntCal13 have been released which include a number of new calibration data sets (Lake Suigetsu sediments, Hulu Cave and Bahamas Speleothem, Tahiti corals). This dissertation contributes 160 new calibration points to fill important gaps in the record where data were previously absent or sparse. With a sampling resolution averaging less than 150 years, the coral record presented here represents the only directly dated (i.e., U-Th) and continuous marine archive spanning the past 50,000 years BP, thereby providing a more detailed and higher resolution $\Delta^{14}C$ record for comparison to published calibration data sets and consensus calibration curves (IntCal13).

Of particular interest in this study is the response of atmospheric ^{14}C to changes in the production of North Atlantic Deep Water (NADW) during times of abrupt climate shifts such as those during the Younger Dryas cold interval (12.9 to 11.6 kyr BP), Bølling/Allerød warm interval (14.5 to 13 kyr BP), and Heinrich Stadial 1 (17.5 to 14.5 kyr BP). NADW production is responsible for net export of ^{14}C produced in the atmosphere to the world's deep oceans. Increases in NADW lowers the ^{14}C content of the atmosphere whereas the atmosphere will accumulate ^{14}C when NADW production is reduced. Deep-sea sediment proxy records suggest changes in NADW during the deglacial [*Charles and Fairbanks*, 1992; *Elmore and Wright*, 2011; *McManus et al.*,

2004; *Piotrowski et al.*, 2004]. Deep-sea sediment proxy records of NADW rely on age models that are based either on calibrated ^{14}C ages, corrected for MRA, or imported chronologies and require assumptions of constant sedimentation rates between age model control points. These sediment records simply do not have the age accuracy or resolution to match records obtained with U-Th dated corals. Only the U-Th dated coral $\Delta^{14}C$ record has the requisite precision and accuracy needed for direct comparison to Greenland ice core chronologies. Our comparisons suggest that rapid climate shifts in the Northern Hemisphere during deglaciation were tied to changes in the strength of North Atlantic overturning.

A second important contribution of this study is a reconstruction the production history of ^{14}C, as controlled by changes in the Earth's geomagnetic field strength. There is substantial evidence the field strength was weaker in the past 50,000 years, during the Laschamp Excursion at 41 kyr BP [*Guillou et al.*, 2004; *Kent et al.*, 2002; *Singer et al.*, 2009] and Mono Lake Excursion, 34-30 kyr BP [*Benson et al.*, 2003; *Cassata et al.*, 2010; *Kent et al.*, 2002; *Liddicoat*, 1992; *Wagner et al.*, 2000]. Spikes in ^{14}C production associated with these excursions should be evident in the record of $\Delta^{14}C$ and therefore U-Th dated corals present an excellent opportunity to constrain the age and duration of these global events.

1.3 Study Sites and sample collection

Coral samples selected in this study are from the Barbados (western Atlantic) offshore drill-core collection from material recovered during three expeditions (RANGER 88-13, M/V NATIVE SPIRIT 2004, and R/V KNORR 189-2). Kiritmati

(Christmas) Island corals (Central Equatorial Pacific) were collected during the R/V MOANA Wave drilling expedition in 1997. Additional corals are from Araki Island (Vanuatu, Western Pacific) sampled from the collection of A. Bloom or collected by R. Fairbanks and C. Brainard during separate field expeditions.

Fossil corals require careful screening before being prepared for radiometric age dating by either the ^{14}C or U-Th method. Samples must be free of secondary mineral phases, such as calcite, that can directly alter both U-Th and ^{14}C ages. Some fossil samples may have been exposed to freshwater diagenesis during subsequent sea level low stands. Persistent exposure to the freshwater lens can modify the U and Th isotopic composition of a sample and generate $^{234}U/^{238}U$ initial ($\delta^{234}U_{initial}$) activity ratios that exceed the expected range for seawater and yield ages that appear too old [*Gallup et al.*, 1994; *Hamelin et al.*, 1991; *Henderson et al.*, 1993]. Throughout this study established sampling screening and strict data quality control criteria are followed [*Chiu et al.*, 2005; *Fairbanks et al.*, 2005]. Only samples with no detectable calcite (less than 0.2 weight percent) were processed for ^{14}C and U-Th dating and only samples with $\delta^{234}U_{initial}$ falling in the range within the acceptable range for corals having maintained closed system behavior (138-152‰) are included in the results. U-Th and U-Pa dating follows the methods detailed in *Mortlock et al.* [2005], as revised in *Abdul et al.* [2016]. All coral age and isotopic data generated and presented in the course of this study is given in Table 1 of the Appendix.

1.4 Overview of Chapters

Chapter 2: Shut-down in North Atlantic Overturning at the start of the Younger Dryas confirmed by tropical Pacific and Atlantic coral $\Delta^{14}C$

Since the ^{14}C content of surface water in which a coral grows is not identical to that of the atmosphere coral ^{14}C ages must be corrected for surface water to atmosphere age difference, commonly known as the marine reservoir age (MRA). Because of its latitudinal dependence it is recommended that MRA corrections be site specific and based on the local offset or ΔR from the global average (~ 400 years). In Chapter 2, Barbados and Kirtimati marine reservoir ages and ΔR are estimated by comparing raw ^{14}C ages of corals to those of tree rings of identical calendar year age. The overlap between corals and tree rings extends from 13.9 to 7.3 kyr BP and provides 74 and 45 independent MRA estimates and its variability at Barbados and Kiritimati, respectively. The data indicate there is variability in the marine reservoir age of tropical Atlantic and Pacific surface water from 13.9 to 7 kyr BP with an interval of lower reservoir age at Barbados at the onset of the Younger Dryas (12.9 kyr BP). Applying constant reservoir corrections to the data produces an increase in $\Delta^{14}C$ at Barbados that leads a similar increase in the Pacific coral or tree ring records. The delayed timing between Atlantic and Pacific $\Delta^{14}C$ records exactly matches modeled predictions that demonstrate shutdown of NADW lowers the ^{14}C age of Atlantic surface water and generates divergent Atlantic and Pacific records $\Delta^{14}C$ [*Singarayer et al.*, 2008]. By 12.5 kyr BP, Atlantic and Pacific coral $\Delta^{14}C$ converge with the tree ring record of $\Delta^{14}C$ and a return to declining values strongly suggests disruption of NADW was short-lived.

This chapter will be submitted to Quaternary Science Reviews, and is authored by R.A. Mortlock, N.A. Abdul, J.D. Wright (all at Rutgers University) with L. Cao (Vaccine Research Center) and R.G. Fairbanks (Columbia University).

Chapter 3: Atmospheric ^{14}C spanning the past 50,000 years from U-Th and ^{14}C dated fossil corals: separating geomagnetic, carbon cycle, and ^{14}C half-life components

In Chapter 3, a record of the atmospheric $^{14}C/^{12}C$ ratio ($\Delta^{14}C$) spanning 50-15 kyr BP is presented based on 156 U-Th and ^{14}C dated coral samples from Barbados and Araki Island. In addition, these data are supplemented with 24 concordant U-Th and U-Pa dates to demonstrate quality control of the U-series dating system. The U-Pa concordancy test has been applied to samples that were exposed to the freshwater table (phreatic lens) or percolating groundwater (vadose) and is the most rigorous test of age accuracy [*Mortlock et al.*, 2005].

Prior to 30 kyr BP, corals generally display younger ^{14}C ages compared to same calendar age Bahamas speleothem data and fall within the scatter of Lake Suigetsu (Japan) and Cariaco Basin (Venezuela) sediment data. ^{14}C age differences between corals and other terrestrial and marine calibration data from 50 to 30 kyr B.P are large (1000 to 3000 years) and cannot be accounted for with MRA corrections to corals ^{14}C ages. The most likely explanation for large age offsets between corals and other data sets is that they are due to dead carbon fractions and $^{230}Th_{initial}$ corrections in the speleothem that have been underestimated and to inaccuracies in deep sea or lake-core sediment age calendar year age models. Data presented in this chapter bolsters the argument that corals have the greatest potential for providing a "backbone" calibration curve to the

limits of radiocarbon dating. Limited only by the availability of "high" quality samples, corals older than 20 kyr BP are not sensitive to either MRA or ^{230}Th initial corrections. Furthermore, the uncertainty in U-Th dating decreases with age so that the uncertainty associated with each calibration and $\Delta^{14}C$ estimate largely reflects the uncertainty in the ^{14}C age. Finally, age accuracy can be critically evaluated for closed-system behavior by virtue of their measured $\delta^{234}U$ initial values and when deemed necessary, U-Pa concordancy age dating. Layer counted sediments that are ^{14}C dated but which require imported age models from U-Th speleothems compound dating error uncertainties and generate unacceptable scatter in records prior to 35 kyr BP

The coral $\Delta^{14}C$ record presented in Chapter 3 confirms earlier studies (Figure 1.4) [*Chiu et al.*, 2007] and demonstrates large-scale features in $\Delta^{14}C$ are largely controlled by changes in production at times of weakened geomagnetic field during the Laschamp Excursion (41 kyr). An important new finding in the updated coral record is an interval of rapidly changing $\Delta^{14}C$ between 32 and 29 kyr BP corresponding to the time of the Mono Lake Excursion, now precisely dated to 31.5 ± 0.2 kyr BP. The $\Delta^{14}C$ record obtained with corals is perhaps the most direct evidence for the Mono Lake Event since: 1) elevated values in $\Delta^{14}C$ can only be explained with an increase in production; and 2) the dating is better constrained compared to paleo-intensity stacked records in deep-sea sediments or from ^{10}Be and ^{36}Cl fluxes measured in ice cores. The improved dating of the Mono Lake event makes it a valuable global stratigraphic marker and places it in importance with the Laschamp event for correlating sediment and ice core records.

When the $\Delta^{14}C$ record is corrected for excess ^{14}C production during the Laschamp and Mono Lake excursions ($\Delta^{14}C_{LMcorr}$), an increase in atmospheric ^{14}C at ~19 kyr BP is

interpreted to reflect increased production associated with the Hilina Pali geomagnetic excursion [*Singer*, 2014; *Teanby et al.*, 2002; *Turrin et al.*, 2013]. Although changes in the magnetic field strength dominate the shape of the $\Delta^{14}C_{LMcorr}$ record, some portion of the linear trend in $\Delta^{14}C_{LMcorr}$ may be due to uncertainties in the half-life of ^{14}C.

Submission of this chapter is planned for *Science or Nature* and will be authored by R.A. Mortlock, N.A. Abdul, J.D.Wright (all at Rutgers University) with L. Cao (Vaccine Research Center) and R.G. Fairbanks (Columbia University).

Chapter 4: Barbados $\Delta^{14}C$ record of deglacial ocean ventilation

The Mystery Interval (17.5 to 14.5 Kyr BP) is an interval of rapidly decreasing $\Delta^{14}C$ [*Broecker*, 2009; *Broecker and Barker*, 2007] and is superimposed on a steady decline in the ^{14}C content of the atmosphere due to the long-term effects of a weaker geomagnetic field known as the Laschamp Excursion (41 kyr BP). The Mystery Interval (MI) corresponds to the time of Heinrich Stadial 1 and a period when episodic ventilation of the deep ocean is believed to have released ^{14}C-depleted CO_2 to the atmosphere. In Chapter 4, paired ^{14}C and U-Th ages obtained from Barbados corals are used to examine the record of $\Delta^{14}C$ between 22 and 13 kyr BP. Difference between coral and Intcal09 $\Delta^{14}C$ strongly suggests the infamous Mystery Interval $\Delta^{14}C$ event is an artifact of an incorrect age model developed in the Cariaco Basin deep-sea core used to compute $\Delta^{14}C$ in IntCal09. After $\Delta^{14}C$ is corrected for excess ^{14}C produced during the Laschamp and Mono Lake Excursions (defined as $\Delta^{14}C_{LMcorr}$), the decline in $\Delta^{14}C$ during the Mystery Interval cannot be distinguished from the long-term trend due to radioactive decay. The increase in $\Delta^{14}C_{LMcorr}$ prior to the Mystery Interval reflects increased production of ^{14}C associated with the Hilina Pali geomagnetic excursion (Chapter 3).

Heinrich Stadial Event 1 (Mystery Interval; 17.5 – 14.5 kyr BP) is associated with increased ice rafted debris in the North Atlantic sediment cores, indicating widespread discharge of icebergs into the North Atlantic, potentially disturbing NADW formation [*G Bond et al.*, 1992; *G C Bond and Lotti*, 1995; *McManus et al.*, 2004]. IntCal13 and Fairbanks0107 calibration curves differ by between 200 to 400 years during Heinrich Stadial 1. The most likely explanations for differences between data sets and calibration curves are: 1) variable MRA at Barbados; 2) variable dead carbon fractions to speleothems; and 3) under-reported ^{230}Th initial corrections to speleothem U-Th ages. Differences between the two data sets indicate that calibration of ^{14}C ages corresponding to Heinrich Stadial 1 remains somewhat ambiguous.

There is strong evidence from δ^{13}C of benthic foraminifera for a dramatic increase in NADW production as the start of the Bølling/Allerød warm interval (14.5 kyr BP). The coral data demonstrates that a rapid decline in Δ^{14}C coincides precisely with the evidence for "turn on" of NADW and provides credible evidence to hypotheses linking changes in NADW production to changes in the ^{14}C content of the atmosphere.

This chapter is being prepared for submission to Quaternary Science Reviews, and is authored by R.A. Mortlock, N.A. Abdul, J.D. Wright (all at Rutgers University), L. Cao (Vaccine Research Center) and R.G. Fairbanks (Rutgers University and Columbia University).

1.5 Acknowledgements

^{14}C dates were conducted at the Center of Accelerator Mass Spectrometry at Lawrence Livermore National Laboratory (T. Guilderson), at the Leibniz Laboratory for

Dating and Isotope Analyses, Christian-Albrechts-Universität, Kiel (P.M. Grootes and M.-J. Nadeau), and the National Ocean Sciences Accelerator Mass Spectrometry Center, Woods Hole Oceanographic Institute (A. McNichol). Technical assistance was provided by A. Cotet and T. Emge. Art Bloom kindly provided his Vanuatu coral collection. C. Brainard and T. Fairbanks provided collected additional Araki corals during 2004 and 2005. This work was supported by grants from the National Science Foundation (OCE09-28446 and OCE05-50900). We acknowledge financial support from the School of Arts and Sciences, and Department of Earth and Planetary Sciences, Rutgers University (NEPTUNE PLUS).

1.6 References

Abdul, N. A., R. A. Mortlock, J. D. Wright, and R. G. Fairbanks (2016), Younger Dryas sea level and meltwater pulse 1B recorded in Barbados reef crest coral *Acropora palmata*, *Paleoceanography*, *31*(2), 330-344, doi:10.1002/2015pa002847.

Adkins, J., and E. Boyle (1997), Changing atmospheric ^{14}C and the record of deep water paleoventilation ages, *Paleoceanography*, *12*, 337-344.

Bard, E., B. Hamelin, R. G. Fairbanks, and A. Zindler (1990), Calibration of the ^{14}C timescale over the past 30,000 years using mass spectrometric U-Th ages from Barbados corals, *Nature*, *345*, 405-410.

Benson, L., J. Liddicoat, J. Smoot, A. Sarna-Wojcicki, R. Negrini, and S. Lund (2003), Age of the Mono Lake excursion and associated tephra, *Quaternary Science Reviews*, *22*(2–4), 135-140, doi:http://dx.doi.org/10.1016/S0277-3791(02)00249-4.

Bond, G., et al. (1992), Evidence for massive discharges of icebergs into the North Atlantic Ocean during the last glacial period *Nature*, *360*, 245-249.

Bond, G. C., and R. Lotti (1995), Iceberg Discharges into the North Atlantic on Millennial Time Scales During the Last Glaciation, *Science*, *267*(5200), 1005-1010, doi:10.1126/science.267.5200.1005.

Broecker, W. (2009), The Mysterious ^{14}C Decline, *Radiocarbon*, *51*(1), 109-119.

Broecker, W., and S. Barker (2007), A 190‰ drop in atmosphere's $\Delta^{14}C$ during the "Mystery Interval" (17.5 to 14.5 kyr), *Earth and Planetary Science Letters*, *256*(1-2), 90-99, doi:10.1016/j.epsl.2007.01.015.

Butzin, M., M. Prange, and G. Lohmann (2005), Radiocarbon simulations for the glacial ocean: The effects of wind stress, Southern Ocean sea ice and Heinrich events, *Earth and Planetary Science Letters*, *235*(1–2), 45-61, doi:http://dx.doi.org/10.1016/j.epsl.2005.03.003.

Cao, L. (2010), High-precision $^{230}Th/^{234}U$ dating of the surface ocean radiocarbon record and its geochemical and geophysical implications.

Cassata, W. S., B. S. Singer, J. C. Liddicoat, and R. S. Coe (2010), Reconciling discrepant chronologies for the geomagnetic excursion in the Mono Basin, California: Insights from new 40Ar/39Ar dating experiments and a revised relative paleointensity correlation, *Quaternary Geochronology*, *5*(5), 533-543, doi:10.1016/j.quageo.2010.02.001.

Charles, C. D., and R. G. Fairbanks (1992), Evidence from Southern Ocean sediments for the effect of North Atlantic deep-water flux on climate, *Nature*, *355*(6359), 416-419.

Cheng, H., R. L. Edwards, J. Hoff, C. D. Gallup, D. A. Richards, and Y. Asmerom (2000), The half-lives of uranium-234 and thorium-230, *Chemical Geology*, *169*(1–2), 17-33, doi:http://dx.doi.org/10.1016/S0009-2541(99)00157-6.

Chiu, T.-C., R. G. Fairbanks, L. Cao, and R. A. Mortlock (2007), Analysis of the atmospheric ^{14}C record spanning the past 50,000 years derived from high-precision $^{230}Th/^{234}U/^{238}U$, $^{231}Pa/^{235}U$ and ^{14}C dates on fossil corals, *Quaternary Science Reviews*, *26*(1-2), 18-36, doi:10.1016/j.quascirev.2006.06.015.

Chiu, T.-c., R. G. Fairbanks, R. A. Mortlock, and A. L. Bloom (2005), Extending the radiocarbon calibration beyond 26,000 years before present using fossil corals,

Quaternary Science Reviews, *24*(16-17), 1797-1808, doi:10.1016/j.quascirev.2005.04.002.

Chiu, T.-C., R. G. Fairbanks, R. A. Mortlock, L. Cao, T. W. Fairbanks, and A. L. Bloom (2006), Redundant $^{230}Th/^{234}U/^{238}U$, $^{231}Pa/^{235}U$ and ^{14}C dating of fossil corals for accurate radiocarbon age calibration, *Quaternary Science Reviews*, *25*(17-18), 2431-2440, doi:10.1016/j.quascirev.2006.01.025.

Edwards, R. L., J. W. Beck, G. S. Burr, D. J. Donahue, J. M. A. Chappell, A. L. Bloom, E. R. M. Druffel, and F. W. Taylor (1993), A Large Drop in Atmospheric $^{14}C/^{12}C$ and Reduced Melting in the Younger Dryas, Documented with ^{230}Th Ages of Corals, *Science*, *260*(5110), 962-968, doi:10.1126/science.260.5110.962.

Edwards, R. L., J. H. Chen, T.-L. Ku, and G. J. Wasserburg (1987), Precise Timing of the Last Interglacial Period from Mass Spectrometric Determination of Thorium-230 in Corals, *Science*, *236*(4808), 1547-1553, doi:10.1126/science.236.4808.1547.

Elmore, A. C., and J. D. Wright (2011), North Atlantic Deep Water and climate variability during the Younger Dryas cold period, *Geology*, *39*(2), 107-110, doi:10.1130/g31376.1.

Elsasser, W., E. P. Ney, and J. R. Winckler (1956), Cosmic-ray intensity and geomagnetism, *Nature*, *178*, 1226-1227.

Fairbanks, R. G., R. A. Mortlock, T.-C. Chiu, L. Cao, A. Kaplan, T. P. Guilderson, T. W. Fairbanks, A. L. Bloom, P. M. Grootes, and M.-J. Nadeau (2005), Radiocarbon calibration curve spanning 0 to 50,000 years BP based on paired $^{230}Th/^{234}U/^{238}U$ and ^{14}C dates on pristine corals, *Quaternary Science Reviews*, *24*(16-17), 1781-1796, doi:10.1016/j.quascirev.2005.04.007.

Friedrich, M., S. Remmele, B. Kromer, J. Hofmann, M. Spurk, F. Kaiser, C. Orcel, and M. Küppers (2004), The 12,460-year Hohenheim oak and pine tree-ring chronology from Central Europe - a unique annual record for radiocarbon calibration and paleoenvironment reconstructions, *Radiocarbon*, *46*(3), 1111-1122.

Gallup, C. D., R. L. Edwards, and R. G. Johnson (1994), The Timing of High Sea Levels Over the Past 200,000 Years, *Science*, *263*(5148), 796-800, doi:10.1126/science.263.5148.796.

Godwin, H. (1962), Half-life of radiocarbon, *Nature*, *195*(4845), 984.

Guillou, H., B. S. Singer, C. Laj, C. Kissel, S. Scaillet, and B. R. Jicha (2004), On the age of the Laschamp geomagnetic excursion, *Earth and Planetary Science Letters*, *227*(3–4), 331-343, doi:http://dx.doi.org/10.1016/j.epsl.2004.09.018.

Hamelin, B., E. Bard, A. Zindler, and R. G. Fairbanks (1991), $^{234}U/^{238}U$ mass spectrometry of corals: How accurate is the U-Th age of the last interglacial period?, *Earth and Planetary Science Letters*, *106*(1–4), 169-180, doi:http://dx.doi.org/10.1016/0012-821X(91)90070-X.

Henderson, G. M., A. S. Cohen, and R. K. O'Nions (1993), $^{234}U/^{238}U$ ratios and ^{230}Th ages for Hateruma Atoll corals: implications for coral diagenesis and seawater $^{234}U/^{238}U$ ratios, *Earth and Planetary Science Letters*, *115*(1), 65-73, doi:http://dx.doi.org/10.1016/0012-821X(93)90213-S.

Hua, Q., M. Barbetti, D. Fink, K. F. Kaiser, M. Friedrich, B. Kromer, V. A. Levchenko, U. Zoppi, A. M. Smith, and F. Bertuch (2009), Atmospheric ^{14}C variations

derived from tree rings during the early Younger Dryas, *Quaternary Science Reviews*, *28*(25-26), 2982-2990, doi:10.1016/j.quascirev.2009.08.013.

Hughen, K. A., J. T. Overpeck, S. J. Lehman, M. Kashgarian, J. Southon, L. C. Peterson, R. Alley, and D. M. Sigman (1998), Deglacial changes in ocean circulation from an extended radiocarbon calibration, *Nature*, *391*(6662), 65-68, doi:http://www.nature.com/nature/journal/v391/n6662/suppinfo/391065a0_S1.html.

Kent, D. V., S. R. Hemming, and B. D. Turrin (2002), Laschamp Excursion at Mono Lake?, *Earth and Planetary Science Letters*, *197*(3–4), 151-164, doi:http://dx.doi.org/10.1016/S0012-821X(02)00474-0.

Key, R. M., A. Kozyr, C. L. Sabine, K. Lee, R. Wanninkhof, J. L. Bullister, R. A. Feely, F. J. Millero, C. Mordy, and T. H. Peng (2004), A global ocean carbon climatology: Results from Global Data Analysis Project (GLODAP), *Global Biogeochem. Cycles*, *18*(4), GB4031, doi:10.1029/2004gb002247.

Kromer, B., M. Friedrich, K. A. Hughen, F. Kaiser, S. Remmele, M. Schaub, and S. Talamo (2004), Late Glacial ^{14}C Ages From a Floating, 1382-Ring Pine Chronology, *Radiocarbon*, *46*(3), 1203-1209.

Lal, D. (Ed.) (1988), *Theoretically expected variations in the terrestrial cosmicray production rates of isotope* North-Holland, Amsterdam, NY.

Liddicoat, J. C. (1992), Mono Lake Excursion in Mono Basin, California, and at Carson Sink and Pyramid Lake, Nevada, *Geophysical Journal International*, *108*(2), 442-452, doi:10.1111/j.1365-246X.1992.tb04627.x.

McManus, J. F., R. Francois, J. M. Gherardi, L. D. Keigwin, and S. Brown-Leger (2004), Collapse and rapid resumption of Atlantic meridional circulation linked to deglacial climate changes, *Nature*, *428*(6985), 834-837, doi:http://www.nature.com/nature/journal/v428/n6985/suppinfo/nature02494_S1.html.

Mortlock, R. A., R. G. Fairbanks, T.-c. Chiu, and J. Rubenstone (2005), $^{230}Th/^{234}U/^{238}U$ and $^{231}Pa/^{235}U$ ages from a single fossil coral fragment by multi-collector magnetic-sector inductively coupled plasma mass spectrometry, *Geochimica et Cosmochimica Acta*, *69*(3), 649-657, doi:10.1016/j.gca.2004.06.033.

Piotrowski, A. M., S. L. Goldstein, S. R. Hemming, and R. G. Fairbanks (2004), Intensification and variability of ocean thermohaline circulation through the last deglaciation, *Earth and Planetary Science Letters*, *225*(1–2), 205-220, doi:http://dx.doi.org/10.1016/j.epsl.2004.06.002.

Reimer, P. B., et al. (2009), IntCal09 and Marine09 Radiocarbon Age Calibration Curves, 0–50,000 Years cal BP, *Radiocarbon*, *51*, 1111-1150.

Reimer, P. B., et al. (2013), IntCal13 and Marine13 Radiocarbon Age Calibration Curves 0-50,000 years Cal BP, *Radiocarbon*, *55*(4), 1869-1887.

Schaub, M., U. Büntgen, K. F. Kaiser, B. Kromer, S. Talamo, K. K. Andersen, and S. O. Rasmussen (2008), Lateglacial environmental variability from Swiss tree rings, *Quaternary Science Reviews*, *27*(1-2), 29-41, doi:10.1016/j.quascirev.2007.01.017.

Singarayer, J. S., D. A. Richards, A. Ridgwell, P. J. Valdes, W. E. N. Austin, and J. W. Beck (2008), An oceanic origin for the increase of atmospheric radiocarbon

during the Younger Dryas, *Geophysical Research Letters*, *35*(14), doi:10.1029/2008gl034074.

Singer, B. S. (2014), A Quaternary geomagnetic instability time scale, *Quaternary Geochronology*, *21*(0), 29-52, doi:http://dx.doi.org/10.1016/j.quageo.2013.10.003.

Singer, B. S., H. Guillou, B. R. Jicha, C. Laj, C. Kissel, B. L. Beard, and C. M. Johnson (2009), $^{40}Ar/^{39}Ar$, K–Ar and $^{230}Th–^{238}U$ dating of the Laschamp excursion: A radioisotopic tie-point for ice core and climate chronologies, *Earth and Planetary Science Letters*, *286*(1-2), 80-88, doi:10.1016/j.epsl.2009.06.030.

Stuiver, M., and P. D. Quay (1980), Changes in Atmospheric Carbon-14 Attributed to a Variable Sun, *Science*, *207*(4426), 11-19, doi:10.1126/science.207.4426.11.

Teanby, N., C. Laj, D. Gubbins, and M. Pringle (2002), A detailed palaeointensity and inclination record from drill core SOH1 on Hawaii, *Physics of the Earth and Planetary Interiors*, *131*(2), 101-140, doi:http://dx.doi.org/10.1016/S0031-9201(02)00032-8.

Turrin, B., D. E. Champion, R. A. Mortlock, R. G. Fairbanks, and C. C. Swisher (2013), $^{40}Ar/^{39}Ar$ and U-series ages of a Late Pleistocene geomagnetic excursion in Western North America: The Hilina Pali event in Western North America? , in *AGU, Fall 2013*, edited, San Francisco.

Wagner, G., J. Beer, C. Laj, C. Kissel, J. Masarik, R. Muscheler, and H. A. Synal (2000), Chlorine-36 evidence for the Mono Lake event in the Summit GRIP ice core, *Earth and Planetary Science Letters*, *181*(1–2), 1-6, doi:http://dx.doi.org/10.1016/S0012-821X(00)00196-5.

1.7 Figures and Tables

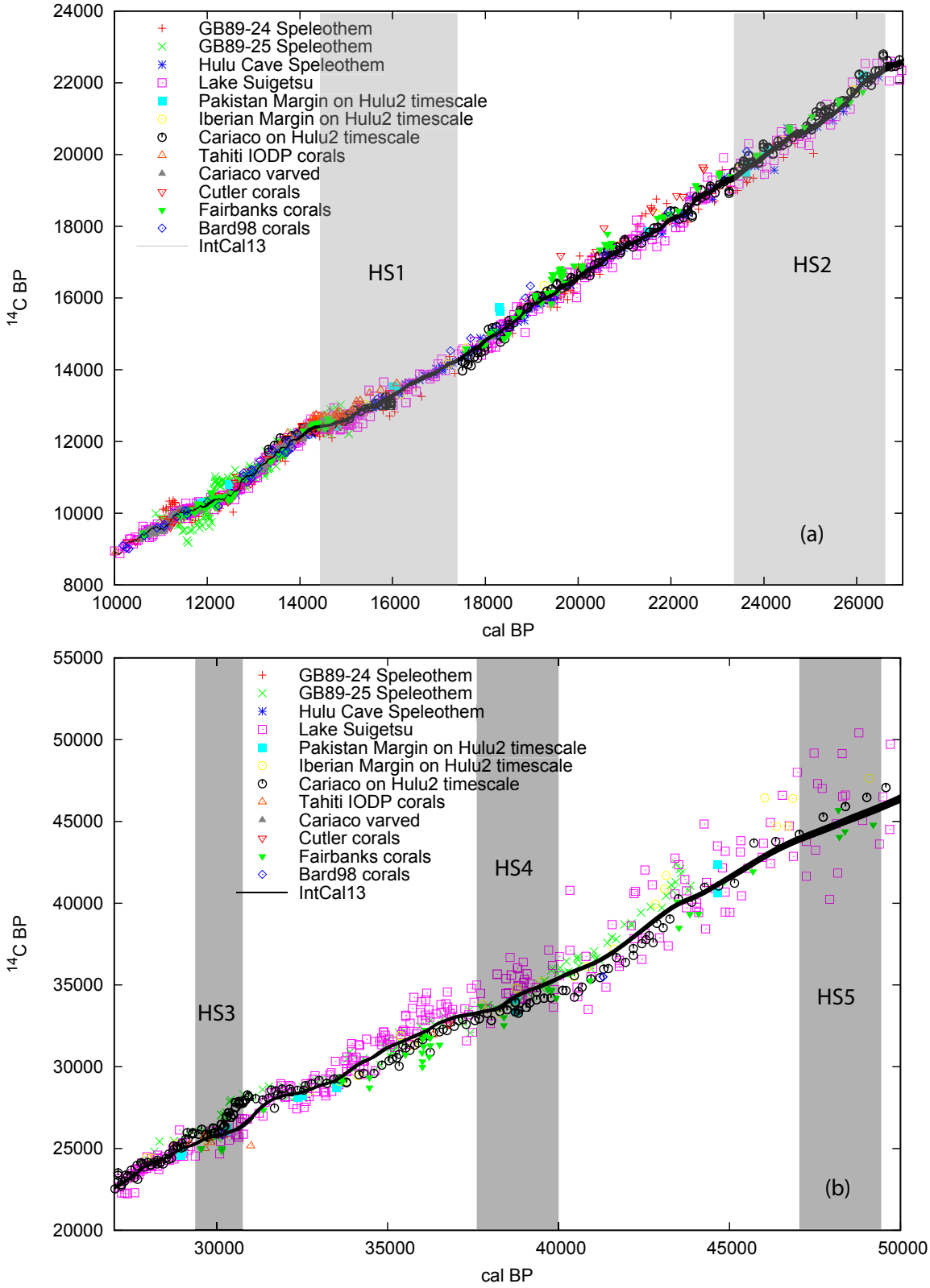
GB89-24 Speleothem
GB89-25 Speleothem
Hulu Cave Speleothem
Lake Suigetsu
Pakistan Margin on Hulu2 timescale
Iberian Margin on Hulu2 timescale
Cariaco on Hulu2 timescale
Tahiti IODP corals
Cariaco varved
Cutler corals
Fairbanks corals
Bard98 corals
IntCal13
HS1
HS2
(a)
^{14}C BP
cal BP
HS3
HS4
HS5
(b)

Figure 1.1: Examples of radiocarbon calibration data sets and calibration curves from IntCal 13 [*Reimer et al.*, 2013].

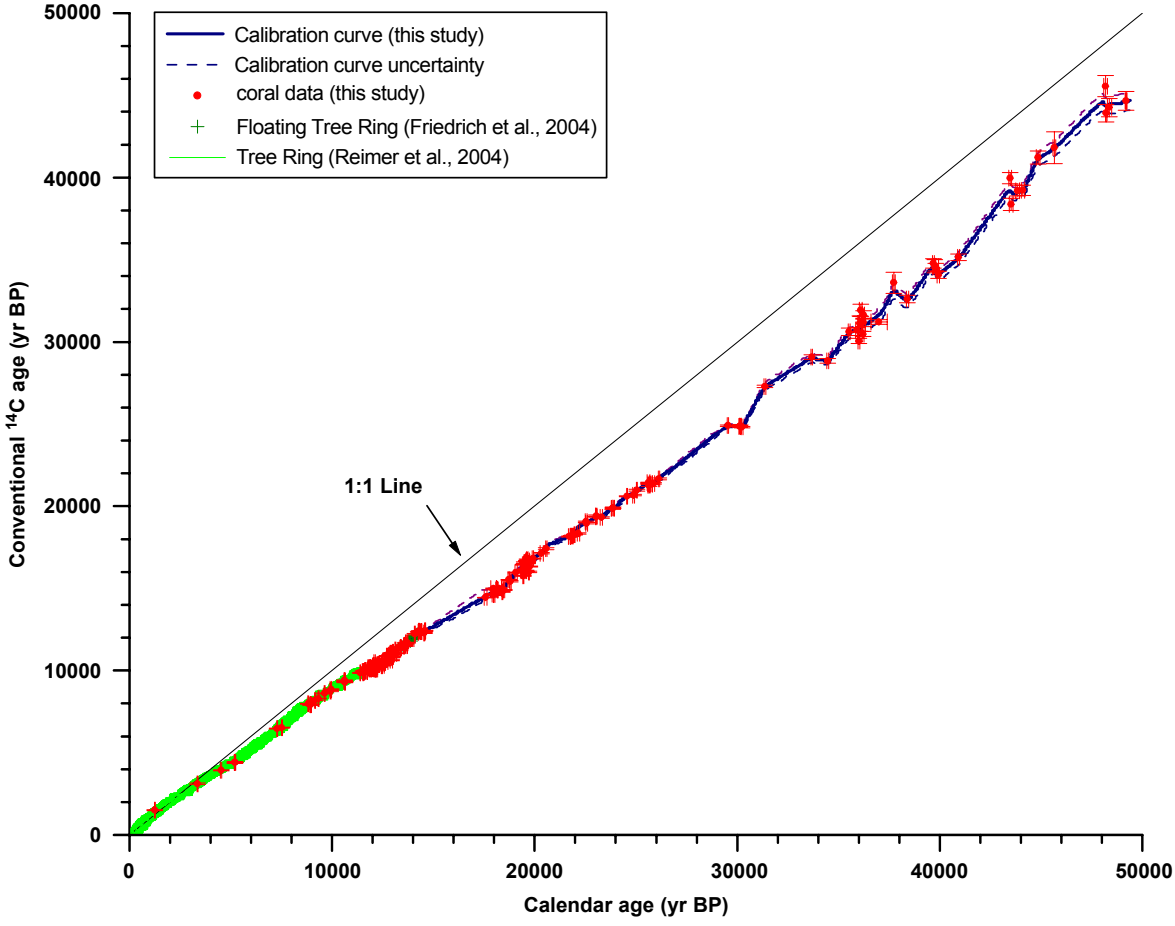
Calibration curve (this study)
Calibration curve uncertainty
coral data (this study)
Floating Tree Ring (Friedrich et al., 2004)
Tree Ring (Reimer et al., 2004)
1:1 Line
Conventional ^{14}C age (yr BP)
Calendar age (yr BP)
0
10000
20000
30000
40000
50000

Figure 1.2: Coral radiocarbon calibration data and calibration curve from [Fairbanks et al. 2005].

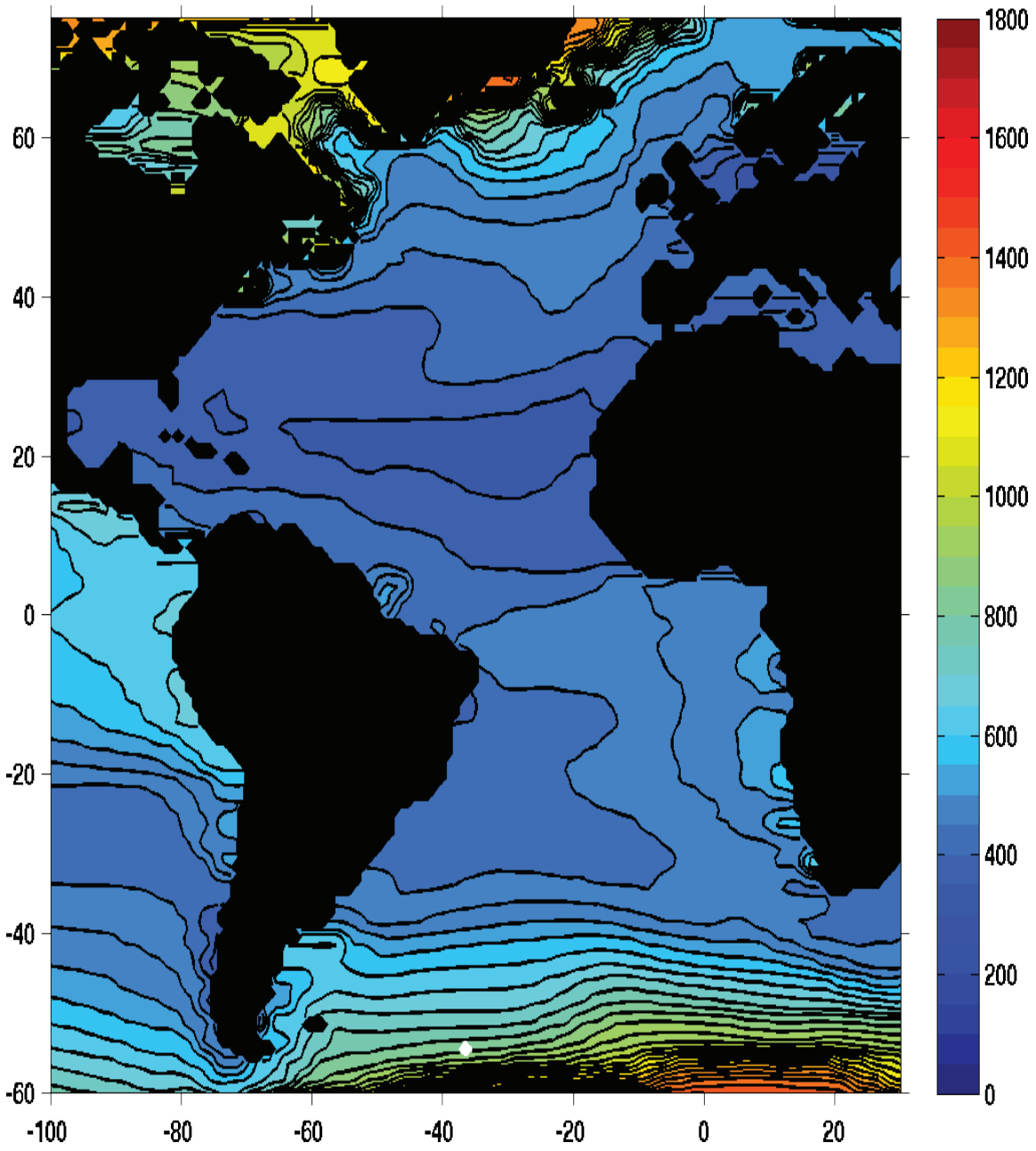
60
40
20
0
-20
-40
-60
-100
-80
-60
-40
-20
0
20
1800
1600
1400
1200
1000
800
600
400
200
0

Figure 1.3: Map of surface water ^{14}C age from 3-D general circulation model, based on radiocarbon reservoir age data set [*Butzin et al.*, 2005]. Scale to the right vertical axis is in ^{14}C years.

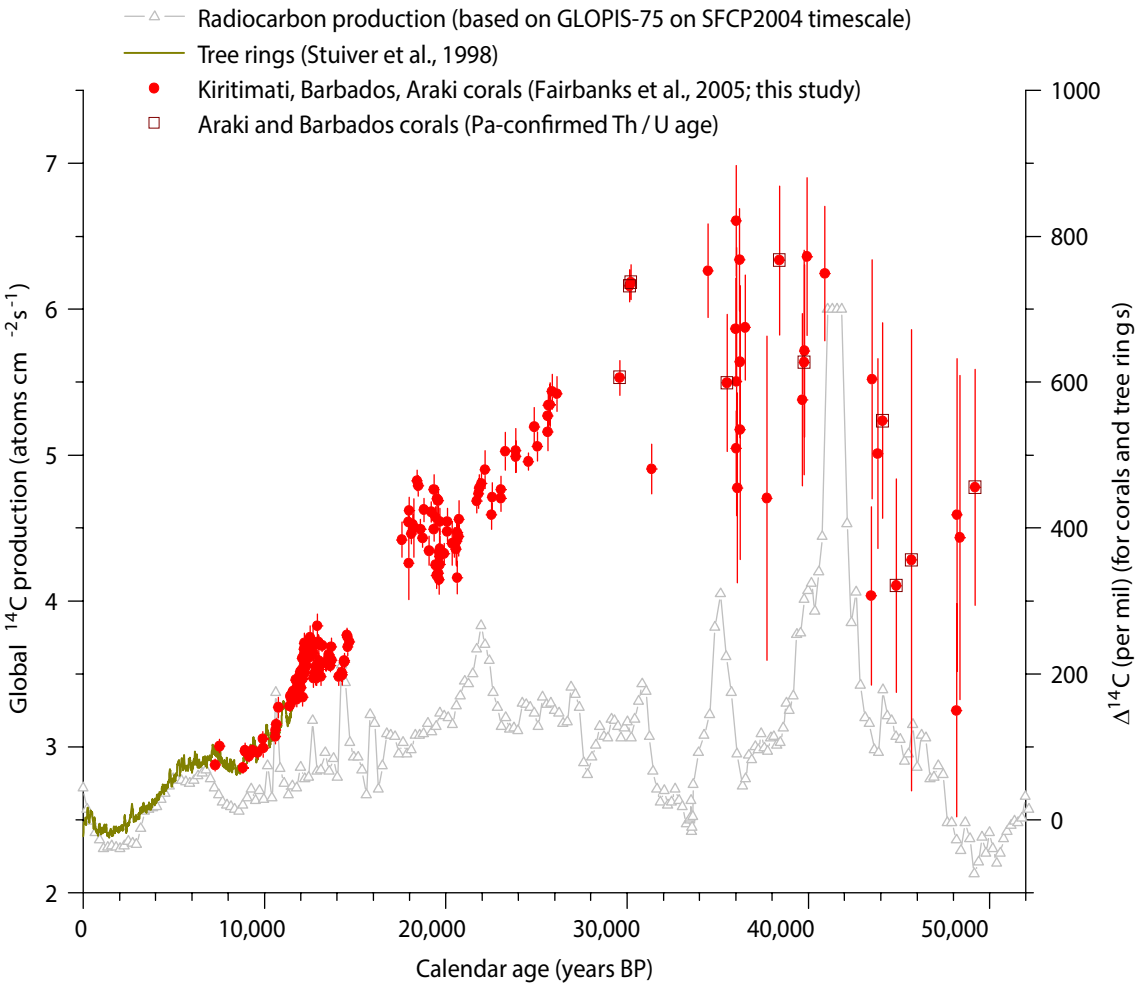
Radiocarbon production (based on GLOPIS-75 on SFCP2004 timescale)
Tree rings (Stuiver et al., 1998)
Kiritimati, Barbados, Araki corals (Fairbanks et al., 2005; this study)
Araki and Barbados corals (Pa-confirmed Th / U age)
Global ^{14}C production (atoms cm $^{-2}$s^{-1})
Δ^{14}C (per mil) (for corals and tree rings)
Calendar age (years BP)
2
3
4
5
6
7
0
200
400
600
800
1000
0
10,000
20,000
30,000
40,000
50,000

Figure 1.4: Atmospheric radiocarbon ($\Delta^{14}C$) reconstruction for the past 50,000 years based on U-Th and ^{14}C dated fossil corals, as published in *Chiu et al.* [2007]

Chapter Two

Shut-down in North Atlantic Overturning at the start of the Younger Dryas confirmed by tropical Pacific and Atlantic Corals $\Delta^{14}C$

2.1 Abstract

The Younger Dryas cold interval (12.86 to 11.65 kyr BP) interrupted the most recent deglaciation with a return to "glacial like" conditions. A shutdown of North Atlantic Deep-Water production (NADW) and disruption of the Atlantic Meridional Overturning Circulation (AMOC), possibly triggered by freshwater input to the North Atlantic, is widely believed to have caused this abrupt climate reversal. Changes in NADW production should be reflected in records of the $^{14}C/^{12}C$ ratio of the atmosphere ($\Delta^{14}C$) since it limits the exchange between surface ocean and atmosphere CO_2 reservoirs. Ocean-atmosphere coupled models consistently show a buildup of ^{14}C in the atmosphere during slowdown or complete shutdown of NADW.

In this study, we present reconstructions of $\Delta^{14}C$ based on paired ^{14}C and U-Th dating of 169 Barbados and Kiritimati surface corals spanning 13.9 to 7.3 kyr BP. The entire data set overlap with tree ring calibration data, thus providing a robust estimate of the marine reservoir age of surface water and its variability at tropical Atlantic and Pacific locations.

Application of constant marine reservoir corrections to coral ^{14}C ages leads to diverging Atlantic and Pacific surface water $\Delta^{14}C$ in both phasing and amplitude, producing a 200 year lead in a 50 to 70‰ rise in $\Delta^{14}C$ at Barbados compared to a similar rise at Kiritimati, at the onset of the Younger Dryas (12.9 kyr BP). Differences between

Atlantic and Pacific $\Delta^{14}C$ records are remarkable in that the data match modeled results demonstrating a shutdown in NADW raises the ^{14}C content of the atmosphere, while simultaneously lowering the ^{14}C age of Atlantic surface water. The precise and accurate dated $\Delta^{14}C$ record obtained with corals confirms that shutdown of NADW occurred at the beginning of the Younger Dryas.

Atlantic coral, Pacific coral, and tree ring $\Delta^{14}C$, all converge by 12.5 kyr BP and thereafter the records display a $\Delta^{14}C$ decrease of about 100‰ by the end of the Younger Dryas (11.6 kyr BP). The more precisely dated coral $\Delta^{14}C$ results indicate NADW shutdown during the Younger Dryas was short lived (i.e., 500 years) and reinvigorated NADW production resulted in a drawdown of atmospheric ^{14}C.

2.2 Introduction

The Younger Dryas climate event in Greenland Ice core records is dated to 12.86 to 11.65 kyr BP (Rasmussen et al., 2006) and was marked by a shift to glacial like conditions during the middle of the last deglaciation. During the Younger Dryas, the North Atlantic polar front and sea-ice boundaries extended further south to more temperate latitudes (Ruddiman and McIntyre, 1981). A shift in Cariaco Basin gray scale corresponding to a simultaneous shift in declining $\delta^{18}O$ in NGRIP is assumed to reflect a subsequent southward shift in the northern polar front and southward shift in the intertropical convergence zone (ITCZ) in response to northern high latitude cooling (Hughen et al., 1998; Hughen et al., 2000; Peterson et al., 2000).

Radiocarbon is produced in the upper atmosphere from the interaction of cosmic rays and nitrogen atoms. Because of changes in shielding effect of the earth's magnetic

the production rate of radiocarbon (^{14}C) in the atmosphere is not a constant and calibration of the radiocarbon time scale is needed in order to convert ^{14}C years to calendar years, essential for measuring time and rates of change for numerous scientific fields. Shallow water fossil corals provide an excellent archive for radiocarbon calibration beyond tree ring records because both the radiocarbon age and Uranium-series (U-Th) age can be generated from the same sample. The paired ages provide an estimate of the $^{14}C/^{12}C$ atmospheric ratio ($\Delta^{14}C$), provided corrections can be made for the local age offset between the surface water HCO_3^- in which the coral grew and the contemporaneous atmosphere, commonly referred to as the marine reservoir age (MRA). This is a requirement for computing accurate $\Delta^{14}C$ because *both* the radiocarbon age and calendar ages can be obtained.

MRA varies globally, ranging from 200 to 1200 years and is strongly dependent upon latitude (Key et al., 2004). The range in MRA is due to partial equilibration of the surface ocean with the atmosphere and from differences in the fraction of ^{14}C depleted sub-surface water that is mixed upwards. The IntCal working group periodically generates a marine ^{14}C curve (e.g., MARINE13) using an ocean-atmosphere box diffusion model (Oeschger et al., 1975), along with marine and terrestrial data from the IntCal13 data-base to derive a "global" estimate of MRA for application to marine carbonates that range between 200 to 500 years (Reimer et al., 2013). However, because of the large variability in MRA observed across the modern ocean it is recommended that MRA corrections be site specific and based on the local offset, or ΔR, defined as the difference in ^{14}C age of a marine sample of known calendar age with its modeled, or MARINE13, age. Simply stated, ΔR represents the regional difference from the global

average (~405 years). MRA, and hence ΔR, can be estimated by a variety of means. When both can be obtained from the same sample, the ^{14}C age of contemporaneous terrestrial material (e.g., wood, leaf material, insects) can be compared to the ^{14}C age of marine fossil material (e.g., carbonate shells). More commonly, MRA is estimated by comparing the raw ^{14}C age in a marine archive to the ^{14}C age in tree rings of identical calendar year age, since the latter is an estimate of the contemporaneous atmosphere. The age difference in ^{14}C years is the MRA. Understandably, beyond the limit of tree ring data (~13.9 kyr BP) (Hua et al., 2009; Kromer et al., 2004) the accuracy of a ^{14}C age in any marine archive (e.g., corals, foraminifera) will be limited by the assumption of a constant reservoir age correction.

The ^{14}C age of tropical surface water is a function of the exchange rate between the atmosphere and ocean but also depends on the pCO_2 of the atmosphere, the fraction of ^{14}C depleted-water mixed into the surface, and to a lesser extent sea surface temperature (SST) (Bard, 1988; Stuiver and Polach, 1977). There is strong evidence that many of these processes (wind speed, SST, pCO_2) varied during different climate states. For example, lower atmospheric pCO_2 during the LGM should have reduced the rate at which radiocarbon diffused from the mixed layer to the atmosphere, resulting in an increase in the average surface ocean to atmosphere ^{14}C age difference by about 150 years (Bard, 1998). In contrast, increased wind speeds predicted for the LGM would have served to increase the rate of CO_2 mixing between the ocean and atmosphere, thereby reducing the radiocarbon atmosphere to surface ocean age difference.

Variable MRA in the tropical Atlantic has been linked to changes in the production of North Atlantic Deep Water (NADW) during the Younger Dryas and

Heinrich Stadial 1 (17.5 – 14.5 kyr BP) stimulated by freshwater input into areas of deep water production (Butzin et al., 2005; Matsumoto and Yokoyama, 2013; Meissner, 2007; Ritz et al., 2008; Singarayer et al., 2008). Ocean models simulating a reduction or shutdown of NADW formation during the Younger Dryas generally result in increased exchange between the surface ocean and atmosphere and or reduction in the volume of aged South Atlantic sourced water, thus decreasing the ocean to atmosphere age difference and leading to lower tropical Atlantic reservoir ages, where as tropical Pacific MRA is less impacted. Direct estimates of MRA during the Younger Dryas at high latitude sites, however, suggest increasing MRA (Bondevik et al., 2006; Cao et al., 2007), perhaps due to a decrease in the rate of atmospheric to ocean exchange with an expansion of sea ice. Similarly, the MRA estimated for Younger Dryas age corals from the western equatorial Pacific have been found to be about 150 years larger than modern values (Burr et al., 2009).

The goals set forth in this chapter are to: 1) combine paired U-Th and ^{14}C dated surface corals overlapping the tree ring record to provide estimates of MRA and ΔR at tropical Atlantic and Pacific Ocean locations; 2) examine potential variability in MRA across abrupt climate boundaries, such as the Younger Dryas/Allerød, that punctuated the most recent deglaciation and that may be related to large changes in thermohaline circulation; and 3) generate independently dated tropical Atlantic and Pacific records of $\Delta^{14}C$ spanning 13.9 to 7.3 kyr BP for comparison to terrestrial $\Delta^{14}C$ records and proxy records of NADW production and to ocean-atmosphere model predictions simulating reduced NADW during the Younger Dryas.

2.3 Materials and Methods

Study site locations are Barbados (13.10° N; 59.32° W) from the western topical Atlantic and Kiritimati Atoll (1.99° N; 157.78° W) from the central equatorial Pacific. MRA estimates and the associated variability at Barbados and Kiritimati is important because corals provide the only directly dated marine archive available for constructing radiocarbon calibration and atmospheric ^{14}C curves (Fairbanks et al., 2005; Reimer et al., 2013) and corals provide critical data to the portions of calibration records where overlapping tree ring records are not available (i.e., beyond 14 kyr BP).

Barbados is located at the western edge of the Atlantic warm pool, where the depth of the surface mixed layer is deepest, ranging from 60 to 80 meters (Ravelo et al., 1990). Surface waters arriving at Barbados have transited the Atlantic subtropical gyres where waters originate with a reservoir age (pre-bomb) of about 250 years and have crossed the equator providing a long atmospheric exchange time. Surface contour maps of ^{14}C show subtropical gyre water today has high bomb ^{14}C, confirming a longer residence time for these waters (Key et al., 2004). Furthermore, coupled ocean models simulating LGM conditions consistently show that an increase in wind stress results in a deepening of the surface mixed layer of the Atlantic Warm Pool (Ravelo et al., 1990) thereby limiting the potential for raising MRA. Although Barbados is expected to be subject to minimal changes in surface water $\Delta^{14}C$ and well suited for buffering large shifts in MRA, constraining variability in these properties beyond modern era data sets (Guilderson et al., 2005) requires validation.

Kiritimati Atoll (a.k.a. Christmas Island) is located close to the equator (2°N) and lies at the eastern edge of the Pacific Warm Pool in the central Pacific and nearest to the

maximum thermal energy associate with the El Nino /La Nina phenomena. At Kiritimati, the warm phase of the El Nino Southern Oscillation (ENSO) results in reduced equatorial upwelling and an increase in SST. Thus, shifts in MRA might be expected due to changes strength of ENSO and related shifts in the proportion of colder, ^{14}C depleted water upwelled from the eastern coast of South America and transported westward via the equatorial counter current. Coral records of $\delta^{18}O$ and $\Delta^{14}C$ in the central equatorial Pacific spanning the last millennium, however, do not show large inter-annual or decadal variability in $\Delta^{14}C$ associated with large changes in $\delta^{18}O$, suggesting radiocarbon in the mixed layer is largely unaffected by changes in ENSO related upwelling (Zaunbrecher et al., 2010).

Coral samples were selected from the Barbados offshore drill-core collection from material recovered during the *RANGER* 88-13 (1988), *M/V NATIVE SPIRIT* 1104 (2004), and *R/V KNORR* 189-2 (2007) expeditions. Offshore drill cores at Kiritimati were recovered in 1997, during *MOANA WAVE* cruise 97-101.

Sample screening and data quality control criteria are reported in Fairbanks et al. (2005) but are briefly described here. Concentric 10 mm and 6 mm drill plugs were taken from coral slabs and mechanically cleaned via sonication. Dried sub–samples were crushed to a powder, and analyzed for evidence of secondary calcite by X-ray Diffraction (XRD). Only samples with "no detectable" calcite (less than 0.2 wt. %, Chiu et al., 2005) were processed further for U-Th and ^{14}C dating. Petrographic thin-section slides were made for a subset of U-Th dated coral samples. We found only traces of secondary aragonite and in insufficient amount to disqualify sample selection in this study.

U-Th dating was determined by Inductively Coupled Mass Spectrometry (ICP-MS) using either a FISONS PLASMA 54 by the methods described in Mortlock et al. (2005) or with a ThermoScientific NEPTUNE PLUS ICP-MS using like-methods and protocols adopted for the PLASMA 54. When using the NEPTUNE PLUS, peak-jumping mode was employed to measure minor isotopes of U and Th with a secondary electron multiplier (SEM) positioned behind a retarding potential quadrupole (RPD). U isotopes were measured with sample -standard bracketing to correct for SEM gain efficiency and drift. Instrument mass fractionation was corrected by monitoring the $^{235}U/^{238}U$ ratio. We found neither systematic nor significant differences in U-series ages in coral samples determined with both instruments (Appendix: Table 1). Based on the measured ^{232}Th concentrations (0.02 to 3 ppb) no corrections were made for initial ^{230}Th. All sample U-Th ages had $\delta^{234}U_{initial}$ falling within the acceptable range for modern and fossil corals that have maintained closed system behavior (138-152‰; Fairbanks et al., 2005). The average precision of the age determination (at 2 s.d.) is better than ± 0.5% and ± 0.2‰ in samples measured with the PLASMA 54 and NEPTUNE PLUS, respectively. As an example, a 12 kyr age coral sample analyzed with the NEPTUNE PLUS yields a remarkable 2 s.d. age uncertainty of ± 20 years, or 5 to 50 times more precise than sediment age models.

Coral samples (30 to 80 mg) were pre-treated by the methods described in Fairbanks et al. (2005) and ^{14}C dated by Accelerator Mass Spectrometry (AMS) at three separate facilities (Center for Accelerator Mass Spectrometry, Lawrence Livermore National Laboratory (LLNL); Leibniz Laboratory for Radiometric Age Determination and Isotope Research (Kiel), Christian Albrecht University; National Ocean Sciences

Accelerator Mass Spectrometry Facility, WHOI (NOSAMS) placing our result in a fully inter-calibrated framework. We used a "radiocarbon dead" fossil coral (AK-H-2; U-Th age ~ 97,000 years BP to apply procedural blank corrections to all fossil coral data. Two to three coral blanks were processed and analyzed with each set of 7 coral samples and the fraction modern carbon (FMC) values for blanks averaged and subtracted from sample values. Coral blank values generated at Kiel and LLNL have been previously reported (Fairbanks et al., 2005). Coral blanks prepared and dated at NOSAMS (n=30) ranged from 0.0005 to 0.0015 FMC and were reproducible within batch runs. The average for all NOSAMS blanks was 0.0011 ± 0.0003 (1 SD) corresponding to a radiocarbon age in excess of 54,700 years. Applying blank corrections to samples in this study generally resulted in increasing the ^{14}C age by 20 years to 40 years, depending on the age of the sample. The reported radiocarbon age uncertainty (2 s.d.) ranged from about 40 to 100 years for samples in this study (Appendix: Table 1).

2.4 Results

MRA corrections to corals were estimated by comparing the radiocarbon age of corals with the age of the contemporaneous atmosphere, as obtained from radiocarbon dated tree-ring sequences of known calendar age. The tree ring chronology has been extended to 13.9 kyr BP via "wiggle" matching of ^{14}C Huon pine tree records (HP-40) from Tasmania (Hua et al., 2009) with European tree ring records (Friedrich et al., 2004; Schaub et al., 2008) and with anchoring of the floating European Late Glacial Pine (LGP) record (Kromer et al., 2004). The HP-40 anchoring is considered to be the most accurate calendar age chronology for the floating LGP ^{14}C dated tree ring sequence (Reimer et al.,

2013). A near constant dead carbon correction of 457 years observed between Hulu Cave speleothem H82 and the extended tree ring sequence is considered to be confirmation of the HP-40 anchoring (Southon et al., 2012). More than one anchoring of the LGP sequence, however, has previously been proposed. For example, whereas the HP-40 anchoring places the end of the LGP floating chronology of Kromer et al. (2004) at 12,597 ± 16 cal yr BP anchoring via the Cariaco Basin varve sediment record in PL07-58PC placed the end of the floating chronology at 12,807 cal yr BP (Hughen et al., 2000). The LGP floating chronology has also been anchored via correlation of the common cosmic production ^{14}C signal in tree rings with the ^{10}Be concentration in Greenland ice cores (Muscheler et al., 2008). That anchoring places the end of the floating chronology closer to 12,500 cal yr BP. Finally, based on comparison of U-Th and ^{14}C dated corals Cao et al. (2007) anchored the floating tree-ring sequence, at ~12.7 kyr BP

The HP-40 anchoring is not without dating uncertainties. For example, ^{14}C ages obtained in Tasmanian trees must be corrected for a 40 year Southern to Northern atmosphere age difference, based on the average offset observed during the past millennium (Hua et al., 2009). It is possible that the atmospheric age offset could have been different at times during deglaciation. For example, a change in the rate of exchange of surface water and the atmosphere in the Southern Ocean may have been impacted by the expansion of sea ice, which has a limiting effect on wind speed and hence ocean-atmospheric exchange. On the other hand, expulsion of salt during sea ice formation increases the density of surface water and enhances vertical mixing with deeper and older water, thereby serving to increase the age of surface water (Bard, 1988). Finally, an increase in Southern Ocean upwelling between 15 and 10 kyr BP, as

suggested by increased opal fluxes (Anderson et al., 2009), may have brought radiocarbon depleted pCO_2 to the surface ocean, thereby increasing the age of surface water. Any increase in the South to North Hemispheric atmospheric ^{14}C age difference during the Younger Dryas would generate a shift the 617-year Huon pine ^{14}C chronology and possibly impact the overlap with the extended absolute tree-ring chronology and the LGP anchoring.

While the HP-40 anchoring of the LGP sequence may not be the final word on linking the 1382-ring chronology to the absolutely dated tree ring chronology, in the discussion to follow, we estimate MRA at Barbados and Kiritimati by comparing coral and tree ring ^{14}C ages of identical calendar age for the period of overlap (13.9 kyr BP to 7.3 kyr BP; Figure 2.1). Following the approach of Southon et al. (2012), we compared coral data directly to the smoothed IntCal13 atmospheric ^{14}C curve, rather than directly to the individual tree ring data sets that comprise the record. To obtain a MRA estimate, coral ^{14}C ages were subtracted from IntCal13 ^{14}C ages averaged over a ± 30-year range, or roughly equivalent to the average 1 s.d. ^{14}C dating uncertainty for the interval of comparison. The uncertainty in each MRA estimate combines the uncertainty in the marine (coral) ^{14}C age with the uncertainty of the contemporaneous atmospheric (IntCal13) ^{14}C age (Figure 2.1).

2.4.1 Barbados and Kiritimati MRA

Barbados MRA estimates span the interval 13.9 to 7.3 kyr BP and range from 2 to 670 years with an average of 320 ± 144 years (1 s.d.; n = 74; Figure 2.2a), or a local offset from the global average MRA (ΔR) equal to -85 years. Kiritimati MRA estimates

span the interval 13.7 to 8.9 kyr BP and range from 100 to 400 years with an average of 314 ± 69 years (n = 45; Figure 2.2b), or ΔR equal to -90 years.

A more rigorous estimate of the uncertainty in MRA can be obtained by $\sqrt{\sigma_{MRA}^2-\sigma_{combined}^2}$, where σ_{MRA} represents the standard deviation (1 s.d.) in MRA and $\sigma_{combined}$ represents the combined average uncertainty in uncorrected coral ^{14}C age and IntCal13 age (± 25 years) for the period of comparison. The revised uncertainty estimate in MRA at Barbados and Kiritimati is ± 138 years and ± 58 years, respectively, and is only slightly reduced since most of the variance is due to a small number of extreme values in each data set. The Barbados estimate of 320 ± 138 years is identical to the value of 320 ± 110 years reported in Reimer et al. (2009) and similar to the value of 365 ± 60 years used to correct ^{14}C ages in the Barbados radiocarbon calibration curve in Fairbanks et al. (2005), both of which were based on smaller data sets (n=22 and n=21, respectively) and identical to the modern Caribbean estimate (312 years) obtained from pre-bomb modern corals (Guilderson et al., 2005). The Kiritimati MRA estimate of 314 ± 58 years (1 s.d.) is within the uncertainty of 335 ± 100 years reported in Fairbanks et al. (2005) and is consistent with $\Delta^{14}C$ measured in pre-bomb modern and 16th century Kiritimati corals indicating a MRA of about 450 and 340 years, respectively (Zaunbrecher et al., 2010) and with the reservoir age estimate of 362 ± 8 years obtained in pre-bomb corals from the Central South Pacific (15°S) (Burr et al., 2009).

The observed variability and range displayed in MRA at Barbados is larger compared to Kiritimati and larger than expected from the average combined ^{14}C dating and IntCal13 uncertainties (1 s.d. of ± 60 years). The stability of Pacific MRA relative to the Atlantic is not unexpected since gradients expressed in the pre-bomb ^{14}C age of

Pacific surface waters are broader and display less variability compared to the Atlantic (Butzin et al., 2005; Key et al., 2004). Furthermore, the much larger size of the Pacific makes it less likely to have the surface reservoir age easily altered. Indeed, high resolution ^{14}C dating of pre-bomb and last millennium corals in the central topical Pacific show little variability in MRA related to changes in ENSO related upwelling (Zaunbrecher et al., 2010).

The overall uncertainty in MRA combines local variability in MRA, dating uncertainties, and short-term changes in the $^{14}C/^{12}C$ ratio of atmospheric CO_2 due to changes in solar production. Tree rings record systematic fluctuations in the ^{14}C content of the atmosphere associated with documented historic sun-spot activity (Stuiver and Braziunas, 1989). Changes in solar output alter the shielding effect of the solar wind to cosmic rays such that during periods of increased solar output and sun spot maxima shielding from cosmic rays is increased and ^{14}C production reduced. Such a phenomena should be recorded as an increase in the calendar to atmosphere ^{14}C age difference, although one would expect production changes in the atmosphere to be attenuated in the surface ocean. Centennial scale $\Delta^{14}C$ variations on the order of 10-20‰, equivalent to 80 to 160 ^{14}C years, have been measured in Younger Dryas and Little Ice Age dated tree rings and are attributed to solar variability (Hua et al., 2009). Therefore, ^{14}C age differences approaching ± 100 ^{14}C years observed in equivalent calendar age corals (Figure 2.1) are similar in scale to those observed in tree ring records and associated with production changes due to solar activity.

The Barbados MRA reconstruction shows a period of extremely low MRA during the early Younger Dryas, not observed in the Kiritimati record (Figure 2.2a and 2.2b).

The anchoring of the floating Late Glacial Pine (LGP) tree-ring record (Hua et al., 2009) generates a ^{14}C "cliff " beginning c.a. 12.7 kyr BP at which time uncorrected ^{14}C ages in four Barbados corals overlap with the IntCal13 estimate of the atmosphere, resulting in MRA corrections of 55 years or less (Figure 2.1 and Figure 2.2a). These extremely low MRA require surface water at Barbados be both isolated from sources of upwelling and in very rapid exchange with the atmosphere, a condition that is not found in modern oceans. Likewise, extreme Barbados MRA estimates of between 600 and 700 years (Figure 2.2a) are not easily reconciled with zonal wind field and paleoceanographic proxy reconstructions in the tropical surface Atlantic Ocean. It is important to consider each U-Th and ^{14}C dated coral sample is an independent and discrete calibration and MRA estimate. This is not the case for the stacked tree-ring radiocarbon record where all gaps or chronology correlations may generate potential dating errors that are cumulative and compounded in the final record. This accordioned uncertainty directly impacts MRA estimates made by comparison of atmospheric and marine radiocarbon records. Nevertheless, these new data, confirmed with replicate U-Th and ^{14}C dating, lend support to prior assertions that MRA was reduced in the tropical Atlantic during the early Younger Dryas (Hua et al., 2009).

That the ^{14}C age of tropical Atlantic surface water was reduced during the onset of the Younger Dryas was based on an abbreviated Barbados coral record and a Cariaco Basin deep sea core (Hua et al., 2009). Those findings prompted the exclusion of all Atlantic-Caribbean calibration data from the 12.90 to 12.55 kyr BP, interval in the IntCal09 and IntCal13 calibration curves (Reimer et al., 2009; Reimer et al., 2013). Indeed, Barbados MRA averages 190 ± 165 years (n = 9) between 12.90 and 12.55 kyr

BP. A recovery to higher Atlantic MRA is achieved by 12.6 kyr BP, although there are also a number of lower MRA values at 13.5 and 12.2 kyr BP (Figure 2a). Kiritimati coral data do not display a shift to lower MRA at the beginning of the Younger Dryas (Figure 2.2b).

The average MRA estimate obtained from Barbados corals overlapping with the continuous tree ring chronology (7.3 to 12.55 kyr BP) is 344 ± 124 years (n = 37). The estimate obtained for the interval preceding the Younger Dryas (13.9 to 12.9 kyr BP) is 338 ± 142 years (n= 30) (Table 2.1). Thus, a record of Atlantic MRA spanning 14 to 7 kyr BP years was interrupted, briefly, with an interval of exceptionally low MRA, and limited to one of the largest and most abrupt climate extremes. Therefore, the results show it is reasonable to apply a constant MRA correction (340 ± 130 years; ΔR = -65 years) to all Barbados coral ^{14}C ages in this, and all subsequent chapters to follow. The 340 ± 130 years estimate is both within a reasonable range for Barbados MRA of surface water and constrained between the estimate for the mean ocean (405 years) and modern values (200-240 years) reported for the Caribbean (Guilderson et al., 2005; Wagner, 2009).

Future coral calibration curves should be revised to account for the brief interval of low Atlantic MRA at the beginning of the Younger Dryas since there is the potential for inaccurate calibration of ^{14}C ages obtained in tropical and subtropical Atlantic deep-sea sediments by over correcting for the MRA. For example, using a constant 400 year MRA correction to 11,300 ^{14}C age obtained from tropical Atlantic foraminifera would result (incorrectly) in a calibrated age of 12,740 calendar years BP and after the start of the Younger Dryas, whereas a MRA correction of 100 years would yield a calibrated age

of 13,080 calendar years BP, thereby placing it at the very end of the Allerød. However, it also important to recognize that ^{14}C dating errors increase exponentially with increasing age so that an applied reservoir age uncertainty of ± 150 years represents less than half of the fractional ^{14}C dating error in samples older than 25,000 ^{14}C years (Figure 2.3).

2.5 Discussion

Application of constant MRA corrections to the coral data produces differences in the placement of the Younger Dryas ^{14}C "cliff" (Figure 2.4 and 2.5). MRA corrected Kiritimati corals plot with the tree ring sequence and Hulu Cave H82 speleothem data (Southon et al., 2012) whereas Barbados corals plot as a ^{14}C "cliff" placed approximately 200 years earlier. Coral data from other Pacific locations (Tahiti and Papua New Guinea) have limited overlap with the Kiritimati data. In addition, those data suffer from much larger ^{14}C dating errors and scatter (Bard et al., 1998; Cutler et al., 2004), thus limiting their usefulness for comparison to the Barbados and Kiritimati data. However, there is very good overlap with the high-resolution Cariaco Basin varve record (Hughen et al., 2004a) and Barbados U-Th dated corals (Figure 2.4 and 2.5), particularly across the Allerød–Younger Dryas boundary, suggesting the Cariaco Basin calendar age chronology, based on counting of varves, is accurate and that constant MRA corrections of 340 and 420 years to these two records, respectfully, are reasonable. Since Atlantic, Caribbean, and Pacific records all represent an archive of the ^{14}C content in the same atmosphere, the divergence between Atlantic corals and Caribbean sediment records from tree rings and Pacific corals must be due to reduced MRA in tropical Atlantic (and Caribbean) surface waters at the start of the Younger Dryas. After 12.6 kyr BP, Atlantic

and Pacific coral records converge indicating the interval of reduced MRA in the tropical Atlantic was brief, lasting about 200 years.

In the discussion to follow, we combine MRA corrected Barbados and Kiritimati coral ^{14}C ages with the paired U-Th ages to generate a record of $\Delta^{14}C$ into and out of the Younger Dryas cold stadial. We then examine the shape of the $\Delta^{14}C$ curve from the mid-Allerød (13.9 kyr BP) through the Younger Dryas and early Holocene in order to isolate variability in $\Delta^{14}C$ from the long-term trend and to identify the geochemical and geophysical mechanisms, global and local, which may have been responsible. Finally, we show that the offset, in timing, between Pacific and Atlantic coral $\Delta^{14}C$ is consistent with modeled predictions of shutdown in NADW and that timing of the shutdown occurred at the same time as the start of the Younger Dryas.

2.5.1 Atmospheric $\Delta^{14}C$ reconstruction

Paired radiocarbon and calendar age data from terrestrial and marine archives provide an estimate of the radiocarbon content of the atmosphere, $\Delta^{14}C$, by the following equation:

$$\Delta^{14}\mathrm{C}\ (‰) = \left(\frac{EXP\ (\lambda_1 * t_1)}{EXP\ (\lambda_C * t_C)} - 1 \right) * 1000 \qquad (1)$$ (after Stuiver and Polach, 1977)

Where t_1 is the calendar age, t_c is the radiocarbon age, λ_1 is the activity constant of ^{14}C based on the consensus (Oxford) half-life of 5730 years and λ_c is the activity constant based on the Libby half-life of 5568 years (Libby, 1955).

Beginning with our reconstruction of $\Delta^{14}C$ at 13.9 kyr BP coral data show a series of ± 50‰ fluctuations in $\Delta^{14}C$ throughout the Allerød, centered around 200‰, and a

decrease of 50‰ starting at 13.2 kyr BP (Figure 2.6). High-frequency variability in $\Delta^{14}C$, most noticeably during the Allerød, is too large to be due to changes in production rates related to solar variability. In fact, the $\Delta^{14}C$ amplitude changes recorded by corals are a factor of two to five more than those measured in tree ring from the last millennium or during the Younger Dryas (Hua et al., 2009; Stuiver and Braziunas, 1989) and attributed to a solar origin. Any fluctuations due to production rate changes in the atmosphere would also be attenuated in the surface ocean. For example, simple box diffusion models incorporating a 10% decrease in production resulted in only a ~40 year increase in reservoir age or equivalent to 5‰ and too small to account for observed variability in the coral $\Delta^{14}C$ (Cao, 2010).

Wind speed can impact the ^{14}C age of surface water as it modifies the mixing rate between the atmosphere and the sea surface. An increase (decrease) in air-sea exchange would serve to decrease (increase) the ^{14}C age difference between the surface-ocean and atmosphere. An Oeschger box-diffusion model simulating a 50% decrease in air-sea exchange generated a 300-year increase in MRA in less than 50 years (Cao, 2010). Therefore, the most likely explanation for rapid $\Delta^{14}C$ fluctuations in the coral record is a change in tropical wind stress and subsequent changes in MRA.

The most salient features in the coral $\Delta^{14}C$ record are the rapid rise of 50 to 70‰ at the onset of the Younger Dryas, the long and large (100‰) decline in $\Delta^{14}C$ during the Younger Dryas. Also, there is a pronounced offset in the timing of the rapid $\Delta^{14}C$ rise in Atlantic and Pacific reconstructions (Figure 2.6). The rise in Atlantic $\Delta^{14}C$ leads both the Pacific and atmospheric (IntCal13) signal by about 200 years. The increase in Atlantic $\Delta^{14}C$ at the start of the Younger Dryas, previously documented in the Cariaco Basin

varve reconstruction (Hughen et al., 2000), can be independently confirmed with U-Th dated Barbados corals (Figure 2.6). The high coherence between the Atlantic and Caribbean marine $\Delta^{14}C$ reconstructions indicates the lead in the record is unlikely to be an artifact of the calendar age model constructed in the sediment core. The divergence in Atlantic and Pacific coral $\Delta^{14}C$ records is a result of a systematic lowering of the surface reservoir age in the Atlantic and Caribbean. Correcting Barbados ^{14}C ages with a constant 340 years artificially increases the calendar age to ^{14}C difference, thereby increasing $\Delta^{14}C$.

After the rise in $\Delta^{14}C$ at the beginning of the Younger Dryas, Atlantic and Pacific corals records converge by 12.5 kyr BP and both display a large and long 100‰ decline, by 11.5 kyr BP. That both the tree ring atmospheric signal (IntCal13) and Atlantic and Pacific coral marine signal (reservoir corrected) overlap in timing and amplitude is diagnostic of an ocean-driven decline. The rate of decline (about 0.1‰ yr^{-1}) during this interval is about four times faster the rate expected from the long-term trend resulting from decay of ^{14}C that followed spikes in production during the Laschamp (41 kyr) and Mono Lake (31.4 kyr) geomagnetic excursion events (Chiu et al., 2007; Durand et al., 2013). We attribute the cause of the rapid decline in $\Delta^{14}C$ to an increase in the strength of NADW overturning following slowdown or shutdown during the early Younger Dryas.

2.5.2 Shutdown of NADW during the Younger Dryas

NADW production is responsible for net export of ^{14}C produced in the atmosphere to the world's deep oceans. Increases in NADW lower the ^{14}C content of the atmosphere whereas the atmosphere will accumulate ^{14}C when NADW production is

reduced. Coupled ocean-atmosphere models show that $\Delta^{14}C$ responds instantaneously to recovery of NADW production with increased NADW production leading to more efficient removal of ^{14}C from the atmosphere and a decrease in $\Delta^{14}C$ (Delaygue et al., 2003; Marchal et al., 2001; Singarayer et al., 2008). Other models, however, challenge the traditional view that a slowdown in NADW should necessarily lead to a buildup of ^{14}C in the atmosphere. Instead, these models generate a decrease in $\Delta^{14}C$ during slowdown of NADW as a result of increased ventilation and release of ^{14}C depleted CO_2 from the Southern Ocean via the bipolar see-saw (Matsumoto and Yokoyama, 2013).

There are many lines of evidence indicating NADW production varied widely during the past 50,000 years and that these fluctuations generated changes in the carbon cycle and produced rapid millennial scale variability in the record of $\Delta^{14}C$ (Adkins and Boyle, 1997; Edwards et al., 1993; Hughen et al., 1998; Muscheler et al., 2000). Geochemical tracer evidence in Atlantic Ocean sediment cores indicate a resumption of AMOC and "turn on" of NADW at the time of the Bølling/Allerød transition onset (~14.5 kyr BP) following a period of weaker NADW production during Heinrich Stadial 1 (Charles and Fairbanks, 1992; McManus et al., 2004). The Younger Dryas is also believed to have been an interval of weaker NADW production (McManus et al., 2004) although the mechanism responsible for a slow-down in AMOC is still a topic for debate. A common feature of models simulating Younger Dryas cooling force NADW shutdown with freshwater input to the North Atlantic and shutdown of the "deep water conveyor belt". These "hosing" experiments generally require freshwater forcing of between 0.1 and 0.4 Sv (Sv = 10^6 m^3 s^{-1}) applied for ~ 1000 years in order to generate and sustain NADW shutdown. The simulations produce $\Delta^{14}C$ increases of about 30 to 50‰,

although the amplitude and duration of the increase is heavily dependent on model parameterization. For example, models employing large changes in wind stress in tropical and subtropical regions, combined with a shutdown of NADW, simulate up to a 70‰ increase at the beginning of the Younger Dryas (Delaygue et al., 2003), thus approaching the higher values indicated by coral data.

While the rise in $\Delta^{14}C$ at the beginning of the Younger Dryas can be simulated with a shutdown of AMOC, the large and long decline following atmospheric buildup of ^{14}C is not reproduced in these same models. A decrease of $\Delta^{14}C$ during the first half of the Younger Dryas was generated, based on the flux of ^{10}Be measured in Greenland Ice, and was attributed to variable production rates, coupled with a decrease in ventilation (Marchal et al., 2001). These simulations, however, did not reproduce the rapid $\Delta^{14}C$ rise at the beginning of the Younger Dryas. A 30‰ decline in atmospheric $\Delta^{14}C$ during the Younger Dryas was generated with ventilation of ^{14}C-depleted CO_2 from the Southern Ocean triggered by freshwater forced shutdown of AMOC via the bi-polar seesaw (Matsumoto and Yokoyama, 2013). However, the model simulations explain only about one half to one-third of the 70 to 100‰-amplitude decline observed in the marine or terrestrial reconstructions (Figure 2.6). Therefore, ocean circulation models can neither reproduce the full amplitude $\Delta^{14}C$ increase at the beginning of the Younger Dryas nor the full amplitude decrease during the Younger Dryas interval, even when incorporating extreme and variable production rates.

One important feature shared by several models is that they make the prediction that when MRA is kept constant the $\Delta^{14}C$ response to NADW shutdown should be different in the Pacific and Atlantic oceans (Matsumoto and Yokoyama, 2013; Singarayer

et al., 2008). In these models, reduced NADW enables Atlantic surface water to remain in exchange with atmosphere for a longer period of time and thus reducing the surface reservoir age and increasing $\Delta^{14}C$. The impact to equatorial Pacific waters is limited, both due to its larger size and because water upwelled in the equatorial Pacific is derived from the Southern Ocean. However, correction of ^{14}C ages with a constant reservoir correction leads to diverging Atlantic and Pacific surface water $\Delta^{14}C$ in both phasing and amplitude (Matsumoto and Yokoyama, 2013).

Differences in the shape of marine and terrestrial derived atmospheric $\Delta^{14}C$ records predicted in models highlight the importance of measuring $\Delta^{14}C$ in different ocean basins. The important contribution of this study is that the $\Delta^{14}C$ records presented here span the entire Younger Dryas and consist of Atlantic and Pacific corals, dated with the precision and accuracy needed to test hypotheses linking atmospheric $\Delta^{14}C$ to shutdown of NADW. There is remarkable similarity in both the phasing and amplitude shift between our Atlantic and Pacific $\Delta^{14}C$ and the predicted changes in MRA presented in the modeling study of Singarayer et al. (2008) (Figure 2.7). Tropical Atlantic surface waters become younger compared to tropical Pacific surface waters due to reduced Atlantic basin ventilation (Delaygue et al., 2003; Matsumoto and Yokoyama, 2013; Singarayer et al., 2008) which is observed as a rise in Atlantic $\Delta^{14}C$, preceding Pacific and atmospheric trends by about 200 years. The midpoint in the Barbados shift to increased $\Delta^{14}C$ is approximately 12.9 kyr BP and is identical, in timing, to the shift observed in the higher density Cariaco Basin record (Figure 2.7). Thus, as interpreted through the Singarayer et al. (2008) ocean-atmospheric model, coral data confirms

NADW shutdown as a likely cause of rapid $\Delta^{14}C$ increase and that shutdown occurred at the same time as the start of the Younger Dryas.

In advancing a mechanism for triggering the Younger Dryas, many have argued a sudden discharge of glacial meltwater freshened and stratified the North Atlantic, thereby disrupting NADW formation and potentially leading to a complete shutdown of AMOC (Broecker et al., 1989; Broecker et al., 1985). A detailed record of sea level spanning the Younger Dryas based on U-Th dated Barbados reef crest species *Acropora palmata* (Abdul et al., 2016) disputes this hypothesis. The *A. palmata* reef crest facies is ecologically restricted to the wave impacted upper 5 m of the water column (Mesolella, 1967) and has proven to be an excellent archive of sea level variability (Abdul et al., 2016; Fairbanks, 1989; Peltier and Fairbanks, 2006). The *A. palmata* record shows a sea level rise of 7 meters during the Younger Dryas with rates of sea level rise that decreased smoothly from 20 mm yr^{-1} at the termination of MWP 1A (13.9 kyr BP), to 4 mm^{-1} by the end of the Younger Dryas, before accelerating again during MWP 1B (11.45 kyr BP) (Abdul et al., 2016). Barbados coral $\Delta^{14}C$ data presented here include 41 of the same *A. palmata* used to construct the sea level curve. The rate of sea level rise and record of $\Delta^{14}C$ can, therefore, be precisely correlated since the records are derived from the same samples or from adjacent samples in the same drill cores (Figure 2.8). Comparison of these records strongly argues against a major melt-water event to have triggered the Younger Dryas. In fact, the rate of sea level rise prior to the Younger Dryas is about 7 mm yr^{-1} (0.07 Sv) and less than that required in freshwater hosing experiments facilitating shutdown of AMOC (Matsumoto and Yokoyama, 2013; Ritz et al., 2008; Singarayer et al., 2008). Finally, the response of $\Delta^{14}C$ is minimal with respect to changes

in the rate of sea level rise (Figure 2.8). We conclude that model driven $\Delta^{14}C$ changes resulting from NADW shutdown during the Younger Dryas and attributed to freshwater input to the North Atlantic are not supported in the record of sea level and suggests the dependence of NADW formation from fresh water forcing may be overestimated or may be more site dependent than simulated in theoretical models.

Proxy evidence for decreased NADW production during the Younger Dryas and during Heinrich Stadials, 60 to 25 kyr BP, are based on decreased $\delta^{13}C$ in benthic foraminifera from the North Atlantic (Elmore and Wright, 2011; Henry et al., 2016), increasing Pa/Th in Bermuda Rise sediments (Henry et al., 2016; McManus et al., 2004), and increasing ε_{Nd} from the South Atlantic (Piotrowski et al., 2005).

The Younger Dryas interval is often compressed, even in high sedimentation rate deep-sea cores. Dating uncertainties imposed by ^{14}C age plateaus and the potential for variable MRA corrections during the Younger Dryas the dating of marine sediments with the radiocarbon chronometer limit the ability for proxy records to accurately constrain the timing or duration of NADW production changes. For example, the canonical evidence for slow down of NADW from the Bermuda Rise (McManus et al., 2004) during the first half of the Younger Dryas corresponds to a 3 cm sampling interval, spanning 300 calendar years.

Reductions in NADW are observed during Marine Isotope Stage 3, inferred from records of benthic $\delta^{13}C$ and Pa/Th (Henry et al., 2016), with the largest reductions associated with Heinrich stadials 4 and 5. That study concluded that increased NADW production led Northern Hemisphere warming by 200 years, based on phasing lag

correlation between NGRIP $\delta^{18}O$ and proxy records, thereby strongly implicating changes in meridional heat transport with abrupt climate change.

The phasing between NADW production proxy records in marine sediment cores with $\delta^{18}O$ of ice cores provides critical insight as to the potential causes for abrupt climate change during the most recent stadial event, the Younger Dryas, but requires precise age correlations between multiple records. We argue the history of $\Delta^{14}C$, and as reconstructed with U-Th dated corals from Atlantic and Pacific locations, provide the best opportunity for investigating the production history of NADW. Sediment proxy data providing a history of NADW production since the Last Glacial Maximum (20 kyr BP) are dated using the radiocarbon chronometer, the accuracy of which is limited by corrections for reservoir age, bioturbation in sediment cores, selective preservation, low temporal resolution, and having to convert ^{14}C ages to calendar age. The use of calibrated ^{14}C ages to date the Younger Dryas is especially problematic since the interval includes a ~ 300 year "radiocarbon plateau" starting at ~13 kyr BP (Figure 2.4) (Reimer et al., 2013). The reconstructed history of NADW production during MIS 3 relies on many of the same proxies (e.g., benthic $\delta^{13}C$, Pa/Th) used to study the Younger Dryas but the age model for the time interval 60-25 kyr BP relies on an imported age model, based on correlation of alkenone-SST in a neighboring core with NGRIP $\delta^{18}O$ (Henry et al., 2016). Furthermore, despite relatively high sedimentation rates, sampling intervals represent 100 to 200 years. We emphasize that each coral $\Delta^{14}C$ in the Younger Dryas record, presented here, represents a discrete data point, and equivalent in duration of time to most tree ring records. With an average sampling resolution of less than 40 years the

$\Delta^{14}C$ record presented here is unmatched by records obtained using deep-sea corals or deep -sea sediments.

2.5.3 Recovery of NADW during the Younger Dryas

In addition to $\Delta^{14}C$, we have plotted the sea surface temperature (SST) history at Barbados, based on calibration of the $\delta^{18}O$ paleo-thermometry in the coral species *A. palmata* (Abdul, 2017) for comparison to NGRIP $\delta^{18}O$. The record is comprised of 45 *A. palmata* for which $\Delta^{14}C$ and SST estimates have been obtained from the same sample. The increase in $\Delta^{14}C$ beginning at 13 kyr BP corresponds precisely in time to a 2 -3°C decrease in SST. Furthermore, the transitions in the two records, as defined by the mid-points in $\Delta^{14}C$ and SST, are 12.96 and 12.92 kyr BP, respectively, and are indistinguishable from the start of the Younger Dryas (12.86 kyr B.P), based on counting errors (±138 years) associated with NGRIP $\delta^{18}O$ (Rasmussen et al., 2006). The SST reconstruction obtained with U-Th dated *A. palmata* is the best-dated paleo-temperature record containing the Younger Dryas cold reversal. That a decrease in tropical Atlantic SST was simultaneous with decreasing surface water reservoir age, and hence increase in $\Delta^{14}C$, is evidence that NADW shutdown and collapse of thermo-haline circulation was simultaneous with Northern Hemispheric cooling, triggering a southward shift in the ITCZ, as reflected in cooling at Barbados and dryer and cooler conditions elsewhere in the Caribbean (Lea et al., 2003; Peterson et al., 2000).

The records of Barbados SST and $\Delta^{14}C$ (Figure 2.8) also reveal that the rapid decline in coral $\Delta^{14}C$ beginning around 12.5 kyr BP was simultaneously mirrored in a SST warming trend, so that recovery of most of the early 2-3°C Younger Dryas cooling

had been largely achieved by 11.9 kyr BP. We interpret a rapid decrease in $\Delta^{14}C$, simultaneously coupled with a warming trend in Barbados SST as a fingerprint for rejuvenation of the thermohaline circulation. Therefore, NADW turn-on preceded the end of the Younger Dryas (11.6 kyr BP). The Younger Dryas $\Delta^{14}C$ and SST records do not support a ~ 200-year phasing of NADW production with Northern Hemisphere warming, as has been interpreted during MIS 3 (Henry et al., 2016). Rather, strengthening of the AMOC was achieved much earlier in the Younger Dryas. Our interpretation of the coral $\Delta^{14}C$ record is therefore consistent with benthic foraminiferal $\delta^{13}C$ records from the Gardar Drift, in the North Atlantic, containing an expanded Younger Dryas section. In that record, increases in benthic foraminiferal $\delta^{13}C$ indicate multiple reorganizations of NADW during the Younger Dryas, with initial recovery of NADW production as early as 12.5 kyr BP (Elmore and Wright, 2011). Finally, the timing of the rise and subsequent decrease of $\Delta^{14}C$ during the Younger Dryas is not particularly well correlated with changes in pCO_2 (Figure 2.8) and suggests that factors other than NADW production, such as release of CO_2 from terrestrial and marine reservoirs, may have contributed to increased atmospheric CO_2 during the Younger Dryas and early Holocene.

2.5.4 Origin of the Younger Dryas

There is evidence that the size of the Atlantic Warm Pool (AWP) impacts circum-North Atlantic climate via the Atlantic Multi-decadal Oscillation mode (Wang et al., 2008). Barbados is located near the center of the tropical Atlantic Warm that spans the Gulf of Mexico, Caribbean Sea and the western tropical North Atlantic. The southward displacement of the ITCZ and resulting decrease in Barbados SST at the start of the

Younger Dryas may indicate a decrease in the overall size of the AWP (Abdul, 2017). The size of the AWP is important in controlling the freshwater balance between Atlantic and Pacific oceans, and hence, the salinity of surface water transported to higher latitudes. Simply stated, a smaller (larger) AWP is associated with increased (reduced) moisture transport from the Atlantic to the Pacific (Wang et al., 2008). Changes in Cariaco Basin sediment properties reflect abrupt shifts in the hydrologic cycle during the last 90,000 years and confirms the potential for large shifts in moisture transport from the Atlantic to Pacific between warm and cold climate transitions (Peterson et al., 2000). Therefore, in the absence of a large input of melt-water to perturb NADW at the start of the Younger Dryas (Abdul et al., 2016), shutdown of NADW production may have initiated in the tropics via progressive freshening of tropical Atlantic and Caribbean waters during Allerød warming which led to a reduction in the salinity of northward surface flow branch of the AMOC. Salinity, rather than temperature, is an important control on NADW formation. A rise in $\Delta^{14}C$ would have soon followed with near collapse of the thermohaline circulation, along with a southward shift in the ITCZ as observed in Cariaco Basin light reflectance records (Hughen et al., 2004b). Cooling in the tropics and the subsequent shrinking of the AWP would have worked to restore the freshwater balance between the Atlantic and Pacific Oceans, thereby increasing the salinity of the northward surface flow branch of the AMOC and return to a strengthening in NADW.

2.6 Conclusions

Using paired U-Th and ^{14}C dated surface corals, I have computed records of marine reservoir age in Atlantic and Pacific surface water and reconstructed the

atmospheric $^{14}C/^{12}C$ ratio ($\Delta^{14}C$) from 13.9 to 7.3 kyr BP. The computed reservoir ages are 340 ± 130 and 314 ± 58 years, at Barbados and Kiritimati, respectively. The coral record spans the Younger Dryas climate reversal, a time when thermohaline circulation was perturbed and heat transport between high and low latitudes reduced. An increase in Atlantic $\Delta^{14}C$ precedes a similar rise in the Pacific by 200 years at the onset of the Younger Dryas. Our coral data confirm model predictions that demonstrate a shutdown of NADW lowers the reservoir age of Atlantic surface water to generate divergent $\Delta^{14}C$ Atlantic and Pacific records. Within ice core and coral dating errors the $\Delta^{14}C$ records precisely date both the shutdown of NADW and 2-3°C decrease in Barbados SST to the start of the Younger Dryas (12.86 kyr BP).

A long and large (100‰) decline in $\Delta^{14}C$ values between 12.6 kyr and 11.6 kyr BP is attributed to rejuvenation of NADW production. The decreasing trend in $\Delta^{14}C$ is simultaneously mirrored with increasing SST at Barbados. Coral $\Delta^{14}C$ and SST records indicates the duration of NADW shutdown during the Younger Dryas, as previously documented with deep-sea sediment tracers in ^{14}C dated sediment cores, has been overestimated. Rather, disruption of NADW during the Younger Dryas was not prolonged but was likely short-lived, with recovery beginning as early as 12.5 kyr BP.

The rate of sea level rise and $\Delta^{14}C$ obtained from same U-Th dated corals excludes a significant melt-water event to have triggered the shutdown of NADW. The simultaneous timing in decreasing tropical Atlantic reservoir age and decreasing tropical Atlantic SST, at the start of the Younger Dryas, but recovery of NADW early on in the Younger Dryas, is consistent with high latitude climate forcing via the tropics, perhaps due perturbations in the salinity balance in the northward surface flow of the AMOC.

2.7 References

Abdul, N. A., 2017, Late Deglaciation (13.9 to 8 kyr BP) Tropical Atlantic Sea Surface Temperature recorded in Barbados reef crest coral *Acropora palmata* PhD]: Rutgers University.

Abdul, N. A., Mortlock, R. A., Wright, J. D., and Fairbanks, R. G., 2016, Younger Dryas sea level and meltwater pulse 1B recorded in Barbados reef crest coral *Acropora palmata*: Paleoceanography, v. 31, no. 2, p. 330-344.

Adkins, J., and Boyle, E., 1997, Changing atmospheric ^{14}C and the record of deep water paleoventilation ages: Paleoceanography, v. 12, p. 337-344.

Anderson, R. F., Ali, S., Bradtmiller, L. I., Nielsen, S. H. H., Fleisher, M. Q., Anderson, B. E., and Burckle, L. H., 2009, Wind-Driven Upwelling in the Southern Ocean and the Deglacial Rise in Atmospheric CO_2: Science, v. 323, no. 5920, p. 1443-1448.

Bard, E., 1988, Correction of accelerator mass spectrometry ^{14}C ages measured in planktonic foraminifera: Paleoceanographic implications: Paleoceanography, v. 3, no. 6, p. 635-645.

Bard, E., 1998, Geochemical and geophysical implications of the radiocarbon calibration: Geochimica et Cosmochimica Acta, v. 62, no. 12, p. 2025-2038.

Bard, E., Arnold, M., Hamelin, B., Tisnerat-Laborde, N., and Cabioch, G., 1998, Radiocarbon calibration by means of mass spectrometric $^{230}Th/^{234}U$ and ^{14}C ages of corals: An updated database including samples from Barbados, Mururoa, and Tahiti: Radiocarbon, v. 40, no. 3, p. 1085-1092.

Bondevik, S., Mangerud, J., Birks, H. H., Gulliksen, S., and Reimer, P., 2006, Changes in North Atlantic Radiocarbon Reservoir Ages During the Allerød and Younger Dryas: Science, v. 312, no. 5779, p. 1514-1517.

Broecker, W. S., Kennett, J. P., Flower, B. P., Teller, J. T., Trumbore, S., Bonani, G., and Wolfli, W., 1989, Routing of meltwater from the Laurentide Ice Sheet during the Younger Dryas cold episode: Nature, v. 341, no. 6240, p. 318-321.

Broecker, W. S., Peteet, D. M., and Rind, D., 1985, Does the ocean-atmosphere system have more than one stable mode of operation?: Nature, v. 315, no. 6014, p. 21-26.

Burr, G. S., Beck, J. W., Corrège, T., Cabioch, G., Taylor, F. W., and Donahue, D. J., 2009, Modern and Pleistocene Reservoir Ages Inferred from South Pacific Corals: Radiocarbon, v. 51, no. 1, p. 319-335.

Butzin, M., Prange, M., and Lohmann, G., 2005, Radiocarbon simulations for the glacial ocean: The effects of wind stress, Southern Ocean sea ice and Heinrich events: Earth and Planetary Science Letters, v. 235, no. 1–2, p. 45-61.

Cao, L., 2010, High-precision $^{230}Th/^{234}U$ dating of the surface ocean radiocarbon record and its geochemical and geophysical implications [PhD: Columbia University, 145 p.

Cao, L., Fairbanks, R. G., Mortlock, R. A., and Risk, M. J., 2007, Radiocarbon reservoir age of high latitude North Atlantic surface water during the last deglacial: Quaternary Science Reviews, v. 26, no. 5–6, p. 732-742.

Charles, C. D., and Fairbanks, R. G., 1992, Evidence from Southern Ocean sediments for the effect of North Atlantic deep-water flux on climate: Nature, v. 355, no. 6359, p. 416-419.

Chiu, T.-C., Fairbanks, R. G., Cao, L., and Mortlock, R. A., 2007, Analysis of the atmospheric ^{14}C record spanning the past 50,000 years derived from high-precision $^{230}Th/^{234}U/^{238}U$, $^{231}Pa/^{235}U$ and ^{14}C dates on fossil corals: Quaternary Science Reviews, v. 26, no. 1-2, p. 18-36.

Chiu, T.-c., Fairbanks, R. G., Mortlock, R. A., and Bloom, A. L., 2005, Extending the radiocarbon calibration beyond 26,000 years before present using fossil corals: Quaternary Science Reviews, v. 24, no. 16-17, p. 1797-1808.

Cutler, K. B., Gray, S. C., Burr, G. S., Edwards, R. L., Taylor, F. W., Cabioch, G., Beck, J. W., Cheng, H., and Moore, J., 2004, Radiocarbon calibration and comparison to 50 kyr with paired ^{14}C and ^{230}Th dating of corals from Vanuatu and Papua New Guinea: Radiocarbon, v. 46, p. 1127-1160.

Delaygue, G., Stocker, T. F., Joos, F., and Plattner, G.-K., 2003, Simulation of atmospheric radiocarbon during abrupt oceanic circulation changes: trying to reconcile models and reconstructions: Quaternary Science Reviews, v. 22, no. 15–17, p. 1647-1658.

Durand, N., Deschamps, P., Bard, E., Hamelin, B., Camoin, G., Thomas, A. L., Henderson, G. M., Yokoyama, Y., and Matsuzaki, H., 2013, Comparison of ^{14}C and U-Th ages in corals form IODP #310 cores offshore Tahiti: Radiocarbon, v. 55, no. 2, p. 1-26.

Edwards, R. L., Beck, J. W., Burr, G. S., Donahue, D. J., Chappell, J. M. A., Bloom, A. L., Druffel, E. R. M., and Taylor, F. W., 1993, A Large Drop in Atmospheric $^{14}C/^{12}C$ and Reduced Melting in the Younger Dryas, Documented with ^{230}Th Ages of Corals: Science, v. 260, no. 5110, p. 962-968.

Elmore, A. C., and Wright, J. D., 2011, North Atlantic Deep Water and climate variability during the Younger Dryas cold period: Geology, v. 39, no. 2, p. 107-110.

Fairbanks, R. G., 1989, A 17,000-year glacio-eustatic sea level record: influence of glacial melting rates on the Younger Dryas event and deep-ocean circulation: Nature, v. 342, no. 6250, p. 637-642.

Fairbanks, R. G., Mortlock, R. A., Chiu, T.-C., Cao, L., Kaplan, A., Guilderson, T. P., Fairbanks, T. W., Bloom, A. L., Grootes, P. M., and Nadeau, M.-J., 2005, Radiocarbon calibration curve spanning 0 to 50,000 years BP based on paired $^{230}Th/^{234}U/^{238}U$ and ^{14}C dates on pristine corals: Quaternary Science Reviews, v. 24, no. 16-17, p. 1781-1796.

Friedrich, M., Remmele, S., Kromer, B., Hofmann, J., Spurk, M., Kaiser, F., Orcel, C., and Küppers, M., 2004, The 12,460-year Hohenheim oak and pine tree-ring chronology from Central Europe - a unique annual record for radiocarbon calibration and paleoenvironment reconstructions: Radiocarbon, v. 46, no. 3, p. 1111-1122.

Guilderson, T. P., Cole, J. E., and Southon, J. R., 2005, Pre-bomb $\Delta^{14}C$ variability and the Suess effect in Cariaco Basin surface waters as recorded in hermatypic corals: Radiocarbon, v. 47, p. 57–65.

Henry, L. G., McManus, J. F., Curry, W. B., Roberts, N. L., Piotrowski, A. M., and Keigwin, L. D., 2016, North Atlantic ocean circulation and abrupt climate change during the last glaciation: Science, v. 353, no. 6298, p. 470-474.

Hua, Q., Barbetti, M., Fink, D., Kaiser, K. F., Friedrich, M., Kromer, B., Levchenko, V. A., Zoppi, U., Smith, A. M., and Bertuch, F., 2009, Atmospheric ^{14}C variations derived from tree rings during the early Younger Dryas: Quaternary Science Reviews, v. 28, no. 25-26, p. 2982-2990.

Hughen, K., Southon, J., Bertrand, C., Frantz, B., and Zermeño, P., 2004a, Cariaco Basin calibration update: revisions to calendar and ^{14}C chronologies for core PL07-58PC: Radiocarbon, v. 46.

Hughen, K. A., Eglinton, T. I., Xu, L., and Makou, M., 2004b, Abrupt Tropical Vegetation Response to Rapid Climate Changes: Science, v. 304, no. 5679, p. 1955-1959.

Hughen, K. A., Overpeck, J. T., Lehman, S. J., Kashgarian, M., Southon, J., Peterson, L. C., Alley, R., and Sigman, D. M., 1998, Deglacial changes in ocean circulation from an extended radiocarbon calibration: Nature, v. 391, no. 6662, p. 65-68.

Hughen, K. A., Southon, J. R., Lehman, S. J., and Overpeck, J. T., 2000, Synchronous Radiocarbon and Climate Shifts During the Last Deglaciation: Science, v. 290, no. 5498, p. 1951-1954.

Key, R. M., Kozyr, A., Sabine, C. L., Lee, K., Wanninkhof, R., Bullister, J. L., Feely, R. A., Millero, F. J., Mordy, C., and Peng, T. H., 2004, A global ocean carbon climatology: Results from Global Data Analysis Project (GLODAP): Global Biogeochem. Cycles, v. 18, no. 4, p. GB4031.

Kromer, B., Friedrich, M., Hughen, K. A., Kaiser, F., Remmele, S., Schaub, M., and Talamo, S., 2004, Late Glacial ^{14}C Ages From a Floating, 1382-Ring Pine Chronology: Radiocarbon, v. 46, no. 3, p. 1203-1209.

Lea, D. W., Pak, D. K., Peterson, L. C., and Hughen, K. A., 2003, Synchroneity of Tropical and High-Latitude Atlantic Temperatures over the Last Glacial Termination: Science, v. 301, no. 5638, p. 1361-1364.

Libby, W. F., 1955, Radiocarbon Dating 2nd Edition, Chicago, Illinois, University of Chicago Press.

Marchal, O., Stocker, T. F., and Muscheler, R., 2001, Atmospheric radiocarbon during the Younger Dryas: production, ventilation, or both?: Earth and Planetary Science Letters, v. 185, no. 3–4, p. 383-395.

Marcott, S. A., Bauska, T. K., Buizert, C., Steig, E. J., Rosen, J. L., Cuffey, K. M., Fudge, T. J., Severinghaus, J. P., Ahn, J., Kalk, M. L., McConnell, J. R., Sowers, T., Taylor, K. C., White, J. W. C., and Brook, E. J., 2014, Centennial-scale changes in the global carbon cycle during the last deglaciation: Nature, v. 514, no. 7524, p. 616-619.

Matsumoto, K., and Yokoyama, Y., 2013, Atmospheric $\Delta^{14}C$ reduction in simulations of Atlantic overturning circulation shutdown: Global Biogeochemical Cycles, v. 27, no. 2, p. 296-304.

McManus, J. F., Francois, R., Gherardi, J. M., Keigwin, L. D., and Brown-Leger, S., 2004, Collapse and rapid resumption of Atlantic meridional circulation linked to deglacial climate changes: Nature, v. 428, no. 6985, p. 834-837.

Meissner, K. J., 2007, Younger Dryas: A data to model comparison to constrain the strength of the overturning circulation: Geophysical Research Letters, v. 34, no. 21, p. n/a-n/a.

Mesolella, K. J., 1967, Zonation of Uplifted Pleistocene Coral Reefs on Barbados, West Indies: Science, v. 156, no. 3775, p. 638-640.

Mortlock, R. A., Fairbanks, R. G., Chiu, T.-c., and Rubenstone, J., 2005, $^{230}Th/^{234}U/^{238}U$ and $^{231}Pa/^{235}U$ ages from a single fossil coral fragment by multi-collector magnetic-sector inductively coupled plasma mass spectrometry: Geochimica et Cosmochimica Acta, v. 69, no. 3, p. 649-657.

Muscheler, R., Beer, J., Wagner, G., and Finkel, R. C., 2000, Changes in deep-water formation during the Younger Dryas event inferred from ^{10}Be and ^{14}C records: Nature, v. 408, no. 6812, p. 567-570.

Muscheler, R., Kromer, B., Bjorck, S., Svensson, A., Friedrich, M., Kaiser, K. F., and Southon, J., 2008, Tree rings and ice cores reveal ^{14}C calibration uncertainties during the Younger Dryas: Nature Geosci, v. 1, no. 4, p. 263-267.

Oeschger, H., Siegenthaler, U., Schotterer, U., and Gugelmann, A., 1975, A box diffusion model to study the carbon dioxide exchange in nature: Tellus, v. 27, no. 2, p. 168-192.

Peltier, W. R., and Fairbanks, R. G., 2006, Global glacial ice volume and Last Glacial Maximum duration from an extended Barbados sea level record: Quaternary Science Reviews, v. 25, no. 23-24, p. 3322-3337.

Peterson, L. C., Haug, G. H., Hughen, K. A., and Röhl, U., 2000, Rapid Changes in the Hydrologic Cycle of the Tropical Atlantic During the Last Glacial: Science, v. 290, no. 5498, p. 1947-1951.

Piotrowski, A. M., Goldstein, S. L., Hemming, S. R., and Fairbanks, R. G., 2005, Temporal Relationships of Carbon Cycling and Ocean Circulation at Glacial Boundaries: Science, v. 307, no. 5717, p. 1933-1938.

Rasmussen, S. O., Andersen, K. K., Svensson, A. M., Steffensen, J. P., Vinther, B. M., Clausen, H. B., Siggaard-Andersen, M. L., Johnsen, S. J., Larsen, L. B., Dahl-Jensen, D., Bigler, M., Röthlisberger, R., Fischer, H., Goto-Azuma, K., Hansson, M. E., and Ruth, U., 2006, A new Greenland ice core chronology for the last glacial termination: Journal of Geophysical Research, v. 111, no. D6, p. D06102.

Ravelo, A. C., Fairbanks, R. G., and Philander, S. G. H., 1990, Reconstructing tropical Atlantic hydrography using planktontic foraminifera and an ocean model: Paleoceanography, v. 5, no. 3, p. 409-431.

Reimer, P. B., Baillie, M. G. L., Bard, E., Bayliss, A., Beck, J. W., Blackwell, P. G., Bronk Ramsey, C., Buck, C. E., Burr, G. S., Edwards, R. L., Friedrich, M., Grootes, P. M., Guilderson, T. P., Hajdas, I., Heaton, T., Hogg, A. G., Hughen, K., Kaiser, F., Kromer, B., McCormac, G., Manning, S., Reimer, R. W., Richards, D. A., Southon, J., Talamo, S., Turney, C., van der Plicht, J., and Weyhenmeyer, C. E., 2009, IntCal09 and Marine09 Radiocarbon Age Calibration Curves, 0–50,000 Years cal BP: Radiocarbon, v. 51, p. 1111-1150.

Reimer, P. B., Bard, E., Bayliss, A., Beck, J. W., Blackwell, P. G., Bronk Ramsey, C., Buck, C. E., Cheng, H., Edwards, R. L., Friedrich, M., Grootes, P. M., Guilderson, T. P., Haflidason, H., Hajdas, I., Hatte, C., Heaton, T., Hoffmann, D. L., Hogg, A. G., Hughen, K., Kaiser, F., Kromer, B., Manning, S., Niu, M., Reimer, R. W., Richards, D. A., Scott, E. M., Southon, J., Staff, R. A., Turney, C., and van der Plicht, J., 2013, IntCal13 and Marine13 Radiocarbon Age Calibration Curves 0-50,000 years Cal BP: Radiocarbon, v. 55, no. 4, p. 1869-1887.

Ritz, S. P., Stocker, T. F., and Müller, S. A., 2008, Modeling the effect of abrupt ocean circulation change on marine reservoir age: Earth and Planetary Science Letters, v. 268, no. 1–2, p. 202-211.

Ruddiman, W., and McIntyre, A., 1981, The North Atlantic Ocean during the last deglaciation: Palaeogeography, Palaeoclimatology, Palaeoecology, v. 35, no. 0, p. 145-214.

Schaub, M., Büntgen, U., Kaiser, K. F., Kromer, B., Talamo, S., Andersen, K. K., and Rasmussen, S. O., 2008, Lateglacial environmental variability from Swiss tree rings: Quaternary Science Reviews, v. 27, no. 1-2, p. 29-41.

Singarayer, J. S., Richards, D. A., Ridgwell, A., Valdes, P. J., Austin, W. E. N., and Beck, J. W., 2008, An oceanic origin for the increase of atmospheric radiocarbon during the Younger Dryas: Geophysical Research Letters, v. 35, no. 14.

Southon, J., Noronha, A. L., Cheng, H., Edwards, R. L., and Wang, Y., 2012, A high-resolution record of atmospheric ^{14}C based on Hulu Cave speleothem H82: Quaternary Science Reviews, v. 33, no. 0, p. 32-41.

Stuiver, M., and Braziunas, T. F., 1989, Atmospheric ^{14}C and century-scale solar oscillations: Nature, v. 338, no. 6214, p. 405-408.

Stuiver, M., and Polach, H., 1977, Discussion; Reporting of ^{14}C data: Radiocarbon, v. 19, p. 353-363.

Wagner, e. a., 2009, Pre-Bomb Surface Water Radiocarbon of the Gulf of Mexico and Caribbean as Recorded in Hermatypic Corals: Radiocarbon, v. 51, p. 947-954.

Wang, C., Lee, S.-K., and Enfield, D. B., 2008, Atlantic Warm Pool acting as a link between Atlantic Multidecadal Oscillation and Atlantic tropical cyclone activity: Geochemistry, Geophysics, Geosystems, v. 9, no. 5, p. Q05V03.

Zaunbrecher, L. K., Cobb, K. M., Beck, J. W., Charles, C. D., Druffel, E. R. M., Fairbanks, R. G., Griffin, S., and Sayani, H. R., 2010, Coral records of central tropical Pacific radiocarbon variability during the last millennium: Paleoceanography, v. 25, no. 4, p. PA4212.

2.8 Figures and Tables

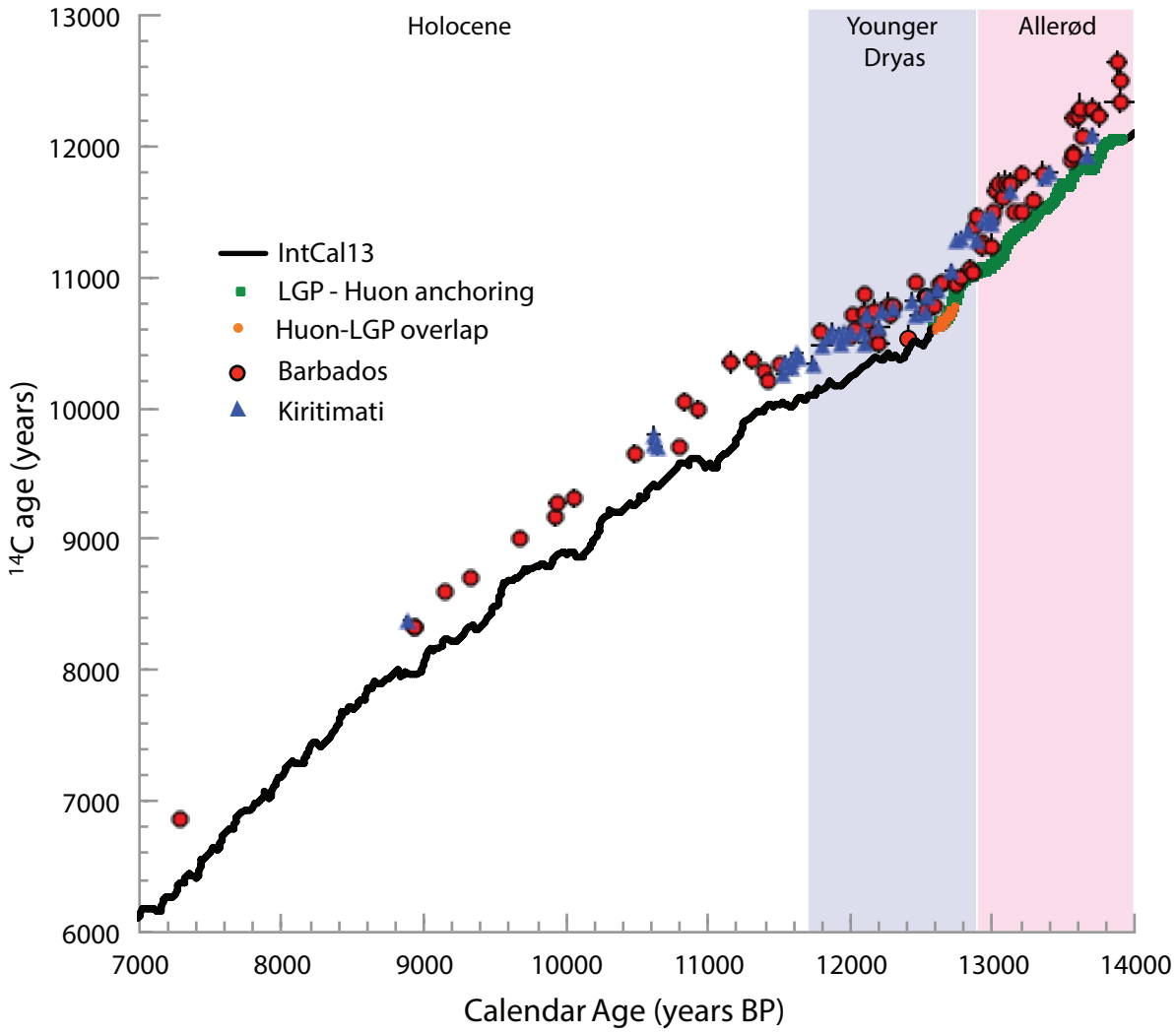
Holocene
Younger Dryas
Allerød
IntCal13
LGP - Huon anchoring
Huon-LGP overlap
Barbados
Kiritimati
^{14}C age (years)
Calendar Age (years BP)
13000
12000
11000
10000
9000
8000
7000
6000
7000
8000
9000
10000
11000
12000
13000
14000

Figure 2.1: ^{14}C age (uncorrected) vs. U-Th (Calendar) age in Barbados (red dots) and Kiritimati (blue triangles) with comparison to IntCal13 (black line) (Reimer et al., 2013). Vertical and horizontal error bars represent 2 s.d. The green portion of IntCal13 curve is the anchored European Late Glacial Pine (LGP) record (Hua et al., 2009). The orange portion of the IntCal13 curve is the interval of overlap between the LGP and Huon Pine tree ring records. The shaded regions represent the Younger Dryas and Bølling Allerød chronozones as defined in (Rasmussen et al., 2006).

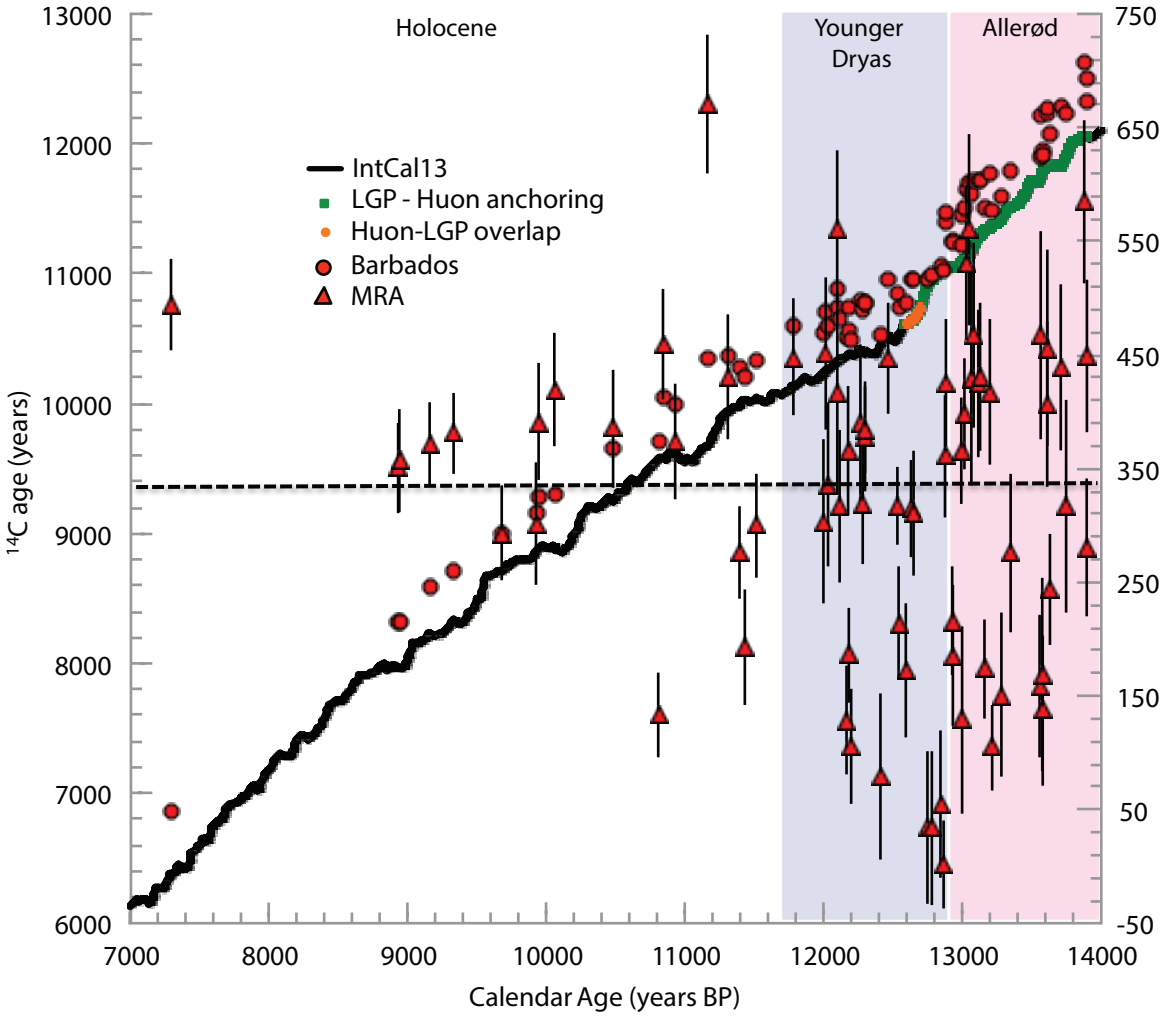
Holocene
Younger Dryas
Allerød
IntCal13
LGP - Huon anchoring
Huon-LGP overlap
Barbados
MRA
^{14}C age (years)
Calendar Age (years BP)
13000
12000
11000
10000
9000
8000
7000
6000
750
650
550
450
350
250
150
50
-50
7000
8000
9000
10000
11000
12000
13000
14000

Figure 2.2a: ^{14}C age (uncorrected) vs. U-Th (Calendar) age in Barbados (red dots) plotted with MRA estimates (red triangles) calculated as the coral- IntCal13 ^{14}C age difference. The dashed black line is the mean MRA at Barbados (340 years). Vertical errors bars are 2 s.d. Black, green, and orange solid lines are as in Figure 2.1.

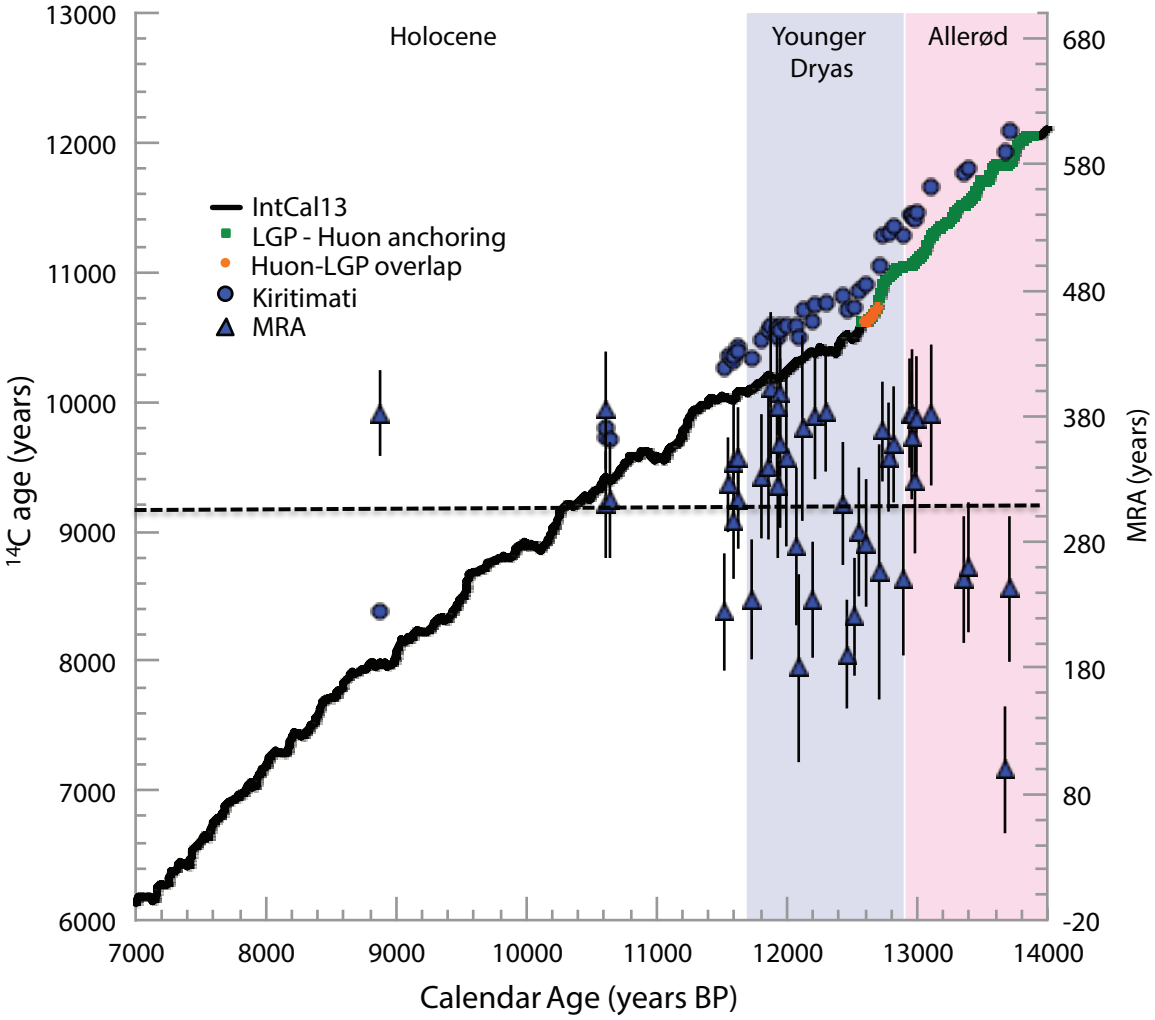
Holocene
Younger Dryas
Allerød
IntCal13
LGP - Huon anchoring
Huon-LGP overlap
Kiritimati
MRA
^{14}C age (years)
MRA (years)
Calendar Age (years BP)
13000
12000
11000
10000
9000
8000
7000
6000
680
580
480
380
280
180
80
-20
7000
8000
9000
10000
11000
12000
13000
14000

Figure 2.2b: ^{14}C age (uncorrected) vs. U-Th (Calendar) age in Kiritimati (blue dots) plotted with MRA estimates (blue triangles) calculated as the coral- IntCal13 ^{14}C age difference. The dashed black line is the mean MRA at Kiritimati (314 years). Vertical errors bars are 2 s.d. Black, green, and orange solid lines are as in Figure 2.1.

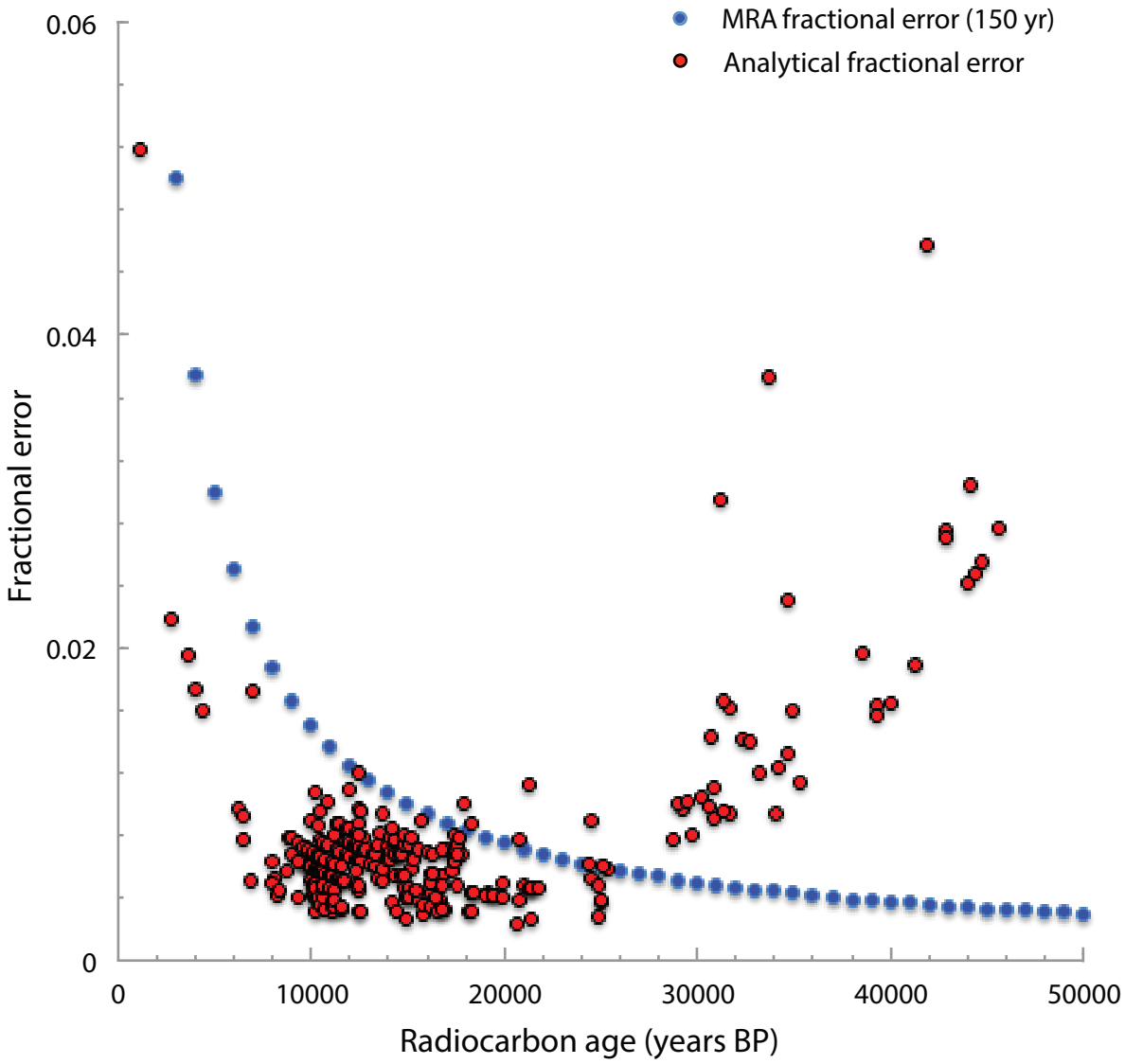
MRA fractional error (150 yr)
Analytical fractional error
0.06
0.04
0.02
0
Fractional error
0
10000
20000
30000
40000
50000
Radiocarbon age (years BP)

Figure 2.3: Fractional error in ^{14}C age associated with 150 year MRA uncertainty plotted with AMS ^{14}C dating error in coral data (this study; Fairbanks et al., 2005).

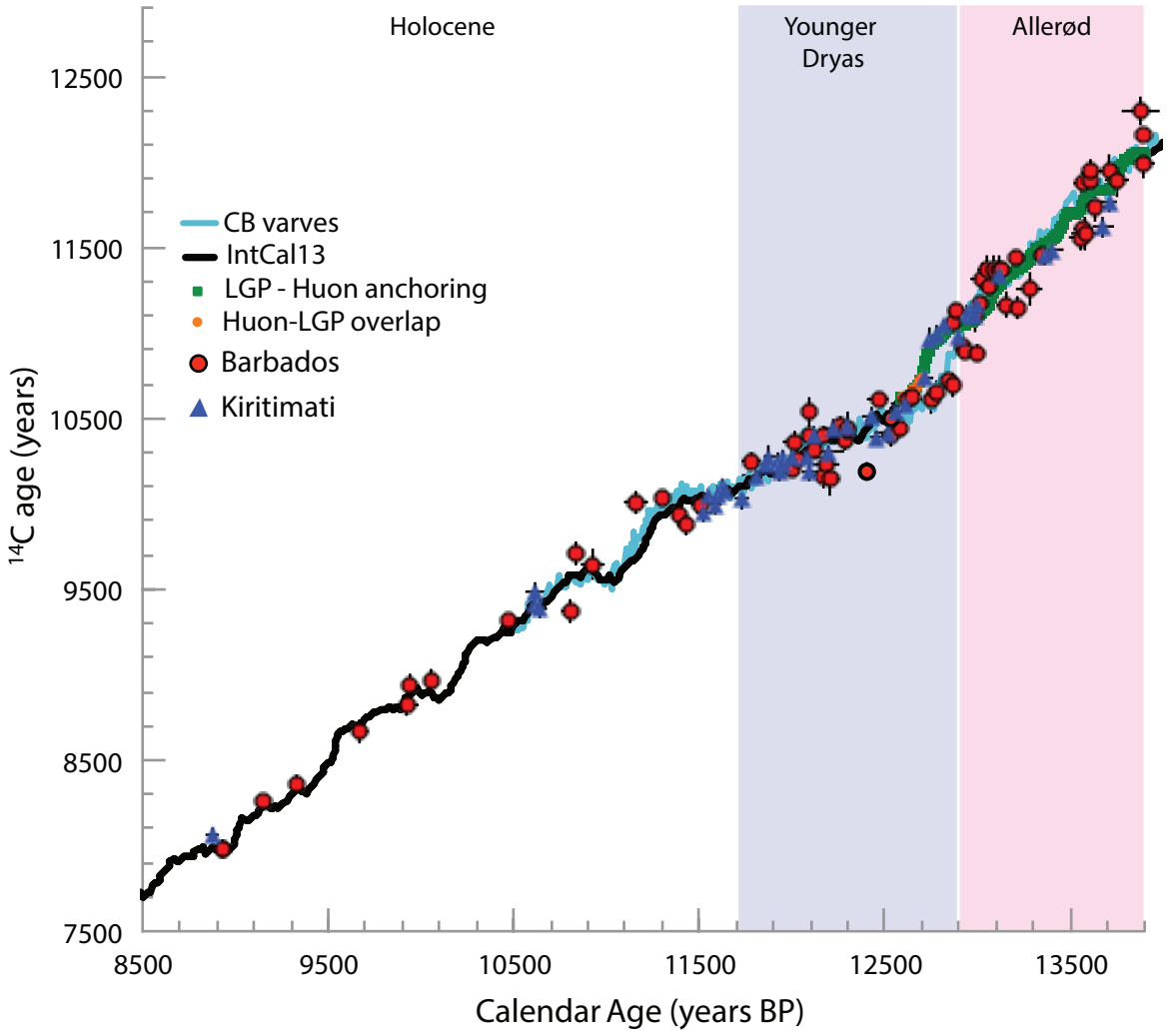
Holocene
Younger Dryas
Allerød
CB varves
IntCal13
LGP - Huon anchoring
Huon-LGP overlap
Barbados
Kiritimati
^{14}C age (years)
12500
11500
10500
9500
8500
7500
8500
9500
10500
11500
12500
13500
Calendar Age (years BP)

Figure 2.4: MRA corrected ^{14}C age vs. Calendar age Barbados (red dots), Kiritimati (blue triangles), Cariaco Basin (light blue line) (Hughen et al., 2004a). Black, green, and orange solid lines are as in Figure 2.1.

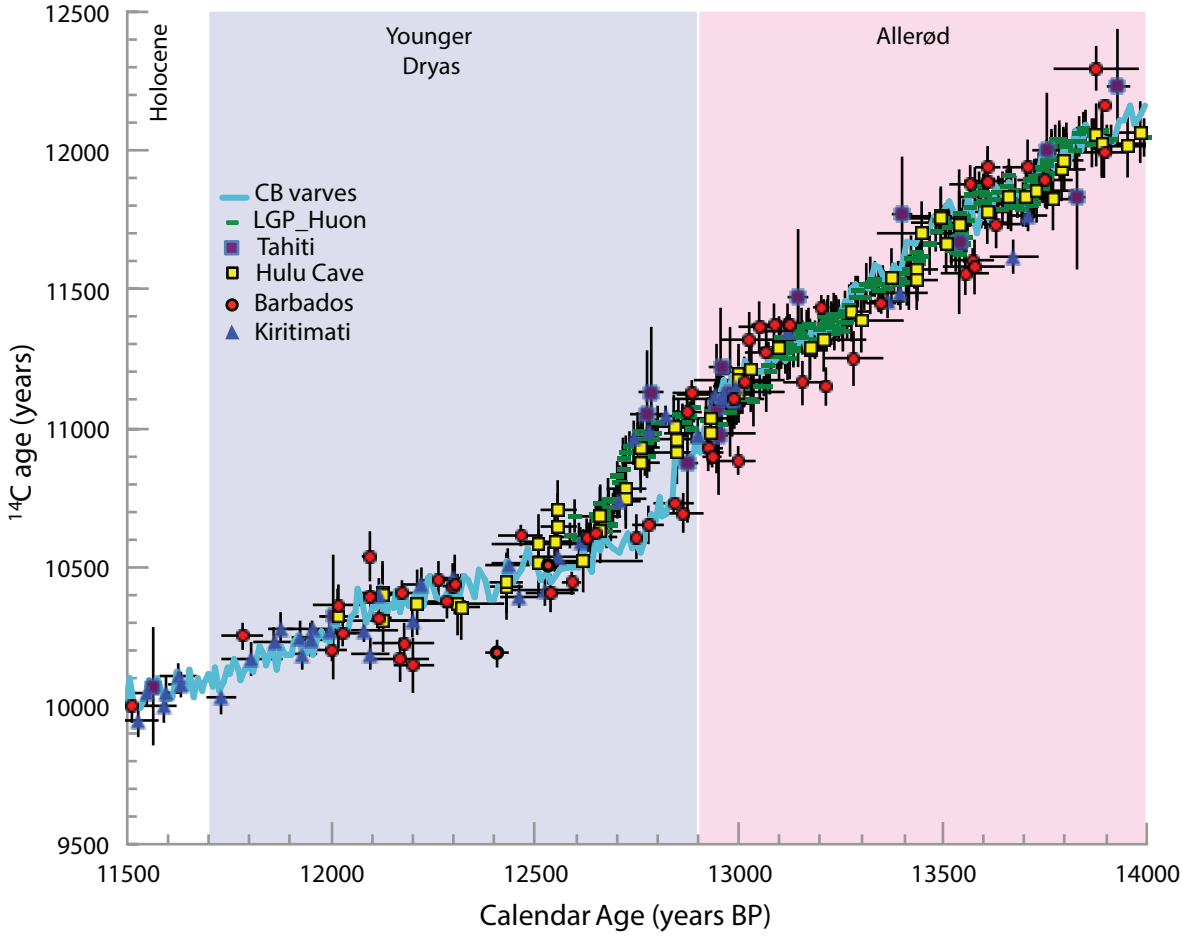
Holocene
Younger
Dryas
Allerød
CB varves
LGP_Huon
Tahiti
Hulu Cave
Barbados
Kiritimati
^{14}C age (years)
12500
12000
11500
11000
10500
10000
9500
11500
12000
12500
13000
13500
14000
Calendar Age (years BP)

Figure 2.5: Expanded view of the 11.5 to 14.0 kyr BP interval. All symbols are as in Figure 2.4. Also, plotted are the anchored (HP-40) LGP tree ring sequence (green bars)(Hua et al., 2009), Tahiti corals (purple squares) (Bard et al., 1998; Durand et al., 2013), Hulu Cave H82 speleothem record (yellow squares) (Southon et al., 2012). Vertical and horizontal error bars represent 2 s.d.

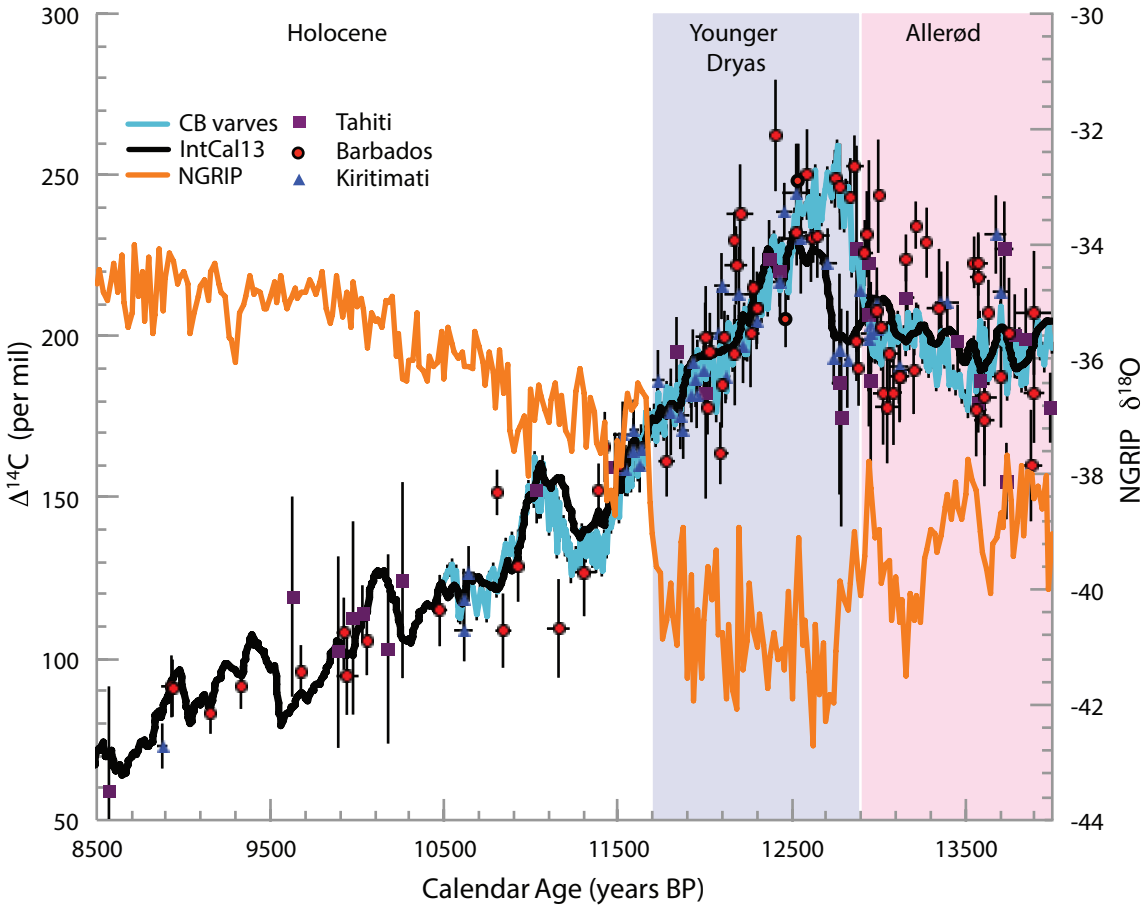
Holocene
Younger Dryas
Allerød
CB varves
IntCal13
NGRIP
Tahiti
Barbados
Kiritimati
300
250
200
150
100
50
-30
-32
-34
-36
-38
-40
-42
-44
8500
9500
10500
11500
12500
13500
Δ14C (per mil)
NGRIP δ18O
Calendar Age (years BP)

Figure 2.6: $\Delta^{14}C$ vs. calendar age: Barbados (red dots), Kiritimati (blue triangles), Tahiti corals (purple squares) (Bard et al., 1998; Durand et al., 2013), Cariaco Basin (light blue line) (Hughen et al., 2004a) and IntCal13 (black line) (Reimer et al., 2013). Vertical and Horizontal error bars are 2 s.d. NGRIP $\delta^{18}O$ (orange line) (Rasmussen et al., 2006).

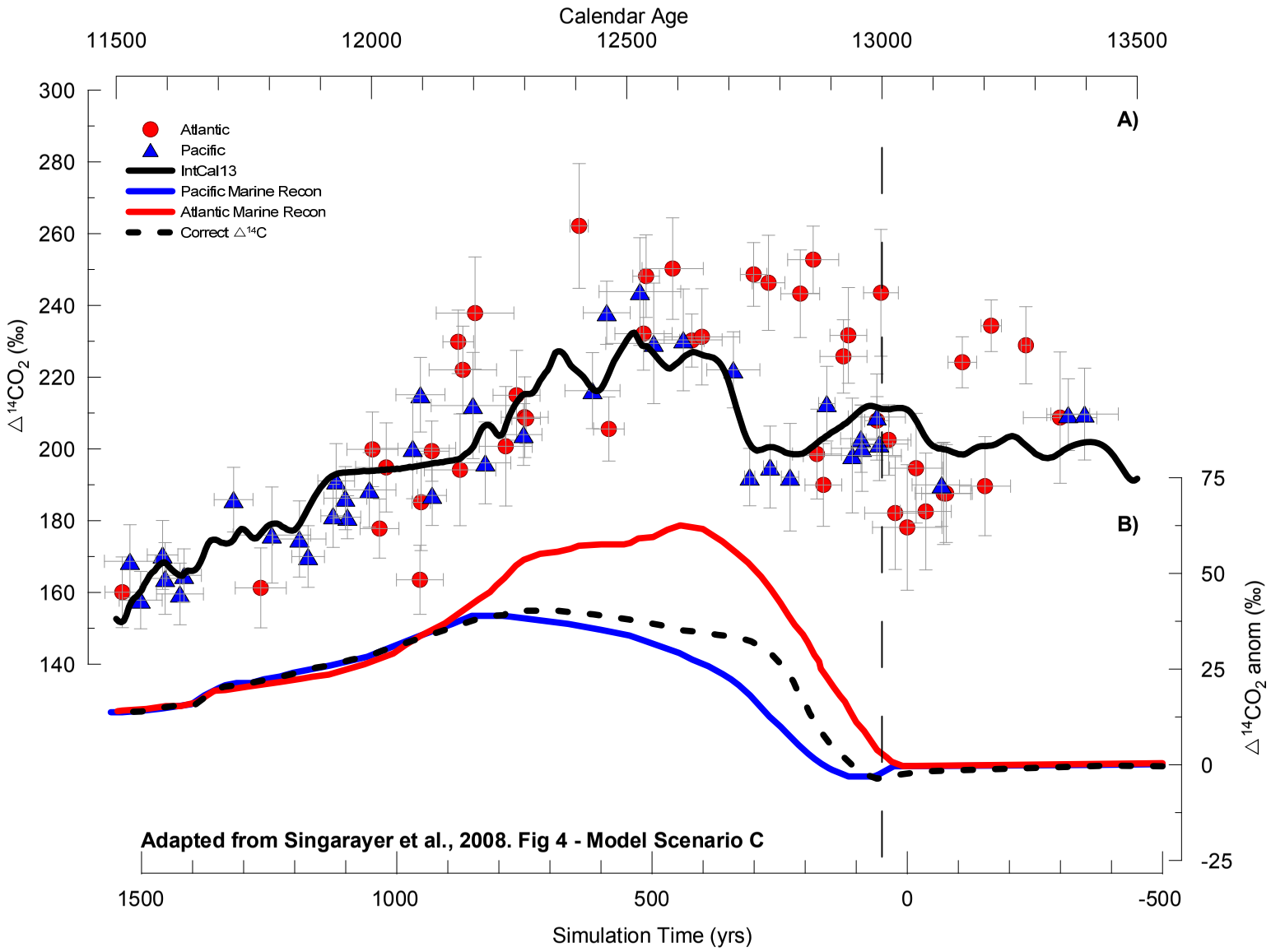
Calendar Age
11500
12000
12500
13000
13500
A)
B)
Atlantic
Pacific
IntCal13
Pacific Marine Recon
Atlantic Marine Recon
Correct △14C
△14CO2 (‰)
△14CO2 anom (‰)
300
280
260
240
220
200
180
160
140
75
50
25
0
-25
1500
1000
500
0
-500
Simulation Time (yrs)
Adapted from Singarayer et al., 2008. Fig 4 - Model Scenario C

Figure 2.7: Barbados and Kiritimati $\Delta^{14}C$ plotted with modeled "C" Atlantic and Pacific $\Delta^{14}C$ response to NADW shutdown (Singarayer et al., 2008). The vertical dashed line represents the start of the freshwater input in the model. Vertical and horizontal error bars represent 2 s.d.

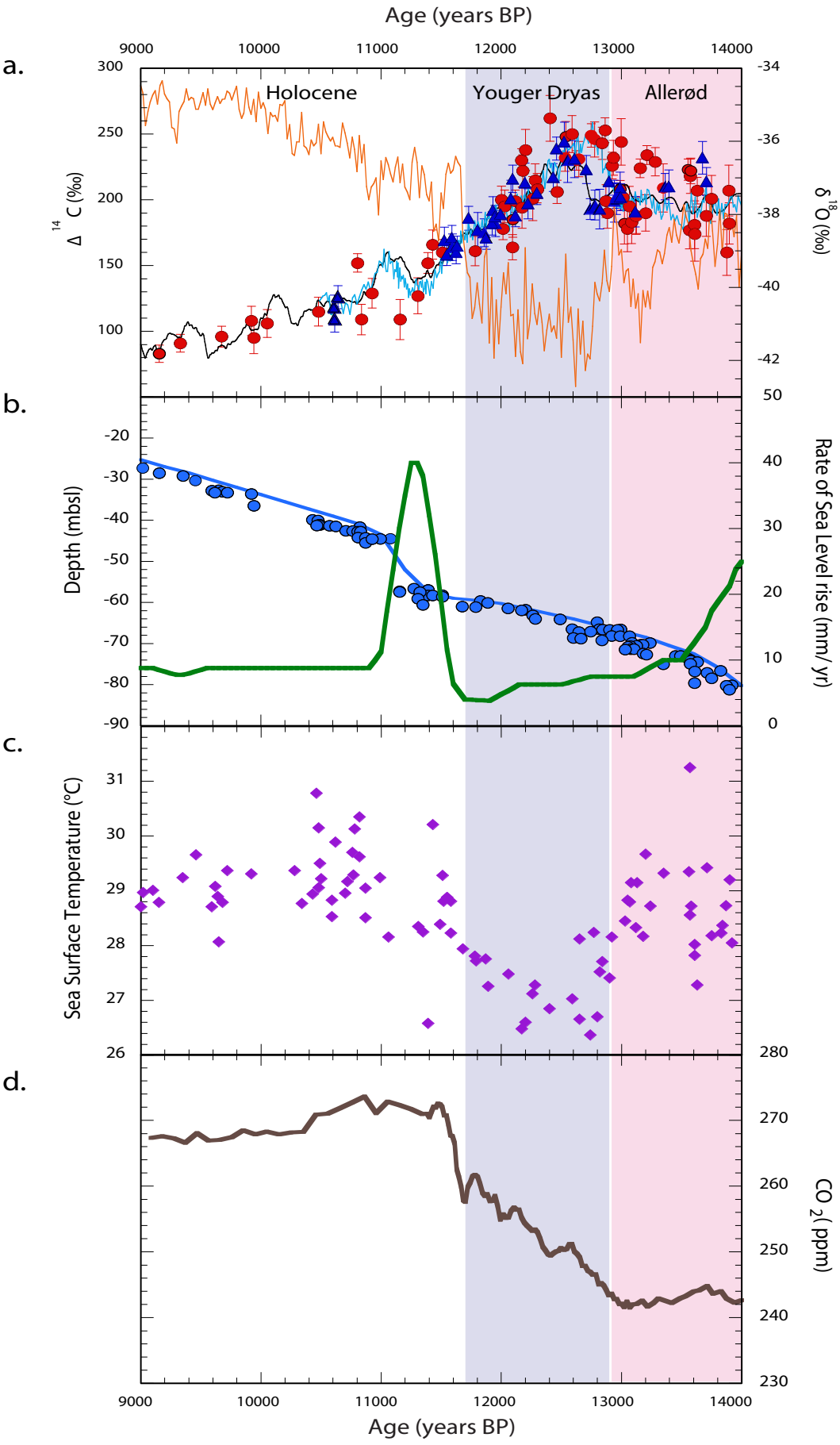
a.
b.
c.
d.
Age (years BP)
9000
10000
11000
12000
13000
14000
Holocene
Younger Dryas
Allerød
Δ 14 C (‰)
δ 18 O (‰)
Depth (mbsl)
Rate of Sea Level rise (mm/ yr)
Sea Surface Temperature (°C)
CO 2 (ppm)

Figure 2.8: (a) Barbados (red dots) and Kiritimati (blue triangles) $\Delta^{14}C$ plotted with NGRIP $\delta^{18}O$ (orange line) (Rasmussen et al., 2006), and Cariaco Basin $\Delta^{14}C$ (light blue line) (Hughen et al., 2004a). (b) Barbados sea-level curve (blue line) constructed with reef crest species Acropora palmata (blue dots) and rate of sea level rise (green line) (Abdul et al., 2016). (c) Barbados SST reconstruction based on *Acropora palmata* (Abdul, 2017). (d) Atmospheric CO_2 record from WDC Antarctic ice core (Marcott et al., 2014).

Location	**13.9 to 7.3 kyr BP**	**12.55 to 7.3 kyr BP**	**13.9 to 12.9 kyr BP**
Barbados	322 ± 144 (n=74)	344 ± 124 (n=37)	338 ± 142 (n=30)
Kiritmati	314 ± 69 (n=45)	318 ± 64 (n=28)	307 ± 93 (n=10)

Table 2.1: Mean reservoir ages calculated for different time intervals at each location. Uncertainties represent 1 s.d.

Chapter Three

Atmospheric ^{14}C record spanning the past 50,000 years from U-Th and ^{14}C dated fossil corals: separating geomagnetic, carbon cycle and ^{14}C half-life components

3.1 Abstract

Coral drilling expeditions offshore Barbados, Kiritimati Atoll, and direct sampling from raised coral terraces on Araki Island provides abundant pristine coral samples for improving the resolution, accuracy and precision of radiocarbon calibration curves and for providing estimates of the $^{14}C/^{12}C$ atmospheric ratio ($\Delta^{14}C$) since 50 kyr BP. In this Chapter, I present a $\Delta^{14}C$ record based on paired radiocarbon and U-Th dating of corals spanning 49.2 to 15 kyr BP. In addition, the data are supplemented with twenty concordant, paired U-Th and U-Pa dates to demonstrate quality control of the uranium series dating system. Consequently, we now have the resolution, precision, and accuracy to more rigorously analyze the various contributions to the $\Delta^{14}C$ signal.

The record of $\Delta^{14}C$ obtained from corals indicates a decline since 50 kyr BP, approximately the limit of radiocarbon dating. The prominent features in this record are due to the long-term effects of short-term periods of weaker geomagnetic field. The earliest is the Laschamp Event at 41 kyr BP. Superimposed on this decline is an interval of rapidly changing $\Delta^{14}C$ between 32 kyr and 29 kyr BP, corresponding to the Mono Lake Excursion, now more precisely dated to between 32.4 to 30.5 kyr BP. After subtraction of the contributions to $\Delta^{14}C$ from increased production during the Laschamp and Mono Lake Excursions ($\Delta^{14}C_{LMcorr}$) there is an 150‰ increase in $\Delta^{14}C_{LMcorr}$ beginning at 27 kyr BP, followed by a plateau in values between 26 and 20 kyr BP,

thereafter followed by a second increase of about 100‰ from 20 to 18 kyr BP. We attribute some contribution to increased $\Delta^{14}C$ beginning at 20 kyr BP to increased production during the Hilina Pali geomagnetic excursion. Models linking large amplitude decreases in $\Delta^{14}C$ beginning 17.5 kyr B.P to ocean ventilation and release of ^{14}C depleted CO_2 exaggerate the shape and scale of the decline by failing to account for production increases due to the Laschamp and Mono Lake Excursions. The residual linear trend in $\Delta^{14}C$ may be due to uncertainties in the half-life of ^{14}C over the entire radiocarbon time scale.

3.2 Introduction

The records of the ^{14}C content of the atmosphere and oceans contain a remarkable array of information about Earth and Solar history. Produced by cosmic rays in the upper atmosphere (Elsasser et al., 1956; Lal, 1988), $^{14}CO_2$ rapidly mixes throughout the troposphere and exchanges with the reactive carbon reservoirs of the oceans and biosphere, where it decays. For the past 11,000 years, fluctuations in the atmospheric $^{14}C/^{12}C$ ratio ($\Delta^{14}C$) have been largely produced by changes in the solar magnetic field (Stuiver and Quay, 1980). Solar magnetic activity and sunspot occurrence have century to decadal-scale variability and are linked to high-frequency variations in $\Delta^{14}C$ (Stuiver and Braziunas, 1989; Stuiver and Quay, 1980). These high-frequency, low amplitude $\Delta^{14}C$ variations are best documented in detailed and spliced tree-ring records (Hua et al., 2009; Reimer et al., 2013a; Stuiver and Braziunas, 1989). Seven data sets consisting of 31 overlapping tree ring chronologies provide over 3853 individual data points and constitute the most detailed and continuous record spanning the past 12.6 kyrs (Reimer et al., 2013a).

On longer time scales, changes in the Earth's magnetic field intensity impact the record of $\Delta^{14}C$ (Bard et al., 1990; Elsasser et al., 1956; Lal, 1988), producing positive $\Delta^{14}C$ anomalies during intervals of weaker geomagnetic field. ^{14}C production is controlled by the interaction of the earth's magnetic field with cosmic rays produced inside and outside of our solar system (Elsasser et al., 1956; Lal, 1988). Many studies have attempted to reconstruct the global paleomagnetic field intensity record using deep-sea sediments (Guyodo and Valet, 1996, 1999; Laj et al., 2004; Laj et al., 2000; Stoner et al., 2002). A compilation of absolute paleointensity records has in turn provided an estimate of the global axial dipole moment for the last 50 kyr (Knudsen et al., 2008). Despite the differences in length and resolution of individual sediment cores and the uncertainties in their chronologies, the reconstructed paleointensity stacks share a common feature: a decreasing trend in paleointensity from the highest value (close to the modern values) at ~50,000 years before present (BP) to the lowest value at ~40,000 years BP, corresponding to the well-known Laschamp event when the earth's magnetic field strength is believed to have approached zero (Laj et al., 2004; Laj et al., 2000).

Changes in deep ocean circulation also play a role in controlling the $^{14}C/^{12}C$ atmospheric ratio. The production of North Atlantic Deep Water (NADW) is a large sink of ^{14}C with times of weaker NADW tied to increases in $\Delta^{14}C$ and vice versa. In the Southern Ocean, ^{14}C-depleted deep water may upwell and lower $\Delta^{14}C$ values. Changes in deep ocean circulation during the most recent deglaciation are believed to be responsible for atmospheric ^{14}C fluctuations observed between 15,000 and 11,000 years (BP) (Adkins and Boyle, 1997; Edwards et al., 1993; Hughen et al., 1998; see Chapter 2, this dissertation), although most carbon models can explain only a small fraction of the

observed variations, even with a complete shutdown of NADW (Delaygue et al., 2003). Atmospheric ^{14}C is also believed to be modulated during episodic ocean ventilation and release of ^{14}C-depleted CO_2 (Broecker, 2009; Marchitto et al., 2007), as is hypothesized during the Mystery Interval (Broecker and Barker, 2007; Denton et al., 2006), corresponding to Heinrich Event 1 (17.5 to 14.5 kyr BP) (Hemming, 2004).

Of practical importance to a wide range of scientific disciplines is calibration of the radiocarbon (^{14}C) time scale, which is needed for converting radiocarbon years to calendar years, essential for measuring time and rates of change for numerous scientific fields. Since the production rate of ^{14}C in the atmosphere is not constant, any radiocarbon date generated from a dated archive (tree rings, corals, marine microfossils) does not represent the "true" or absolute age of the sample and therefore all ^{14}C ages must be converted to calendar age via some other direct dating method (e.g., U-series dating) or via indirect dating (e.g., tree ring counting or sediment layer counting). Radiocarbon dates can be converted by means of radiocarbon calibration curves based on direct dating (Fairbanks et al., 2005) or a combination of direct dating and indirect dating through correlations and splicing data segments and assumptions about what constitutes an annual layer and whether all years are accounted for in layered deposits (Reimer et al., 2009; Reimer et al., 2013a).

Tree rings records from northern Europe provide precise and overlapping correlated data sets for the time period 0 to ~12.6 kyr BP (Reimer et al., 2013a). Wiggle matching of ^{14}C dated Huon (Tasmania) pine-tree records (Hua et al., 2009) with European tree ring records (Friedrich et al., 2004; Schaub et al., 2008) has permitted an anchoring to the floating European Late Glacial Pine (LGP) record (Kromer et al., 2004),

thereby extending the tree ring chronology to 13.9 kyr BP (Reimer et al., 2013a). Beyond tree ring records, radiocarbon calibration must rely on terrestrial ^{14}C dated archives such as layered lake sediments assumed to be annual (Ramsey et al., 2012) or precipitated cave deposits (speleothems) to extend calibration back through time (Beck et al., 2001; Hoffmann et al., 2010; Southon et al., 2012).

As an alternative to terrestrial records, marine archives such as ^{14}C dated shallow water fossil corals (Bard et al., 1998; Bard et al., 1990; Cutler et al., 2004; Durand et al., 2013; Edwards et al., 1993; Fairbanks et al., 2005) and ^{14}C dated deep-sea sediments (Bard et al., 2004; Hughen et al., 2006) are variously used by the radiocarbon community for radiocarbon calibration. Corals provide an excellent archive for radiocarbon calibration beyond tree ring records because both the radiocarbon age and Uranium-series, U-Th, age can be generated from the same sample. Provided corrections can be made for the age offset between the surface water in which the coral grew and the contemporaneous atmosphere (marine reservoir age or MRA correction), the paired ages provide an independent and discrete calibration and $\Delta^{14}C$ data point. This is a requirement of computing accurate $\Delta^{14}C$ because *both* the radiocarbon age and calendar ages can be measured. The main limitation to using corals for radiocarbon calibration is the lack of suitable samples. Fossil corals exposed to the corrosive effects of the freshwater (phreatic) lens may become diagenetically altered and yield unreliable U-Th and or ^{14}C ages (Gallup et al., 1994; Hamelin et al., 1991). This is particularly true with the dating of older samples when trace amounts of secondary marine cements can result in unacceptably large offsets in radiocarbon ages (Chiu et al., 2005; Yokoyama, 2000).

Calibration data generated via ^{14}C dated foraminifera in deep-sea sediments have no direct calendar dates and require assigned calendar ages which are based on visual correlations of sediment proxy or color variability, geochemical records to distant atmospheric climate proxy records in layer counted ice cores, or U-Th dated speleothems, located thousands of kilometers away. These distant climate indices are subject to proxy interpretations, correlation errors in identifying and assigning "tie points", uncertainties in ice core chronologies, phase lags between indices recording the same climate signals, and the assumption of constant sedimentation rates between age model control points. Furthermore, a disadvantage to using deep-seas core chronologies tied to ice core records is that multiple age models have been constructed in Greenland ice cores with differences between chronologies exceeding 3000 to 5000 years prior to 25 kyr BP (Southon, 2004). Nevertheless, further refinement of ice core chronologies makes deep-sea sediments an attractive archive for radiocarbon calibration since they provided high-resolution records back to the limits of radiocarbon dating (50 kyr BP).

For more than five decades, the radiocarbon scientific community has compiled and evaluated data sets to build a robust consensus radiocarbon calibration curve (IntCal04, IntCal09, IntCal13). Despite the need in many scientific fields for a "static" calibration curve, periodic updates with the addition of new data sets and the removal of problematic data often result in generating differences in calibration curves. Thus, radiocarbon calibration continues to be a "work in progress" (Reimer et al., 2013a).

In this study, we pursue an independent $\Delta^{14}C$ curve based exclusively on paired U-Th and ^{14}C age determinations, supplemented with U-Pa ages, on corals from our offshore drill core collection from Barbados (13.10°N; 59.32 °W) in the western tropical

Atlantic and from the uplifted coral reefs of Araki Island (15.63°S; 166.93° E) in the western Pacific to compile a record of $\Delta^{14}C$ 50 kyr to 15 kyr BP The record presented here consists of 155 individual samples and doubles the number of samples used to construct our initial coral $\Delta^{14}C$ record (Chiu et al., 2007) and calibration curve (Fairbanks et al., 2005). With an average sampling resolution of 200 years, this study represents the only directly-dated continuous marine record to span the past 50 kyr and thereby provides a stand-alone "backbone" or "gold standard" record of marine $\Delta^{14}C$ for comparison to other archive data and to reconstructions of the earth's magnetic field.

3.3 Materials and Methods

Coral samples were selected from the Barbados offshore drill-core collection from material recovered during the *R/V RANGER* 88-13 (1988) and *R/V KNORR* 189-2 (2007) wire-line drilling expeditions. Araki Island (Vanuatu) corals used in this study were sampled from the uplifted Holocene and Marine Isotope Stage (MIS) 3 reef sequences (Urmos, 1985) and are from the collection of A. Bloom (1972) or collected during field expeditions conducted in 2004 and 2005 by R. Fairbanks, T. Fairbanks, and C. Brainard.

Sample screening and data quality control criteria followed Fairbanks et al. (2005) but are briefly described here. Concentric 10 mm and 6 mm drill plugs were taken from coral slabs and mechanically cleaned via sonication. Dried sub–samples were crushed to a powder, and analyzed for evidence of secondary calcite by X-ray Diffraction (XRD). Only samples with "no detectable" calcite (less than 0.2 wt. %, Chiu et al., 2005) were processed further for U-Th and radiocarbon dating. A "less than 0.2 weight %" criterion is now the accepted screening level for fossil coral used for radiocarbon calibration

studies (Durand et al., 2013; Reimer et al., 2013b). Petrographic thin-section slides were made for a representative number of U-Th dated coral samples to check for microstructure preservation and absence of aragonite needles. Secondary aragonite was minimal at best and no samples were disqualified based on this criterion in this study.

3.3.1 U-series dating

U-Th dating was determined by Inductively Coupled Mass Spectrometry (ICP-MS) using either a FISONS PLASMA 54 by the methods described in Mortlock et al. (2005) or with a ThermoScientific NEPTUNE PLUS ICP-MS using like-methods and protocols adopted for the PLASMA 54 (Abdul et al., 2016). Specifically, measurements made with the NEPTUNE PLUS employed peak-jumping mode to measure minor isotopes of U and Th with a secondary electron multiplier (SEM) positioned behind a retarding potential quadrupole. U isotopes were measured with sample-standard bracketing to correct for SEM gain efficiency and drift. Instrument mass fractionation was corrected by monitoring the $^{235}U/^{238}U$ ratio. We found neither systematic nor significant differences in U-series ages in coral samples determined with both instruments (Appendix; Table 1). Based on the measured ^{232}Th concentrations (0.02 to 3 ppb), no corrections were made for initial ^{230}Th and we rejected any U-Th age where the $\delta^{234}U_{initial}$ did not fall within the acceptable range for modern and fossil corals that have maintained closed system behavior (138-152‰; Fairbanks et al., 2005). The average precision of the age determination (at 2 s.d) is better than ±0.5% and ±0.2‰ in samples measured with the PLASMA 54 and NEPTUNE PLUS, respectively. As an example, a 30,000 year-old coral sample analyzed with the NEPTUNE PLUS yields a remarkable 2

s.d. age uncertainty of ± 60 years, or 5 to 50 times more precise than sediment age models.

$^{231}Pa/^{235}U$ dating was applied to representative samples that were exposed to the freshwater table (phreatic lens) during sea level low-stands (i.e., 30 kyr reef at Barbados) or the vadose (Araki Island) as a further check for Uranium-series closed system. Paired U-Th and U-Pa ages were considered concordant when the $^{231}Pa/^{235}U$ age fell within ± 2% of the associated U-Th age (Chiu et al., 2006; Mortlock et al., 2005). The average precision in the U-Pa ages is about 1.5% (2 s.d.). Twenty-four out of 28 samples dated by both U-Th and U-Pa methods passed the test of concordancy (Appendix; Table 1).

As per our coral radiocarbon calibration classification, all but five coral samples reported in this study are ranked as Category I through Category V samples (see Fairbanks et al., 2005). Four Araki corals are ranked as Category VI samples as they did not pass the age U-Th and U-Pa age concordancy test at ± 2%. One Category III sample (RGF 12-30-3) was found to contain 0.3 wt. % calcite. Nevertheless, we have included these five samples in all figures since they provide valuable comparison data for an under-sampled time interval (i.e., 49 to 30 kyr BP).

3.3.2 Radiocarbon dating methods

Coral samples (30 to 80 mg) were pre-treated by the methods described in Fairbanks et al. (2005) and ^{14}C dated by Accelerator Mass Spectrometry (AMS) at three separate facilities (Center for Accelerator Mass Spectrometry, Lawrence Livermore National Laboratory (LLNL); Leibniz Laboratory for Radiometric Age Determination and Isotope Research (Kiel), Christian Albrecht University; National Ocean Sciences Accelerator Mass Spectrometry Facility, WHOI (NOSAMS) placing our result in a fully

inter-calibrated framework. We used a "radiocarbon dead" fossil coral (AK-H-2; U-Th age ~ 97 kyr BP to apply procedural blank corrections to all fossil coral data. Two to three coral blanks were processed and analyzed with each set of 7 coral samples and the fraction modern carbon (FMC) values for blanks averaged and subtracted from sample values. Coral blank values generated at Kiel, LLNL, and NOSAMS are reported elsewhere (Fairbanks et al., 2005; see Chapter 2) but were reproducible within batch runs and ranged from 0.0005 to 0.0015 FMC, corresponding to a radiocarbon age in excess of 55 kyr. Applying coral blank corrections to samples in this study generally resulted in increasing the ^{14}C age by 20 years to 80 years in samples younger than 25 kyr BP and about 200 to 1000 years in samples older than 35 kyr BP. The 1 s.d. uncertainty in our coral blank correction measured at NOSAMS and averaged over individual 10 batch runs was ± 0.00021 FMC and close to what has been estimated in our prior study (Fairbanks et al., 2005). Propagating the blank uncertainty at 2 s.d. through the ^{14}C age or $\Delta^{14}C$ calculation has little impact in samples of calendar age younger than 35 kyr BP. However, including a blank uncertainty of ± 0.00042 FMC with the ^{14}C age error increases the total ^{14}C age uncertainty in samples older than 40 kyr by 50%, thereby making it a significant component in estimating the overall uncertainty in $\Delta^{14}C$.

3.3.3 Barbados and Araki reservoir age estimates

The radiocarbon age of a coral living in surface water must be corrected for the age difference between the water and atmosphere. The age difference is due to the incomplete isotopic equilibration and mixing between subsurface waters of older age. Today, the marine reservoir age (MRA) is between 300 and 500 years in the tropical and subtropical regions (20°N to 20°S) and in the general area of our study (Butzin et al.,

2005; Key et al., 2004). The reservoir age at Barbados and Araki was computed by subtracting the conventional (uncorrected) ^{14}C age from the ^{14}C age of same calendar year tree rings, as estimated by the smoothed IntCal13 atmospheric ^{14}C curve (Reimer et al., 2013a) for the period of overlap (13.9 kyr BP to 7.3 kyr BP; see Chapter 2) .

The computed reservoir age applied to all Barbados coral ^{14}C ages is 340 ± 130 years (see Chapter 2). The Araki-Santo Island MRA estimate is 470 ± 220 years (n = 9), based on samples collected from the uplifted late Holocene age coral terrace. The Araki estimate is somewhat larger than the previously obtained value of 365 years (Fairbanks et al., 2005), but includes two estimates in excess of 700 years. Elimination of the two high values lowers the estimate to 380 ± 130 years, a value consistent with pre-bomb corals at Vanuatu (362 ± 8 years) and with estimates from Younger Dryas to mid Holocene age corals at other western Pacific sites: Vanuatu (394 ± 87 years; n =3) (Paterne et al., 2004), Urelapa (332 ±115 years; n=12), and Tasmaloum (486 ± 155; n = 7) (Cutler et al., 2004). To maintain consistency in reporting Araki data we have applied the MRA correction of 365 years as reported in (Fairbanks et al., 2005) to all new data obtained in this study (Appendix; Table 1).

3.3.4 ^{14}C age uncertainties

^{14}C age accuracy is limited by the assumption of applying constant reservoir age corrections, particularly for time intervals when tree ring records are not available for comparison. Processes such as wind speed, pCO_2 are important in controlling the ^{14}C age of surface water (Bard, 1988) and are likely to have varied during different climate states. There is credible evidence that the MRA at Barbados may have less than 100 years at the onset of the Younger Dryas (12.9 kyr BP) (see Chapter 2) and perhaps as high as 600

years during the Mystery Interval (17.5 to 15 kyr BP) as is discussed in Chapter 4 of this dissertation. Barbados lies near the western edge of the Atlantic warm pool where the surface mixed layer is between 60 and 80 meters deep (Levitus and Boyer, 1994; Ravelo et al., 1990; Stansfield et al., 1995) and where surface waters arriving at Barbados have transited the Atlantic subtropical gyres and crossed the equator providing a long atmospheric exchange time. Thus, Barbados is predicted to be well suited for buffering large shifts in MRA. The range in MRA estimates calculated for Barbados from 13.9 to 7.3 kyr BP (Chapter 2) is therefore unexpectedly large (0 to 600 years). Some portion of MRA variability is likely due to production changes in the atmosphere related to solar output; however, a reservoir age of zero years at Barbados requires that surface water must have been in equilibrium with the atmosphere and removed from sources of upwelling, a condition that is not found in the modern ocean. Nevertheless, an independently dated Caribbean record from Cariaco basin based on annual varve layer counting anchored to tree ring data sets (Hughen et al., 2004b) also suggests lower MRA at the start of the Younger Dryas (Hua et al., 2009) and thereby requires that reduced MRA would have been widespread in the tropical Atlantic unless there is an error in the anchoring of the floating tree ring radiocarbon chronology (Reimer et al., 2013a).

The uncertainty in MRA corrections becomes much less significant, particularly with samples older than 20 kyr BP because the analytical uncertainty in the ^{14}C measurement increases exponentially with age (Chiu et al., 2007). This is especially relevant for the Araki Island and MIS 3 Barbados samples where AMS ^{14}C measurement uncertainty dominates age error estimates and the uncertainty in $\Delta^{14}C$. It is in this age range that the accuracy of ^{14}C dating depends largely on constraining the fraction of

modern carbon (FMC) that may have been introduced during sample processing. High and variable processing blanks can introduce erroneous structure in radiocarbon calibration curves and calculated $\Delta^{14}C$ that have been interpreted as rapid changes in production (Beck et al., 2001).

3.4 Results

The coral record presented here spans 49.2 to 15 kyr BP (Figure 3.1a) and consists of 155 discrete samples and represent five times the coral data published elsewhere for this same time interval (Bard et al., 1998; Cutler et al., 2004; Durand et al., 2013). Except for a few brief data gaps the coral record is nearly continuous, with an average resolution of 240 years, and less than 100 years from 26 - 15 kyr BP, or a resolution comparable to speleothem and sediment records. In contrast to speleothem records and deep-sea cores (where sampling intervals may represent decades to centuries and where calibration data may be inherently smoothed) each individual coral sample represents a few years of coral growth, thereby generating redundancy in data and potential for identifying higher resolution structure in calibration and $\Delta^{14}C$ curves.

3.4.1 The 50 to 34 kyr BP Interval

Available records for comparison to Araki coral data for the interval 49.2 to 34 kyr BP include U-Th dated speleothems (Hoffmann et al., 2010), varve sequences from Lake Suigetsu, Japan (Ramsey et al., 2012), and deep-sea sediments from Caricao Basin (Hughen et al., 2006) and Iberian and Pakistan margins (Bard et al., 2013) (Figure 3.1a). Although the sediment records provide high-density data to the IntCal13 calibration curves, their chronologies must be considered inter-dependent since they require transfer

of calendar age chronologies from a reference record to the undated sediment record (Heaton et al., 2013). For example, the calendar year age model in the Lake Suigetsu SG06 core was obtained by assuming ^{14}C features in the varve record correlate to similar features in U-Th dated Bahamas speleothems (Ramsey et al., 2012) 12,000 km away, a process commonly referred to as wiggle matching. Calendar ages assigned in the Cariaco Basin and Iberian-Pakistan sediment cores were obtained based on correlating tie points between climate and geochemical proxy records via a revised (Hulu2) U-Th dated $\delta^{18}O$ chronology (Bard et al., 2013; Hughen et al., 2006; Reimer et al., 2013a), a groundwater signal located 15,000 and 11,000 km away, respectively. Since the Cariaco Basin and Iberian-Pakistan records use the same reference record for generating the individual calendar age models they tend to follow the similar trends in plots of radiocarbon vs. calendar age (Figure 3.1a). One clear lesson from Project SPECMAP is that individual climate or ocean proxy signals may appear similar but they usually contain a phase shift due to different time constants for different climate or regional systems (Martinson et al., 1987). Allowances for phase shifts between signals are not considered by the IntCal compilations.

Araki corals for the interval 49.2 to 34 kyr BP generally display younger ^{14}C ages compared to same calendar age speleothem and Lake Suigetsu varves (Hoffmann et al., 2010; Ramsey et al., 2012) (Figure 3.1a) with age differences by as much as 2000 years. Twenty-four of the 37 corals were dated by the U-Pa method and 20 of these generated concordant U-Th and U-Pa ages, thereby providing robust quality control of the U-series dating system (Figure 3.2; Appendix Table 1).

A number of Bahamas speleothem ^{14}C ages are 2000 to 3000 years older than same calendar year age corals. These age differences are too large to be attributed to dating errors or MRA corrections to Araki ^{14}C ages. One explanation is that the dead carbon fraction (DFC) may have been larger and more variable than the assumed 2075 ± 540 years (Hoffmann et al., 2010). Speleothems also require age corrections due to $^{230}Th_{initial}$. In the Bahamas speleothem, the U-Th age corrections were 300-400 years, based on a $^{230}Th/^{232}Th_{initial}$ activity ratio of 7.8 ± 4 (Hoffmann et al., 2010). In addition, unlike corals, paired ^{14}C and U-Th ages in speleothems cannot be obtained from the same sampling interval or subsample. Slow growth rates and low U concentrations make it necessary to sample adjacent to the ^{14}C-sampled intervals so that sufficient material is obtained to generate a U-Th age. Distance-age models must then be generated in order to assign U-Th ages corresponding to the ^{14}C-dated intervals, with the underlying assumption that were no growth hiatuses.

Iberian, Pakistan, and Cariaco Basin sediment data are more or less consistent with the Araki coral data and generally overlap within the estimated ^{14}C dating uncertainties, typically in the range of ± 300 to 600 years at 2 s.d. (Figure 3.1a and 3.1b). Araki data falls within the scatter of values displayed in the high-density Lake Suigetsu record. However, the increased scatter in Lake Suigetsu ^{14}C ages prohibits interpretation of age differences and indicates contamination may contribute to ^{14}C dating artifacts in the Lake Suigetsu record.

3.4.2 The 34 to 28 kyr BP Interval

Comparison of calibration data 34 to 28 kyr BP shows large ^{14}C age differences of up to 3000 years (Figure 3.1b) between coral and other archives. Two Barbados corals

indicate a rapid decrease in ^{14}C age between 32.36 and 31.52 kyr BP during which time the calendar to radiocarbon age difference increases from 3000 to 6000 years. Between 31.5 and 29.6 kyr, BP six Barbados corals display nearly uniform ^{14}C age, averaging 25.06 ± 0.44 kyr BP (2 s.d.). From 31.5 to 28.6 kyr BP coral ^{14}C ages decreased by only ~1000 years. Tahiti coral data spanning the same interval (Durand et al., 2013) are consistent with the Barbados coral data, with a number of samples either overlapping or plotting within uncertainties representing combined dating errors (± 200 years) and MRA variability (± 200 years). In contrast to the coral data, both Cariaco Basin sediments and the Bahamas speleothem show rapidly decreasing ^{14}C ages beginning around 30.5 kyr BP corresponding to the time when corals show an interval of plateauing ^{14}C age. Lake Suigetsu data scatter between corals, Cariaco Basin sediments, and speleothems (Figure 3.1b) and does not provide confirmation of either of the disparate records.

That there should be such large differences in calibration data from 34 to 30 kyr BP is surprising since ^{14}C-dating errors in this age range are relatively small (± 100 to ± 200 years at 2 s.d.) and so better overlap between different data sets would be expected. The accuracy of the coral data is supported by Barbados and Tahiti corals both having $\delta^{234}U_{initial}$ values falling within the accepted range for seawater and closed system samples. In addition, four of the Barbados corals constraining the ^{14}C "plateau" age have concordant U-Th and U-Pa dates (Chiu et al., 2006), thereby confirming accuracy in the radiometric dating. Finally, differences of 3000 years in ^{14}C age between corals and other archives are an order of magnitude too large to be attributed to MRA corrections.

Calendar ages corresponding to ^{14}C dated planktonic foraminifera from Cariaco Basin have not been measured but are assigned based on correlation of gray scale in the

sediment core to proxy records in ice cores and cave deposits. An earlier age model using ODP Hole 1002D was based on correlation of gray scale to GISP $\delta^{18}O$ (Hughen et al., 2004a). That age model was later revised based on U-Th dated Hulu Cave $\delta^{18}O$ record (Hughen et al., 2006) and the ^{14}C-Calendar age pairings incorporated into the IntCal09 calibration curves. Most recently, calendar ages in the sediment core were recalculated based on an updated high-resolution U-Th dated Hulu Cave $\delta^{18}O$ record (Cariaco-Hulu2) and included in IntCal13 (Reimer et al., 2013a). The revised age model shifts calendar ages by about 1000 years, younger, throughout the 32 to 28 kyr BP interval, thereby producing large shifts ^{14}C ages compared to corals (Figure 3.3). The large shifts in calendar age displayed with the Cariaco Basin sediment data illustrate potential shortcomings when calibration data rely on imported chronologies. The selection of tie points is subjective and may occasionally lead to identifying "false positives" which generate abrupt and unrealistic changes in sedimentation rates (this dissertation, Chapter 4; Chiu et al., 2007). More importantly, the underlying principle in all tied chronologies is that events linking proxy records are assumed to be simultaneous. In the example above, changes in color in the Cariaco Basin core were assumed to be simultaneous with changes in $\delta^{18}O$ preserved in a Chinese cave deposit and linked to changes in the strength of the East Asian monsoon. Our observation of large offsets between Cariaco Basin sediment data from 32 to 28 kyr BP is not unlike the findings in Chiu et al. (2007) and where it was demonstrated that the selection of tie points in the Cariaco-GISP2 and Cariaco-Hulu age models generated large and rapid shifts in sedimentation rates and large shifts in calendar ages during Marine Isotope Stage 3 and the Mystery Interval (see Chapter 4). Radiocarbon calibration data relying on imported

chronologies should be first confirmed with independent (i.e., U-Th dated) chronologies to identify potential miss-correlation in tie points.

Large age differences between Bahamas speleothems and corals in the 32 to 28 kyr BP interval (Figure 3.1b) are more difficult to reconcile since both represent U-Th dated archives. Higher and more variable dead carbon fraction (e.g., 3000 – 5000 years) than the assumed value of 2075 years (Hoffmann et al., 2010) would be required to explain the large offsets in ^{14}C ages. Climate records obtained from speleothems and deep sea cores indicate large changes in the hydrologic cycle during Marine Isotope Stage 3 (Carolin et al., 2013; Peterson et al., 2000; Wang et al., 2001) which may have led to changes in vegetation patterns, root depth and soil formation, and the chemistry of groundwater across D/O events, thereby modifying the DCF of $CaCO_3$ precipitating in caves. We note that a variable dead carbon fraction in GB-24-1 is likely required during the Younger Dryas portion of the record in order to explain ^{14}C age plateaus and cliffs that are not reproduced in either tree ring or coral records (Hoffmann et al., 2010).

The 32.6 to 27.8 kyr B.P interval in GB89-25-3 consists of 26 modeled-ages, generated from a cubic spline fit to 12 U-Th dated samples. The U-Th dated intervals themselves produce pronounced changes in growth rate, from ~30 to 150 mm kyr^{-1}, corresponding to the time interval where the coral and speleothem data diverge, whereas the smooth spline fit averages out the abrupt shifts in growth rates (Hoffmann et al., 2010). The spline fit age model also incorporates two U-Th ages corrected for $^{230}Th_{initial}$ and inclusion of the $^{230}Th_{initial}$ corrected U-Th ages shifts the spline fit age model to younger calendar age by 400 to 600 years between 32 and 30 kyr BP. Therefore, in addition to DCF corrections that may be larger and more variable through time, modeled

U-Th ages assigned to corresponding ^{14}C ages in GB89-25-3 may be subject to abrupt changes in speleothem growth rate, not accounted for in distance-age models as well as variable ^{230}Th corrections.

3.4.3 The 26 to 18 kyr BP Interval

From 26 to 18 kyr BP the agreement between coral, speleothem, and sediment data improves and generally overlap within combined dating uncertainties, and uncertainties in MRA and DCF corrections (Figure 3.1a). The good overlap between U-Th dated archives (Barbados coral and Hulu Cave and Bahamas speleothem) and calibration data obtained from deep sea cores (e.g., Cariaco Basin, Lake Suigetsu, Pakistan Margin) indicates their respective age models used to assign calendar ages for the 26 to18 kyr BP interval are reasonably robust (Figure 3.1b).

3.4.4 Calibration curve comparison

Paired U-Th and ^{14}C dating of Barbados corals provided an initial calibration data set and demonstrated U-Th ages provided a powerful tool for calibrating the radiocarbon time scale beyond tree ring records. Bard et al. (1990) show that the consensus radiocarbon calibration curve was in error by 1000 years at 10 kyr BP based on the Dye 3 and Camp Century ice core chronology and the age for the Younger Dryas climate event (Hammer et al., 1986). Subsequently, the missing 1000 years was found in Greenland GSIP2 ice core chronologies and attributed to the undercounting of annual layers in the Dye 3 ice core (Alley et al., 1993). In Fairbanks et al. (2005), a stand-alone radiocarbon calibration curve was constructed exclusively from coral data. The curve was offered as an alternative to calibration curves that incorporated data sets with inferred calendar ages

based on correlation of local proxies in deep-sea cores to ice core proxies or other distant climate proxies and without assumptions of constancy of sedimentation rates. The coral calibration curve was based on hierarchical Bayesian modeling to compute an age distribution for a given set of samples on the basis of a given uncertainty in the their radiocarbon age, assuming no error in their calendar age. Unlike other calibration curves such as IntCal09 and IntCal13, the coral based curve met the requirement that each data point in the calibration curve had a measured calendar age and radiocarbon age with known errors, independent of one another (Fairbanks et al., 2005). The curve was subsequently updated with additional data in 2007 (FAIRBANKS0107). That calibration could be used to convert radiocarbon ages to calendar ages using an online conversion program that included a rigorous error estimate. Data presented in Figure 3.4 bolsters our argument that corals provide the greatest potential for providing a "backbone" calibration curve beyond tree ring records, or beyond 14 kyr BP and to the limits of radiocarbon dating. Limited only by the availability of suitable samples, corals in this age range are neither sensitive to MRA corrections to measured ^{14}C ages nor are they subject to U-Th age corrections due to $^{230}Th_{initial}$. Corals are also the only archive for which $\delta^{234}U_{initial}$ provides a rigorous test of "closed system" behavior and their relatively high U content (ppm) and unlimited sample size make corals ideal for applying concordant U-Pa age testing. Unlike speleothems, corals are free from DCF corrections that may exceed several thousand years and from age-depth corrections and inherent smoothing of calibration data since both the U-Th and ^{14}C ages are obtained from the same sample. Layer counted sediments that are ^{14}C dated but which require imported age models from U-Th speleothems, compound dating error uncertainties and generate unacceptable

scatter in records prior to 35 kyr BP (Figure 3.1a). Finally, corals permit inter-lab calibrations of ages that are not possible with sample limited cave deposits.

Comparison of the coral calibration curve (Fairbanks0107) with the consensus IntCal09 and Intcal13 curves 50 to 25 kyr BP show the three curves share a similar "bowed up" shape where the offset between the ^{14}C age and calendar age from the 1:1 line increases from about 4000 years at 48 kyr BP to maximum values of about 6000 years at 30 kyr B.P (Figure 3.4). Since both IntCal09 and Intcal13 incorporate all but 10 of the Araki coral data presented in this study the agreement between the Incal and FAIRBANKS0107 calibration curves in this older portion is somewhat expected. However, inclusion of Bahamas speleothem (Hoffmann et al., 2010) and Iberian and Pakistan margin foraminiferal data (Bard et al., 2013) generally displaces the IntCal13 curve to older ^{14}C and younger calendar age compared to coral data and the coral based curve (Figure 3.4). Scatter within individual data sets that contribute to IntCal13 increases about the calibration curve with increasing age (Figure 3.1a). However, because of its higher data density and small calendar age uncertainties, the Lake Suigetsu record generally determines the shape of the IntCal13 calibration curve when it diverges from other records (Figure 3.1a). This is particularly true for the 32 to 29 kyr BP interval where the Intcal13 curve does not follow the trend established with the Bahamas speleothem or Cariaco Basin data but rather follows the trend set by Lake Suigetsu data. Despite considerable scatter in ^{14}C ages associated with samples older than 35 kyr BP, ^{14}C ages will, however, typically convert to calendar ages that agree to within 1000 to 2000 years regardless of the choice of calibration curve. After 26 kyr BP, the coral-based and IntCal13 curves largely converge on the same solution (Figure 3.4) and differences

between curves are consistent with ^{14}C dating errors and with uncertainties in MRA and DCF corrections associated with corals and speleothems, respectively.

In our future calibration efforts it will be important to obtain quality coral samples to fill data gaps and to address discrepancies between different data sets, particularly for the time intervals 34 to 28 kyr BP and 43 to 40 kyr BP. These intervals represent important times slices to archaeologists and anthropologists who rely on estimates of calendar ages from ^{14}C ages obtained in bone and charcoal and dating of upper Paleolithic cave art for reconstructing migration routes taken by modern humans across Europe and the Near East (Sauvet, 2016). The intervals also correspond to rapid shifts in high latitude climate, as characterized by Heinrich Events 3, 4, and 5 (Bond and Lotti, 1995; Hemming, 2004), Dansgaard-Oeschger Events 4-13 (Dansgaard et al., 1993), and Antarctic Isotope Maxima (Members, 2006). The intervals also contain the Laschamp and Mono Lake geomagnetic excursions (Benson et al., 2003; Gillot et al., 1979; Guillou et al., 2004; Kent et al., 2002) when the earth's magnetic field weakened to zero or near zero field strength. In the discussion to follow, we use the paired ^{14}C and U-Th coral ages to generate a record of the $^{14}C/^{12}C$ atmospheric ratio to identify and confirm the predicted ^{14}C production increases due to geomagnetic excursions during the past 50 kyr.

3.5 Discussion

Paired ^{14}C and calendar age data from terrestrial and marine archives provide an estimate of the radiocarbon content of the atmosphere ($\Delta^{14}C_{atm}$) by the following equation:

$$\Delta^{14}\mathrm{C}\ (‰) = \left(\frac{EXP\ (\lambda_1 * t_1)}{EXP\ (\lambda_C * t_C)} - 1 \right) * 1000 \quad (1)$$

(Stuiver and Polach, 1977) where t_1 is the calendar age, t_c is the radiocarbon age, λ_1 is the activity constant of ^{14}C based on the consensus (Oxford) half-life of 5730 years and λ_c is the activity constant based on the Libby half-life of 5568 years (Libby, 1955).

3.5.1 Coral Record of Atmospheric $\Delta^{14}C$

Chiu et al. (2007) generated an atmospheric $\Delta^{14}C$ record since 50 kyr BP based on U-Th and ^{14}C dated fossil corals. Fourteen of the samples older than 28 kyr BP had U-Th ages confirmed with concordant U-Pa ages. That record showed an increase in $\Delta^{14}C$ from 50 kyr BP to a maximum at 40 kyr BP and subsequent decline of $\Delta^{14}C$ from 35 kyr BP to the present, consistent with the predicted role of the Laschamp geomagnetic field excursion on the long-term trend of the $\Delta^{14}C$ record (Figure 3.5). Chiu et al. (2007) concluded that the amplitude of coral $\Delta^{14}C$ was a factor of two higher than carbon box models (Beck et al., 2001; Hughen et al., 2004a) or ^{14}C production scenarios predict, leading the authors to propose a significant linear component of the long-term $\Delta^{14}C$ trend might be due to inaccuracies in the generally accepted ^{14}C decay constant. In our study, we have supplemented the $\Delta^{14}C$ record presented in Chiu et al. (2007) with 70 new dated samples, including 10 new coral U-Th ages anchored with concordant U-Pa ages. The updated coral $\Delta^{14}C$ record reveals structure in $\Delta^{14}C$ not previously resolved or sufficiently constrained with data in Chiu et al. (2007). Two such features are a rapid spike in $\Delta^{14}C$ shortly after 32 kyr BP and a $\Delta^{14}C$ plateau between 20 and 18 kyr BP (Figure 3.5).

3.5.2 The Laschamp and Mono Lake Excursions

The Laschamp Excursion is the best-documented geomagnetic event recorded in the past 50,000 years (Guyodo and Valet, 1996; Laj et al., 2000). First identified in France, in lava flows having low paleointensity and anomalous paleomagnetic directions, the rocks were later dated to between 40.4 and 40.7 (± 2) kyr BP (Guillou et al., 2004; Singer et al., 2009). The most recent estimate of the age of the Laschamp excursion is based on U-Th dating and layer counting in a North American speleothem and constrains the event to having taken place between 42.25 to 39.70 kyr BP, with the main phase estimated to have occurred 41.1 ± 0.35 kyr BP (Lascu et al., 2016). Four of our Araki coral data span the main phase of the event (Appendix; Table 1) and include two $\Delta^{14}C$ estimates in excess of 1000‰ (Figure 3.5). Error bars associated with $\Delta^{14}C$ estimates prior to 35 kyr BP are large as ^{14}C-dating uncertainties and blank corrections in these samples translate to large uncertainties (± 200 to 400‰) in $\Delta^{14}C$. Nevertheless, the coral data are consistent with increased ^{14}C production at a time when the field strength is believed to have decreased to near zero. Because of the relatively large radiocarbon dating error bars, the decline in $\Delta^{14}C$ due to decay and the subsequent recovery in the geomagnetic field strength only loosely correlate with paleointensity stack records following Laschamp (Figure 3.5). It is evident that interpretation of the history of atmospheric ^{14}C prior to 34 kyr BP continues to be limited by radiocarbon dating precision and that better precision and rigorous blank monitoring are needed.

Barbados coral data show a rapid $\Delta^{14}C$ increase from 400‰ to 900‰ between two samples, from 32.36 ± 0.03 kyr BP to 31.52 ± 0.06 kyr BP. The increase is followed by a rapid decrease of about 400‰ by 29.6 kyr BP. The rapid decrease in $\Delta^{14}C$

corresponds to the two thousand year ^{14}C age plateau of 25.06 ± 0.44 ^{14}C kyr (Figure 3.1b). Several Tahiti coral $\Delta^{14}C$ (Durand et al., 2013) also overlap with the Barbados data. Taken together the combined coral record displays a much larger amplitude change in $\Delta^{14}C$ compared to the IntCal13 (Reimer et al., 2013a) curve (Figure 3.5). The lower amplitude $\Delta^{14}C$ signal in the smoothed IntCal13 estimate 31-28 kyr BP reflects the reliance on an indirectly dated record, specifically on the higher density Lake Suigetsu data which shifts the IntCal13 curve to older ^{14}C and younger calendar age by several thousand years (Figure 3.4) and hence to lower $\Delta^{14}C$ compared to coral estimates of $\Delta^{14}C$ (Figure 3.5).

We believe that the Lake Suigetsu data set is in error. The most likely explanation is that there are errors in calendar ages resulting from the mapping of the SG06 time scale onto the speleothem U-Th time-scale as well as potential cumulative errors introduced in generating an "event free depth scale" (i.e., removal of turbidites, tephras) from a composite depth scale (Ramsey et al., 2012). Several Lake Suigetsu data overlap with coral $\Delta^{14}C$ at ~31 kyr BP, but these data were determined to be outliers in the $\Delta^{14}C$ record (Ramsey et al., 2012). The match between Lake Suigetsu and GB89-25-3 speleothem data is not particularly good prior to 25 kyr BP. Nevertheless, the dependence of the $SG06_{2012}$ chronology on the U-Th Bahamas speleothem time scale introduces a biasing and rejection of data that cannot be confirmed with coral data. Accordingly, we see no a priori reason why the coral U-Th time-scale could not serve as an alternative calendar age model for the SG06 ^{14}C chronology.

An increase in $\Delta^{14}C$ from ~500‰ to 950‰ after 32 kyr BP is much too large to be caused by changes in solar output or the carbon cycle. In fact, $\Delta^{14}C$ variations induced

by solar activity and changes in the carbon cycle are much less detectable through time as the $\Delta^{14}C$ record loses its resolution due to the increasing relative errors of radiocarbon dating and or the availability of continuous archived records. Although the radiocarbon age external precision degrades with age, the magnitude of the $\Delta^{14}C$ signal fluctuations increases with age due to the enormous effects of the Laschamp excursion. As a result, the $\Delta^{14}C$ "signal to noise" ratio does not change dramatically over the past 50,000 years. Therefore, the large and rapid increase in $\Delta^{14}C$ is best explained by an increase in production during zero or near zero geomagnetic field strength. We conclude that the large and rapid rise measured in $\Delta^{14}C$ between two samples dated at 32.36 ± 0.03 kyr BP and 31.51 ± 0.06 kyr BP corresponds to the Mono Lake Excursion, initially identified in North American Great Basin sediment cores (Benson et al., 2003; Liddicoat, 1992; Liddicoat, 1996; Liddicoat and Coe, 1979) and later confirmed in North and South Atlantic Ocean deep sea core records (Channell, 2006a; Stoner et al., 2002).

The age of the Mono Lake excursion was previously determined by ^{14}C dating of sediments above and below Ash #15 at Pyramid Lake, CA and provided an age estimate of between 33.3 and 31.5 kyr BP based on the GISP2 time scale (Benson et al., 2003). The age of the Mono Lake excursion remains somewhat controversial as it has been argued that ^{14}C and $^{40}Ar/^{39}Ar$ dating uncertainties associated with the same ash layer at the Wilson Creek Formation, Mono Lake, CA and its type locality, make it indistinguishable from the Laschamp event (Cassata et al., 2010; Cox et al., 2012; Kent et al., 2002; Zimmerman et al., 2006). Regardless, as to whether the event recorded at Mono Lake represents an excursion distinct from Laschamp there is widespread evidence from paleointensity records in deep sea sediments (Channell, 2006a; Laj et al., 2000;

Stoner et al., 2002) and ^{36}Cl accumulation records in Greenland ice cores (Wagner et al., 2000) of an excursion event that post-dates the Laschamp, sometime between 34 and 30 kyr BP. We conclude that our record of $\Delta^{14}C$ obtained with high precision and high-accuracy U-Th dated corals provide much better constraints on the timing and duration of the Mono Lake excursion to date and confirm it as a global event. Although additional data will provide better constraints for the exact timing of the initial rise in atmospheric ^{14}C, data in Figure 3.5 can be used to estimate the duration of the Mono Lake excursion. Based on the width of the $\Delta^{14}C$ spike measured at one-half the amplitude, we estimate the duration to be about 2000 years (32– 30 kyr BP) with peak intensity sometime around 31.5 ± 0.2 kyr BP. The decrease in $\Delta^{14}C$ following the production event is better constrained with data and we estimate the e-folding time (the time for the signal to decrease to 1/e) in the decline to be about 14,000 years and is consistent with natural decay of ^{14}C within the oceanic reservoir. Our dating of the Mono Lake excursion agrees with the age of the peak in ^{36}Cl measured in Summit GRIP ice core (~32 kyr BP), identified between Dansgaard-Oeschger (D-O) events 6 and 7. The estimated duration of 2000 years is consistent with numerical modeling suggesting geomagnetic excursions correspond to short-term geomagnetic processes in the outer liquid core (Gubbins, 1999). The 400‰ increase in $\Delta^{14}C$ also matches the predicted increase estimated with modeling of production rates applying a zero- magnetic field of ~2000 year duration (Lal, 1988; Lal and Charles, 2007).

In contrast to ^{14}C and ^{36}Cl records, there is no pronounced peak in the flux of cosmogenic ^{10}Be recorded in ice cores corresponding to the time of the Mono Lake event (Figure 3.5) (Finkel and Nishiizumi, 1997; Muscheler et al., 2005; Muscheler et al.,

2004). Estimates of ^{10}Be fluxes are, however, highly dependent upon the accuracy of ice core age models and changes in the transport of precipitation. Therefore, although there is a good correlation between ^{10}Be and ^{14}C recorded at Summit during the Holocene, associated with solar variability and the 205-yr de Vries cycle (Wagner et al., 2001), ^{10}Be fluxes recorded during MIS 3 may not necessarily be linearly related to global production rates associated with geomagnetic field strength.

Comparison of the stacked NAPIS-75 and SAPIS paleointensity records with our Δ^{14}C reconstruction does not show a particularly good correlation between low intensity values and high Δ^{14}C corresponding to the age of the Mono Lake Excursion (Figure 3.5). We attribute the mismatch between the stacked paleo-intensity records and coral Δ^{14}C to imprecision in the age models constructed for the individual records that are combined to produce the composite stack. For example, the age model constructed for the 11 - 41 kyr BP interval in ODP Site 1089 and used as a reference core in the SAPIS paleointensity stack (Stoner et al., 2003) was generated based on a comparison of planktonic and benthic δ^{18}O to records in a ^{14}C dated companion core, RC11-83 (Charles et al., 1996). That age model relied on only a few calibration data older than 25 kyr BP to convert ^{14}C years to calendar years and so the calendar ages were considered to be only accurate to within ± 1500 years. Recalibration of the ^{14}C ages in RC11-83 with updated curves such as IntCal13, or FAIRBANKS0107 do not improve upon the original age model in Site 1089 as discrepancies among calibration data 34 -30 kyr BP (Figure 3.1b and Figure 3.4) can produce a range calendar year estimates that differ by 1500 years. Thus, radiocarbon calibration limits the accuracy of age models in paleointensity records obtained from deep-sea cores containing a history of strength of the earth's magnetic field. With our

record of $\Delta^{14}C$ constructed with Barbados corals, we are confident that we have identified and dated the ^{14}C production spike associated with the Mono Lake excursion. The accurate dating of this event could provide a powerful stratigraphic marker for correlating paleointensity records from around the globe if verified in revised paleointensity records.

3.5.3 Corrections to the $\Delta^{14}C$ coral record

Lal and Charles (2007) adjusted a 50,000-year record of $\Delta^{14}C$ reconstructed from Cariaco Basin sediments by removing the contributions from the Laschamp and Mono Lake excursions. Their record of residual $\Delta^{14}C$ showed constant values of about 300‰ during 28-17 kyr BP followed by rapid drop beginning at 17 kyr BP. The plateau in $\Delta^{14}C$ was attributed to changes in ocean circulation, and also to an increase in the expansion sea ice in the southern ocean, resulting in isolation of a fraction (>20%) of the oceanic reservoir from mixing with the atmosphere. The decline in $\Delta^{14}C$ after 17 kyr BP was attributed to the mixing of the isolated reservoir back into the atmosphere. The calendar year age model for the Cariaco Basin sediment core that served as a target $\Delta^{14}C$ record in Lal and Charles (2007) has since been revised (Hughen et al., 2006; Reimer et al., 2013a), thereby producing changes in both the shape and amplitude of $\Delta^{14}C$ variations 35 -25 kyr BP that differ during the interval corresponding to Mono Lake. Equipped with an expanded coral record we can now apply corrections to coral $\Delta^{14}C$ data to remove the influence of the Laschamp and Mono Lake excursions. The distinct advantage of using coral $\Delta^{14}C$ for a target atmospheric record is that the data are calculated based on measured calendar ages, rather than calendar ages that have been assigned based on modeled ages in sediment cores. With 85 data points spanning the 50 to 20 kyr BP interval, the coral record has sufficient data density to make identification and subtraction

of excess ^{14}C from known geomagnetic events possible. For simplicity, we model Laschamp as an instantaneous increase in production of ^{14}C, sufficient to raise the atmospheric content 500‰ from pre-excursion background values of 450‰ to a maximum value of 950‰, based on the average of four coral $\Delta^{14}C$ data spanning 41.35 ± 0.35 kyr BP. In our simulation, atmospheric ^{14}C is allowed to decay from 41 kyr BP with the consensus half-life (5730 years) and the contributions from Laschamp subtracted from Barbados coral $\Delta^{14}C$ and plotted as the residual or $\Delta^{14}C_{Lcorr}$ (Figure 3.6). Corrections for Mono Lake are calculated based on $\Delta^{14}C_{Lcorr}$ in Figure 3.5 and is modeled as an increase above background of 400‰ at 31 kyr BP. Plots comparing $\Delta^{14}C$ and $\Delta^{14}C_{LMcorr}$ demonstrate that corrections made for excess ^{14}C from the Laschamp and Mono Lake excursions are significant. For example, contributions from the Laschamp and Mono Lake events to $\Delta^{14}C$ at 25 kyr BP are about 100‰ and 200‰, respectively, constituting about one-half of the raw $\Delta^{14}C$ estimate.

Our computed $\Delta^{14}C_{LMcorr}$ record shows an increase of 150‰ between 28 and 26 kyr BP followed by plateau, centered around 250‰, from 26-20 kyr BP. Therefore, while the general shape of $\Delta^{14}C_{LMcorr}$ obtained with corals is similar to that computed using Cariaco Basin sediments as a target record (Lal and Charles, 2007), the plateau observed in our coral record is about one-half the magnitude and of shorter duration. While there are no coral data available for the interval 28- 26 kyr BP, three H82 speleothem samples date within the interval and have $\Delta^{14}C$ values of 550 to 525‰, yielding $\Delta^{14}C_{LMcorr}$ = 220‰ and consistent with our coral data. Therefore, the combined coral and speleothem data suggest a rise in $\Delta^{14}C_{LMcorr}$ likely began prior to 27 kyr BP (Figure 3.6).

Corrections to the $\Delta^{14}C$ raw data and computed $\Delta^{14}C_{LMcorr}$ are sensitive to the selection of "peak" $\Delta^{14}C$ values associated with the two excursion events. The absolute values of $\Delta^{14}C$ and $\Delta^{14}C_{LMcorr}$ are also sensitive to the accuracy of the ^{14}C half-life in equation 1. For example, substitution of the calorimetry estimate of the half-life (6030 years) as measured by Jenks and Sweeton (1952) in place of the consensus half-life (5568 years) reduces $\Delta^{14}C$ estimates by about half and generates values more or less consistent with global production and atmospheric models and with combined sources of variability (i.e., dating errors) (Chiu et al., 2007). Regardless of the parameters chosen to calculate $\Delta^{14}C_{LMcorr}$, the relative shape of $\Delta^{14}C_{LMcorr}$ would remain unchanged. Therefore, a "relative" increase of 150‰ prior to 27 kyr BP must be due to increased production rates, perhaps in conjunction changes in ocean circulation. Both the SAPIS and NAPIS-75 stacked records display a second paleointensity minimum that post-dates the Mono Lake excursion, implying a weakened geomagnetic field and hence increased production of ^{14}C. The timing of the increase in atmospheric ^{14}C at 27 kyr BP also coincides with a 30 meter ice equivalent lowering of relative sea level (RSL) as reconstructed with the reef crest building coral *Acropora palmata* at Barbados (Peltier and Fairbanks, 2006). A drop in sea level associated with rapid buildup of the Northern Hemisphere ice sheets may have perturbed AMOC and reduced deep-water formation, thus contributing to a buildup of ^{14}C in the atmosphere. An expansion of sea ice in the Southern Ocean at this time may also have contributed to the increase in $\Delta^{14}C$ by reducing the rate of gas exchange between the atmosphere and surface-ocean. An increase in $\Delta^{14}C_{LMcorr}$ due to an expansion in sea ice and reduction in gas exchange is consistent with an observed negative shift in mid-depth benthic $\delta^{13}C$ after 28 kyr BP (Lal and Charles, 2007; Pahnke

and Zahn, 2005).

An important finding in correcting raw $\Delta^{14}C$ for the Laschamp and Mono Lake contributions is the removal of rapid and large amplitude directional changes in $\Delta^{14}C$ and overall reduction in short-term variability. This is because correcting $\Delta^{14}C$ removes the inherent biasing introduced with the sudden addition of excess ^{14}C atoms and their subsequent removal into the ocean and exponential decay during production events. For example, during the interval, 26 to 20 kyr BP, coral $\Delta^{14}C$ declines from 600 to 400‰, at a rate of 50‰ kyr^{-1} where as $\Delta^{14}C_{LMcorr}$ displays uniform values, averaging 250 ± 60‰ (Figure 3.6). Therefore, variability in $\Delta^{14}C_{LMcorr}$ is more consistent with combined dating errors (20 -30‰), variability in MRA (10-20‰), and solar-related production changes (10-20‰), whereas neither the shape, nor variability displayed in the uncorrected $\Delta^{14}C$ record over this same interval, are easily explained by geochemical or geophysical processes (e.g., production changes, ocean circulation).

3.5.4 Hilina Pali Excursion

From 20 to 18 kyr BP, $\Delta^{14}C_{LMcorr}$ increases by about 100‰. A build-up of atmospheric ^{14}C could have resulted from a reduction in NADW production. However, the timing of the inferred NADW slow down or shut down conflicts with Pa/Th evidence in North Atlantic deep-sea sediments that indicate NADW production did not slow or stall until the start of Heinrich Event 1 (17.5 kyr BP) although Nd_{ε} measured in a South Atlantic deep sea core during the Last Glacial Maximum suggests NADW was already reduced prior to 18 kyr BP (Piotrowski et al., 2004). Regardless, a 100‰ increase is twice the amplitude change that ocean-atmosphere models are able to generate with a complete shutdown of NADW (Delaygue et al., 2003). We attribute a contribution to

increased atmospheric ^{14}C prior to Heinrich 1 to increased production rates during the Hilina Pali geomagnetic excursion. Although not as well documented in paleomagnetic records as Laschamp or Mono Lake, the Hilina Pali is characterized by anomalous behavior in declination, inclination, and paleointensity measured in basalts from Hawaii, China, and western USA (Singer, 2014; Teanby et al., 2002; Turrin et al., 2013). $^{40}Ar/^{39}Ar$ ages in these lavas indicate an age of about 17 ± 1 ka for the Hilina Pali excursion where as calibrated ^{14}C ages on Hawaiian basalts suggest an age of closer to 20 kyr BP (Coe et al., 1978). The coral record indicates increasing $\Delta^{14}C_{LMcorr}$ between 20 and 18 kyr BP, consistent with the age of the Hilina Pali, when dating uncertainties are taken into account.

A fair criticism of the Barbados $\Delta^{14}C$ record is that it does not account for variability due to local variability in MRA. A doubling of MRA to 700 years would be required to account for a 100‰ increase $\Delta^{14}C_{LMcorr}$ observed 20 to 18 kyr BP. It is important to note, however, that there is good overlap between Barbados coral and Hulu Cave speleothem calibration data from 26 to 18 kyr BP (Figure 3.1a) and that both records show the same amplitude and directional change in $\Delta^{14}C$ over the interval corresponding to the Hilina Pali event. We cite the similarities between terrestrial based and marine based $\Delta^{14}C$ records as evidence that the same geophysical and geochemical processes controlled both and therefore the increase in $\Delta^{14}C$ observed in Barbados corals is not due to variable MRA corrections. Rather, the increase in ^{14}C production confirms the predicted increase that would result from a weakened magnetic field during the Hilina Pali excursion and is confirmed by overlapping marine and terrestrial records.

3.5.5 Radiocarbon half-life uncertainty

The coral radiocarbon data and calibration curve presented in Figure 3.4 is strikingly linear. Over the entire 50,000-year span, the differences between the paired coral ^{14}C ages and the U-Th ages increase proportionately with time. The "selection" of the ^{14}C half-life value is one parameter that would create a "proportional offset" between the calendar age and the ^{14}C age. The computed $\Delta^{14}C$ value also depends on the value of the half-life used in Equation 1, although the uncertainty in $\Delta^{14}C$, which increases exponentially, is largely insensitive to the half-life (Chiu et al., 2007). While the uncertainty in $\Delta^{14}C$ represents the combined uncertainties in ^{14}C and calendar year ages, it is ^{14}C measurement error and blank correction that dominate the overall $\Delta^{14}C$ uncertainty in samples older than 35 kyr BP. For example, the uncertainty in $\Delta^{14}C$ is increased by about 50% if a blank uncertainty of ± 0.00042 FMC is propagated through the calculation of $\Delta^{14}C$ (Figure 3.6).

Substitution of the calorimetry estimate of the ^{14}C half-life (6030 years) in place of the consensus half-life (5730 years) removes about one-half of the proportional ^{14}C – calendar year age offset observed in the calibration curve (Figure 3.7a). Furthermore, when $\Delta^{14}C$ is re-calculated with the 6030 year half-life estimates are reduced by a factor of two (Figure 3.7b) and generate values consistent with global production and atmospheric models, and pre-Laschamp values that are close to modern values (Chiu et al., 2007). Other studies, however, contend that the ^{14}C half-life could be 2% shorter, as opposed to being 5% longer (Roberts and Southon, 2007). Regardless of presumed inaccuracies in the ^{14}C half-life, any conventional ^{14}C age shall continue to be converted to a calendar age using radiocarbon calibration curves such as IntCal13 or

Fairbanks0107. However, a strict interpretation of the $\Delta^{14}C$ atmospheric record including the uncertainties, and its geochemical and geophysical causes requires that the half-life is accurately known.

3.6 Conclusions

An updated atmospheric ^{14}C record for the past 50 BP, includes 155 individually ^{14}C and U-Th dated samples, supplemented with twenty-four concordant U-Pa dates, thereby generating the most continuous directly dated marine $\Delta^{14}C$ record for comparison to other archive data sets. Past changes $\Delta^{14}C$ since 50 kyr BP were dominated by increases in production during the Laschamp (41 kyr BP) and Mono Lake (31 kyr BP), geomagnetic excursions. After correcting for the combined effects of these two excursions an increase in $\Delta^{14}C$ beginning around 20 kyr BP appears to correlate with increased production during the Hilina Pali Excursion (19 to18 kyr BP). Although changes in the geomagnetic field strength dominate the shape of the $\Delta^{14}C$ record since 50 kyr BP, some portion of the linear trend in residual in $\Delta^{14}C$ may be due to uncertainties in the half-life of ^{14}C over the entire radiocarbon time scale.

The coral $\Delta^{14}C$ record provides the most accurate and precise dating of the Mono Lake Excursion and places it with the Laschamp event in importance as a valuable stratigraphic and marker in time for correlating sediment and ice core records. $\Delta^{14}C$ records are consistent with duration estimates of ~ 2000 years for the Laschamp and Mono Lake geomagnetic excursion events.

3.7 Acknowledgements

J. Stoner kindly provided the SAPIS and NAPIS 75 paleointensity data. R. Muscheler generously provided the ^{10}Be flux data.

3.8 References

Abdul, N. A., Mortlock, R. A., Wright, J. D., and Fairbanks, R. G., 2016, Younger Dryas sea level and meltwater pulse 1B recorded in Barbados reef crest coral *Acropora palmata*: Paleoceanography, v. 31, no. 2, p. 330-344.

Adkins, J., and Boyle, E., 1997, Changing atmospheric ^{14}C and the record of deep water paleoventilation ages: Paleoceanography, v. 12, p. 337-344.

Alley, R. B., Meese, D. A., Shuman, C. A., Gow, A. J., Taylor, K. C., Grootes, P. M., White, J. W. C., Ram, M., Waddington, E. D., Mayewski, P. A., and Zielinski, G. A., 1993, Abrupt increase in Greenland snow accumulation at the end of the Younger Dryas event: Nature, v. 362, no. 6420, p. 527-529.

Bard, E., 1988, Correction of accelerator mass spectrometry ^{14}C ages measured in planktonic foraminifera: Paleoceanographic implications: Paleoceanography, v. 3, no. 6, p. 635-645.

Bard, E., Arnold, M., Hamelin, B., Tisnerat-Laborde, N., and Cabioch, G., 1998, Radiocarbon calibration by means of mass spectrometric $^{230}Th/^{234}U$ and ^{14}C ages of corals: An updated database including samples from Barbados, Mururoa, and Tahiti: Radiocarbon, v. 40, no. 3, p. 1085-1092.

Bard, E., Hamelin, B., Fairbanks, R. G., and Zindler, A., 1990, Calibration of the ^{14}C timescale over the past 30,000 years using mass spectrometric U-Th ages from Barbados corals: Nature, v. 345, p. 405-410.

Bard, E., Menot, G., Rostek, F., Licari, L., Boning, P., Edwards, L., Cheng, H., Wang, Y., and Heaton, T., 2013, Radiocarbon calibration/comparison records based on marine sediments from the Pakistan and Iberian Margins: Radiocarbon, v. 55, no. 4, p. 1999-2019.

Bard, E., Rostek, F., and Ménot-Combes, G., 2004, Radiocarbon calibration beyond 20,000 ^{14}C yr B.P. by means of planktonic foraminifera of the Iberian Margin: Quaternary Research, v. 61, no. 2, p. 204-214.

Beck, J. W., Richards, D. A., Lawrence , R., Edwards, Silverman, B. W., Smart, P. L., Donahue, D. J., Hererra-Osterheld, S., Burr, G. S., Calsoyas, L., Timothy , A. J., Jull, and Biddulph, D., 2001, Extremely Large Variations of Atmospheric 14C Concentration During the Last Glacial Period: Science, v. 292, no. 5526, p. 2453-2458.

Benson, L., Liddicoat, J., Smoot, J., Sarna-Wojcicki, A., Negrini, R., and Lund, S., 2003, Age of the Mono Lake excursion and associated tephra: Quaternary Science Reviews, v. 22, no. 2–4, p. 135-140.

Bond, G. C., and Lotti, R., 1995, Iceberg Discharges into the North Atlantic on Millennial Time Scales During the Last Glaciation: Science, v. 267, no. 5200, p. 1005-1010.

Broecker, W., 2009, The Mysterious ^{14}C Decline: Radiocarbon, v. 51, no. 1, p. 109-119.

Broecker, W., and Barker, S., 2007, A 190‰ drop in atmosphere's $\Delta^{14}C$ during the "Mystery Interval" (17.5 to 14.5 kyr): Earth and Planetary Science Letters, v. 256, no. 1-2, p. 90-99.

Butzin, M., Prange, M., and Lohmann, G., 2005, Radiocarbon simulations for the glacial ocean: The effects of wind stress, Southern Ocean sea ice and Heinrich events: Earth and Planetary Science Letters, v. 235, no. 1–2, p. 45-61.

Carolin, S. A., Cobb, K. M., Adkins, J. F., Clark, B., Conroy, J. L., Lejau, S., Malang, J., and Tuen, A. A., 2013, Varied Response of Western Pacific Hydrology to Climate Forcings over the Last Glacial Period: Science, v. 340, no. 6140, p. 1564-1566.

Cassata, W. S., Singer, B. S., and Cassidy, J., 2008, Laschamp and Mono Lake geomagnetic excursions recorded in New Zealand: Earth and Planetary Science Letters, v. 268, no. 1–2, p. 76-88.

Cassata, W. S., Singer, B. S., Liddicoat, J. C., and Coe, R. S., 2010, Reconciling discrepant chronologies for the geomagnetic excursion in the Mono Basin, California: Insights from new 40Ar/39Ar dating experiments and a revised relative paleointensity correlation: Quaternary Geochronology, v. 5, no. 5, p. 533-543.

Channell, J., 2006a, Late Brunhes polarity excursions (Mono Lake, Laschamp, Iceland Basin and Pringle Falls) recorded at ODP Site 919 (Irminger Basin): Earth and Planetary Science Letters, v. 244, no. 1-2, p. 378-393.

Channell, J. E. T., 2006b, Late Brunhes polarity excursions (Mono Lake, Laschamp, Iceland Basin and Pringle Falls) recorded at ODP Site 919 (Irminger Basin): Earth and Planetary Science Letters, v. 244, no. 1–2, p. 378-393.

Channell, J. E. T., Hodell, D. A., and Curtis, J. H., 2012, ODP Site 1063 (Bermuda Rise) revisited: Oxygen isotopes, excursions and paleointensity in the Brunhes Chron: Geochemistry, Geophysics, Geosystems, v. 13, no. 2, p. n/a-n/a.

Charles, C. D., LynchStieglitz, J., Ninnemann, U. S., and Fairbanks, R. G., 1996, Climate connections between the hemisphere revealed by deep sea sediment core ice core correlations: Earth and Planetary Science Letters, v. 142, p. 19-27.

Chiu, T.-C., Fairbanks, R. G., Cao, L., and Mortlock, R. A., 2007, Analysis of the atmospheric ^{14}C record spanning the past 50,000 years derived from high-precision $^{230}Th/^{234}U/^{238}U$, $^{231}Pa/^{235}U$ and ^{14}C dates on fossil corals: Quaternary Science Reviews, v. 26, no. 1-2, p. 18-36.

Chiu, T.-c., Fairbanks, R. G., Mortlock, R. A., and Bloom, A. L., 2005, Extending the radiocarbon calibration beyond 26,000 years before present using fossil corals: Quaternary Science Reviews, v. 24, no. 16-17, p. 1797-1808.

Chiu, T.-C., Fairbanks, R. G., Mortlock, R. A., Cao, L., Fairbanks, T. W., and Bloom, A. L., 2006, Redundant $^{230}Th/^{234}U/^{238}U$, $^{231}Pa/^{235}U$ and ^{14}C dating of fossil corals for accurate radiocarbon age calibration: Quaternary Science Reviews, v. 25, no. 17-18, p. 2431-2440.

Coe, R. S., Gromme, S., and Mankinen, E. A., 1978, Geomagnetic Paleointensities from Radiocarbon-Dated Lava Flows on Hawaii and the Question of the Pacific Nondipole Low: Journal of Geophysical Research, v. 83, p. 1740-1756.

Cox, S. E., Farley, K. A., and Hemming, S. R., 2012, Insights into the age of the Mono Lake Excursion and magmatic crystal residence time from (U-Th)/He and 230Th dating of volcanic allanite: Earth and Planetary Science Letters, v. 319–320, p. 178-184.

Cutler, K. B., Gray, S. C., Burr, G. S., Edwards, R. L., Taylor, F. W., Cabioch, G., Beck, J. W., Cheng, H., and Moore, J., 2004, Radiocarbon calibration and comparison to 50 kyr with paired ^{14}C and ^{230}Th dating of corals from Vanuatu and Papua New Guinea: Radiocarbon, v. 46, p. 1127-1160.

Dansgaard, W., Johnsen, S. J., Clausen, H. B., Dahl-Jensen, D., Gundestrup, N. S., Hammer, C. U., Hvidberg, C. S., Steffensen, J. P., Sveinbjornsdottir, A. E., Jouzel, J., and Bond, G., 1993, Evidence for general instability of past climate from a 250-kyr ice-core record: Nature, v. 364, no. 6434, p. 218-220.

Delaygue, G., Stocker, T. F., Joos, F., and Plattner, G.-K., 2003, Simulation of atmospheric radiocarbon during abrupt oceanic circulation changes: trying to reconcile models and reconstructions: Quaternary Science Reviews, v. 22, no. 15–17, p. 1647-1658.

Denton, G. H., Broecker, W. S., and Alley, R. B., 2006, The mystery interval 17.5 to 14.5 kyrs ago: PAGES NEWS, v. 14, no. 2, p. 14-16.

Durand, N., Deschamps, P., Bard, E., Hamelin, B., Camoin, G., Thomas, A. L., Henderson, G. M., Yokoyama, Y., and Matsuzaki, H., 2013, Comparison of ^{14}C and U-Th ages in corals form IODP #310 cores offshore Tahiti: Radiocarbon, v. 55, no. 2, p. 1-26.

Edwards, R. L., Beck, J. W., Burr, G. S., Donahue, D. J., Chappell, J. M. A., Bloom, A. L., Druffel, E. R. M., and Taylor, F. W., 1993, A Large Drop in Atmospheric $^{14}C/^{12}C$ and Reduced Melting in the Younger Dryas, Documented with ^{230}Th Ages of Corals: Science, v. 260, no. 5110, p. 962-968.

Elsasser, W., Ney, E. P., and Winckler, J. R., 1956, Cosmic-ray intensity and geomagnetism: Nature, v. 178, p. 1226-1227.

Fairbanks, R. G., Mortlock, R. A., Chiu, T.-C., Cao, L., Kaplan, A., Guilderson, T. P., Fairbanks, T. W., Bloom, A. L., Grootes, P. M., and Nadeau, M.-J., 2005, Radiocarbon calibration curve spanning 0 to 50,000 years BP based on paired $^{230}Th/^{234}U/^{238}U$ and ^{14}C dates on pristine corals: Quaternary Science Reviews, v. 24, no. 16-17, p. 1781-1796.

Finkel, R. C., and Nishiizumi, K., 1997, Beryllium 10 concentrations in the Greenland Ice Sheet Project 2 ice core from 3–40 ka: Journal of Geophysical Research: Oceans, v. 102, no. C12, p. 26699-26706.

Friedrich, M., Remmele, S., Kromer, B., Hofmann, J., Spurk, M., Kaiser, F., Orcel, C., and Küppers, M., 2004, The 12,460-year Hohenheim oak and pine tree-ring chronology from Central Europe - a unique annual record for radiocarbon calibration and paleoenvironment reconstructions: Radiocarbon, v. 46, no. 3, p. 1111-1122.

Gallup, C. D., Edwards, R. L., and Johnson, R. G., 1994, The Timing of High Sea Levels Over the Past 200,000 Years: Science, v. 263, no. 5148, p. 796-800.

Gillot, P. Y., Labeyrie, J., Laj, C., Valladas, G., Guérin, G., Poupeau, G., and Delibrias, G., 1979, Age of the Laschamp paleomagnetic excursion revisited: Earth and Planetary Science Letters, v. 42, no. 3, p. 444-450.

Godwin, H., 1962, Half-life of radiocarbon: Nature, v. 195, no. 4845, p. 984.

Gubbins, D., 1999, The distinction between geomagnetic excursions and reversals: Geophysical Journal International, v. 137, no. 1, p. F1-F3.

Guillou, H., Singer, B. S., Laj, C., Kissel, C., Scaillet, S., and Jicha, B. R., 2004, On the age of the Laschamp geomagnetic excursion: Earth and Planetary Science Letters, v. 227, no. 3–4, p. 331-343.

Guyodo, Y., and Valet, J.-P., 1996, Relative variations in geomagnetic intensity from sedimentary records: the past 200,000 years: Earth and Planetary Science Letters, v. 143, no. 1–4, p. 23-36.

-, 1999, Global changes in intensity of the Earth's magnetic field during the past 800 kyr: Nature, v. 399, no. 6733, p. 249-252.

Hamelin, B., Bard, E., Zindler, A., and Fairbanks, R. G., 1991, $^{234}U/^{238}U$ mass spectrometry of corals: How accurate is the U-Th age of the last interglacial period?: Earth and Planetary Science Letters, v. 106, no. 1–4, p. 169-180.

Hammer, C. U., Clausen, H. B., and Tauber, H., 1986, Ice-core dating of the Pleistocen/Holocene Boundary applied to a calibration of the ^{14}C time scale: Radiocarbon, v. 28, no. 2A, p. 284-291.

Heaton, T. J., Bard, E., and Hughen, K., 2013, Elastic tie pointing- transferring chronlogies between records via a gaussian process : Radiocarbon, v. 55, no. 4, p. 1975-1997.

Hemming, S. R., 2004, Heinrich events: Massive late Pleistocene detritus layers of the North Atlantic and their global climate imprint: Reviews of Geophysics, v. 42, no. 1.

Hoffmann, D. L., Beck, J. W., Richards, D. A., Smart, P. L., Singarayer, J. S., Ketchmark, T., and Hawkesworth, C. J., 2010, Towards radiocarbon calibration beyond 28ka using speleothems from the Bahamas: Earth and Planetary Science Letters, v. 289, no. 1-2, p. 1-10.

Hua, Q., Barbetti, M., Fink, D., Kaiser, K. F., Friedrich, M., Kromer, B., Levchenko, V. A., Zoppi, U., Smith, A. M., and Bertuch, F., 2009, Atmospheric ^{14}C variations derived from tree rings during the early Younger Dryas: Quaternary Science Reviews, v. 28, no. 25-26, p. 2982-2990.

Hughen, K., Lehman, S., Southon, J., Overpeck, J., Marchal, O., Herring, C., and Turnbull, J., 2004a, ^{14}C Activity and Global Carbon Cycle Changes over the Past 50,000 Years: Science, v. 303, no. 5655, p. 202-207.

Hughen, K., Southon, J., Bertrand, C., Frantz, B., and Zermeño, P., 2004b, Cariaco Basin calibration update: revisions to calendar and ^{14}C chronologies for core PL07-58PC: Radiocarbon, v. 46.

Hughen, K., Southon, J., Lehman, S., Bertrand, C., and Turnbull, J., 2006, Marine-derived ^{14}C calibration and activity record for the past 50,000 years updated from the Cariaco Basin: Quaternary Science Reviews, v. 25, no. 23-24, p. 3216-3227.

Hughen, K. A., Overpeck, J. T., Lehman, S. J., Kashgarian, M., Southon, J., Peterson, L. C., Alley, R., and Sigman, D. M., 1998, Deglacial changes in ocean circulation from an extended radiocarbon calibration: Nature, v. 391, no. 6662, p. 65-68.

Jenks, G. H., and Sweeton, F. H., 1952, Calorimetric Determination of the Relationship between the Half-Life and Average Beta-Energy of C^{14}: Physical Review v. 86, p. 803-804.

Kent, D. V., Hemming, S. R., and Turrin, B. D., 2002, Laschamp Excursion at Mono Lake?: Earth and Planetary Science Letters, v. 197, no. 3–4, p. 151-164.

Key, R. M., Kozyr, A., Sabine, C. L., Lee, K., Wanninkhof, R., Bullister, J. L., Feely, R. A., Millero, F. J., Mordy, C., and Peng, T. H., 2004, A global ocean carbon climatology: Results from Global Data Analysis Project (GLODAP): Global Biogeochem. Cycles, v. 18, no. 4, p. GB4031.

Kissel, C., Guillou, H., Laj, C., Carracedo, J. C., Nomade, S., Perez-Torrado, F., and Wandres, C., 2011, The Mono Lake excursion recorded in phonolitic lavas from Tenerife (Canary Islands): Paleomagnetic analyses and coupled K/Ar and Ar/Ar dating: Physics of the Earth and Planetary Interiors, v. 187, no. 3–4, p. 232-244.

Knudsen, M. F., Riisager, P., Donadini, F., Snowball, I., Muscheler, R., Korhonen, K., and Pesonen, L. J., 2008, Variations in the geomagnetic dipole moment during the Holocene and the past 50 kyr: Earth and Planetary Science Letters, v. 272, no. 1-2, p. 319-329.

Kromer, B., Friedrich, M., Hughen, K. A., Kaiser, F., Remmele, S., Schaub, M., and Talamo, S., 2004, Late Glacial ^{14}C Ages From a Floating, 1382-Ring Pine Chronology: Radiocarbon, v. 46, no. 3, p. 1203-1209.

Laj, C., Kissel, C., and Beer, J., 2004, High Resolution Global Paleointensity Stack Since 75 kyr (GLOPIS-75) Calibrated to Absolute Values: Geophysical Monograph Series, v. 145, p. 255-265.

Laj, C., Kissel, C., Mazaud, A., Channell, J., and Beer, J., 2000, North Atlantic paleointensity stack since 75 ka (NAPIS-75) and the duration of the Laschamp Event: Royal Society of London, v. 358, p. 1009-1025.

Lal, D., 1988, Theoretically expected variations in the terrestrial cosmicray production rates of isotope *in* Castagnoli, G. C., ed., Solar–Terrestrial Relationships and the Earth Environment in the Last Millennia: Amsterdam, NY, North-Holland.

Lal, D., and Charles, C., 2007, Deconvolution of the atmospheric radiocarbon record in the last 50,000 years: Earth and Planetary Science Letters, v. 258, no. 3–4, p. 550-560.

Lascu, I., Feinberg, J. M., Dorale, J. A., Cheng, H., and Edwards, R. L., 2016, Age of the Laschamp excursion determined by U-Th dating of a speleothem geomagnetic record from North America: Geology.

Levitus, S., and Boyer, T. P., 1994, World Atlas.

Libby, W. F., 1955, Radiocarbon Dating 2nd Edition, Chicago, Illinois, University of Chicago Press.

Liddicoat, J. C., 1992, Mono Lake Excursion in Mono Basin, California, and at Carson Sink and Pyramid Lake, Nevada: Geophysical Journal International, v. 108, no. 2, p. 442-452.

Liddicoat, J. C., 1996, Mono Lake Excursion In the Lahontan Basin, Nevada: Geophysical Journal International, v. 125, no. 2, p. 630-635.

Liddicoat, J. C., and Coe, R. S., 1979, Mono Lake geomagnetic excursion: Journal of Geophysical Research: Solid Earth, v. 84, no. B1, p. 261-271.

Marchitto, T. M., Lehman, S. J., Ortiz, J. D., Fluckiger, J., and van Geen, A., 2007, Marine radiocarbon evidence for the mechanism of deglacial atmospheric CO_2 rise: Science, v. 316, no. 5830, p. 1456-1459.

Martinson, D. G., Pisias, N. G., Hays, J. D., Imbrie, J., Moore Jr, T. C., and Shackleton, N. J., 1987, Age dating and the orbital theory of the ice ages: Development of a high-resolution 0 to 300,000-year chronostratigraphy: Quaternary Research, v. 27, no. 1, p. 1-29.

Members, E. C., 2006, One-to-one coupling of glacial climate variability in Greenland and Antarctica: Nature, v. 444, no. 7116, p. 195-198.

Mortlock, R. A., Fairbanks, R. G., Chiu, T.-c., and Rubenstone, J., 2005, $^{230}Th/^{234}U/^{238}U$ and $^{231}Pa/^{235}U$ ages from a single fossil coral fragment by multi-collector magnetic-sector inductively coupled plasma mass spectrometry: Geochimica et Cosmochimica Acta, v. 69, no. 3, p. 649-657.

Muscheler, R., Beer, J., Kubik, P. W., and Synal, H. A., 2005, Geomagnetic field intensity during the last 60,000 years based on ^{10}Be and ^{36}Cl from the Summit ice cores and ^{14}C: Quaternary Science Reviews, v. 24, no. 16-17, p. 1849-1860.

Muscheler, R., Beer, J., Wagner, G., Laj, C., Kissel, C., Raisbeck, G. M., Yiou, F., and Kubik, P. W., 2004, Changes in the carbon cycle during the last deglaciation as indicated by the comparison of ^{10}Be and ^{14}C records: Earth and Planetary Science Letters, v. 219, no. 3-4, p. 325-340.

Pahnke, K., and Zahn, R., 2005, Southern Hemisphere Water Mass Conversion Linked with North Atlantic Climate Variability: Science, v. 307, no. 5716, p. 1741-1746.

Paterne, M., Ayliffe, L., Arnold, M., Cabioch, G., Tisnérat-Laborde, N., C., H., E., D., and Bard, E., 2004, Paired ^{14}C and $^{230}Th/U$ dating of surface corals from the Marquesas and Vanuata (Sub-Equatorial Pacific) in the 3000 to 15,000 cal yr Interval: Radiocarbon, v. 46, p. 551-566.

Peltier, W. R., and Fairbanks, R. G., 2006, Global glacial ice volume and Last Glacial Maximum duration from an extended Barbados sea level record: Quaternary Science Reviews, v. 25, no. 23-24, p. 3322-3337.

Peterson, L. C., Haug, G. H., Hughen, K. A., and Röhl, U., 2000, Rapid Changes in the Hydrologic Cycle of the Tropical Atlantic During the Last Glacial: Science, v. 290, no. 5498, p. 1947-1951.

Piotrowski, A. M., Goldstein, S. L., Hemming, S. R., and Fairbanks, R. G., 2004, Intensification and variability of ocean thermohaline circulation through the last deglaciation: Earth and Planetary Science Letters, v. 225, no. 1–2, p. 205-220.

Ramsey, C. B., Staff, R. A., Bryant, C. L., Brock, F., Kitagawa, H., van der Plicht, J., Schlolaut, G., Marshall, M. H., Brauer, A., Lamb, H. F., Payne, R. L., Tarasov, P. E., Haraguchi, T., Gotanda, K., Yonenobu, H., Yokoyama, Y., Tada, R., and Nakagawa, T., 2012, A Complete Terrestrial Radiocarbon Record for 11.2 to 52.8 kyr B.P: Science, v. 338, no. 6105, p. 370-374.

Ravelo, A. C., Fairbanks, R. G., and Philander, S. G. H., 1990, Reconstructing tropical Atlantic hydrography using planktontic foraminifera and an ocean model: Paleoceanography, v. 5, no. 3, p. 409-431.

Reimer, P. B., Baillie, M. G. L., Bard, E., Bayliss, A., Beck, J. W., Blackwell, P. G., Bronk Ramsey, C., Buck, C. E., Burr, G. S., Edwards, R. L., Friedrich, M., Grootes, P. M., Guilderson, T. P., Hajdas, I., Heaton, T., Hogg, A. G., Hughen, K., Kaiser, F., Kromer, B., McCormac, G., Manning, S., Reimer, R. W., Richards, D. A., Southon, J., Talamo, S., Turney, C., van der Plicht, J., and Weyhenmeyer, C. E., 2009, IntCal09 and Marine09 Radiocarbon Age Calibration Curves, 0–50,000 Years cal BP: Radiocarbon, v. 51, p. 1111-1150.

Reimer, P. B., Bard, E., Bayliss, A., Beck, J. W., Blackwell, P. G., Bronk Ramsey, C., Buck, C. E., Cheng, H., Edwards, R. L., Friedrich, M., Grootes, P. M., Guilderson, T. P., Haflidason, H., Hajdas, I., Hatte, C., Heaton, T., Hoffmann, D. L., Hogg, A. G., Hughen, K., Kaiser, F., Kromer, B., Manning, S., Niu, M., Reimer, R. W., Richards, D. A., Scott, E. M., Southon, J., Staff, R. A., Turney, C.,

and van der Plicht, J., 2013a, IntCal13 and Marine13 Radiocarbon Age Calibration Curves 0-50,000 years Cal BP: Radiocarbon, v. 55, no. 4, p. 1869-1887.

Reimer, P. J., Bard, E., Bayliss, A., Beck, J. W., Blackwell, P. G., Bronk Ramsey, C., Brown, D. M., Buck, C. E., Edwards, L., Friedrich, M., Grootes, P. M., Guilderson, T. P., Haflidason, H., Hajdas, I., Hatte, C., Heaton, T., Hogg, A. G., Hughen, K., Kaiser, F., Kromer, B., Manning, S., Reimer, R. W., Richards, D. A., Scott, E. M., Southon, J., Turney, C., and van de Plicht, J., 2013b, Selection and Treatment of Data for Radiocarbon Calibration: an Update to the International Calibration (IntCal) Criteria: Radiocarbon, v. 55, no. 4, p. 1923-1945.

Roberts, M. L., and Southon, J., 2007, A preliminary determination of the absoluted $^{14}C/^{12}C$ ratio of OX-1A: Radiocarbon, v. 49, no. 2, p. 441-445.

Sauvet, G., 2016, Paleolithic culture behind the veil of chronology: Journal of Archaeological Science: Reports.

Schaub, M., Büntgen, U., Kaiser, K. F., Kromer, B., Talamo, S., Andersen, K. K., and Rasmussen, S. O., 2008, Lateglacial environmental variability from Swiss tree rings: Quaternary Science Reviews, v. 27, no. 1-2, p. 29-41.

Singer, B., Jicha, B., He, H., and Zhu, R., 40Ar/39Ar Evidence for a 17 ka Geomagnetic Field Excursion at Changbaishan Volcano, Northeastern China, *in* Proceedings AGU Fall Meeting Abstracts2011, Volume 1, p. 04.

Singer, B. S., 2014, A Quaternary geomagnetic instability time scale: Quaternary Geochronology, v. 21, no. 0, p. 29-52.

Singer, B. S., Guillou, H., Jicha, B. R., Laj, C., Kissel, C., Beard, B. L., and Johnson, C. M., 2009, $^{40}Ar/^{39}Ar$, K–Ar and $^{230}Th–^{238}U$ dating of the Laschamp excursion: A radioisotopic tie-point for ice core and climate chronologies: Earth and Planetary Science Letters, v. 286, no. 1-2, p. 80-88.

Southon, J., 2004, A Radiocarbon Perspective on Greenland Ice-Core Chronologies: Can we use Ice Cores for ^{14}C Calibration?: Radiocarbon, v. 46, p. 1239-1259.

Southon, J., Noronha, A. L., Cheng, H., Edwards, R. L., and Wang, Y., 2012, A high-resolution record of atmospheric ^{14}C based on Hulu Cave speleothem H82: Quaternary Science Reviews, v. 33, no. 0, p. 32-41.

Stansfield, K. L., Bowman, M. J., Fauria, S. J., and Wilson, T. C., 1995, Water mass and coastal current variability near Barbados, West Indies: Journal of Geophysical Research: Oceans, v. 100, no. C12, p. 24819-24830.

Stoner, J. S., Channell, J. E. T., Hodell, D. A., and Charles, C. D., 2003, A ~580 kyr paleomagnetic record from the sub-Antarctic South Atlantic (Ocean Drilling Program Site 1089): Journal of Geophysical Research: Solid Earth, v. 108, no. B5, p. n/a-n/a.

Stoner, J. S., Laj, C., Channell, J. E. T., and Kissel, C., 2002, South Atlantic and North Atlantic geomagnetic paleointensity stacks (0–80 ka): implications for inter-hemispheric correlation: Quaternary Science Reviews, v. 21, no. 10, p. 1141-1151.

Stuiver, M., and Braziunas, T. F., 1989, Atmospheric ^{14}C and century-scale solar oscillations: Nature, v. 338, no. 6214, p. 405-408.

Stuiver, M., and Polach, H., 1977, Discussion; Reporting of ^{14}C data: Radiocarbon, v. 19, p. 353-363.

Stuiver, M., and Quay, P. D., 1980, Changes in Atmospheric Carbon-14 Attributed to a Variable Sun: Science, v. 207, no. 4426, p. 11-19.

Svensson, A., Andersen, K. K., Bigler, M., Clausen, H. B., Dahl-Jensen, D., Davies, S. M., Johnsen, S. J., Muscheler, R., Parrenin, F., Rasmussen, S. O., Röthlisberger, R., Seierstad, I., Steffensen, J. P., and Vinther, B. M., 2008, A 60 000 year Greenland stratigraphic ice core chronology: Clim. Past, v. 4, no. 1, p. 47-57.

Teanby, N., Laj, C., Gubbins, D., and Pringle, M., 2002, A detailed palaeointensity and inclination record from drill core SOH1 on Hawaii: Physics of the Earth and Planetary Interiors, v. 131, no. 2, p. 101-140.

Turrin, B., Champion, D. E., Mortlock, R. A., Fairbanks, R. G., and Swisher, C. C., 2013, $^{40}Ar/^{39}Ar$ and U-series ages of a Late Pleistocene geomagnetic excursion in Western North America: The Hilina Pali event in Western North America? , AGU, Fall 2013, Volume GP31A-06: San Francisco.

Urmos, J. P., 1985, Oxygen isotopes, sea levels, and uplift of reef terraces, Araki Island, Vanuatu [M.S.: Cornell University, 123 p.

Wagner, G., Beer, J., Laj, C., Kissel, C., Masarik, J., Muscheler, R., and Synal, H. A., 2000, Chlorine-36 evidence for the Mono Lake event in the Summit GRIP ice core: Earth and Planetary Science Letters, v. 181, no. 1–2, p. 1-6.

Wagner, G., Beer, J., Masarik, J., Muscheler, R., Kubik, P. W., Mende, W., Laj, C., Raisbeck, G. M., and Yiou, F., 2001, Presence of the Solar de Vries Cycle (~205 years) during the Last Ice Age: Geophysical Research Letters, v. 28, no. 2, p. 303-306.

Wang, Y. J., Cheng, H., Edwards, R. L., An, Z. S., Wu, J. Y., Shen, C.-C., and Dorale, J. A., 2001, A High-Resolution Absolute-Dated Late Pleistocene Monsoon Record from Hulu Cave, China: Science, v. 294, no. 5550, p. 2345-2348.

Yokoyama, Y., Esat, T.M., Lambeck, K., Fifield, L.K., 2000, Last ice age millennial scale climate changes recorded in Huon Peninsula corals: Radiocarbon, v. 42, no. 3, p. 383-401.

Zimmerman, S. H., Hemming, S. R., Kent, D. V., and Searle, S. Y., 2006, Revised chronology for late Pleistocene Mono Lake sediments based on paleointensity correlation to the global reference curve: Earth and Planetary Science Letters, v. 252, no. 1–2, p. 94-106.

3.9 Figures and Tables

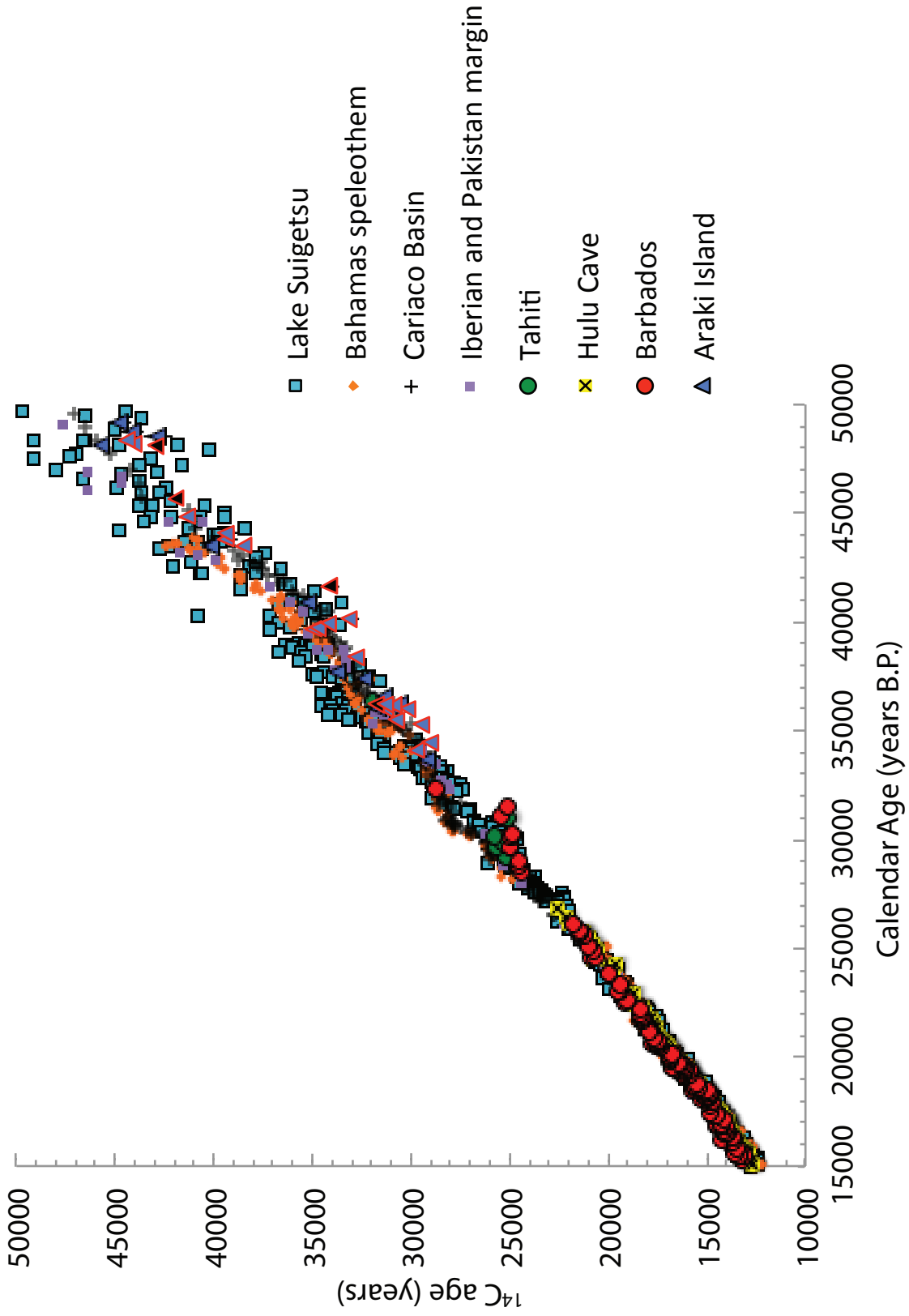
Lake Suigetsu
Bahamas speleothem
Cariaco Basin
Iberian and Pakistan margin
Tahiti
Hulu Cave
Barbados
Araki Island
14C age (years)
Calendar Age (years B.P.)
10000
15000
20000
25000
30000
35000
40000
45000
50000

Figure 3.1a: Comparison of marine reservoir corrected coral 14C age vs. calendar age (50 to 15 kyr BP) with calibration data from Cariaco Basin, Lake Suigetsu, Iberian and Pakistan Margins (Bard et al., 2013; Ramsey et al., 2012; Reimer et al., 2013a), Bahamas (Hoffmann et al., 2010) and China (Hulu Cave) speleothems (Southon et al., 2012), and Tahiti corals (Durand et al., 2013). Vertical error bars (Araki data only) are 2 s.d. Araki samples with concordant U-Th and U-Pa ages are blue triangles outlined in red. Barbados samples concordant U-Th and U-Pa ages are red dots outlined in blue. Araki corals failing to pass the test of concordancy (Mortlock et al., 2005) are black triangles outlined in red.

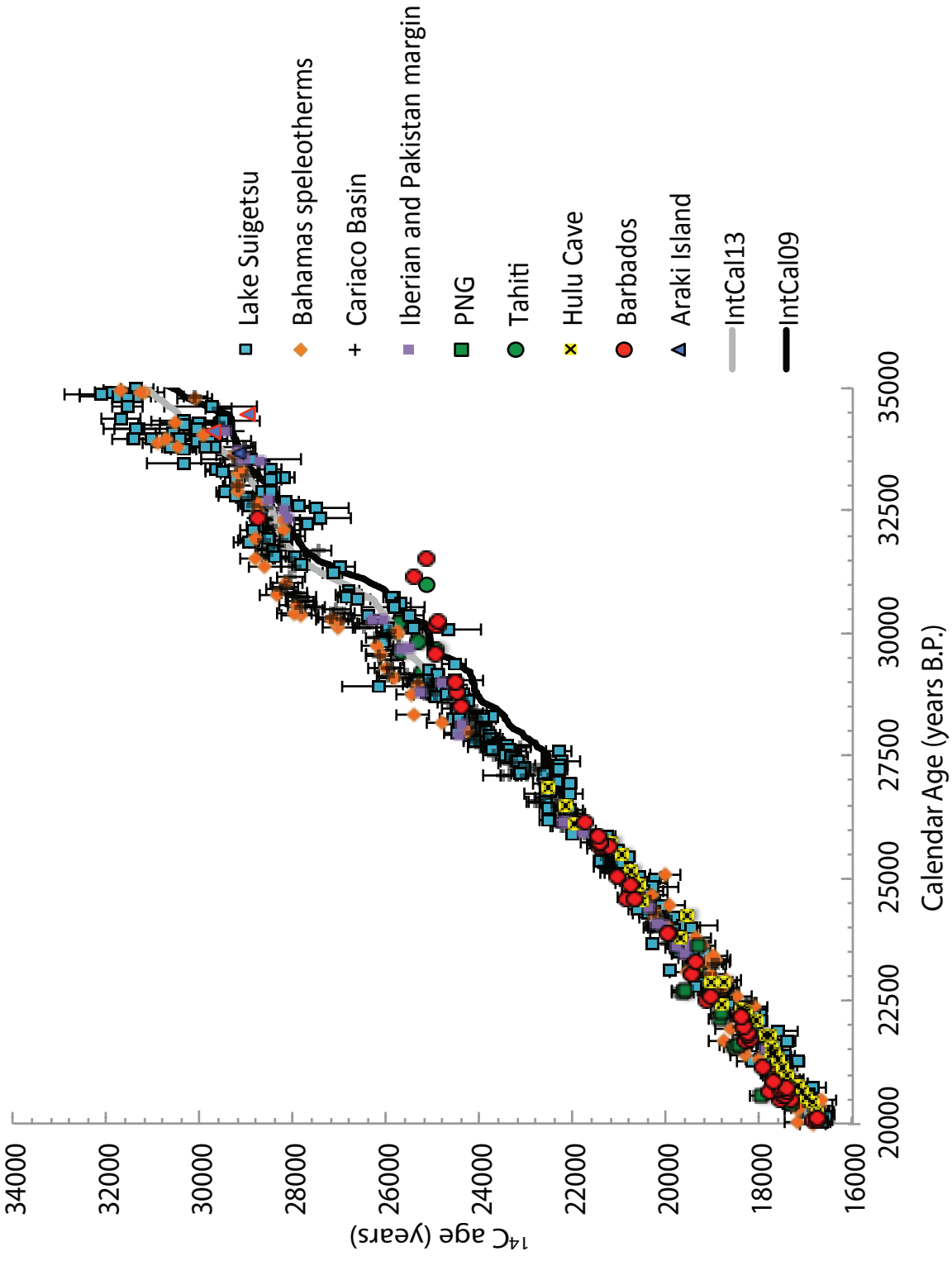
Lake Suigetsu
Bahamas speleotherms
Cariaco Basin
Iberian and Pakistan margin
PNG
Tahiti
Hulu Cave
Barbados
Araki Island
IntCal13
IntCal09
34000
32000
30000
28000
26000
24000
22000
20000
18000
16000
14C age (years)
20000
22500
25000
27500
30000
32500
35000
Calendar Age (years B.P.)

Figure 3. 1b: Expanded 35 to 20 kyr BP interval. Same data and symbols as in Figure 3.1a. Additional coral data from Papua New Guinea (Cutler et al., 2004). Intcal09 and Intcal13 curves in black and gray, respectively. 1 s.d. errors are represented by vertical lines or are smaller than the size of the data point (e.g. Araki, Barbados, and Tahiti corals, Hulu Cave speleothem).

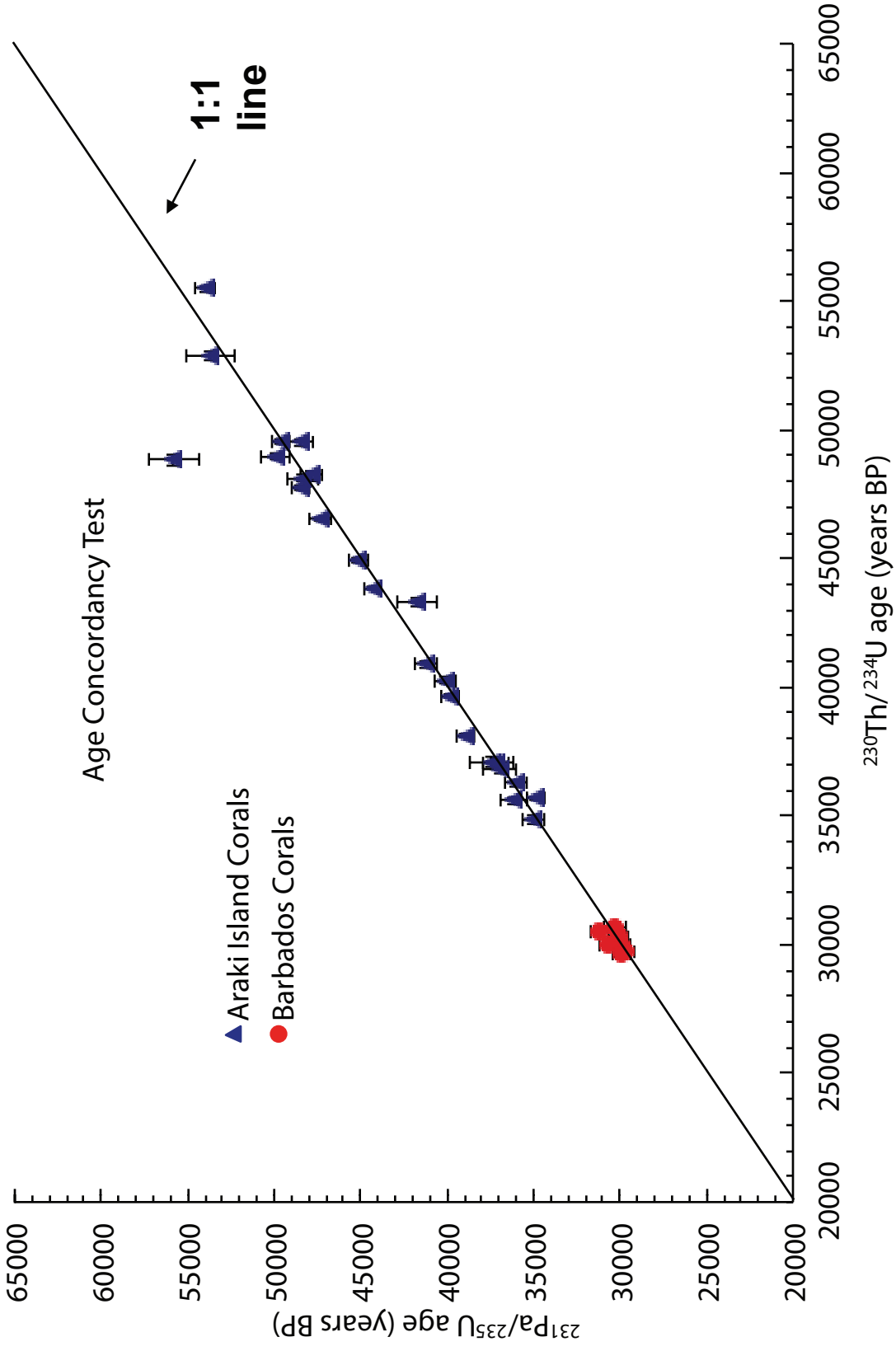
Age Concordancy Test
1:1 line
Araki Island Corals
Barbados Corals
$^{231}Pa/^{235}U$ age (years BP)
$^{230}Th/^{234}U$ age (years BP)
20000
25000
30000
35000
40000
45000
50000
55000
60000
65000

Figure 3. 2: U-Th age vs. U-Pa age for Barbados and Araki Island coral (this study; Chiu et al., 2007; Chiu et al., 2006; Mortlock et al., 2005). Vertical error bars represent 2-sigma errors. Horizontal error bars are smaller than the size of the data symbol.

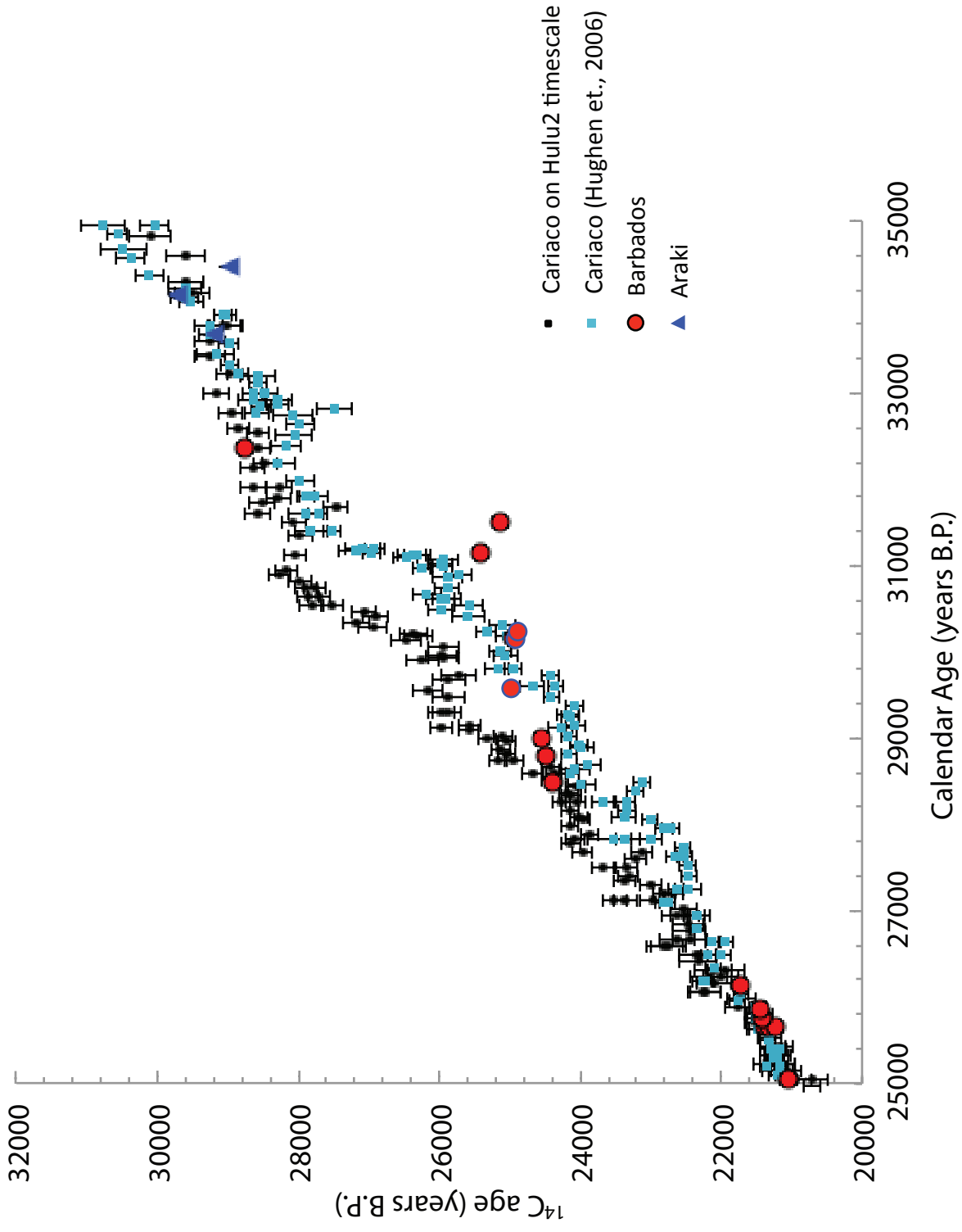
Cariaco on Hulu2 timescale
Cariaco (Hughen et., 2006)
Barbados
Araki
14C age (years B.P.)
Calendar Age (years B.P.)
20000
22000
24000
26000
28000
30000
32000
25000
27000
29000
31000
33000
35000

Figure 3.3: Barbados and Araki corals (35 to 25 kyr BP) plotted with Cariaco Basin sediments based on Hulu2 (Reimer et al., 2013a) and Hulu (Hughen et al., 2006) age models. 1 s.d. errors are represented by vertical lines or are smaller than the size of the data point.

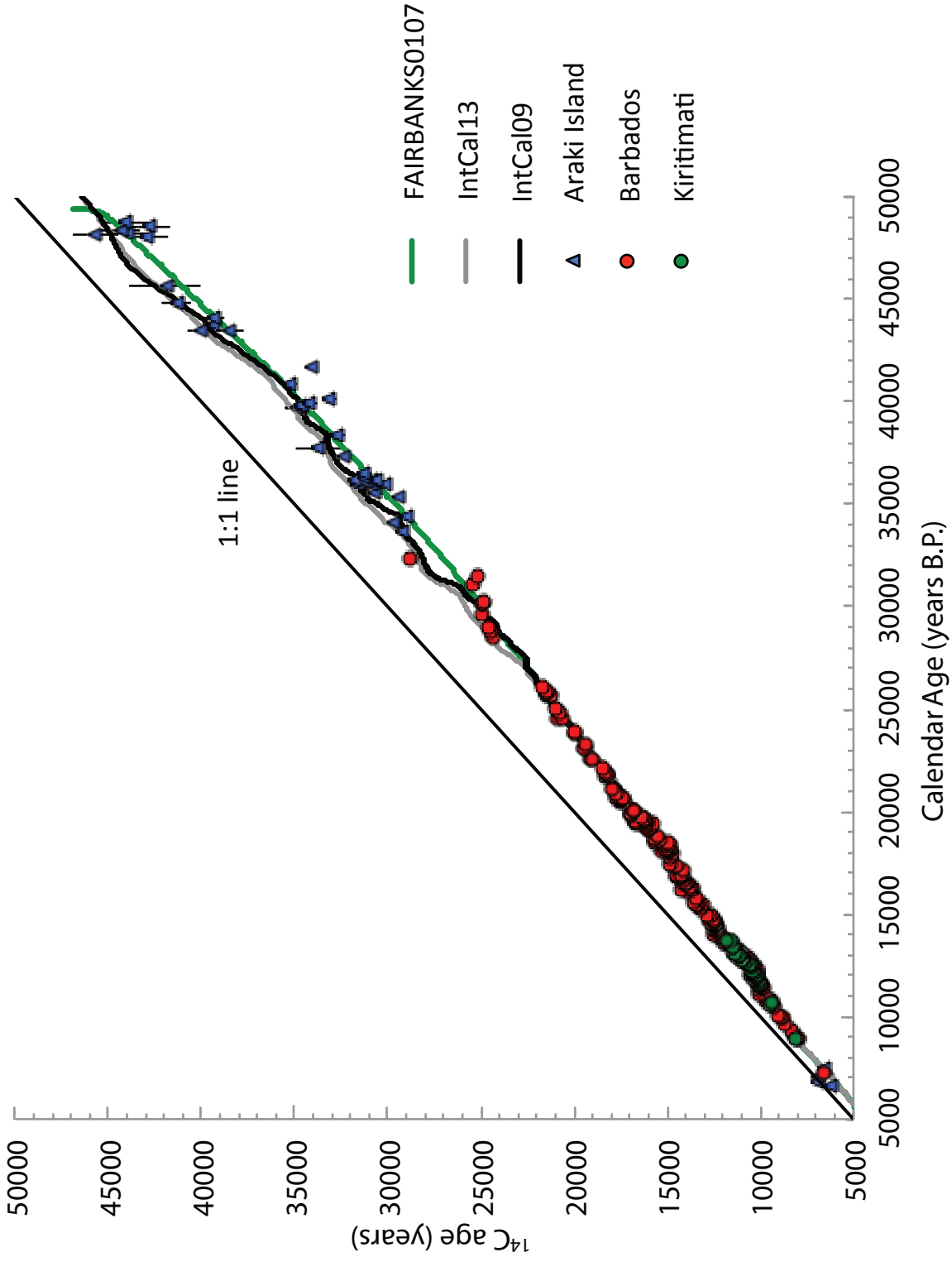
FAIRBANKS0107
IntCal13
IntCal09
Araki Island
Barbados
Kiritimati
1:1 line
^{14}C age (years)
Calendar Age (years B.P.)
5000
10000
15000
20000
25000
30000
35000
40000
45000
50000

Figure 3.4: Coral calibration curve of FAIRBANKS0107 (green line) with all coral data (50 to 5 kyr BP) plotted with 2 s.d. error bars. IntCal13 (Reimer et al., 2013a) and IntCal09 (Reimer et al., 2009) calibration curves in gray and black, respectively.

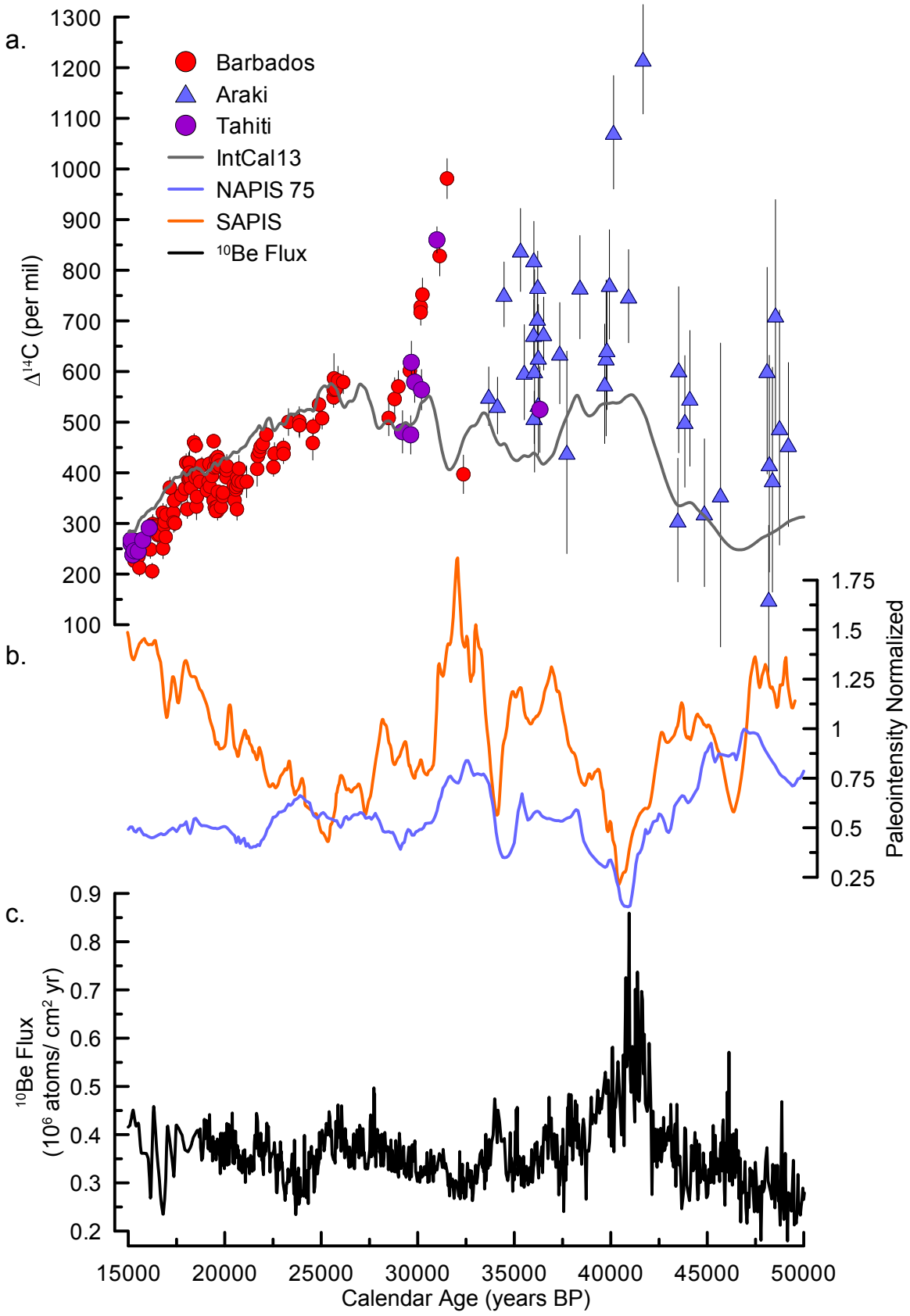
a.
b.
c.
Barbados
Araki
Tahiti
IntCal13
NAPIS 75
SAPIS
10Be Flux
Δ14C (per mil)
Paleointensity Normalized
10Be Flux
(10^6 atoms/ cm^2 yr)
Calendar Age (years BP)
1300
1200
1100
1000
900
800
700
600
500
400
300
200
100
1.75
1.5
1.25
1
0.75
0.5
0.25
0.9
0.8
0.7
0.6
0.5
0.4
0.3
0.2
15000
20000
25000
30000
35000
40000
45000
50000

Figure 3.5: (a) $\Delta^{14}C$ based on Araki, Barbados, and Tahiti corals (Durand et al., 2013) compared with IntCal13 (Reimer et al., 2013a) atmospheric curve (gray line). Vertical lines represent 2 s.d. (b) SAPIS (orange line) and NAPIS-75 (blue line) stacked relative paleointensity records (Stoner et al., 2002). (c) ^{10}Be flux (black line) from GISP2 and GRIP ice cores (Muscheler et al., 2005) based on the GICC05 time scale (Svensson et al., 2008). Note the paleointensity minimum and peak in ^{10}Be flux at 41 kyr BP corresponds to the Laschamp excursion.

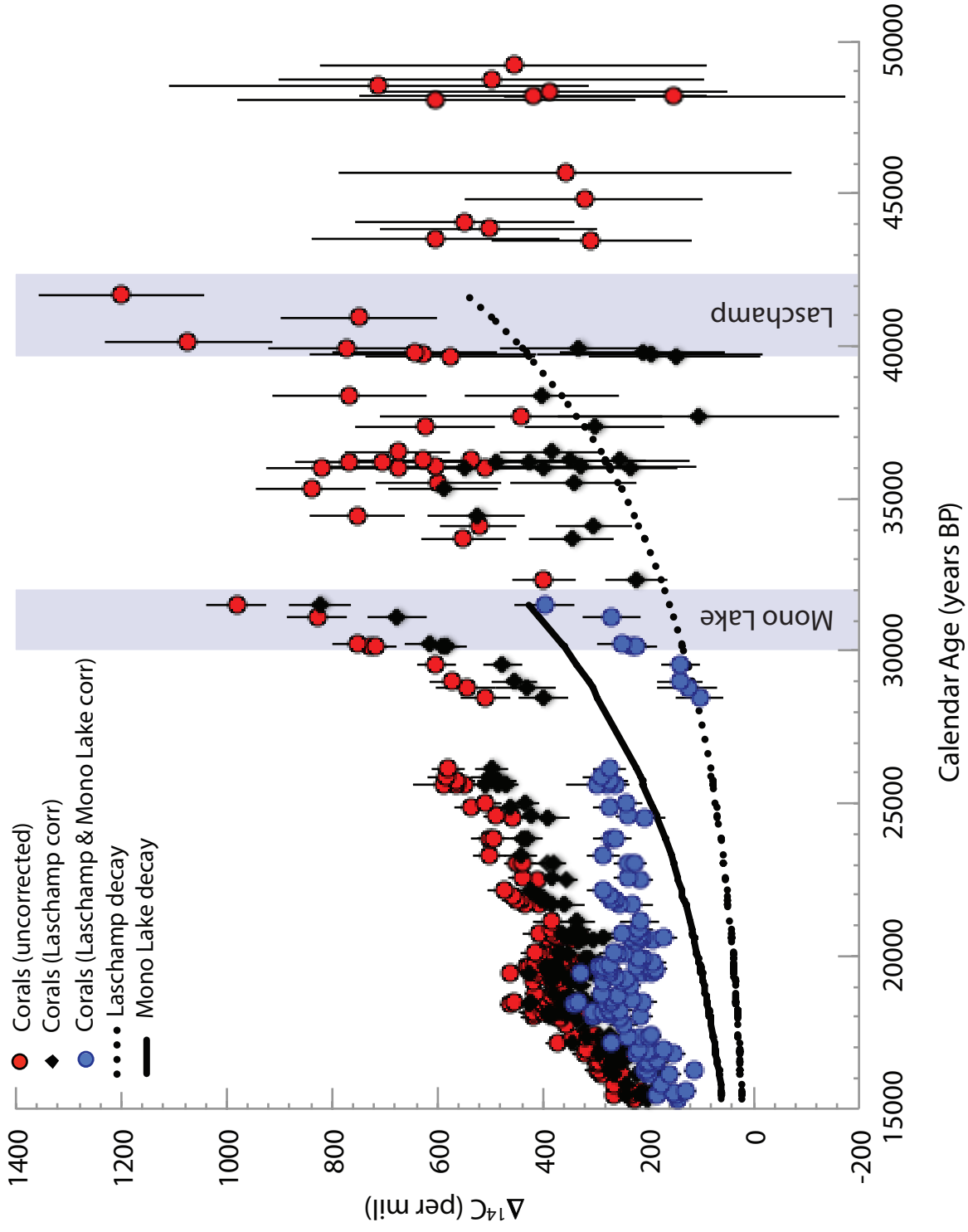
Corals (uncorrected)
Corals (Laschamp corr)
Corals (Laschamp & Mono Lake corr)
Laschamp decay
Mono Lake decay
Mono Lake
Laschamp
Δ14C (per mil)
Calendar Age (years BP)
1400
1200
1000
800
600
400
200
0
-200
15000
20000
25000
30000
35000
40000
45000
50000

Figure 3.6: Raw (i.e. uncorrected) coral $\Delta^{14}C$ (red dots), and $\Delta^{14}C$ recalculated after corrections for Laschamp (black diamond) and Mono Lake Excursions (blue dots). Vertical error bars are 2 s.d. and include a 0.000042 FMC blank uncertainty propagated through the calculation of the $\Delta^{14}C$ error. Dotted black line is the modeled decay of Laschamp and the solid black line is the modeled decay of Mono Lake. Shaded areas represent estimated duration of the Laschamp (Lascu et al., 2016) and Mono Lake (this study) excursions.

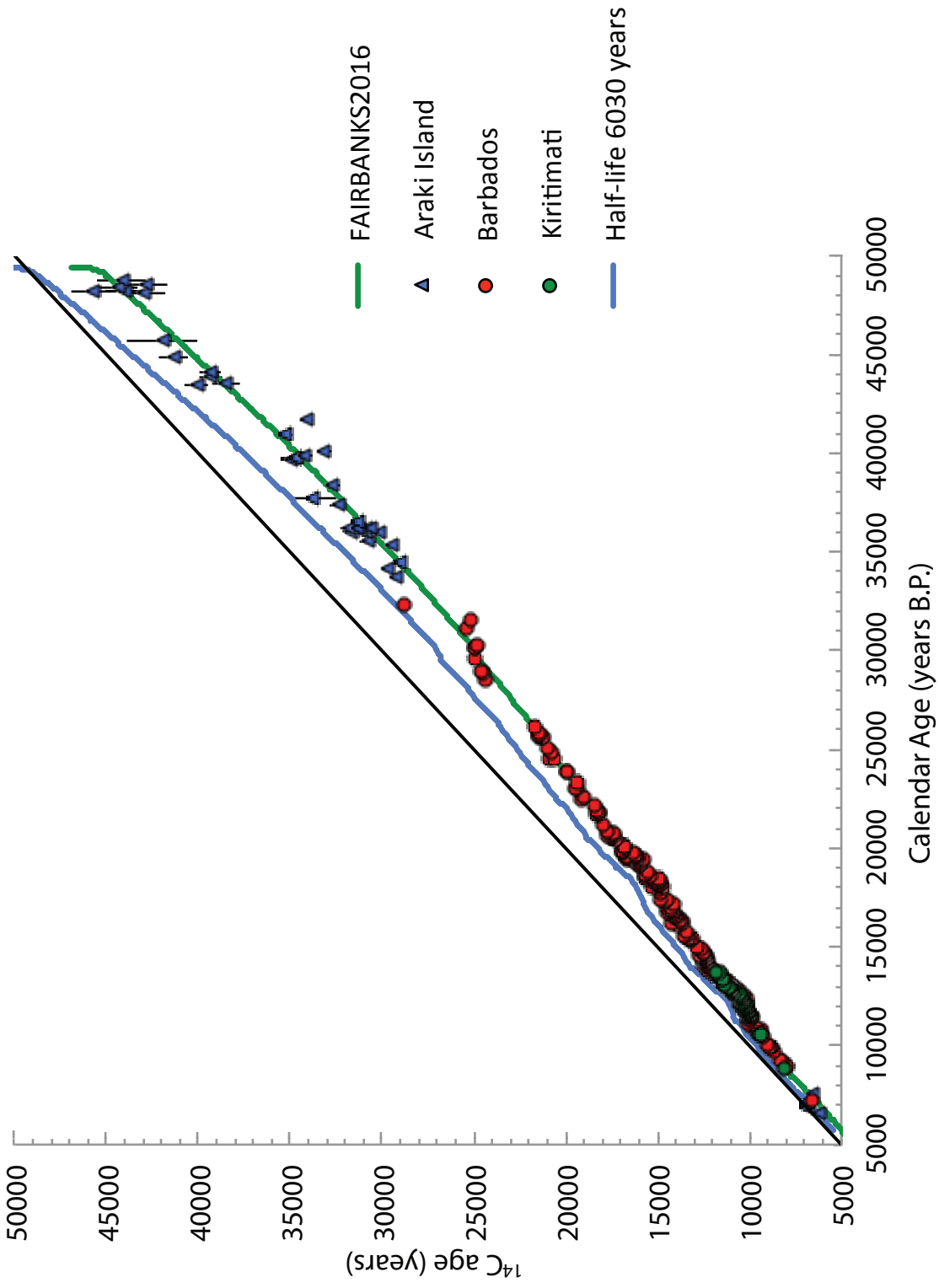
FAIRBANKS2016
Araki Island
Barbados
Kiritimati
Half-life 6030 years
^{14}C age (years)
Calendar Age (years B.P.)
5000
10000
15000
20000
25000
30000
35000
40000
45000
50000

Figure 3.7a: Coral calibration curve of FAIRBANKS0107 (green line) plotted with all coral data (50 to 5 kyr BP). Vertical error bars are 2 s.d. 1:1 line added for reference. FAIRBANKS0107 curve re-plotted (blue line) using ^{14}C half-life of 6030 years (Jenks and Sweeton, 1952).

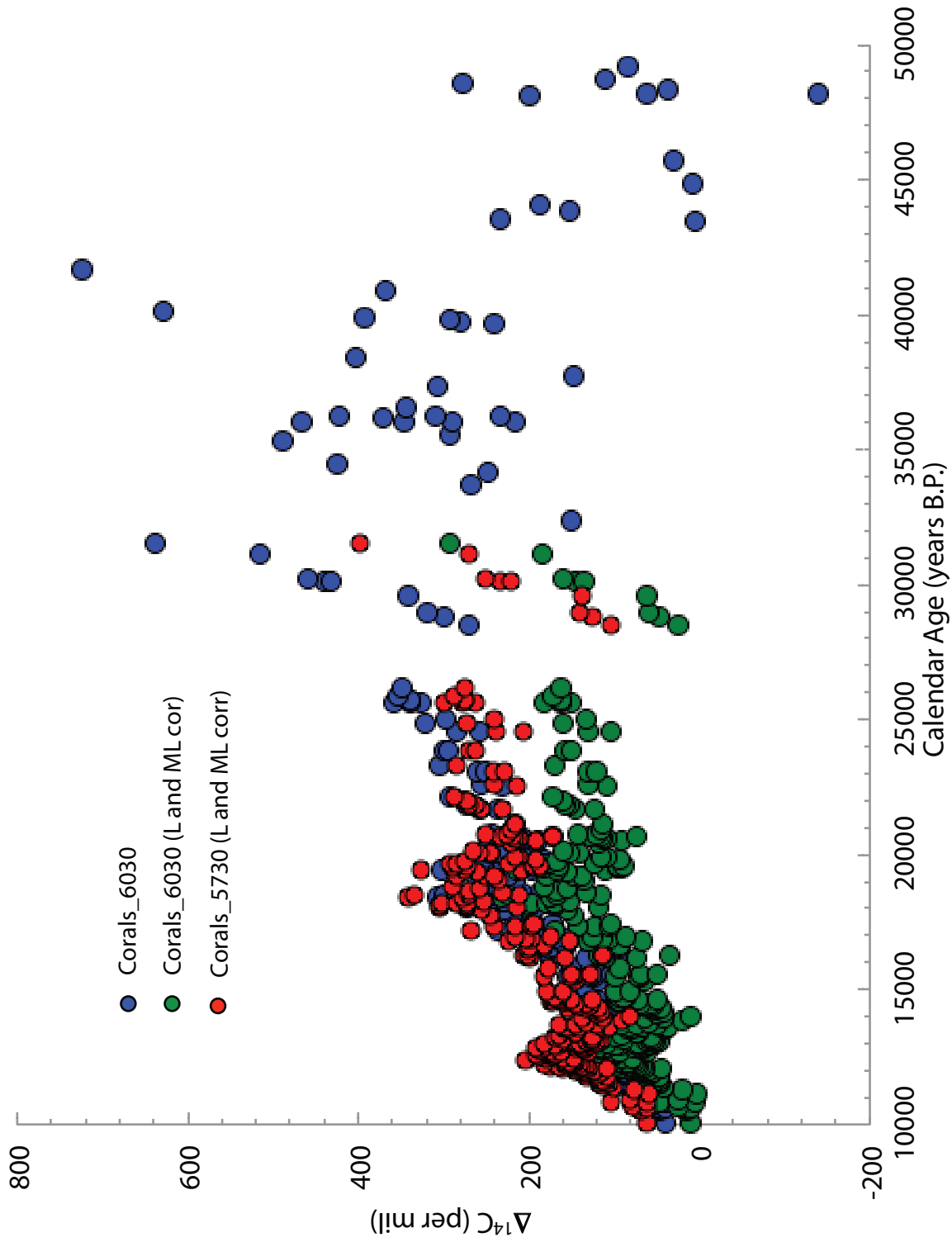
Corals_6030
Corals_6030 (L and ML cor)
Corals_5730 (L and ML corr)
Δ14C (per mil)
800
600
400
200
0
-200
10000
15000
20000
25000
30000
35000
40000
45000
50000
Calendar Age (years B.P.)

Figure 3.7b: Coral $\Delta^{14}C$ and residual (Laschamp and Mono Lake corrected) $\Delta^{14}C$ recalculated using the 6030 year half-life (Jenks and Sweeton, 1952) for comparison to residual $\Delta^{14}C$ calculated using the consensus half-life of 5730 years (Godwin, 1962).

Hilina Pali	**Age (kyr BP)**	**Duration (kyr)**	**Method**
This study	18.5 (1)	19.5 - 18	$\Delta^{14}C$
Singer et al. (2011)	17 (1)		$^{40}Ar/^{39}Ar$
Turrin et al. (2013)	17 (1)		$^{40}Ar/^{39}Ar$
Coe et al. (1978)	20		^{14}C
Mono Lake			
This study	31.5 (0.2)	32-30	$\Delta^{14}C$
Laj et al. (2004)	34		paleointensity
(Channell, 2006b)	33	34 -32	paleointensity
Cassata et al. (2008)	32		$^{40}Ar/^{39}Ar$
Kissel et al. (2011)	32	34-32	$^{40}Ar/^{39}Ar$, K/Ar
Laschamp			
This study	41.4 (0.35)		$\Delta^{14}C$
Guillou et al. (2004)	40.4 (2)		$^{40}Ar/^{39}Ar$, K/Ar
Laj et al. (2004)	40		paleointensity
Cassata et al. (2008)	41		$^{40}Ar/^{39}Ar$
Singer et al. (2009)	41		$^{40}Ar/^{39}Ar$
Channell et al. (2012)	40.8	0.5	paleointensity
Lascu et al. (2016)	41.1 (0.35)	42.25-39.70	Magnetic properties in U-Th dated speleothem

Table 3.1: Age estimates in dated magnetic excursions, as summarized in (Singer, 2014).

Chapter Four

Barbados $\Delta^{14}C$ record of deglacial ocean ventilation

4.1 Abstract

The relative concentration of ^{14}C in the atmosphere ($\Delta^{14}C$) is a balance between production, the fluxes into and out of the deep-ocean and fluxes into and out of other large carbon reservoirs. Estimates of $\Delta^{14}C$ indicate a rather steady ^{14}C decline in the atmosphere for the past 40,000 years due to the long-term effects of a weaker geomagnetic field during the Laschamp (41 kyr BP) and Mono Lake Events (~32 kyr BP). Superimposed on this steady decline was an interval of rapidly changing $\Delta^{14}C$ between 17.5 kyr and 14 kyr BP that has been attributed to changes in deep ocean ventilation. In this chapter, I use paired U-Th and ^{14}C dated corals from Barbados to directly compute a marine-based record of $\Delta^{14}C$ from 22 to 13 kyr BP, independent of inter-hemispheric proxy/chronology correlations, to evaluate the possible role of changing atmosphere-deep ocean exchange in controlling the fluctuations from the long-term trend observed in $\Delta^{14}C$.

There is strong evidence from $\delta^{13}C$ of benthic foraminifera and water mass proxy tracer data sampled from an array of deep-sea cores for an increase in the production of NADW beginning at 14.5 kyr BP. A sharp decline in coral derived $\Delta^{14}C$ coincides with the proxy evidence for the switch 'on' of NADW during the last deglacial period and provides credible evidence to hypotheses linking changes in NADW production to changes in the ^{14}C content of the atmosphere.

More debatable is the evidence for a 190‰ decline in $\Delta^{14}C$ during the Mystery Interval (17.5 to 14.5 kyr BP) attributed to episodic ventilation of the deep ocean. The

Barbados coral data demonstrates that the Mystery Interval $\Delta^{14}C$ "event" is 1) an artifact of an incorrect age model applied to a Cariaco Basin sediment core used to compute $\Delta^{14}C$ in IntCal09 and 2) has been overestimated by failure to correct $\Delta^{14}C$ records for excess radiocarbon produced during the Laschamp and Mono Lake geomagnetic excursions. An increase in "corrected" $\Delta^{14}C_{LMcorr}$ beginning at 20 kyr BP may correlate with increased cosmogenic production during the Hilina Pali geomagnetic excursion.

Systematic offsets between corals and Hulu Cave (China) speleothem H82 $\Delta^{14}C$ data between 18 and 15 kyr BP are most likely due to local artifacts such as variable dead carbon and $^{230}Th_{initial}$ age corrections in the H82 record, as well as distance-age models and sample depth corrections, the extent of which may be obscured by the exceedingly slow and variable growth rate of the H82 specimen. Alternatively, attributing age offsets between corals and H82 during the Mystery Interval, entirely to marine reservoir corrections, requires sustained tropical Atlantic surface water ^{14}C age of 500 to 700 years. These conditions appear unlikely since a lowering in reservoir age at Barbados would be predicted with reduced NADW during the Mystery Interval, as has been similarly documented at the onset of the Younger Dryas.

4.2 Introduction

Variable North Atlantic Deep Water (NADW) production may be one of the key amplifiers of global climate change, enhancing the impact of Milankovitch's relatively small zonal radiation cycles. Project SPECMAP first demonstrated that, "*variations in 'North Atlantic' polar surface waters are highly coherent and in phase within the 95% confidence interval with deep-ocean $\delta^{13}C$ over 'Milankovitch' bands and at higher*

frequencies, suggesting a link between the deep and shallow North Atlantic circulation (Mix and Fairbanks, 1985). On shorter time scales and with greater dating accuracy and precision, abrupt changes in Northern Hemisphere climate during the most recent deglaciation, as interpreted in ice core and marine sediment records, are believed to coincide with changes in the production of NADW and atmospheric circulation patterns. Ocean models indicate that ice sheet meltwater may be a forcing mechanism for variable NADW as simulations of freshwater added to the surface ocean from retreating continental ice sheets impacted areas of deep-water formation in both Northern and Southern Hemispheres (Manabe and Stouffer, 1995; Weaver et al., 2003).

There are other proxy tracers of NADW circulation patterns, such as the Cd/Ca nutrient proxy (Boyle and Keigwin, 1987), εNd provenance tracer (Piotrowski et al., 2005), and Pa-Th scavenging tracer (McManus et al., 2004) that are compatible with $\delta^{13}C$ evidence but their discussions are beyond the scope of this chapter. Instead, the focus here is on carbon isotope tracers, exclusively; ^{12}C, ^{13}C and ^{14}C.

$\delta^{13}C$ records obtained from benthic foraminifera provide strong and geographically and oceanographically coherent evidence for changes in the relative fluxes of NADW Atlantic during deglaciation (Boyle and Keigwin, 1987; Charles and Fairbanks, 1992; Oppo and Fairbanks, 1987; Oppo et al., 1990). However, reconstructions of $\delta^{13}C$ and water mass gradients are sensitive to the selection of water mass end-member values, end-member mixing, oxidation and re-mineralization of organic material in the water column, and changes in carbon reservoirs that may also introduce dating errors in age models. In addition, the history of $\delta^{13}C$ in the Southern Ocean may not necessarily only reflect changes in the relative aging of water masses and

hence, in the strength of Atlantic Meridional Ocean Circulation (AMOC). For example, differences in the $\delta^{13}C$ between deep and intermediate depth waters in the Southern Ocean are strongly correlated to Northern Hemisphere climate records and the strength of the South East Asian Monsoon suggesting both are linked via the atmosphere to North Atlantic variability on millennial timescales (Charles et al., 2010), perhaps through the influence of sea ice on the positioning of the ITCZ. Finally, nearly uniform $\delta^{13}C$ values in Circumpolar Deep Water (CPW) and Antarctic Bottom Water (AABW) may render the tracer less suited for identifying changes in the relative fluxes of theses water masses during past ventilation events in the Southern Ocean.

On shorter time-scales radiocarbon (^{14}C) content of ocean water provides a less ambiguous tracer for estimating the age of a water mass as it provides a direct measure of the time of isolation since it was last in exchange with the contemporaneous atmosphere. In the modern ocean, a significant fraction of the ^{14}C produced in the atmosphere is entrained in North Atlantic Deep Water (NADW), where ^{14}C decays as NADW is slowly mixed with the world's deep ocean. In other locations, particularly the Southern Ocean, aged ^{14}C-depleted deep waters are returned to the surface ocean where exchange with the atmosphere lowers the ^{14}C content. Therefore, we expect that significant fluctuations in NADW production should be evident in the $^{14}C/^{12}C$ ratio of the atmosphere ($\Delta^{14}C$) or in a record of western tropical-ocean surface waters that are nearly equilibrated with the atmosphere. Here, we identify the role of changing atmosphere to deep ocean exchange using the ^{14}C tracer measured in surface corals of known age to better constrain the natural distortions of the radiocarbon clock (i.e., $\Delta^{14}C$) and to better understand the physics regulating the ^{14}C system. Of particular interest is the response of $\Delta^{14}C$ during

time intervals when ocean proxy records suggest episodic ventilation of the Southern Ocean, beginning around 17.5 kyr BP (the Mystery Interval) and a "turn on" of NADW at the time of the Bølling to Allerød transition (~14.5 kyr BP).

4.2.1 The Mystery Interval

The Mystery Interval (MI) is assigned the period ~ 17.5 to 14.5 kyr BP (Denton et al., 2006) and in ice core and marine sediment records corresponds to Heinrich Stadial 1 (Hemming, 2004). The MI is most often associated and/or defined by a 190‰ decrease in the atmospheric $^{14}C/^{12}C$ ratio ($\Delta^{14}C$) as computed from the IntCal09 radiocarbon calibration curve (Broecker, 2009; Reimer et al., 2009). The decline in $\Delta^{14}C$ from 17.5 to 14.5 kyr BP is not believed to be due to decreased production since the ^{14}C decrease is not accompanied by a parallel decrease in ^{10}Be accumulation recorded in ice cores (Finkel and Nishiizumi, 1997).

Because the ocean represents a much larger reservoir of carbon compared to the atmosphere, the decline in $\Delta^{14}C$ during the MI is generally attributed to the transfer of radiocarbon-depleted CO_2 from the deep ocean reservoir to the surface ocean and to the atmosphere (i.e., the ventilation hypothesis; Broecker and Barker, 2007). Indeed, a reconstruction of $\Delta^{14}C$ at intermediate water depth (700 m) in the eastern North Pacific (Baja) shows very large $\Delta^{14}C$ depletions (-450‰), relative to the contemporaneous atmosphere during the MI (Marchitto et al., 2007) and is often cited as the "smoking gun" for the ventilation hypothesis. The Baja record has subsequently been validated by $\Delta^{14}C$ records obtained from the Arabian Sea (Bryan et al., 2010) and eastern equatorial Pacific (Stott et al., 2009), showing even larger radiocarbon depletions during the MI. Large depletions in ocean $\Delta^{14}C$ at intermediate depths during the MI generally track a parallel

decline in atmospheric $\Delta^{14}C$ as reconstructed in IntCal09 (Reimer et al., 2009) and coincide with the rise in pCO_2 (Marcott et al., 2014; Monnin et al., 2001) and with increases in Southern Ocean upwelling (Anderson et al., 2009). Paired ^{14}C and U-series dated deep-sea corals from the Drake Passage also provide evidence for ^{14}C depleted Circumpolar Deep Water (CPDW) prior to 18 kyr BP, followed by a Southern Ocean that was well-ventilated Southern Ocean by 14.5 kyr BP (Burke and Robinson, 2012) and U-Th dated deep-sea corals from the South Atlantic indicate ^{14}C depleted AAIW penetrating to the coast of Brazil during the MI (Mangini et al., 2010). Thus, taken together, multiple lines of evidence are consistent with release of ^{14}C-depleted CO_2 from Southern Ocean waters during the MI resulting in a dilution of the $^{14}C/^{12}C$ atmospheric ratio.

That a widespread ocean ventilation event occurred during the MI, however, remains controversial. For example, ^{14}C dated benthic foraminifera from the North Pacific indicate the ventilation rate of the deep Pacific actually slowed during the MI (Lund, 2013; Lund et al., 2011), opposite to what is predicted by the ventilation hypothesis. In addition, a number of marine sediment records from the Atlantic and Pacific Oceans provide little to no evidence for radiocarbon depleted AAIW during the MI at locations where depletions are expected (Cléroux et al., 2011; De Pol-Holz et al., 2010; Rose et al., 2010; Sortor and Lund, 2011). Nor does the timing of the atmospheric ^{14}C decline, when corrected for production, mirror a synchronous *p*CO2 rise during the MI, thereby arguing $\Delta^{14}C$ changes cannot simply be explained by release of CO_2 from the ocean (Hain et al., 2014). Finally, ocean models indicate the volume of glacial-age water requiring isolation to reduce the ^{14}C of deep-water sufficiently to lower the atmosphere $^{14}C/^{12}C$ ratio during the MI results in anoxia and $CaCO_3$ dissolution, neither of which are

observed in deep sea core records, thereby suggesting mid-depth $\Delta^{14}C$ anomalies recorded in sediment archives, such as Baja and the Arabian Sea, might represent regional phenomena (Hain et al., 2011). Models such as these, however, may have over-estimated the volume of "older" water needed to ventilate in order to generate the observed decrease in atmospheric $\Delta^{14}C$ (Burke and Robinson, 2012).

The bulk of evidence supporting widespread ventilation of a ^{14}C depleted glacial ocean reservoir during the MI comes from ventilation ages calculated from the ^{14}C age difference between co-existing planktonic and benthic foraminifera in deep-sea sediment cores (Broecker et al., 1988; Duplessy et al., 1989; Shackleton et al., 1988). Ventilation ages provide an estimate of the extent of isolation of surface to deep water from the atmosphere but are subject to ^{14}C dating artifacts stemming from bioturbation, species-specific dissolution, and radiocarbon contamination. In addition, benthic to planktonic foraminifera age differences can be biased by variable depth habitats in the pore waters and water column and by changes in the ^{14}C content of surface water and the atmosphere that may not have been accounted for (i.e., marine reservoir age corrections; Adkins and Boyle, 1997). The vulnerability of marine microfossils to ^{14}C dating artifacts may account for an extreme range in ventilation ages estimated for the LGM. For example, age estimates in the deep Atlantic and Pacific Oceans during the LGM range from "modern like" values (1600 years) to as old as 5000 years (Barker et al., 2010; Broecker et al., 2004; Sikes et al., 2000; Skinner et al., 2010; Thornalley et al., 2011).

Ventilation ages and ocean $\Delta^{14}C$ can be estimated independent of radiocarbon calibration by generating calendar ages for ^{14}C dated benthic foraminifera via stratigraphic correlation of sediment proxy data. Reconstructions such as these have no

direct calendar dates and require assigned calendar ages which are based on visual correlations of sediment proxy or color variability, geochemical records to distant atmospheric climate proxy records in layer counted ice cores, or U-Th dated speleothems, located thousands of kilometers away. These distant climate indices are subject to proxy interpretations, correlation errors in identifying and assigning "tie points", uncertainties in ice core chronologies, the assumption of constant sedimentation rates between age model control points, and disregard potential leads and lags between climate records. As an example, age models in North Atlantic deep-sea cores have been constructed from stratigraphic correlation between % *Neogloboquadrina pachyderma sinistral* (s) and Greenland ice core $\delta^{18}O$ (Thornalley et al., 2011). % *N. pachyderma (s)*, however, reaches near saturation at 100% abundance during the MI, thus limiting tie point identification. Consequently, the technique may not be well suited during this time interval for correlating deep-sea proxy records with ice core $\delta^{18}O$. Conversely, abrupt changes in proxy data marking the Bølling/Allerød and Younger Dryas climate transitions provide numerous tie-points, but may lead to instantaneous and large changes in sedimentation rates and hence, the potential for generating artifacts in deep-sea core $\Delta^{14}C$ reconstructions.

Finally, use of the ^{14}C tracer in identifying episodic ventilation events such as those proposed during the most recent deglaciation requires that atmospheric and marine $\Delta^{14}C$ reconstructions be placed on the same absolute (calendar year) time scale for direct comparison. Periodic updates to radiocarbon calibration curves often include additions of new data and removal of problematic calibration data sets. These updates can translate to large differences (100's to 1000's years) in calibrated ^{14}C ages and generate large

differences in the magnitude and timing of atmospheric $\Delta^{14}C$ curves that is the target for comparison.

Shallow water fossil corals provide an excellent archive for radiocarbon calibration beyond tree ring records because both the radiocarbon age and Uranium-series (U-Th) age can be generated from the same sample. Provided corrections can be made for the age offset between the surface water in which the coral grew and the contemporaneous atmosphere (marine reservoir age or MRA correction), the paired ages provide an estimate of $\Delta^{14}C$. This is a requirement for computing accurate $\Delta^{14}C$ because *both* the radiocarbon age and calendar age can be directly obtained from the same sample.

The Barbados coral record presented here spans the time interval 22 to 13 kyr BP, consists of 142 paired U-Th and ^{14}C dated samples, and adds 87 new paired age data to the record of Fairbanks et al. (2005) that was adopted in the IntCal 09 and IntCal13 calibration curves (Reimer et al., 2009; Reimer et al., 2013). MRA corrections to measured ^{14}C ages and estimates of MRA uncertainty are based on overlap of 74 Barbados corals with tree ring sequences (see Chapter 2). The Barbados coral record represents the only continuous and directly dated marine archive for this time interval and thereby provides an independent estimate as to the timing, duration, and magnitude of change in $\Delta^{14}C$ for comparison to other marine and terrestrial archive records and to consensus calibration curves (IntCal09 and IntCal13; Reimer et al., 2009; Reimer et al., 2013).

4.3 Materials and Methods

All coral samples were selected from the Barbados offshore drill-core collection from material recovered during the RANGER 88-13 (1988) and R/V KNORR 189-2 (2007) expeditions. Sample screening and data quality control criteria are as reported in Fairbanks et al. (2005). All samples were analyzed for evidence of secondary calcite by X-ray Diffraction (XRD) and only samples with "no detectable" calcite (less than 0.2 weight %, Chiu et al., 2005) were processed for U-Th and radiocarbon dating. Petrographic thin-section slides were made for a representative number of U-Th dated coral samples. We found no evidence of extensive secondary aragonite to disqualify sample selection in this study.

U-Th dating methods are described in detail in Chapter 2. In summary isotopic measurements were made by Inductively Coupled Mass Spectrometry (ICP-MS) using either a FISONS PLASMA 54 by the methods described in Mortlock et al. (2005) or with a ThermoScientific NEPTUNE PLUS ICP-MS using like-methods and protocols adopted for the PLASMA 54. Based on the measured ^{232}Th concentrations (0.02 to 3 ppb) no corrections were made for initial ^{230}Th. All U-Th ages had $\delta^{234}U_{initial}$ that fell within the acceptable range for modern and fossil corals that have maintained closed system behavior (138-152‰; Fairbanks et al., 2005). The average precision of the age determination (at 2 s.d.) is better than ± 0.5% and ± 0.2‰ in samples measured with the PLASMA 54 and NEPTUNE PLUS, respectively (Table 1). As an example, a 20 kyr BP coral sample analyzed with the NEPTUNE PLUS yields a remarkable 2 s.d. age uncertainty of ± 50 years or less, or 5 to 50 times more precise than sediment age models.

Coral samples (30 to 80 mg) were pre-treated by the methods described in Fairbanks et al. (2005) and ^{14}C dated by Accelerator Mass Spectrometry (AMS) at three separate facilities (Center for Accelerator Mass Spectrometry, Lawrence Livermore National Laboratory (LLNL); Leibniz Laboratory for Radiometric Age Determination and Isotope Research, Christian Albrecht University (Kiel); National Ocean Sciences Accelerator Mass Spectrometry Facility, WHOI (NOSAMS) placing our result in a fully inter-calibrated framework. A "radiocarbon dead" fossil coral (AK-H-2; U-Th age ~ 97 kyr BP was used to apply procedural blank corrections to all fossil coral data (Fairbanks et al., 2005). Two to three coral blanks were processed and analyzed with each set of 7 coral samples and the fraction modern carbon (FMC) values for blanks averaged and subtracted from sample values. Coral blank values generated at Kiel, LLNL, and NOSAMS are reported elsewhere (Fairbanks et al., 2005; Chapters 2 and 3) but generally ranged between 0.0005 to 0.0015 FMC and were reproducible within batch runs. Average blank corrections typically corresponded to a radiocarbon age in excess of 55 kyr. Applying coral blank corrections to samples in this study generally resulted in increased ^{14}C ages by 30 years to 60 years in 11.5 and 18.0 ^{14}C kyr corals, respectively.

4.4 Results

4.4.1 Marine Reservoir Age Corrections

All measured coral radiocarbon ages must be corrected for the local offset between the $^{14}C/^{12}C$ ratio of surface water and that of the atmosphere, commonly referred to as the marine reservoir age (MRA) correction. The global average MRA is estimated to be about 400 years and depends on latitude, ranging from 200 to 1200 years with

higher values in polar regions (Key et al., 2004). The range in MRA is due to partial equilibration of the surface ocean with the atmosphere and from differences in the fraction of ^{14}C depleted sub-surface water that is mixed upwards. Due to the large variability in MRA observed across the modern ocean it is recommended that MRA corrections be site specific and based on the local offset, or ΔR, defined as the difference in ^{14}C age of a marine sample of known calendar age with its modeled (i.e., MARINE13) ^{14}C age.

Large shifts in MRA are not predicted for Barbados as it is positioned far from zones of upwelling and lies at the western edge of the Atlantic Warm Pool, where the depth of the surface mixed layer is deepest, ranging between 60 and 80 meters (Ravelo et al., 1990). Importantly, Barbados is located within the western Atlantic Ocean entirely outside of the Caribbean Sea and its influences. Surface waters arriving at Barbados have transited the Atlantic subtropical gyres and crossed the equator providing a long atmospheric exchange time and surface ocean maps of ^{14}C show subtropical gyre water has high bomb ^{14}C, confirming a longer residence time for these waters (Key et al., 2004).

Past MRA at Barbados is estimated to be 340 ± 130 years (ΔR = -65 years) based on comparison of uncorrected ^{14}C Barbados coral ages with tree ring sequences spanning 13.9 and 7.3 kyr BP (Chapter 2). The observed variability is somewhat larger than the combined reported radiometric dating-errors. This suggests that there may be under-reported errors in the composite tree-ring calendar chronology, under estimates of radiocarbon blank corrections, precision differences between radiocarbon sample runs not adequately captured by internal standards, or marine reservoir age variability due to

changing air-sea exchange rates. For example, a Oeschger box diffusion model, simulating a 50% decrease in air-sea exchange generates a 300-year increase in MRA in less than 50 years (Cao, 2010). Coupled ocean models, however, simulating LGM conditions show that an increase in wind stress results in a deepening of the surface mixed layer of the Atlantic Warm Pool (Ravelo et al., 1990) thereby potentially limiting an increase in MRA. Some variability in the Barbados MRA record could also be due to changes in solar output, although production changes in the atmosphere would be attenuated in the surface ocean. Simple box diffusion models confirm that relatively large changes in production rates produce only minor (less than 50 years) changes in MRA (Cao, 2010).

4.4.2 Marine Reservoir Age variability

The accuracy of a coral ^{14}C age is limited by the assumption of a uniform reservoir age correction, particularly in samples for which tree ring records are not available for comparison (i.e., samples older than 13.9 kyr BP). The ^{14}C age of tropical surface water is dependent upon a number of processes such as the exchange rate between the atmosphere and ocean, pCO_2 of the atmosphere, the fraction of ^{14}C depleted-water mixed into the surface, changing sea ices limits, and sea level (Bard, 1988; Stuiver and Polach, 1977) and there is strong evidence that many of these processes (e.g., wind speed, sea level, pCO_2) have varied during different climate states.

Very low MRA of 60 years and less are estimated for Barbados at the onset of the Younger Dryas (12.9 to 12.7 kyr BP) (Chapter 2). Very low MRA estimates such as these are highly unusual since they require that surface water be both isolated from sources of upwelling and in equilibrium with atmospheric pCO_2, a condition that is not

found in the modern ocean. Low MRA at Barbados and at Cariaco Basin in the Caribbean at the start of the Younger Dryas was previously reported (Hua et al., 2009) but can now been confirmed with new coral data and be directly linked to decreased production of North Atlantic Deep Water (NADW) via records of $\Delta^{14}C$ (Chapter 2). Ocean models simulating a reduction or shutdown of NADW formation generally result in increased exchange between the surface ocean and atmosphere, thus decreasing the ocean to atmosphere age difference and leading to lower reservoir ages in Atlantic surface water compared to the Pacific (Matsumoto and Yokoyama, 2013; Muscheler et al., 2008; Singarayer et al., 2008). A 200-year delay in the rise in $\Delta^{14}C$ in Atlantic versus Pacific corals at the start of the Younger Dryas is consistent with modeled results (Singarayer et al., 2008) whereby shutdown of NADW lowers Atlantic MRA to generate differences in the trajectories of Atlantic and Pacific $\Delta^{14}C$ (Chapter 2).

With the exception of the start of the Younger Dryas extreme MRA estimates are infrequent and it is therefore appropriate to apply a constant reservoir age of 340 ± 130 years (ΔR = -65 years) to all coral ^{14}C ages included in this study. A 340 year MRA correction is within a reasonable range for surface water, constrained between the estimate for the mean ocean (~ 400 years) and modern Caribbean estimate (312 years) obtained from pre-bomb modern corals (Guilderson et al., 2005) and estimates reported elsewhere in the Caribbean (200-240 years) (Wagner, 2009). Finally, since the radiocarbon dating error increases exponentially with age, the uncertainty in MRA corrections becomes less significant in samples older than 15 kyr BP and makes only a small contribution to the calculation of $\Delta^{14}C$.

4.4.3 Radiocarbon during the Mystery Interval

U-Th and ^{14}C dating results indicate that new Barbados calibration data are entirely consistent with previous data and our coral-based radiocarbon calibration curve (Fairbanks0107, 2007). This update provides critical data (n = 28) to the 17.5 to 15 kyr BP portion of the record where coverage was previously sparse or entirely absent (Figure 4.1). By comparison, the MARINE13 database contains only 10 U-Th and ^{14}C dated coral corresponding to this same time interval and relies more heavily on marine sediment and terrestrial archive records to constrain the MARINE13 and IntCal13 calibration curves (Reimer et al., 2013).

Comparison of Barbados coral data with calibration data from Cariaco Basin sediments (Hughen et al., 2006), Hulu Cave stalagmite (Southon et al., 2012), and Tahiti corals (Bard et al., 1998; Durand et al., 2013) reveals some similarities but also some striking differences (Figure 4.2). From 22 to 20 kyr BP Barbados coral data is reasonably consistent with Cariaco Basin sediment and Pacific coral data although coral ^{14}C ages tend to be 300 to 600 years older than same calendar age H82 stalagmite. From 20 to 18 kyr BP corals and H82 data overlap but from 18 to 15 kyr BP Barbados coral ^{14}C ages are systematically older, by 200 to 400 years, compared to H82, and 700 to 1000 ^{14}C years older compared to Cariaco Basin foraminifera. Tahiti coral data overlap with Barbados corals during the MI, although the data are too sparse to make a robust comparison prior to 16 kyr BP

From 15 to 13 kyr BP Barbados corals display good overlap with other marine and terrestrial calibration data and reaffirm a radiocarbon age plateau between 15 and 14.2 kyr BP (Figure 4.2). The average ^{14}C age of Barbados corals (n=25) across this

plateau is 12.49 ± 0.10 kyr BP (1 s.d.) and within error of the plateau age measured in Tahiti corals (12.58 ± 0.11 kyr (n=31); Durand et al., 2013). After ~ 14 kyr BP, Barbados ^{14}C ages decline until the beginning of the Younger Dryas (12.9 kyr BP) when Barbados coral ^{14}C ages rapidly decrease, displaying a ^{14}C age "cliff" that is similarly observed in tree ring records (Chapter 2).

4.4.4 High-frequency variations in radiocarbon records

The updated Barbados calibration record suggests that an increase in coral data density has not necessarily translated directly to a decrease in scatter (Figure 4.1 and Figure 4.2). This is particularly true for the interval 22 kyr to 15 kyr BP when corals of same calendar age display differences in ^{14}C age of between 200 and 600 years and larger than would be expected from combined dating errors (2 s.d. ± 100 ^{14}C years) or variability in MRA (± 130 years). Outliers in the Barbados coral record appear neither systematic nor biased to high or low ^{14}C age and replicate ^{14}C and U-Th ages agree to within 2 s.d. (Appendix; Table 1), indicating we have not underestimated dating errors. Changes in solar production can only account for about one-half of the observed high-frequency variability (Stuiver and Braziunas, 1989; Stuiver and Quay, 1980) in ^{14}C age. Changes in global ^{14}C production rates related to changes in magnetic field strength could also contribute to ^{14}C age scatter. However, a modulation of ± 50% of the modern geomagnetic field strength would be required to generate an appreciable change in the global production rate of ^{14}C (Elsasser et al., 1956; Lal, 1988), an event that is not likely to have occurred on timescales of decades to centuries or at the frequency suggested by our data.

In comparison, the H82 record displays much less scatter in a plot of U-Th vs. ^{14}C age (Figure 4.2). Slow growth rates (6 to 30 mm kyr^{-1}) in the speleothem limit sampling resolution to about one-millimeter intervals so that each sample integrates about 30 to 150 years of the record, whereas coral subsamples represent a few years of growth. Therefore, reduced sampling resolution in the stalagmite generates inherent smoothing of higher-frequency variability that might be associated with changes in ^{14}C production rates or variability related to changes in the dead carbon fraction (DCF).

4.4.5 Comparison of Tropical Atlantic calibration data

^{14}C age offsets reported between Cariaco Basin planktonic foraminifera and H82 speleothem (Southon et al., 2012) during the MI have been attributed to lower MRA at Cariaco Basin (Reimer et al., 2013), perhaps in response to a shutdown in Atlantic Meridional Overturning Circulation (AMOC) (McManus et al., 2004). Evidence for lower MRA at Cariaco Basin prompted the removal of the 17.5 to 16 kyr BP portion of the Cariaco record from the IntCal13 and MARINE13 data sets and their replacement with the H82 stalagmite and Lake Suigetsu SG06 varve calibration data. The SG06 calendar age model is, however, tied to the U-Th dated H82 speleothem via wiggle matching of ^{14}C records (Ramsey et al., 2012) and so SG06 calibration data (not shown) generally follow the trend established with the H82 record (Reimer et al., 2013). These data substitutions directly account for the well-defined differences between the IntCal09 and IntCal13 curves during the MI and displayed in Figure 4.1.

With abundant new coral data from Barbados for comparison, we consider it very unlikely that 400 to 1000-year ^{14}C age offsets between corals and Cariaco Basin foraminifera during the MI (Figure 4.2) can be explained by MRA corrections to ^{14}C ages

in these data sets. Today, both locations have MRAs of 300-400 years, as shown by surface water ^{14}C contours (Butzin et al., 2005; Key et al., 2004), and in good agreement with Guilderson et al. (2005) estimated pre-bomb radiocarbon age of Cariaco Basin surface water (312 years) and consistent with our estimate at Barbados (340 years). Moreover, the close proximity to one another (separated by less than 700 km) makes it highly unlikely that Barbados and Cariaco Basin would be separated by strong gradients in the radiocarbon age of surface water during the past. The good overlap between Barbados and Cariaco Basin records both prior to and following the MI, especially from 14 to 11 kyr BP (Chapter 2) indicate MRA corrections imposed at these two sites are reasonable and suggest relatively uniform MRA across several millennia. Indeed, reconciling large ^{14}C age differences between Barbados corals and Cariaco Basin foraminifera during the MI with MRA corrections, would require an increase in MRA at Barbados to 700 years simultaneous with a lowering of MRA to 0 years at Cariaco Basin. It can be argued that a shallower basin sill depth during the LGM would have limited exchange between the Cariaco Basin and Caribbean Sea to lower the radiocarbon age of the mixed layer at Cariaco Basin (Southon et al., 2012). However, we note Barbados and Cariaco Basin records do not diverge until after ~ 17.5 kyr BP (Figure 4.2) and therefore, the discrepancy between ^{14}C records does not appear to correlate with minimum basin sill depth or with abrupt jumps in sea level (Peltier and Fairbanks, 2006).

We attribute offsets between Barbados coral and Cariaco Basin calibration data during the MI to inaccuracies in assigning calendar year ages to ^{14}C dated planktonic foraminifera in the Cariaco Basin sediment core. Calendar year age assignments in ODP Hole 1002D are presently based on an age model constructed via correlation of color

changes (gray scale) to a composite $\delta^{18}O$ record obtained from U-Th dated Hulu Cave (China) stalagmites (Hughen et al., 2006; Wang et al., 2001). The study sites are 15,000 km apart. The Hulu cave-based age model represents a revision to an earlier age model where a calendar year chronology was constructed based on correlation of sediment core gray scale changes to the $\delta^{18}O$ record in Greenland ice cores (Hughen et al., 2004; Hughen et al., 2006).

The MI portion of the Hulu Cave-Cariaco Basin tied calendar year age model was constructed by assigning visual tie points at ~ 15, 16, 17 and 17.5 kyr BP, corresponding to the mid-point of abrupt changes identified in 1002D reflectance and two overlapping stalagmite $\delta^{18}O$ records. Calendar year ages were assigned to Hole 1002D sample depth intervals assuming constant sedimentation rates between tie points. The resulting chronology generates unnaturally large and instantaneous shifts in implied sedimentation rates during the MI (Figure 4.3) that precisely coincide with the timing of large calendar year age offsets between Barbados corals and Cariaco Basin foraminifera (Figure 4.2). Rather than being due to large differences in MRA corrections between Barbados and Cariaco Basin surface waters, we conclude that tie point selection, corresponding to 17.5 to 15.0 kyr BP, in the Hole 1002D reflectance record (Hughen et al., 2006) has stretched the age to depth relationship in the Cariaco Basin sediment core and generated a calendar year age model that contains more years than the true number of calendar years. The analysis is similar to that of Chiu et al. (2007) who demonstrated that the assignment of tie points between Site 1002D reflectance and Greenland ice core $\delta^{18}O$ from 30 to 50 kyr BP generated large variations in sedimentation rates at Cariaco Basin and large shifts in the slope of $\Delta^{14}C$ versus age.

Divergence in the Barbados and Cariaco Basin calibration records during the MI highlights an important distinction between our approach to using coral archives for calibration, where both the calendar age and radiocarbon age be directly measured from the same sample, as opposed to the IntCal approach, where calibration data from sediment records are incorporated. The accuracy of the Hulu-Cariaco Basin tied chronology assumes, implicitly, synchronous phasing between two far-field climate records responding to Northern Hemisphere cooling as inferred from Greenland ice core $\delta^{18}O$ records. This is the underlying assumption in all tied chronologies. Yet, Charles et al. (1994) and Liu et al. (2012) both show in their models that $\delta^{18}O$ in Greenland ice responds not only to temperature but also to changes in the source of moisture (North Atlantic versus Pacific). Furthermore, Project SPECMAP demonstrated that individual climate or ocean proxy signals may appear similar but they usually contain a phase shift due to different time constants for different climate or regional systems (Martinson et al., 1987). It is, therefore, reasonable to expect different time constants or phasing between the atmosphere/ground water $\delta^{18}O$ signal in Hulu Cave due to changes in the intensity of the Southeast Asian monsoon and the sedimentation rate signal in the Cariaco Basin due to variable South American river runoff. Moreover, large and rapid shifts in Greenland ice $\delta^{18}O$, often used to correlate proxy records, remain difficult to reconcile solely with changes in North Atlantic cooling since the high latitude contribution to the meridional heat flux is small compared to the atmospheric flux from the tropics (Wunsch, 2006).

4.4.6 Barbados Coral and Hulu Cave Stalagmite (H82) comparison

Several factors could account for the systematic ^{14}C and or U-Th age offsets observed between coral and H82 data during the MI and prior to 20 kyr BP (Figure 4.2).

Like corals, speleothems are not pure recorders of atmospheric radiocarbon. Speleothem ^{14}C ages must be corrected for the dead carbon fraction (DCF) or the amount of dead carbon introduced from dissolution of the carbonate host rock and from CO_2 generated in soils during microbial respiration. DCF can vary with changes in cave ventilation, the residence time of water as it percolates through the vadose, or with changes in biological activity in soils above the cave that may be influenced by vegetation cover, temperature, and soil moisture (Genty et al., 2001; Hendy, 1971). In H82, a DCF of 452 ± 50 years was estimated based on comparison of uncorrected speleothem ^{14}C ages with the ^{14}C age of same calendar year age tree rings (Southon et al., 2012). A uniform DCF of 452 ± 50 years also produced a good match between H82 and DCF corrected Bahamas speleothem data (Beck et al., 2001; Hoffmann et al., 2010) in samples older than 13.9 kyr BP suggesting the assumption of constant DCF corrections in both records was valid. The match, however, between dead-carbon corrected H82 and Bahamas speleothem data during the Younger Dryas is not particularly good where ^{14}C age differences in excess of 500 years are observed between speleothems (Hoffmann et al., 2010; Southon et al., 2012).

U-Th dating of corals and speleothems via mass spectrometry yield very precise ages, but U-Th ages may require corrections for initial ^{230}Th for dating accuracy. In surface corals, age corrections for initial ^{230}Th are unnecessary since it can be assumed the seawater in which the coral grew contained no initial ^{230}Th as it is readily scavenged. In spelothems, however, initial ^{230}Th incorporated into cave stalagmites or stalactites may not be negligible and depends on the mineral composition and age of the host carbonate bedrock. Therefore, speleothems typically require corrections for initial ^{230}Th that are

based on measured ^{232}Th concentrations and an assumed or measured initial (or detrital) $^{230}Th/^{232}Th$ ratio. U-Th ages obtained in H82 were corrected based on an assumed $^{230}Th/^{232}Th$ initial ratio of 4.4 ppm (Wang et al., 2001). Due to low ^{232}Th concentrations, these age corrections are small, resulting in corrections of a few decades or less (Southon et al., 2012). Speleothems from other locations, however, have been found to display $^{230}Th/^{232}Th$ initial ratios as large as 60 to 120 ppm, based on isochron analysis (Carolin et al., 2013; Hoffmann et al., 2010; Partin et al., 2007) so that samples containing even relatively minor concentrations of ^{232}Th (< 50 parts per trillion) required U-Th age corrections of between 50 and 200 years. If the $^{230}Th/^{232}Th$ activity ratio in H82 is larger than the assumed 4.4 ppm value, then corrections to U-Th ages have been underestimated, thereby increasing the calendar age difference between the stalagmite and corals.

MRA at Barbados greater than the assumed 340 years could also contribute to offsets in ^{14}C ages between the corals and H82 observed during the MI and prior to 20 kyr BP but would require that the age of Atlantic surface water be as old as 600 to 800 years, or similar to the age of mid to high latitudes surface waters today in Southern Ocean (Butzin et al., 2005; Key et al., 2004). Calibration data from Tahiti and Papua New Guinea corals during the MI interval are limited but generally plot with Barbados corals (Figure 4.2), implying that any shift to increased MRA during the MI and LGM in the tropical Atlantic must have been accompanied by a similar shift in the tropical Pacific. Modeled MRA estimates for the Caribbean, based on iterative tuning of radiocarbon chronologies to a target atmospheric $\Delta^{14}C$ record, generate an extreme range in MRA estimates (300 to 900 years) during the MI and LGM (Butzin et al., 2012).

However, the Caribbean MRA reconstructions rely on model tuning to an atmospheric $\Delta^{14}C$ represented by Cariaco Basin $\Delta^{14}C$ data (Hughen et al., 2006). For reasons discussed above, we do not believe the Cariaco Basin serves as a reliable atmospheric ^{14}C record during the MI and therefore question the validity of the modeled MRA results of Butzin et al. (2012).

Paleo-reconstructions for the glacial ocean suggests higher alkalinity (Yu and Elderfield, 2007), lower pCO_2, and an ocean, that was on average, older (see Sarnthein et al., 2013). In today's ocean there is a strong linear correlation between decreasing $\Delta^{14}C$ and increasing alkalinity or Total CO_2 (Rubin and Key, 2002). Assuming the slope of the alkalinity- $\Delta^{14}C$ relationship in the glacial ocean was similar to the modern (Key et al., 2004) an increase in alkalinity of the deep ocean of about 25 μmol kg^{-1} during the LGM would translate to a mean age increase of about 200 years. Presumably, any increase in the mean ocean-atmosphere age difference would be reflected in the surface ocean and recorded by corals. ^{14}C dated foraminifera records obtained from Southern Ocean sediment cores suggest older AAIW during HS1 (Skinner et al., 2010). More poorly ventilated (older) AABW may have outcropped further to the south and mixed into CPDW along isopycnals in response to the retreat of sea ice during Southern Ocean warming. Subsequent mixing of "aged" CPDW with AAIW, in turn would have increased the ^{14}C age of the latter to be eventually transported to the western Atlantic Warm Pool and upwelled near Barbados. ^{14}C dated benthic foraminifera obtained at intermediate depth sites in the North Atlantic indicate extremely old (~ 5000 years) AAIW penetrating into northern high latitudes during the MI (Thornalley et al., 2011) although other results suggest the Arctic Ocean and Nordic Seas, rather than AAIW, may

have been the source of poorly ventilated water to the North Atlantic (Thornalley et al., 2015). To summarize, systematic offsets between Barbados coral and Hulu Cave speleothem calibration data, particularly during the MI, could be due to under-reported marine reservoir corrections to corals, over-reported dead carbon corrections to speleothem ^{14}C ages and under-reported initial ^{230}Th corrections to speleothem U-Th ages. But it seems unlikely that a single one of these factors accounts for discrepancies between archives. Additional coral data from other Atlantic and Pacific locations may be needed to identify and resolve the relative importance of factors contributing to generate large age differences between data sets.

4.5 Discussion

4.5.1 Atmospheric $\Delta^{14}C$ reconstructions

Paired radiocarbon and calendar age data from terrestrial and marine archives provide an estimate of the radiocarbon content of the atmosphere ($\Delta^{14}C_{atm}$) by the following equation:

$$\Delta^{14}\mathrm{C}\ (‰) = \left(\frac{EXP\ (\lambda_1 * t_1)}{EXP\ (\lambda_C * t_C)} - 1 \right) * 1000 \qquad (1)$$

(after Stuiver and Polach, 1977) where t_1 is the calendar age, t_c is the radiocarbon age, λ_1 is the activity constant of ^{14}C based on the consensus (Oxford) half-life of 5730 years and λ_c is the activity constant based on the Libby half-life of 5568 years (Libby, 1955).

The Barbados coral record exhibits four distinct features in $\Delta^{14}C$: (1) scatter that is distributed about the long-term trend in $\Delta^{14}C$ due to decreased production due to an

increase in the Earth's geomagnetic field strength following the Laschamp and Mono Lake geomagnetic excursions (Chiu et al., 2007; Chapter 3); (2) uniform $\Delta^{14}C$ from 20 to 18 kyr BP, distinct from the predicted decreasing long-term trend (3) a decline during the Mystery Interval of 90 ± 10‰; and (4) a more rapid decline in $\Delta^{14}C$ of 70 ± 10‰ from 14.7 to 14.0 kyr BP

4.5.2 Atmospheric Radiocarbon, Ocean Ventilation, and Sea Level

During the past 50,000 years changes in the Earth's magnetic field strength have controlled the ^{14}C content of the atmosphere with positive anomalies in $\Delta^{14}C$ produced during periods of weaker magnetic field (Bard et al., 1990; Elsasser et al., 1956; Lal, 1988). On shorter time scales, fluctuations in $\Delta^{14}C$ were produced by changes in the solar magnetic field (Stuiver and Quay, 1980). Changes in the carbon cycle also impact atmospheric ^{14}C as carbon is transferred between ocean and terrestrial reservoirs. For example, NADW production is responsible for net export of ^{14}C produced in the atmosphere to the world's deep oceans. Increases in NADW lowers the ^{14}C content of the atmosphere whereas the atmosphere will accumulate ^{14}C when NADW production is reduced. Coupled ocean-atmosphere models show that $\Delta^{14}C$ responds instantaneously to recovery of NADW production with increased NADW production leading to more efficient removal of ^{14}C from the atmosphere and a decrease in $\Delta^{14}C$ (Delaygue et al., 2003; Singarayer et al., 2008; Stocker and Wright, 1996).

There are multiple lines of evidence indicating NADW production varied widely during the past 50,000 years and that these fluctuations generated changes in the carbon cycle and produced rapid millennial scale variability in the record of $\Delta^{14}C$ (Adkins and Boyle, 1997; Edwards et al., 1993; Hughen et al., 1998; Muscheler et al., 2000). For

example, a rapid rise in $\Delta^{14}C$ at the onset of the Younger Dryas (12.9 kyr BP) recorded in terrestrial and marine records (Hughen et al., 1998; Hughen et al., 2000; Chapter 2) corresponds, in timing, to a slow-down of NADW, as evidenced by geochemical proxy data from Atlantic Ocean sediment cores (Elmore and Wright, 2011; McManus et al., 2004; Piotrowski et al., 2005). In the following discussion, we isolate and correct for variability in $\Delta^{14}C$ from the long-term production trend and examine the shape of the $\Delta^{14}C$ curve from 22 kyr to 13 kyr BP to propose geochemical and geophysical mechanisms, global and local, which may be responsible.

4.5.3 The 22 kyr to 18 kyr BP Interval

Corals display a decrease in $\Delta^{14}C$ from 22 to 20 kyr BP of about 50‰ (Figure 4.4a) although scatter in the data makes it difficult to resolve a meaningful trend-line. The record in H82 better illustrates decreasing $\Delta^{14}C$ over this time interval although values are offset, in comparison to coral data $\Delta^{14}C$, by about +50‰, or equivalent to about 400 years as observed in plots of ^{14}C age versus calendar age (Figure 4.2). The decline in $\Delta^{14}C$ can be attributed to the long-term increase in the Earth's geomagnetic field strength, following periods of weaker field and increased production associated with the Laschamp (41 kyr BP) and Mono Lake (31.5 kyr BP) geomagnetic excursions (Chiu et al., 2007; Chapter 3). From 20 to 18 kyr BP corals and speleothem $\Delta^{14}C$ records overlap with more uniform values centered around 400‰ (Figure 4.4a). Coral $\Delta^{14}C$ ranges between 300 and 400‰ at 19.5 kyr BP. The increased scatter in coral $\Delta^{14}C$ compared to the smooth H82 record is puzzling as it represents 500 to 800 year ^{14}C age differences in same calendar age samples and corresponds in time to a ^{14}C age cliff in the coral data (Figure 4.2). Despite increased scatter, the similarity in marine and terrestrial

$\Delta^{14}C$ records indicates the $\Delta^{14}C$ plateau 19.5 to 18 kyr BP resulted from an "excess" of atmospheric radiocarbon via a common mechanism and is not due to local changes in MRA at Barbados or DCF at Hulu Cave.

4.5.4 The 18 to 15 kyr BP Interval

Reconstructions of $\Delta^{14}C$ at intermediate depths in different ocean basins suggest offsets from the contemporaneous atmosphere as large as 400 to 500‰ during the MI and ventilation ages in deep and intermediate waters as old as 5000 years (see Sarnthein, 2011). The decrease in $\Delta^{14}C$ during the MI coincides with a 40 ppm rise in atmospheric pCO_2 (Marcott et al., 2014; Monnin et al., 2001). This correlation has led to the hypothesis that the decline in $\Delta^{14}C$ is attributed to release of ^{14}C depleted-CO_2 from the ocean. The hypothesis is further supported from the $\delta^{13}C$ record of CO_2 ($\delta^{13}C_{atm}$) in Antarctic ice cores that indicates a release of ^{14}C depleted-carbon from the ocean to the atmosphere beginning at 18 kyr BP (Schmitt et al., 2012). Several marine sediment records show no evidence for ^{14}C-depleted waters penetrating to intermediate depths and thereby contradict a release of radiocarbon depleted CO_2 to the atmosphere (Cléroux et al., 2011; De Pol-Holz et al., 2010; Rose et al., 2010; Sortor and Lund, 2011). Hain et al. (2014) cite similar inconsistencies with the ventilation hypothesis but also argue that differences in the timing of the deglacial decrease in modeled atmospheric $\Delta^{14}C$ with the pCO_2 increase, measured in ice cores, do not support the simplistic view of a large release of ^{14}C depleted CO_2 during the MI.

When smoothed, the Barbados coral record of $\Delta^{14}C$ shows a decrease of only ~90 ± 10‰ during the MI (Figure 4.4a) and at a rate that is similar to the long-term decay trend (Chiu et al., 2007; Durand et al., 2013). The H82 record displays a similar decline

although values are systematically 25‰ to 50‰ higher compared to coral $\Delta^{14}C$, or equivalent to the observed 200 to 400-year offsets observed in their respective ^{14}C ages (Figure 4.2). Neither corals, nor H82 support the timing or magnitude change in atmospheric $\Delta^{14}C$ during the MI, as constructed in IntCal09 (Figure 4.4a). The exaggerated shape of the IntCal09 estimate $\Delta^{14}C$ during the MI, particularly the shift to higher $\Delta^{14}C$, is directly due to incorporation of paired ^{14}C and calendar age data obtained from the Cariaco Basin deep-sea sediment core. Tie point selection in ODP Hole 1002D generated an age model in the Cariaco Basin sediment core that shifted calendar year ages, older, by 700 to 1000 years 17.5 to 15 kyr BP. Increasing the calendar to ^{14}C age difference produces a diagonal shift to higher amplitude $\Delta^{14}C$ beginning at 17 kyr BP and sharp decline beginning at 16.5 kyr BP (Figure 4.2 and Figure 4.4a).

4.5.5 The 15 to 13 kyr BP Interval

Arguably, the most remarkable feature in the deglacial record of atmospheric radiocarbon is a rapid decrease in $\Delta^{14}C$ values from 14.7 to 14.1 kyr BP (Figure 4.4b). The precision in ^{14}C dating of corals is vastly improved in samples younger than 15 kyr BP thereby reducing the scatter in $\Delta^{14}C$ and allowing for better comparison between different data sets. Barbados coral $\Delta^{14}C$ overlap with Tahiti coral and H82 values to and display a decrease in $\Delta^{14}C$ of about 70 ± 10‰. The decline in $\Delta^{14}C$ corresponds to the ^{14}C plateau age (Figure 4.2) and to an interval when production of atmospheric ^{14}C was balanced with its loss by natural decay. Following the $\Delta^{14}C$ decline corals and speleothem display relatively uniform $\Delta^{14}C$ values that vary around 200‰.

The decrease in $\Delta^{14}C$ beginning at 14.7 kyr BP coincides with both the $^{13}C/^{12}C$ tracer of NADW history measured in foraminifera (Charles and Fairbanks, 1992) and the

Pa/Th tracer of NADW production measured in deep sea sediments (McManus et al., 2004) and provides credible evidence to hypotheses linking changes in NADW production to changes in the ^{14}C content of the atmosphere (Figure 4.5). The apparent turn-on of NADW and shift in $^{14}C/^{12}C$ also corresponds to an interval of accelerated sea-level rise, Melt Water Pulse (MWP) 1A, originally identified at Barbados (Fairbanks, 1989) and later confirmed at the Sunda Shelf (Hanebuth et al., 2000) and Tahiti (Deschamps et al., 2012), when sea level rose 15 meters with rates of sea level rise approaching 25 mm yr^{-1} (Figure 4.5). The Barbados sea-level record is constructed from the species *Acropora palmata*, considered to be the benchmark coral for estimating past sea level (Fairbanks 1989). Coral data in this study (Appendix; Table 1) include a large number of the same *A. palmata* samples used to construct the deglacial sea level curve (Abdul et al., 2016; Fairbanks et al., 2016; Peltier and Fairbanks, 2006) and so the atmospheric $\Delta^{14}C$ record can be unequivocally tied to MWP-1A since the records are derived from the same cores and in most instances, from the same U-Th and ^{14}C dated samples. Therefore, there is clear evidence from both NADW proxy and $\Delta^{14}C$ records that NADW production was increased at the time of MWP-1A. This finding would appear counter intuitive since injection of freshwater to sensitive regions of NADW formation is thought to slow down or stall AMOC (Delaygue et al., 2003; Stocker and Wright, 1996). Instead, NADW formation was robust even in the face of a large documented meltwater pulse and may support claims that a significant contribution to MWP 1A was from melting of the Antarctica ice sheet, as predicted by Glacial Isostatic Adjustment (GIA) ice models simulating the eustatic or global sea level rise during deglaciation (Bassett et al., 2007; Bassett et al., 2005; Clark et al., 2002; Deschamps et

al., 2012). General circulation models, in turn, demonstrate that freshwater added to the location of AAIW formation can trigger NADW production thereby warming the North Atlantic and leading to the Bølling /Allerød warm interval (Weaver et al., 2003).

A $\delta^{13}C$ record from Southern Ocean core RC11-83 supports a turn-on of NADW, albeit via "a false start", as early as 15.2 kyr BP (Charles and Fairbanks, 1992). That resumption in NADW production may have preceded the major pulse of MWP-1A and a shift in the $\delta^{18}O$ of Greenland ice by ~ 400 to 600 years (Figure 4.5) is not likely to be an artifact of constructed age models for the deep-sea cores or ice core records. Rather, the delayed response of MWP-1A to climate shifts is consistent with theoretical calculations of the ice sheet response to abrupt atmospheric shifts based on equilibrium models (Cuffey and Paterson, 2010). A rejuvenation of NADW prior to Bølling/Allerød warming and MWP-1A implies that persistent freshening of the Southern Ocean from sea ice melting during the later stages of HS1 was sufficient to produce the density differences between NADW and AAIW needed to reactivate AMOC (Bianchi and Gersonde, 2004; Knorr and Lohmann, 2003). Once reinvigorated, increased NADW production and the associated pole-ward heat transport may have provided a necessary amplifier for ice sheet melting, culminating in MWP-1A (Charles and Fairbanks, 1992).

The decline in $\Delta^{14}C$ beginning at 14.7 kyr BP also corresponds to abrupt increases in the greenhouse gases (GHG) pCO_2 and CH_4 (Figure 4.5) (Marcott et al., 2014). Permafrost thawing at high latitudes during the early phase of MWP-1A, rather than increased NADW production, is thought to have released large quantities of GHG and ^{14}C depleted carbon (Köhler et al., 2014). As modeled with Tahiti corals, an injection of 125 Pg of nearly ^{14}C-free carbon released over 200 years beginning at 14.6 kyr BP

generated a 55‰ decrease in $\Delta^{14}C$ and 22 ppm increase in pCO_2 (Köhler et al., 2014). The Barbados coral $\Delta^{14}C$ and sea level record is, however, inconsistent with this strict interpretation of the Tahiti $\Delta^{14}C$ and sea level records for a number of reasons. First, Barbados and Hulu Cave data indicate that the full amplitude shift in atmospheric $\Delta^{14}C$ during the Bølling/Allerød took place in a period of 400 to 600 years (Figure 4.4b). Closer inspection of Tahiti coral $\Delta^{14}C$ and associated dating uncertainties indicates the proposed 200-year release window is not well constrained and that Tahiti, Barbados, and Hulu Cave $\Delta^{14}C$ records cannot be readily distinguished from one another (Figure 4.4b). Second, Barbados *A. palmata* corals constrain MWP-1A from 14.7 to 13.9 kyr BP with highest rates of sea level rise not achieved until 14.1 kyr BP (Fairbanks et al., unpublished data) or several centuries after both pCO_2 and CH_4 concentrations had plateaued (Figure 4.5). Finally, the molar activity of $^{14}CO_2$ (calculated as the quantity of $^{14}CO_2$ per mole of air) continued to increase after 14.7 kyr BP (Svetlik et al., 2013) thus making it unlikely that the decrease in $\Delta^{14}C$ observed from 14.7 to 14.0 kyr BP can be entirely attributed to dilution of the atmosphere with injection of ^{14}C-free carbon. Rather, the similarity in both the amplitude and timing of overlapping terrestrial (speleothem) and marine (coral) $\Delta^{14}C$ signals is strong evidence that ocean circulation was the most likely source for the decrease in $\Delta^{14}C$ from 14.7 to 14.0 kyr BP and that the decline involved removal of ^{14}C from the atmosphere via rapid exchange between carbon reservoirs.

4.5.6 Contribution to $\Delta^{14}C$ from the Laschamp and Mono Lake Excursions

Imbedded in the atmospheric $\Delta^{14}C$ record are two periods of increased production at a time of weaker geomagnetic field strength during the Laschamp (~41 kyr) (Lascu et al., 2016; Singer et al., 2009) and Mono Lake excursions (31.5 kyr BP) (Chapter 3). In

order to identify $\Delta^{14}C$ fluctuations that may be superimposed on the long-term trend and attributed to changes in deep-ocean ventilation or production the raw $\Delta^{14}C$ record must be corrected for excess production of ^{14}C during the Laschamp and Mono Lake geomagnetic excursions and its subsequent decay. In the discussion to follow I present a record of residual $\Delta^{14}C$, or $\Delta^{14}C_{LMcorr}$, from 22 to 13 kyr BP by extending the approach applied in Chapter 3.

The impact of production changes due to Laschamp and Mono Lake on the deglacial history of $\Delta^{14}C$ is illustrated in Figure 4.6. In contrast to a decline in uncorrected $\Delta^{14}C$ from 22 to 20 kyr BP $\Delta^{14}C_{LMcorr}$ displays relatively constant values of between 200 and 250‰. From 20 to 18 kyr BP, uncorrected $\Delta^{14}C$ values are relatively uniform, whereas $\Delta^{14}C_{LMcorr}$ increases by about 60 to 80‰, with values peaking at around 18.5 kyr BP (Figure 4.6). During the Mystery Interval the decrease in $\Delta^{14}C_{LMcorr}$ is about 70‰ or about one-third to one-half the amplitude decline computed in IntCal09 or IntCal13, respectively (Figure 4.6). The rate of decrease in $\Delta^{14}C_{LMcorr}$ during the MI is about 0.025 ‰ yr^{-1} or roughly equivalent to the expected long-term trend due to natural decay. Therefore, after $\Delta^{14}C$ is corrected for increased production during the Laschamp and Mono Lake excursions, the decline in $\Delta^{14}C$ during the MI and attributed to episodic ventilation of the deep ocean cannot be readily distinguished from the long-term trend.

Another interesting observation in the $\Delta^{14}C_{LMcorr}$ record is that besides a much lower overall decrease in $\Delta^{14}C$ during the MI, $\Delta^{14}C_{LMcorr}$ shows an increase of about 60 - 80‰, *prior* to the MI (Figure 4.6). An increase of this amplitude is difficult to reconcile entirely with changes in the carbon cycle. An increase of 80‰ cannot be simulated in ocean-atmospheric coupled models even with a complete turn-off of NADW (Delaygue

et al., 2003; Stocker and Wright, 1996). Furthermore, proxy data suggest NADW production had already weakened prior to 20 kyr BP (Piotrowski et al., 2005). Finally, the similarity between coral and speleothem raw $\Delta^{14}C$ (Figure 4.4a) argues that the feature in $\Delta^{14}C_{LMcorr}$ is not likely to be an artifact of MRA corrections to coral ^{14}C ages.

An increase of 60 to 80‰ in $\Delta^{14}C_{LMcorr}$ can be reasonably generated with increased production estimates based on changes in the relative intensity of the geomagnetic dipole (Lal, 1988). The record of $\Delta^{14}C_{LMcorr}$ from 20 to 18 kyr BP may be evidence for increased radiocarbon production associated with the Hilina Pali geomagnetic excursion. The Hilina Pali event was first identified in paleointensity and inclination measurements taken in Hawaiian lava flows and documents a geomagnetic field excursion at around 20 kyr BP, based on ^{14}C dating. (Coe et al., 1978; Teanby et al., 2002). Lavas from China and from the western United States display low paleointensities and transitional Virtual Geomagnetic poles (VGP), consistent with the Hilina Pali excursionoid event (Singer, 2014; Turrin et al., 2013). The age of the Hilina Pali Event, as determined by $^{40}Ar/^{39}Ar$ dating of these same lava flows, suggests a younger age of about 17 ± 1 kyr BP (Singer, 2014; Turrin et al., 2013). Our record of $\Delta^{14}C_{LMcorr}$ record indicates increased production as early as 19 kyr BP. Virtual axial dipole moment (VADM) reconstructions based on ^{10}Be accumulation rates in ice cores do not provide convincing evidence for a weakened field at this time (Frank et al., 1997; Muscheler et al., 2005; Muscheler et al., 2004) although estimates of ^{10}Be fluxes measured in ice cores are highly dependent upon the accuracy of ice core age models and changes in precipitation transport. $\Delta^{14}C$ records calculated from ^{10}Be fluxes or paleointensity stacked-records do not indicate a spike in atmospheric ^{14}C corresponding to the Hilina

Pali event (Hain et al., 2014; Muscheler et al., 2005). Nevertheless, we maintain the record of $\Delta^{14}C$ obtained with fossil corals and corrected for excess ^{14}C due to the Laschamp and Mono Lake Excursions can be considered as the most direct and reliably dated record of production changes associated with the Hilina Pali event. Additional records of $\Delta^{14}C$ with sufficient resolution, derived from both marine and atmospheric archives, and more precisely dated lava flows (i.e., U-Th) will be needed to confirm and constrain records of $\Delta^{14}C_{LMcorr}$ and the timing and duration of the Hilina Pali excursion. One might speculate as to whether or not the scatter in $\Delta^{14}C_{LMcorr}$ observed at 19.5 kyr BP represents decadal-scale variability in production rate that reflect instability in the geomagnetic dipole.

The contributions from Laschamp and Mono Lake to excess atmospheric ^{14}C at 14.5 kyr BP are 20‰ and 54‰, respectively (Figure 4.6) but have little impact on the shape of the decline in $\Delta^{14}C_{LMcorr}$ during the Bølling/Allerød (Figure 4.6). Excess ^{14}C associated with the Hilina Pali event and its subsequent decay would shift $\Delta^{14}C_{LMcorr}$ higher, by about 30 to 40‰ during the Bølling/Allerød but would not alter the amplitude change observed from 14.7 to 14.1 kyr BP attributed to switch on of NADW.

4.6 Conclusions

We have computed a record of the atmospheric $^{14}C/^{12}C$ ratio from 22 to 13 kyr BP with 142 U-Th and ^{14}C dated Barbados corals, providing the only directly dated marine record to span the entire LGM to Holocene time interval. Forty-three of these samples correspond to the Mystery Interval (17.5 to 14.5 kyr BP). After correcting for excess ^{14}C produced during the Laschamp (41 kyr) and Mono Lake (31.5 kyr) geomagnetic excursions, our estimate of the residual $\Delta^{14}C$ ($\Delta^{14}C_{LMcorr}$) during the Mystery Interval

cannot be readily distinguished from the long-term trend. Attempts linking records of atmospheric ^{14}C with those of ocean ventilation 17.5 to 14.5 kyr BP (Bryan et al., 2010; Burke and Robinson, 2012; Marchitto et al., 2007) suffer from two shortcomings: 1) reliance on $\Delta^{14}C$ target records (e.g., IntCal09) that erroneously exaggerated the amplitude decrease in $\Delta^{14}C$ and 2) a failure to correct for the compounded contributions of increases in $\Delta^{14}C$ from the Laschamp and Mono Lake Excursions. The record of $\Delta^{14}C_{LMcorr}$ reveals a period of increased atmospheric ^{14}C preceding the Mystery Interval that we attribute to increased production during a period of weakened geomagnetic field strength (Hilina Pali Excursion).

A sharp decrease in $\Delta^{14}C$ beginning at 14.7 kyr coincides with deep-sea core proxy evidence for the switch 'on' of NADW during the last deglacial period and provides credible evidence to hypotheses linking changes in NADW production to changes in the ^{14}C content of the atmosphere. A decrease in $^{14}C/^{12}C$ atmospheric ratio from 14.7 kyr to 14.0 kyr BP also corresponds to a time of high latitude Northern Hemispheric warming, increased GHG, and to a rapid rise in sea level (MWP-1A). This coincidence is, perhaps, the strongest evidence to date that the rate of NADW production is one of the key amplifiers of the Milankovitch Theory of climate change.

Large offsets in age and in $\Delta^{14}C$ records observed between Barbados corals and IntCal09 curves are due to inaccuracies in the calendar age model constructed in the Cariaco Basin deep-sea core. The Pacific Tahiti calibration data points are generally in agreement with the Atlantic Barbados data set thereby making a strong case for the combined coral record.

Age and $\Delta^{14}C$ differences between Barbados coral and Tahiti coral data and Hulu Cave stalagmite data and Intcal13 during the MI are most likely due to a combination of reduced dead carbon fractions and under-reported initial ^{230}Th corrections to U-Th ages in Hulu Cave H82 data. Many factors determine whether alternating dissolution followed by re-precipitation of individual cave deposits occurs that can add additional distortion to $\Delta^{14}C$ records. These include changes in cave temperature, humidity, changes in climate precipitation patterns, soil thickness and type, changes in vegetation and amount of carbon dioxide in the vadose waters. All of these parameters change with changing climate. In addition, the accuracy of calibration and $\Delta^{14}C$ data in the slow growing H82 specimen may be compromised since "paring" of calendar ages with ^{14}C ages must be accomplished via interpolation between adjacent U-Th dates. Systematic offsets between corals and H82 during the Mystery Interval are more difficult to reconcile with marine reservoir corrections, as it would require sustained tropical Atlantic surface water ^{14}C age of 500 to 700 years, a condition that is not found in the modern ocean or in the late deglacial- Holocene history of marine reservoir age at Barbados. Lastly, reproducible $\Delta^{14}C$ cave records from cave deposits around the world must be achieved before H82 archive can be considered to be reliable.

4.7 References

Abdul, N. A., Mortlock, R. A., Wright, J. D., and Fairbanks, R. G., 2016, Younger Dryas sea level and meltwater pulse 1B recorded in Barbados reef crest coral *Acropora palmata*: Paleoceanography, v. 31, no. 2, p. 330-344.

Adkins, J., and Boyle, E., 1997, Changing atmospheric ^{14}C and the record of deep water paleoventilation ages: Paleoceanography, v. 12, p. 337-344.

Anderson, R. F., Ali, S., Bradtmiller, L. I., Nielsen, S. H. H., Fleisher, M. Q., Anderson, B. E., and Burckle, L. H., 2009, Wind-Driven Upwelling in the Southern Ocean and the Deglacial Rise in Atmospheric CO_2: Science, v. 323, no. 5920, p. 1443-1448.

Bard, E., 1988, Correction of accelerator mass spectrometry ^{14}C ages measured in planktonic foraminifera: Paleoceanographic implications: Paleoceanography, v. 3, no. 6, p. 635-645.

Bard, E., Arnold, M., Hamelin, B., Tisnerat-Laborde, N., and Cabioch, G., 1998, Radiocarbon calibration by means of mass spectrometric $^{230}Th/^{234}U$ and ^{14}C ages of corals: An updated database including samples from Barbados, Mururoa, and Tahiti: Radiocarbon, v. 40, no. 3, p. 1085-1092.

Bard, E., Hamelin, B., Fairbanks, R. G., and Zindler, A., 1990, Calibration of the ^{14}C timescale over the past 30,000 years using mass spectrometric U-Th ages from Barbados corals: Nature, v. 345, p. 405-410.

Barker, S., Knorr, G., Vautravers, M. J., Diz, P., and Skinner, L. C., 2010, Extreme deepening of the Atlantic overturning circulation during deglaciation: Nature Geosci, v. 3, no. 8, p. 567-571.

Bassett, S. E., Milne, G. A., Bentley, M. J., and Huybrechts, P., 2007, Modelling Antarctic sea-level data to explore the possibility of a dominant Antarctic contribution to meltwater pulse IA: Quaternary Science Reviews, v. 26, no. 17–18, p. 2113-2127.

Bassett, S. E., Milne, G. A., Mitrovica, J. X., and Clark, P. U., 2005, Ice Sheet and Solid Earth Influences on Far-Field Sea-Level Histories: Science, v. 309, no. 5736, p. 925-928.

Beck, J. W., Richards, D. A., Lawrence , R., Edwards, Silverman, B. W., Smart, P. L., Donahue, D. J., Hererra-Osterheld, S., Burr, G. S., Calsoyas, L., Timothy , A. J., Jull, and Biddulph, D., 2001, Extremely Large Variations of Atmospheric 14C Concentration During the Last Glacial Period: Science, v. 292, no. 5526, p. 2453-2458.

Bianchi, C., and Gersonde, R., 2004, Climate evolution at the last deglaciation: the role of the Southern Ocean: Earth and Planetary Science Letters, v. 228, no. 3–4, p. 407-424.

Boyle, E. A., and Keigwin, L., 1987, North Atlantic thermohaline circulation during the past 20,000 years linked to high-latitude surface temperature: Nature, v. 330, no. 6143, p. 35-40.

Broecker, W., 2009, The Mysterious ^{14}C Decline: Radiocarbon, v. 51, no. 1, p. 109-119.

Broecker, W., and Barker, S., 2007, A 190‰ drop in atmosphere's $\Delta^{14}C$ during the "Mystery Interval" (17.5 to 14.5 kyr): Earth and Planetary Science Letters, v. 256, no. 1-2, p. 90-99.

Broecker, W., Barker, S., Clark, E., Hajdas, I., Bonani, G., and Stott, L., 2004, Ventilation of the Glacial Deep Pacific Ocean: Science, v. 306, no. 5699, p. 1169-1172.

Broecker, W. S., Andree, M., Bonani, G., Wolfli, W., Klas, M., Mix, A., and Oeschger, H., 1988, Comparison between radiocarbon ages obtained on coexisting planktonic foraminifera: Paleoceanography, v. 3, no. 6, p. 647-657.

Bryan, S. P., Marchitto, T. M., and Lehman, S. J., 2010, The release of ^{14}C-depleted carbon from the deep ocean during the last deglaciation: Evidence from the Arabian Sea: Earth and Planetary Science Letters, v. 298, no. 1–2, p. 244-254.

Burke, A., and Robinson, L. F., 2012, The Southern Ocean's role in carbon exchange during the last deglaciation: Science, v. 335, no. 6068, p. 557-561.

Butzin, M., Prange, M., and Lohmann, G., 2005, Radiocarbon simulations for the glacial ocean: The effects of wind stress, Southern Ocean sea ice and Heinrich events: Earth and Planetary Science Letters, v. 235, no. 1–2, p. 45-61.

-, 2012, Readjustment of glacial radiocarbon chronologies by self-consistent three-dimensional ocean circulation modeling: Earth and Planetary Science Letters, v. 317-318, p. 177-184.

Cao, L., 2010, High-precision $^{230}Th/^{234}U$ dating of the surface ocean radiocarbon record and its geochemical and geophysical implications [PhD: Columbia University, 145 p.

Carolin, S. A., Cobb, K. M., Adkins, J. F., Clark, B., Conroy, J. L., Lejau, S., Malang, J., and Tuen, A. A., 2013, Varied Response of Western Pacific Hydrology to Climate Forcings over the Last Glacial Period: Science, v. 340, no. 6140, p. 1564-1566.

Charles, C. D., and Fairbanks, R. G., 1992, Evidence from Southern Ocean sediments for the effect of North Atlantic deep-water flux on climate: Nature, v. 355, no. 6359, p. 416-419.

Charles, C. D., Pahnke, K., Zahn, R., Mortyn, P. G., Ninnemann, U., and Hodell, D. A., 2010, Millennial scale evolution of the Southern Ocean chemical divide: Quaternary Science Reviews, v. 29, no. 3–4, p. 399-409.

Charles, C. D., Rind, D., Jouzel, J., Koster, R. D., and Fairbanks, R. G., 1994, Glacial-Interglacial Changes in Moisture Sources for Greenland: Influences on the Ice Core Record of Climate: Science, v. 263, no. 5146, p. 508-511.

Chiu, T.-C., Fairbanks, R. G., Cao, L., and Mortlock, R. A., 2007, Analysis of the atmospheric ^{14}C record spanning the past 50,000 years derived from high-precision $^{230}Th/^{234}U/^{238}U$, $^{231}Pa/^{235}U$ and ^{14}C dates on fossil corals: Quaternary Science Reviews, v. 26, no. 1-2, p. 18-36.

Chiu, T.-c., Fairbanks, R. G., Mortlock, R. A., and Bloom, A. L., 2005, Extending the radiocarbon calibration beyond 26,000 years before present using fossil corals: Quaternary Science Reviews, v. 24, no. 16-17, p. 1797-1808.

Clark, P. U., Mitrovica, J. X., Milne, G. A., and Tamisiea, M. E., 2002, Sea-Level Fingerprinting as a Direct Test for the Source of Global Meltwater Pulse IA: Science, v. 295, no. 5564, p. 2438-2441.

Cléroux, C., deMenocal, P., and Guilderson, T., 2011, Deglacial radiocarbon history of tropical Atlantic thermocline waters: absence of CO_2 reservoir purging signal: Quaternary Science Reviews, v. 30, no. 15–16, p. 1875-1882.

Coe, R. S., Gromme, S., and Mankinen, E. A., 1978, Geomagnetic Paleointensities from Radiocarbon-Dated Lava Flows on Hawaii and the Question of the Pacific Nondipole Low: Journal of Geophysical Research, v. 83, p. 1740-1756.

Cuffey, K., and Paterson, W. S., 2010, The Physics of Glaciers, Oxford, UK, Elsevier, 704 p.:

Cutler, K. B., Gray, S. C., Burr, G. S., Edwards, R. L., Taylor, F. W., Cabioch, G., Beck, J. W., Cheng, H., and Moore, J., 2004, Radiocarbon calibration and comparison to 50 kyr with paired ^{14}C and ^{230}Th dating of corals from Vanuatu and Papua New Guinea: Radiocarbon, v. 46, p. 1127-1160.

De Pol-Holz, R., Keigwin, L., Southon, J., Hebbeln, D., and Mohtadi, M., 2010, No signature of abyssal carbon in intermediate waters off Chile during deglaciation: Nature Geosci, v. 3, no. 3, p. 192-195.

Delaygue, G., Stocker, T. F., Joos, F., and Plattner, G.-K., 2003, Simulation of atmospheric radiocarbon during abrupt oceanic circulation changes: trying to reconcile models and reconstructions: Quaternary Science Reviews, v. 22, no. 15–17, p. 1647-1658.

Denton, G. H., Broecker, W. S., and Alley, R. B., 2006, The mystery interval 17.5 to 14.5 kyrs ago: PAGES NEWS, v. 14, no. 2, p. 14-16.

Deschamps, P., Durand, N., Bard, E., Hamelin, B., Camoin, G., Thomas, A. L., Henderson, G. M., Okuno, J., and Yokoyama, Y., 2012, Ice-sheet collapse and sea-level rise at the Bolling warming 14,600 years ago: Nature, v. 483, no. 7391, p. 559-564.

Duplessy, J. C., Arnold, M., Bard, E., Juillet-Leclerc, A., Kallel, N., and Labeyrie, L., 1989, AMS ^{14}C study of transient events and the ventilaton rate of the Pacific Intermediate water during the last deglaciation: Radiocarbon, v. 31, no. 3, p. 493-502.

Durand, N., Deschamps, P., Bard, E., Hamelin, B., Camoin, G., Thomas, A. L., Henderson, G. M., Yokoyama, Y., and Matsuzaki, H., 2013, Comparison of ^{14}C and U-Th ages in corals form IODP #310 cores offshore Tahiti: Radiocarbon, v. 55, no. 2, p. 1-26.

Edwards, R. L., Beck, J. W., Burr, G. S., Donahue, D. J., Chappell, J. M. A., Bloom, A. L., Druffel, E. R. M., and Taylor, F. W., 1993, A Large Drop in Atmospheric $^{14}C/^{12}C$ and Reduced Melting in the Younger Dryas, Documented with ^{230}Th Ages of Corals: Science, v. 260, no. 5110, p. 962-968.

Elmore, A. C., and Wright, J. D., 2011, North Atlantic Deep Water and climate variability during the Younger Dryas cold period: Geology, v. 39, no. 2, p. 107-110.

Elsasser, W., Ney, E. P., and Winckler, J. R., 1956, Cosmic-ray intensity and geomagnetism: Nature, v. 178, p. 1226-1227.

Fairbanks0107, 2007, Updated radiocarbon calibration curve available at http://www.radiocarbon.ldeo.columbia.edu.

Fairbanks, R. G., 1989, A 17,000-year glacio-eustatic sea level record: influence of glacial melting rates on the Younger Dryas event and deep-ocean circulation: Nature, v. 342, no. 6250, p. 637-642.

Fairbanks, R. G., Mortlock, R. A., Chiu, T.-C., Cao, L., Kaplan, A., Guilderson, T. P., Fairbanks, T. W., Bloom, A. L., Grootes, P. M., and Nadeau, M.-J., 2005,

Radiocarbon calibration curve spanning 0 to 50,000 years BP based on paired $^{230}Th/^{234}U/^{238}U$ and ^{14}C dates on pristine corals: Quaternary Science Reviews, v. 24, no. 16-17, p. 1781-1796.

Fairbanks, R. G., Mortlock, R. A., Wright, J. D., Abdul, N., and Mey, J., 2016, The Barbados sea level curve (MS in prep.).

Finkel, R. C., and Nishiizumi, K., 1997, Beryllium 10 concentrations in the Greenland Ice Sheet Project 2 ice core from 3–40 ka: Journal of Geophysical Research: Oceans, v. 102, no. C12, p. 26699-26706.

Frank, M., Schwarz, B., Baumann, S., Kubik, P. W., Suter, M., and Mangini, A., 1997, A 200 kyr record of cosmogenic radionuclide production rate and geomagnetic field intensity from 10Be in globally stacked deep-sea sediments1: Earth and Planetary Science Letters, v. 149, no. 1–4, p. 121-129.

Genty, D., Baker, A., Massault, M., Proctor, C., Gilmour, M., Pons-Branchu, E., and Hamelin, B., 2001, Dead carbon in stalagmites: carbonate bedrock paleodissolution vs. ageing of soil organic matter. Implications for 13C variations in speleothems: Geochimica et Cosmochimica Acta, v. 65, no. 20, p. 3443-3457.

Guilderson, T. P., Cole, J. E., and Southon, J. R., 2005, Pre-bomb $\Delta^{14}C$ variability and the Suess effect in Cariaco Basin surface waters as recorded in hermatypic corals: Radiocarbon, v. 47, p. 57–65.

Hain, M. P., Sigman, D. M., and Haug, G. H., 2011, Shortcomings of the isolated abyssal reservoir model for deglacial radiocarbon changes in the mid-depth Indo-Pacific Ocean: Geophysical Research Letters, v. 38, no. 4.

-, 2014, Distinct roles of the Southern Ocean and North Atlantic in the deglacial atmospheric radiocarbon decline: Earth and Planetary Science Letters, v. 394, p. 198-208.

Hanebuth, T., Stattegger, K., and Grootes, P. M., 2000, Rapid Flooding of the Sunda Shelf: A Late-Glacial Sea-Level Record: Science, v. 288, no. 5468, p. 1033-1035.

Hemming, S. R., 2004, Heinrich events: Massive late Pleistocene detritus layers of the North Atlantic and their global climate imprint: Reviews of Geophysics, v. 42, no. 1.

Hendy, C. H., 1971, The isotopic geochemistry of speleothems — I. The calculation of the effects of different modes of formation on the isotopic composition of speleothems and their applicability as palaeoclimatic indicators: Geochimica et Cosmochimica Acta, v. 35, no. 8, p. 801-824.

Hoffmann, D. L., Beck, J. W., Richards, D. A., Smart, P. L., Singarayer, J. S., Ketchmark, T., and Hawkesworth, C. J., 2010, Towards radiocarbon calibration beyond 28ka using speleothems from the Bahamas: Earth and Planetary Science Letters, v. 289, no. 1-2, p. 1-10.

Hua, Q., Barbetti, M., Fink, D., Kaiser, K. F., Friedrich, M., Kromer, B., Levchenko, V. A., Zoppi, U., Smith, A. M., and Bertuch, F., 2009, Atmospheric ^{14}C variations derived from tree rings during the early Younger Dryas: Quaternary Science Reviews, v. 28, no. 25-26, p. 2982-2990.

Hughen, K., Lehman, S., Southon, J., Overpeck, J., Marchal, O., Herring, C., and Turnbull, J., 2004, ^{14}C Activity and Global Carbon Cycle Changes over the Past 50,000 Years: Science, v. 303, no. 5655, p. 202-207.

Hughen, K., Southon, J., Lehman, S., Bertrand, C., and Turnbull, J., 2006, Marine-derived ^{14}C calibration and activity record for the past 50,000 years updated from the Cariaco Basin: Quaternary Science Reviews, v. 25, no. 23-24, p. 3216-3227.

Hughen, K. A., Overpeck, J. T., Lehman, S. J., Kashgarian, M., Southon, J., Peterson, L. C., Alley, R., and Sigman, D. M., 1998, Deglacial changes in ocean circulation from an extended radiocarbon calibration: Nature, v. 391, no. 6662, p. 65-68.

Hughen, K. A., Southon, J. R., Lehman, S. J., and Overpeck, J. T., 2000, Synchronous Radiocarbon and Climate Shifts During the Last Deglaciation: Science, v. 290, no. 5498, p. 1951-1954.

Key, R. M., Kozyr, A., Sabine, C. L., Lee, K., Wanninkhof, R., Bullister, J. L., Feely, R. A., Millero, F. J., Mordy, C., and Peng, T. H., 2004, A global ocean carbon climatology: Results from Global Data Analysis Project (GLODAP): Global Biogeochem. Cycles, v. 18, no. 4, p. GB4031.

Knorr, G., and Lohmann, G., 2003, Southern Ocean origin for the resumption of Atlantic thermohaline circulation during deglaciation: Nature, v. 424, no. 6948, p. 532-536.

Köhler, P., Knorr, G., and Bard, E., 2014, Permafrost thawing as a possible source of abrupt carbon release at the onset of the Bølling/Allerød: Nat Commun, v. 5.

Lal, D., 1988, Theoretically expected variations in the terrestrial cosmicray production rates of isotope *in* Castagnoli, G. C., ed., Solar–Terrestrial Relationships and the Earth Environment in the Last Millennia: Amsterdam, NY, North-Holland.

Lascu, I., Feinberg, J. M., Dorale, J. A., Cheng, H., and Edwards, R. L., 2016, Age of the Laschamp excursion determined by U-Th dating of a speleothem geomagnetic record from North America: Geology.

Libby, W. F., 1955, Radiocarbon Dating 2nd Edition, Chicago, Illinois, University of Chicago Press.

Liu, Z., Carlson, A. E., He, F., Brady, E. C., Otto-Bliesner, B. L., Briegleb, B. P., Wehrenberg, M., Clark, P. U., Wu, S., Cheng, J., Zhang, J., Noone, D., and Zhu, J., 2012, Younger Dryas cooling and the Greenland climate response to CO_2: Proceedings of the National Academy of Sciences.

Lund, D. C., 2013, Deep Pacific ventilation ages during the last deglaciation: Evaluating the influence of diffusive mixing and source region reservoir age: Earth and Planetary Science Letters, v. 381, no. 0, p. 52-62.

Lund, D. C., Mix, A. C., and Southon, J., 2011, Increased ventilation age of the deep northeast Pacific Ocean during the last deglaciation: Nature Geosci, v. 4, no. 11, p. 771-774.

Manabe, S., and Stouffer, R. J., 1995, Simulation of abrupt climate change induced by freshwater input to the North Atlantic Ocean: Nature, v. 378, no. 6553, p. 165-167.

Mangini, A., Godoy, J. M., Godoy, M. L., Kowsmann, R., Santos, G. M., Ruckelshausen, M., Schroeder-Ritzrau, A., and Wacker, L., 2010, Deep sea corals off Brazil verify a poorly ventilated Southern Pacific Ocean during H2, H1 and the Younger Dryas: Earth and Planetary Science Letters, v. 293, no. 3-4, p. 269-276.

Marchitto, T. M., Lehman, S. J., Ortiz, J. D., Fluckiger, J., and van Geen, A., 2007, Marine radiocarbon evidence for the mechanism of deglacial atmospheric CO_2 rise: Science, v. 316, no. 5830, p. 1456-1459.

Marcott, S. A., Bauska, T. K., Buizert, C., Steig, E. J., Rosen, J. L., Cuffey, K. M., Fudge, T. J., Severinghaus, J. P., Ahn, J., Kalk, M. L., McConnell, J. R., Sowers, T., Taylor, K. C., White, J. W. C., and Brook, E. J., 2014, Centennial-scale changes in the global carbon cycle during the last deglaciation: Nature, v. 514, no. 7524, p. 616-619.

Martinson, D. G., Pisias, N. G., Hays, J. D., Imbrie, J., Moore Jr, T. C., and Shackleton, N. J., 1987, Age dating and the orbital theory of the ice ages: Development of a high-resolution 0 to 300,000-year chronostratigraphy: Quaternary Research, v. 27, no. 1, p. 1-29.

Matsumoto, K., and Yokoyama, Y., 2013, Atmospheric $\Delta^{14}C$ reduction in simulations of Atlantic overturning circulation shutdown: Global Biogeochemical Cycles, v. 27, no. 2, p. 296-304.

McManus, J. F., Francois, R., Gherardi, J. M., Keigwin, L. D., and Brown-Leger, S., 2004, Collapse and rapid resumption of Atlantic meridional circulation linked to deglacial climate changes: Nature, v. 428, no. 6985, p. 834-837.

Monnin, E., Indermühle, A., Dällenbach, A., Flückiger, J., Stauffer, B., Stocker, T. F., Raynaud, D., and Barnola, J.-M., 2001, Atmospheric CO_2 Concentrations over the Last Glacial Termination: Science, v. 291, no. 5501, p. 112-114.

Mortlock, R. A., Fairbanks, R. G., Chiu, T.-c., and Rubenstone, J., 2005, $^{230}Th/^{234}U/^{238}U$ and $^{231}Pa/^{235}U$ ages from a single fossil coral fragment by multi-collector magnetic-sector inductively coupled plasma mass spectrometry: Geochimica et Cosmochimica Acta, v. 69, no. 3, p. 649-657.

Muscheler, R., Beer, J., Kubik, P. W., and Synal, H. A., 2005, Geomagnetic field intensity during the last 60,000 years based on ^{10}Be and ^{36}Cl from the Summit ice cores and ^{14}C: Quaternary Science Reviews, v. 24, no. 16-17, p. 1849-1860.

Muscheler, R., Beer, J., Wagner, G., and Finkel, R. C., 2000, Changes in deep-water formation during the Younger Dryas event inferred from ^{10}Be and ^{14}C records: Nature, v. 408, no. 6812, p. 567-570.

Muscheler, R., Beer, J., Wagner, G., Laj, C., Kissel, C., Raisbeck, G. M., Yiou, F., and Kubik, P. W., 2004, Changes in the carbon cycle during the last deglaciation as indicated by the comparison of ^{10}Be and ^{14}C records: Earth and Planetary Science Letters, v. 219, no. 3-4, p. 325-340.

Muscheler, R., Kromer, B., Bjorck, S., Svensson, A., Friedrich, M., Kaiser, K. F., and Southon, J., 2008, Tree rings and ice cores reveal ^{14}C calibration uncertainties during the Younger Dryas: Nature Geosci, v. 1, no. 4, p. 263-267.

Oppo, D. W., and Fairbanks, R. G., 1987, Variability in the deep and intermediate water circulation of the Atlantic Ocean during the past 25,000 years: Northern Hemisphere modulation of the Southern Ocean: Earth and Planetary Science Letters, v. 86, no. 1, p. 1-15.

Oppo, D. W., Fairbanks, R. G., Gordon, A. L., and Shackleton, N. J., 1990, Late Pleistocene Southern Ocean $\delta^{13}C$ variability: Paleoceanography, v. 5, no. 1, p. 43-54.

Partin, J. W., Cobb, K. M., Adkins, J. F., Clark, B., and Fernandez, D. P., 2007, Millennial-scale trends in west Pacific warm pool hydrology since the Last Glacial Maximum: Nature, v. 449, no. 7161, p. 452-455.

Peltier, W. R., and Fairbanks, R. G., 2006, Global glacial ice volume and Last Glacial Maximum duration from an extended Barbados sea level record: Quaternary Science Reviews, v. 25, no. 23-24, p. 3322-3337.

Piotrowski, A. M., Goldstein, S. L., Hemming, S. R., and Fairbanks, R. G., 2005, Temporal Relationships of Carbon Cycling and Ocean Circulation at Glacial Boundaries: Science, v. 307, no. 5717, p. 1933-1938.

Ramsey, C. B., Staff, R. A., Bryant, C. L., Brock, F., Kitagawa, H., van der Plicht, J., Schlolaut, G., Marshall, M. H., Brauer, A., Lamb, H. F., Payne, R. L., Tarasov, P. E., Haraguchi, T., Gotanda, K., Yonenobu, H., Yokoyama, Y., Tada, R., and Nakagawa, T., 2012, A Complete Terrestrial Radiocarbon Record for 11.2 to 52.8 kyr B.P: Science, v. 338, no. 6105, p. 370-374.

Rasmussen, S. O., Andersen, K. K., Svensson, A. M., Steffensen, J. P., Vinther, B. M., Clausen, H. B., Siggaard-Andersen, M. L., Johnsen, S. J., Larsen, L. B., Dahl-Jensen, D., Bigler, M., Röthlisberger, R., Fischer, H., Goto-Azuma, K., Hansson, M. E., and Ruth, U., 2006, A new Greenland ice core chronology for the last glacial termination: Journal of Geophysical Research, v. 111, no. D6, p. D06102.

Ravelo, A. C., Fairbanks, R. G., and Philander, S. G. H., 1990, Reconstructing tropical Atlantic hydrography using planktontic foraminifera and an ocean model: Paleoceanography, v. 5, no. 3, p. 409-431.

Reimer, P. B., Baillie, M. G. L., Bard, E., Bayliss, A., Beck, J. W., Blackwell, P. G., Bronk Ramsey, C., Buck, C. E., Burr, G. S., Edwards, R. L., Friedrich, M., Grootes, P. M., Guilderson, T. P., Hajdas, I., Heaton, T., Hogg, A. G., Hughen, K., Kaiser, F., Kromer, B., McCormac, G., Manning, S., Reimer, R. W., Richards, D. A., Southon, J., Talamo, S., Turney, C., van der Plicht, J., and Weyhenmeyer, C. E., 2009, IntCal09 and Marine09 Radiocarbon Age Calibration Curves, 0–50,000 Years cal BP: Radiocarbon, v. 51, p. 1111-1150.

Reimer, P. B., Bard, E., Bayliss, A., Beck, J. W., Blackwell, P. G., Bronk Ramsey, C., Buck, C. E., Cheng, H., Edwards, R. L., Friedrich, M., Grootes, P. M., Guilderson, T. P., Haflidason, H., Hajdas, I., Hatte, C., Heaton, T., Hoffmann, D. L., Hogg, A. G., Hughen, K., Kaiser, F., Kromer, B., Manning, S., Niu, M., Reimer, R. W., Richards, D. A., Scott, E. M., Southon, J., Staff, R. A., Turney, C., and van der Plicht, J., 2013, IntCal13 and Marine13 Radiocarbon Age Calibration Curves 0-50,000 years Cal BP: Radiocarbon, v. 55, no. 4, p. 1869-1887.

Rose, K. A., Sikes, E. L., Guilderson, T. P., Shane, P., Hill, T. M., Zahn, R., and Spero, H. J., 2010, Upper-ocean-to-atmosphere radiocarbon offsets imply fast deglacial carbon dioxide release: Nature, v. 466, no. 7310, p. 1093-1097.

Rubin, S. I., and Key, R. M., 2002, Separating natural and bomb-produced radiocarbon in the ocean: The potential alkalinity method: Global Biogeochemical Cycles, v. 16, no. 4, p. 1105.

Sarnthein, M., 2011, Paleoclimate. Northern meltwater pulses, CO_2, and changes in Atlantic convection: Science, v. 331, no. 6014, p. 156-158.

Sarnthein, M., Schneider, B., and Grootes, P. M., 2013, Peak glacial ^{14}C ventilation ages suggest major draw-down of carbon into the abyssal ocean: Clim. Past Discuss., v. 9, no. 1, p. 925-965.

Schmitt, J., Schneider, R., Elsig, J., Leuenberger, D., Lourantou, A., Chappellaz, J., Köhler, P., Joos, F., Stocker, T. F., Leuenberger, M., and Fischer, H., 2012,

Carbon Isotope Constraints on the Deglacial CO_2 Rise from Ice Cores: Science, v. 336, no. 6082, p. 711-714.

Shackleton, N. J., Duplessy, J. C., Arnold, M., Maurice, P., Hall, M. A., and Cartlidge, J., 1988, Radiocarbon age of last glacial Pacific deep water: Nature, v. 335, no. 6192, p. 708-711.

Sikes, E. L., Samson, C. R., Guilderson, T. P., and Howard, W. R., 2000, Old radiocarbon ages in the southwest Pacific Ocean during the last glacial period and deglaciation: Nature, v. 405, no. 6786, p. 555-559.

Singarayer, J. S., Richards, D. A., Ridgwell, A., Valdes, P. J., Austin, W. E. N., and Beck, J. W., 2008, An oceanic origin for the increase of atmospheric radiocarbon during the Younger Dryas: Geophysical Research Letters, v. 35, no. 14.

Singer, B. S., 2014, A Quaternary geomagnetic instability time scale: Quaternary Geochronology, v. 21, no. 0, p. 29-52.

Singer, B. S., Guillou, H., Jicha, B. R., Laj, C., Kissel, C., Beard, B. L., and Johnson, C. M., 2009, $^{40}Ar/^{39}Ar$, K–Ar and $^{230}Th–^{238}U$ dating of the Laschamp excursion: A radioisotopic tie-point for ice core and climate chronologies: Earth and Planetary Science Letters, v. 286, no. 1-2, p. 80-88.

Skinner, L. C., Fallon, S., Waelbroeck, C., Michel, E., and Barker, S., 2010, Ventilation of the Deep Southern Ocean and Deglacial CO_2 Rise: Science, v. 328, no. 5982, p. 1147-1151.

Sortor, R. N., and Lund, D. C., 2011, No evidence for a deglacial intermediate water $\Delta^{14}C$ anomaly in the SW Atlantic: Earth and Planetary Science Letters, v. 310, no. 1-2, p. 65-72.

Southon, J., Noronha, A. L., Cheng, H., Edwards, R. L., and Wang, Y., 2012, A high-resolution record of atmospheric ^{14}C based on Hulu Cave speleothem H82: Quaternary Science Reviews, v. 33, no. 0, p. 32-41.

Stocker, T. F., and Wright, D. G., 1996, Rapid changes in ocean circulation and atmospheric radiocarbon: Paleoceanography, v. 11, no. 6, p. 773-795.

Stott, L., Southon, J., Timmermann, A., and Koutavas, A., 2009, Radiocarbon age anomaly at intermediate water depth in the Pacific Ocean during the last deglaciation: Paleoceanography, v. 24, no. 2.

Stuiver, M., and Braziunas, T. F., 1989, Atmospheric ^{14}C and century-scale solar oscillations: Nature, v. 338, no. 6214, p. 405-408.

Stuiver, M., and Polach, H., 1977, Discussion; Reporting of ^{14}C data: Radiocarbon, v. 19, p. 353-363.

Stuiver, M., and Quay, P. D., 1980, Changes in Atmospheric Carbon-14 Attributed to a Variable Sun: Science, v. 207, no. 4426, p. 11-19.

Svetlik, I., Povinec, P. P., Brabcova, K. P., Fejgl, M., Tomaskova, L., and Turek, K., 2013, Estimating the Amount of $^{14}CO_2$ in the Atmosphere During the Holocene and Glacial Periods: Radiocarbon, v. 55, no. Nr. 2-3, p. 1546-1555.

Teanby, N., Laj, C., Gubbins, D., and Pringle, M., 2002, A detailed palaeointensity and inclination record from drill core SOH1 on Hawaii: Physics of the Earth and Planetary Interiors, v. 131, no. 2, p. 101-140.

Thornalley, D. J., Barker, S., Broecker, W. S., Elderfield, H., and McCave, I. N., 2011, The deglacial evolution of North Atlantic deep convection: Science, v. 331, no. 6014, p. 202-205.

Thornalley, D. J. R., Bauch, H. A., Gebbie, G., Guo, W., Ziegler, M., Bernasconi, S. M., Barker, S., Skinner, L. C., and Yu, J., 2015, A warm and poorly ventilated deep Arctic Mediterranean during the last glacial period: Science, v. 349, no. 6249, p. 706-710.

Turrin, B., Champion, D. E., Mortlock, R. A., Fairbanks, R. G., and Swisher, C. C., 2013, $^{40}Ar/^{39}Ar$ and U-series ages of a Late Pleistocene geomagnetic excursion in Western North America: The Hilina Pali event in Western North America? , AGU, Fall 2013, Volume GP31A-06: San Francisco.

Wagner, e. a., 2009, Pre-Bomb Surface Water Radiocarbon of the Gulf of Mexico and Caribbean as Recorded in Hermatypic Corals: Radiocarbon, v. 51, p. 947-954.

Wang, Y. J., Cheng, H., Edwards, R. L., An, Z. S., Wu, J. Y., Shen, C.-C., and Dorale, J. A., 2001, A High-Resolution Absolute-Dated Late Pleistocene Monsoon Record from Hulu Cave, China: Science, v. 294, no. 5550, p. 2345-2348.

Weaver, A. J., Saenko, O. A., Clark, P. U., and Mitrovica, J. X., 2003, Meltwater Pulse 1A from Antarctica as a Trigger of the Bølling-Allerød Warm Interval: Science, v. 299, no. 5613, p. 1709-1713.

Wunsch, C., 2006, Abrupt climate change: An alternative view: Quaternary Research, v. 65, no. 2, p. 191-203.

Yu, J., and Elderfield, H., 2007, Benthic foraminiferal B/Ca ratios reflect deep water carbonate saturation state: Earth and Planetary Science Letters, v. 258, no. 1–2, p. 73-86.

4.8 Figures and Tables

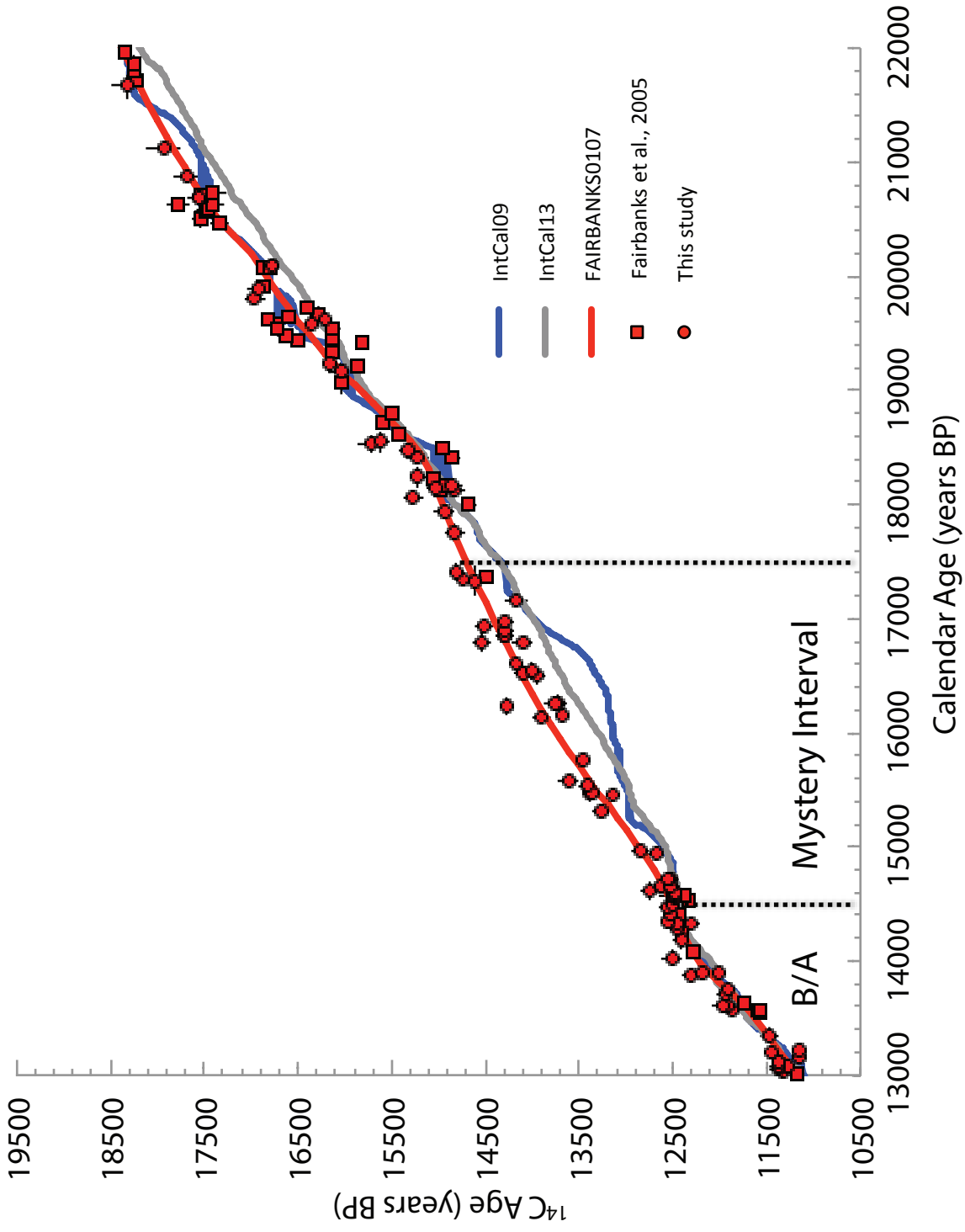
19500
18500
17500
16500
15500
14500
13500
12500
11500
10500
14C Age (years BP)
13000
14000
15000
16000
17000
18000
19000
20000
21000
22000
Calendar Age (years BP)
B/A
Mystery Interval
IntCal09
IntCal13
FAIRBANKS0107
Fairbanks et al., 2005
This study

Figure 4.1: MRA corrected ^{14}C age vs. Calendar ages: Red filled circles Barbados coral (this study). Red filled squares are Barbados coral data from Fairbanks et al. (2005). Red line is the Fairbanks0107calibration curve. Grey line is the IntCal13 (Reimer et al., 2013) calibration curve and the blue line is the IntCal09 calibration curve(Reimer et al., 2009). Vertical and horizontal errors bars are 2 s.d.

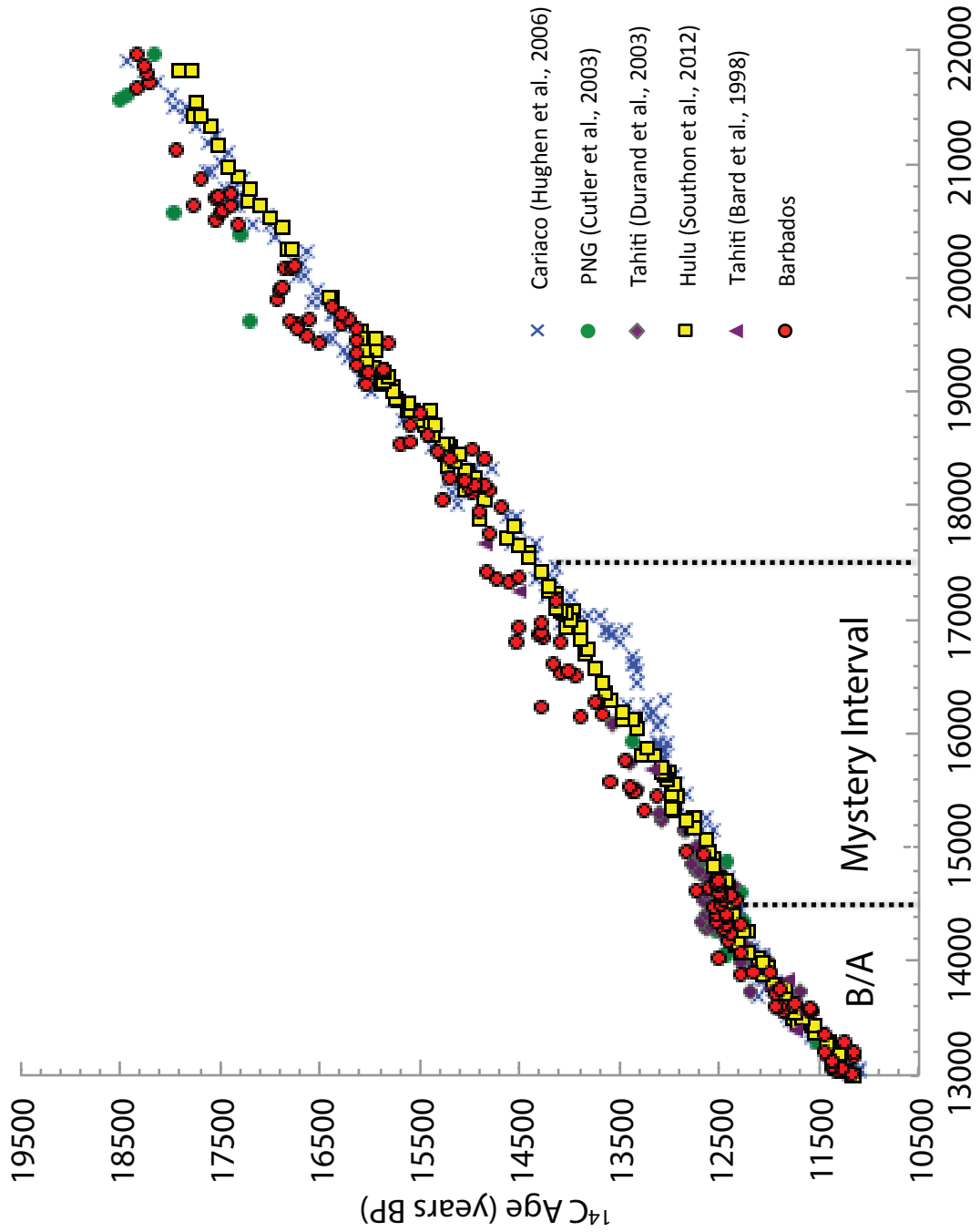
Cariaco (Hughen et al., 2006)
PNG (Cutler et al., 2003)
Tahiti (Durand et al., 2003)
Hulu (Southon et al., 2012)
Tahiti (Bard et al., 1998)
Barbados
B/A
Mystery Interval
Calendar Age (years BP)
14C Age (years BP)
19500
18500
17500
16500
15500
14500
13500
12500
11500
10500
13000
14000
15000
16000
17000
18000
19000
20000
21000
22000

Figure 4.2: ^{14}C age vs. Calendar age Barbados (red dots), Cariaco Basin (light blue cross), Papua New Guinea, green dots (Cutler et al., 2004), Tahiti, purple diamonds (Durand et al., 2013) and green triangles (Bard et al., 1998), and Hulu Cave H82, yellow squares (Southon et al., 2012).

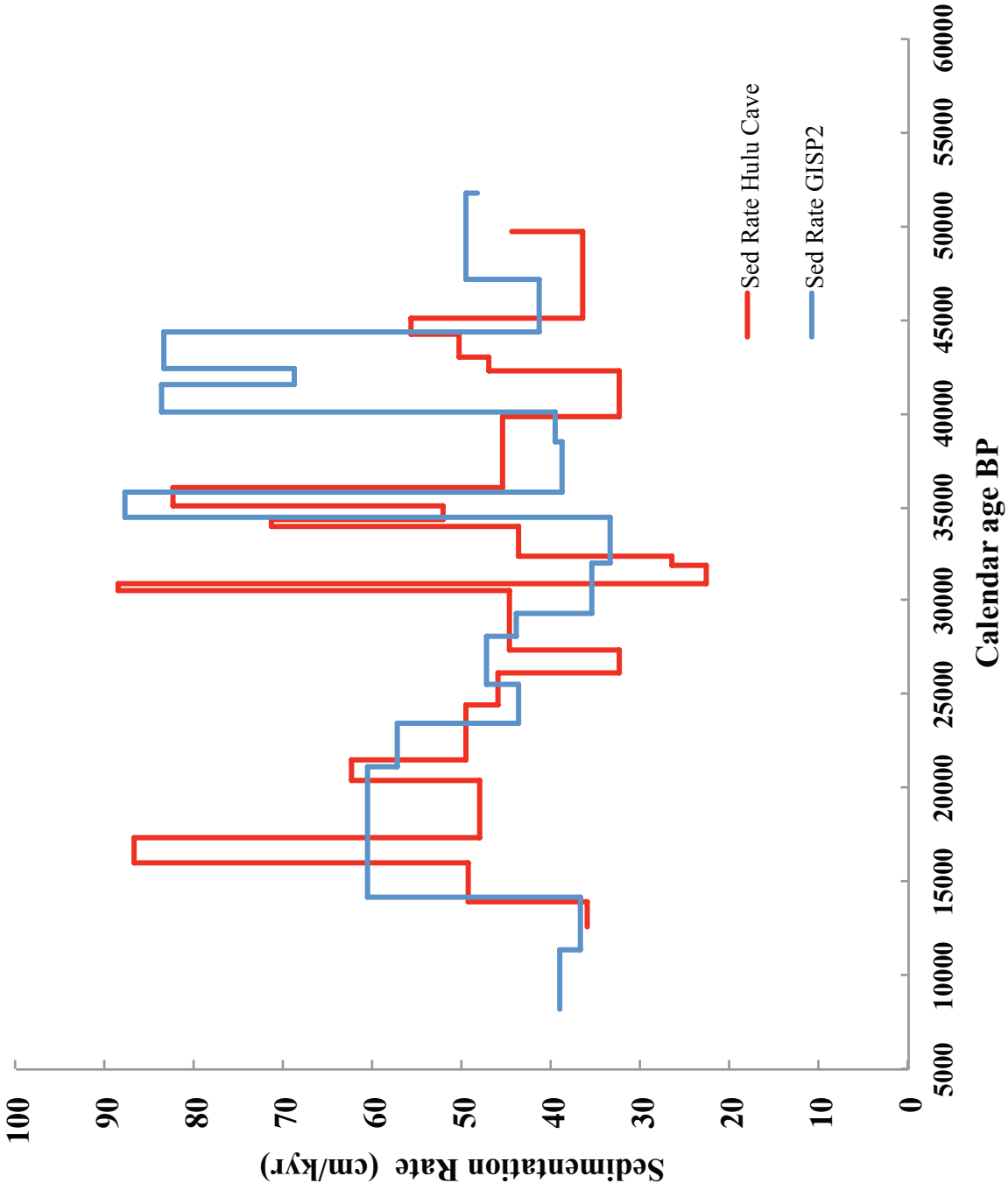
Sedimentation Rate (cm/kyr)
100
90
80
70
60
50
40
30
20
10
0
5000
10000
15000
20000
25000
30000
35000
40000
45000
50000
55000
60000
Calendar age BP
Sed Rate Hulu Cave
Sed Rate GISP2

Figure 4.3: Calculated sedimentation rates vs. Calendar Age for Cariaco Basin ODP 1002D based on the GISP ice core chronology (Hughen et al., 2004) and Hulu Cave U-Th chronology (Hughen et al., 2006). Sedimentation rates from GISP2 reported as in Chiu et al. (2007).

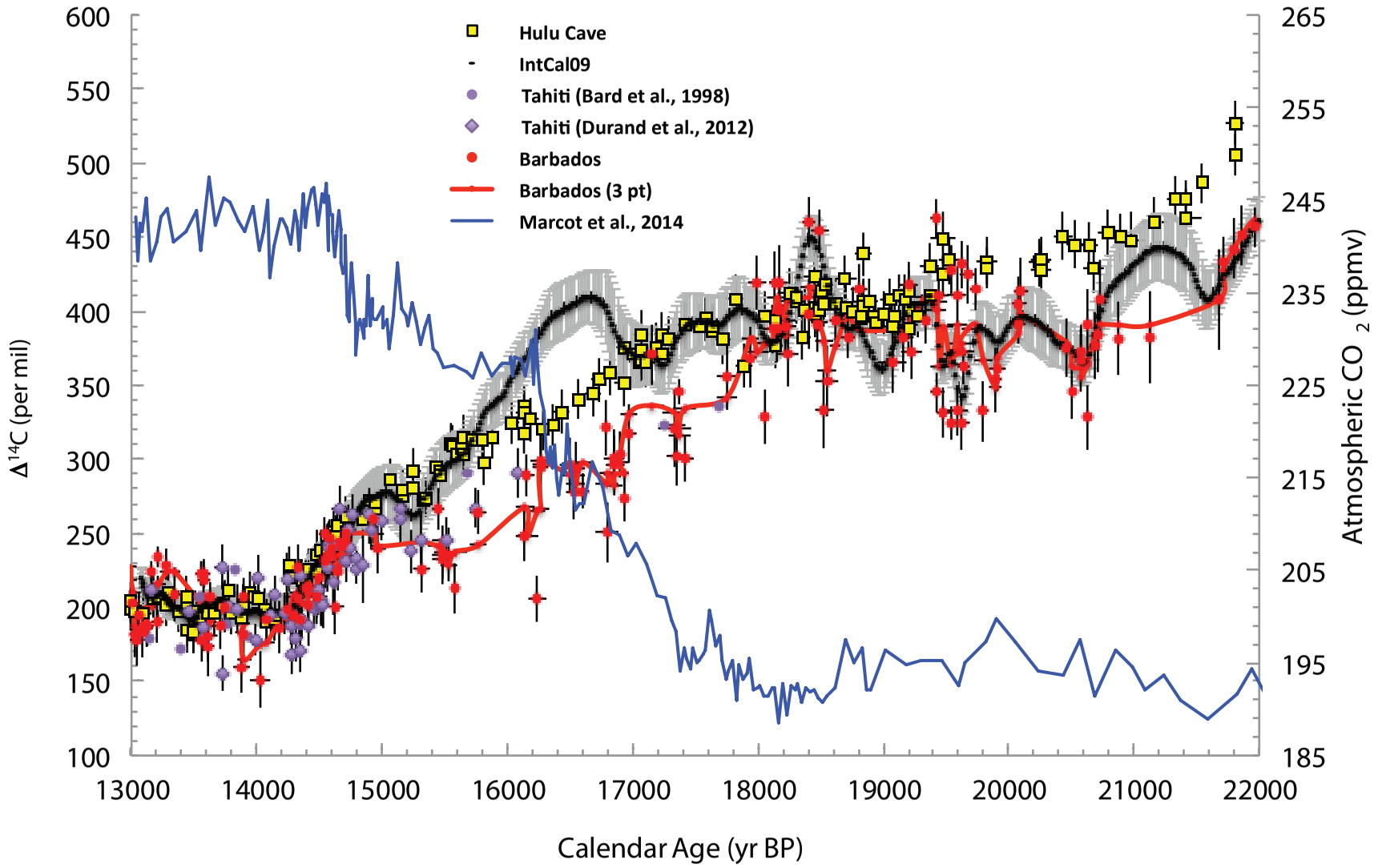
Hulu Cave
IntCal09
Tahiti (Bard et al., 1998)
Tahiti (Durand et al., 2012)
Barbados
Barbados (3 pt)
Marcot et al., 2014
Δ14C (per mil)
Atmospheric CO 2 (ppmv)
Calendar Age (yr BP)
600
550
500
450
400
350
300
250
200
150
100
265
255
245
235
225
215
205
195
185
13000
14000
15000
16000
17000
18000
19000
20000
21000
22000

Figure 4.4a: $\Delta^{14}C$ vs. calendar age: Barbados (red dots and 3-point running mean), Tahiti corals (purple diamonds), H82 speleothem, (yellow diamonds) and IntCal13 (black line). pCO_2 (blue line) from WDC06A-7 (Marcott et al., 2014). Error bars are 2 s.d.

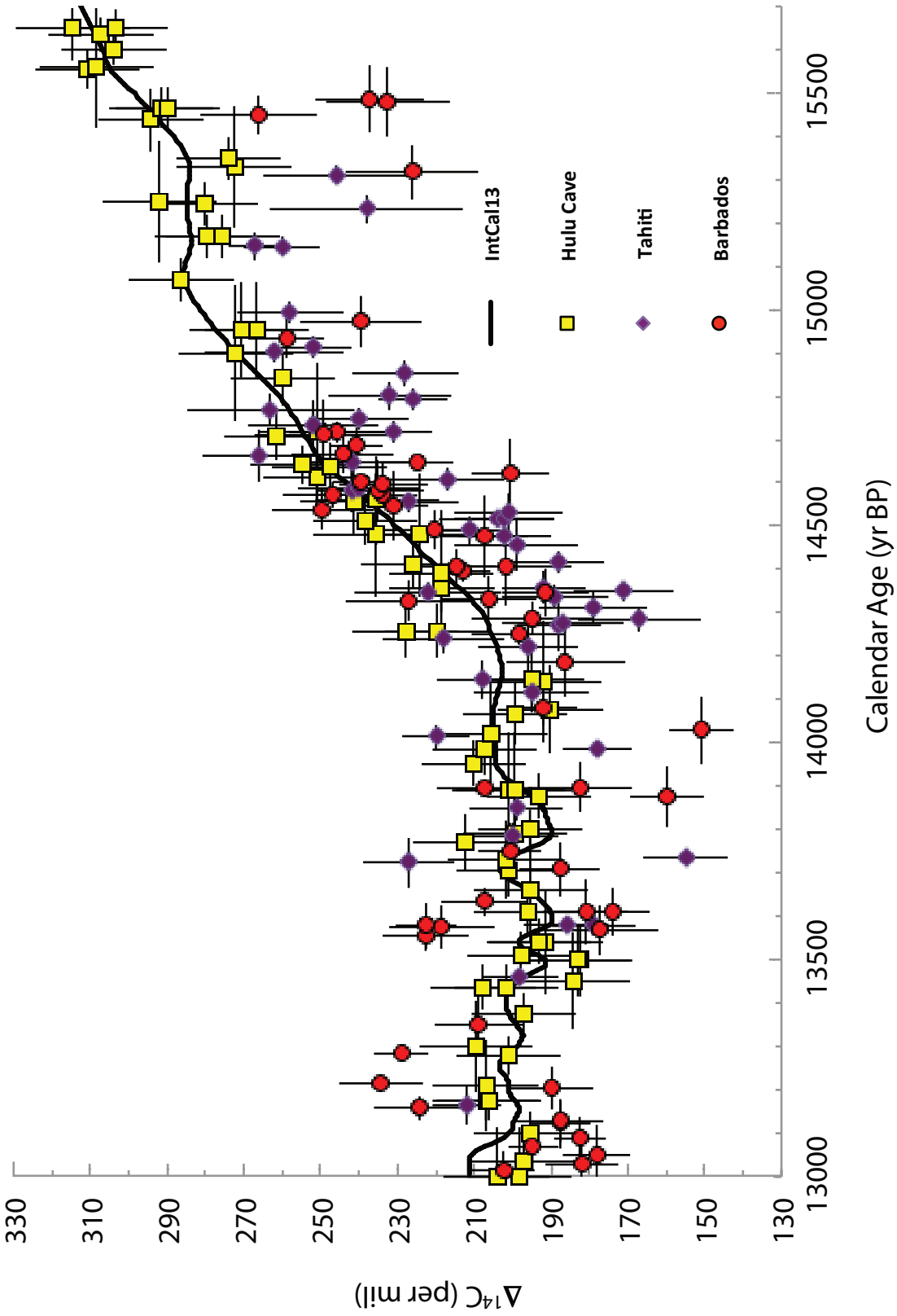
Δ14C (per mil)
330
310
290
270
250
230
210
190
170
150
130
13000
13500
14000
14500
15000
15500
Calendar Age (yr BP)
IntCal13
Hulu Cave
Tahiti
Barbados

Figure 4.4b: 13 to 15.7 kyr BP record of $\Delta^{14}C$. Symbols are as in Figure 4a.

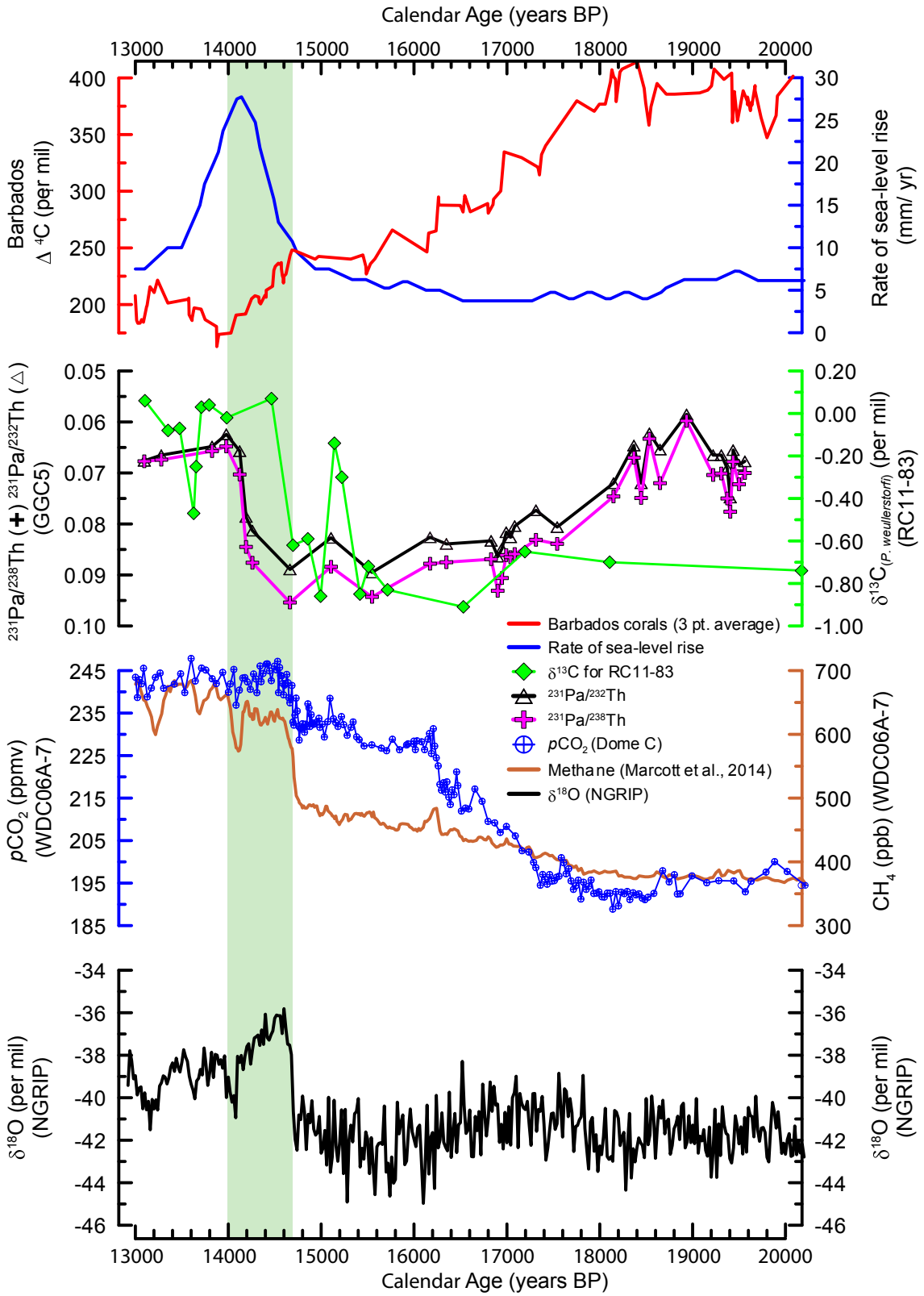
Calendar Age (years BP)
13000
14000
15000
16000
17000
18000
19000
20000
Barbados
Δ 14C (per mil)
400
350
300
250
200
Rate of sea-level rise
(mm/ yr)
30
25
20
15
10
5
0
231Pa/238Th (+) 231Pa/232Th (△)
(GGC5)
0.05
0.06
0.07
0.08
0.09
0.10
δ13C(P. wuellerstorfi) (per mil)
(RC11-83)
0.20
0.00
-0.20
-0.40
-0.60
-0.80
-1.00
Barbados corals (3 pt. average)
Rate of sea-level rise
δ13C for RC11-83
231Pa/232Th
231Pa/238Th
pCO2 (Dome C)
Methane (Marcott et al., 2014)
δ18O (NGRIP)
pCO2 (ppmv)
(WDC06A-7)
245
235
225
215
205
195
185
CH4 (ppb) (WDC06A-7)
700
600
500
400
300
δ18O (per mil)
(NGRIP)
-34
-36
-38
-40
-42
-44
-46
Calendar Age (years BP)

Figure 4.5. Comparison of coral $\Delta^{14}C$ with ocean and atmospheric proxy records. 3-point running mean of Barbados coral $\Delta^{14}C$ (red line; left axis) plotted with the rate of sea level rise (thin blue line; right axis) from Fairbanks et al., (unpublished data), RC11-83 benthic $\delta^{13}C$ (green line; right axis) from Charles and Fairbanks (1992) plotted on revised age model using AMS ^{14}C dates calibrated with (Fairbanks0107, 2007), Pa/Th activity (purple and black line; left axis) from Bermuda rise (McManus et al., 2004) plotted on revised age model using AMS ^{14}C dates calibrated with (Fairbanks0107, 2007), pCO_2 (thick blue line; left axis) and CH_4 (thin brown line; right axis) from WDC06A-7 (Marcott et al., 2014) and North Greenland Ice Core Project (NGRIP) $\delta^{18}O$ (thin black line) plotted on the GICC05 timescale (Rasmussen et al., 2006). Shaded area highlights 14.7 to 14.0 kyr BP.

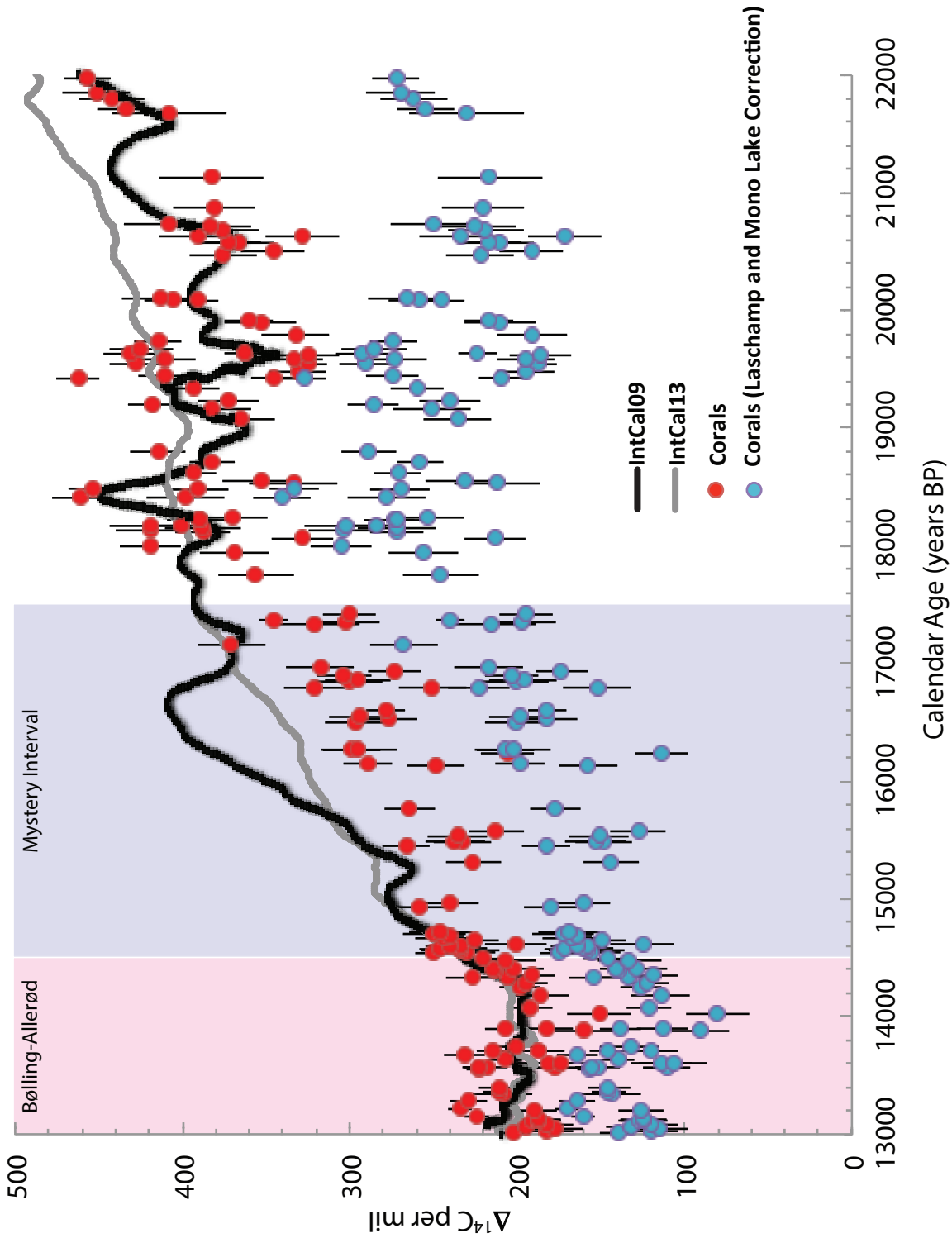
Bølling-Allerød
Mystery Interval
IntCal09
IntCal13
Corals
Corals (Laschamp and Mono Lake Correction)
Δ14C per mil
500
400
300
200
100
0
13000
14000
15000
16000
17000
18000
19000
20000
21000
22000
Calendar Age (years BP)

Figure 4.6. Barbados coral $\Delta^{14}C$ (red dots), Barbados coral $\Delta^{14}C_{LMcorr}$ (lightly shaded blue dots), IntCal09 and IntCal13 $\Delta^{14}C$ curves (black and gray lines, respectively. Vertical error bars are 2 s.d.

Chapter Five

5.1 Conclusions from the Dissertation

Radiocarbon (^{14}C) is a powerful tracer for reconstructing past changes in ocean processes such as the reorganization of the deep convective circulation and can be utilized for investigating the apparent synchronicity of changes in Atlantic meridional overturning circulation (AMOC) with abrupt climate change. The half-life of ^{14}C is 5730 years and comparable to the mixing time of the ocean (1500 years) and so ^{14}C can mix throughout the surface and deep ocean, atmosphere and biosphere reactive carbon reservoirs. Yet, its relatively long half-life makes it well suited for measuring the times and rates of change to the limit of ^{14}C dating (50,000 years BP).

Of particular importance to the scientific community is the record of the atmospheric $^{14}C/^{12}C$ ratio ($\Delta^{14}C$) since the Last Glacial Maximum (25 kyr BP) to the present when atmospheric ^{14}C is thought to have responded to large changes in the production of North Atlantic Deep Water and to the release of ^{14}C depleted CO_2 during ventilation of the Southern Ocean. In this dissertation, I have used paired U-Th and ^{14}C ages obtained from pristine fossil corals to reconstruct a record of $\Delta^{14}C$ that spans 49.2 to 7.4 kyr BP, consisting of 312 individually dated coral samples. 160 of these represent data generated during the course of this study and fill important gaps in existing records.

The decline of the atmospheric $\Delta^{14}C$ from 50 kyr BP to the present is well documented in a number of individual records (Chiu et al., 2007; Hoffmann et al., 2010; Hughen et al., 2006; Ramsey et al., 2012; Southon et al., 2012) and in compiled calibration curves (Reimer et al., 2009; Reimer et al., 2013). Although the general shape

of the $\Delta^{14}C$ curves is similar, there are differences between data sets that are much larger than those predicted from dating uncertainties alone and argues that there are inaccuracies in ^{14}C and or calendar ages with one or more of the individual marine and terrestrial archives.

The accuracy of a coral ^{14}C age depends on the marine reservoir correction which accounts for the age offset between the surface water that a coral grew in and that of the atmosphere. Is it, therefore, important that reasonable and robust estimates of the marine reservoir age and estimates of its variability be made in order to correct raw ^{14}C ages. In Chapter 2, I estimated the marine reservoir age for Barbados and Kirtimati by comparing raw ^{14}C ages with those of tree rings of the same calendar year for the time interval of overlap (13.9 to 7.4 kyr BP). High-frequency and random variability in reservoir ages of ± 100 years can be explained by changes in wind stress and solar output. However, a 200-year interval of low (less than 100 years) reservoir age is observed at Barbados corresponding to the onset of the Younger Dryas cold interval (12.9-12.7 kyr BP). This period of low reservoir age in the tropical Atlantic is not observed in the tropical Pacific coral record. The observation of an interval of low reservoir age is compelling evidence for slow-down of NADW as it reflects a smaller contribution of older deep water reaching to low latitudes in the Atlantic. Constant marine reservoir corrections made to coral data produces divergent Atlantic and Pacific records of $\Delta^{14}C$, as predicted with ocean-atmosphere circulation models simulating shut-down of NADW (Singarayer et al., 2008). The record of coral $\Delta^{14}C$ suggests the strength of NADW production resumed early into the Younger Dryas (12.5 kyr BP)

On longer time scales, changes in Earth's magnetic field intensity impact $\Delta^{14}C$ (Bard et al., 1990; Elsasser et al., 1956; Lal, 1988) where positive anomalies in $\Delta^{14}C$ are generated during a weaker field. A measure of the reliability of a $\Delta^{14}C$ record is that it should exhibit recognizable ^{14}C production spikes, and hence positive anomalies in $\Delta^{14}C$, during known geomagnetic excursions such as the Laschamp (41 kyr) and Mono Lake (34-30 kyr) events. The distinct advantage to using fossil corals to investigate changes in ^{14}C production back in time is that marine reservoir corrections in the most extreme (e.g., 0 to 500 years) become insignificant when computing $\Delta^{14}C$ values beyond 20 kyr BP. This is not the case with the speleothem data that may require large (2,000 year) dead carbon corrections to ^{14}C ages and where the assumption of constancy of dead carbon corrections is not constrained beyond the tree ring record (13.9 kyr BP).

To compliment and confirm U-Th dating accuracy, the U-Pa dating method was applied to 28 coral samples used to construct $\Delta^{14}C$ for the 28 to 50 kyr BP interval. The U-Pa concordancy test is the most rigorous test of the accuracy of the U-series dating system.

In Chapter 3, both the Laschamp and Mono Lake events were identified with large positive anomalies in coral $\Delta^{14}C$. These increases are due to increased production in the atmosphere during zero or near zero magnetic field strength. The $\Delta^{14}C$ record obtained with Barbados corals provides the most accurate and precise dating of the Mono Lake event (31.5 ± 0.2 kyr BP) and places it in importance with the Laschamp excursion.

Having identified the timing and amplitude $\Delta^{14}C$ change associated with the Laschamp and Mono Lake events, the raw $\Delta^{14}C$ record was corrected for the excess ^{14}C produced and plotted as the residual value, defined as $\Delta^{14}C_{LMcorr}$. Plots comparing

$\Delta^{14}C_{LMcorr}$ with $\Delta^{14}C$ show characteristically different features. For example, from 28 to 26 kyr $\Delta^{14}C_{LMcorr}$ values increase and then plateau until 20 kyr BP where as $\Delta^{14}C$ declines over this same time interval. An important consequence of correcting $\Delta^{14}C$ is the removal of rapid and large amplitude directional changes in $\Delta^{14}C$ such as the 200‰ decline from 26 to 20 kyr BP. The $\Delta^{14}C_{LMcorr}$ record shows increasing values sometime after 20 kyr BP and is a feature that has not been previously identified. The hypothesis presented here is that the increase represents increased production associated with a third "excursionoid" event; the Hilina Pali geomagnetic excursion (Singer et al., 2011; Turrin et al., 2013).

A comparison between $\Delta^{14}C_{LMcorr}$ calculated with the consensus half-life (5730 years) and that calculated by Jenks and Sweeton (1952) (6030 years) demonstrates that some portion of the linear trend in $\Delta^{14}C_{LMcorr}$ may be related to the uncertainty in the ^{14}C half-life.

Superimposed on the steady decline in atmospheric ^{14}C (Chapter 3) are two episodes of rapidly decreasing $\Delta^{14}C$ between 17.5 and 14 kyr BP that have been attributed to changes in ocean ventilation and resumption of NADW production. The main product of Chapter 4 is the interpretation of the $\Delta^{14}C$ record from 22 to 13 kyr BP based on 142 U-Th and ^{14}C dated fossil corals from Barbados. A constant marine reservoir correction of 340 years was applied to all coral ^{14}C ages based on the findings in Chapter 2. The record includes 28 new data points corresponding from 17 to 15 kyr BP and to an interval in Intcal13 and Marine13 that is under-represented with coral data and until now has largely relied on marine sediment and terrestrial archives to generate calibration and $\Delta^{14}C$ curves.

An important observation is that a comparison of coral calibration data with other data sets during the Mystery Interval show corals are systematically 400 to 1000 years older, compared to Cariaco Basin sediments (Hughen et al., 2006) and 200-400 years older compared to same calendar age speleothems. When the $\Delta^{14}C$ records are compared, the 190‰ decline observed in IntCal09 (Reimer et al., 2009) and attributed to Southern Ocean ventilation is not supported with coral data. Since marine reservoir corrections cannot account for the age offset between corals and Cariaco Basin foraminifera, I have concluded that differences in the records during the Mystery Interval are due to inaccurate calendar age assignments to Cariaco Basin ^{14}C dated sediment data. The Cariaco Basin deep-sea core age model contains more years than the true number of years. Errors in the Cariaco Basin age model reflect errors in the selection of tie points between the gray scale record in the deep-sea core and $\delta^{18}O$ record in the U-Th dated Hulu Cave (China) speleothem.

When coral $\Delta^{14}C$ values are corrected for excess ^{14}C production from the combined Laschamp and Mono Lake events (Chapter 3) the decline in residual or $\Delta^{14}C_{LMcorr}$ is only about 60‰ and cannot be distinguished from the long-term trend. I have concluded that studies linking records of declining atmospheric ^{14}C during the Mystery Interval suffer from two shortcomings: 1) $\Delta^{14}C$ target records that erroneously exaggerated the shape of the $\Delta^{14}C$ curve (i.e., IntCal09) due to the reliance on Cariaco Basin sediment data; and 2) failure to correct $\Delta^{14}C$ for the compounded contributions from the Laschamp and Mono Lake excursions. The record of $\Delta^{14}C_{LMcorr}$ does not support the hypothesis attributing a decline in atmospheric ^{14}C during the Mystery Interval to a synchronous release of ^{14}C-depleted CO_2.

In Chapter 4, I show that a sharp decline in $\Delta^{14}C$ coincides with switch-on of NADW as inferred from both the $\delta^{13}C$ tracer of NADW history measured in foraminifera (Charles and Fairbanks, 1992) and Pa/Th tracer of NADW production measured in deep-sea sediments (McManus et al., 2004). Barbados $\Delta^{14}C$ data overlap with Tahiti coral (Durand et al., 2013) and Hulu Cave speleothem data (Southon et al., 2012) and provides credible evidence to hypotheses linking changes in NADW production to changes in the ^{14}C content of the atmosphere. The turn-on of NADW also corresponds to an interval of accelerated sea level rise during Melt Water Pulse 1A when rates of sea level approached 25 mm yr^{-1}(Deschamps et al., 2012; Fairbanks, 1989). Rather than a slow-down in AMOC during freshwater input to the ocean, NADW was reinvigorated and the associated pole-ward heat transport may have been an amplifier for ice sheet melting, culminating in MWP-1A.

The 22-13 kyr BP $\Delta^{14}C$ record obtained with Barbados corals supports model simulations showing that only changes in NADW production can produce the sharp decline observed beginning at 14.7 kyr BP and that release of CO_2 to the atmosphere from increased upwelling in the Southern Ocean played a lesser role to contributing to overall deglacial $\Delta^{14}C$ decline (Hain et al., 2014).

5.2 Future Work

Accurate estimates of the marine reservoir corrections to ^{14}C ages in corals and foraminifera are necessary for constructing accurate records of $\Delta^{14}C$ and age models in deep-sea sediment cores. The observation of very low reservoir ages in tropical Atlantic surface water at the onset of the Younger Dryas (Chapter 2) tied to a slow-down of

NADW is an important observation but the amplitude and timing can be better constrained with the dating of more Younger-Dryas and late Holocene age Barbados corals. Also needing additional data coverage is the interval 14 to 13 kyr BP when intervals of lower MRA are also observed, perhaps signaling a weakening of NADW prior to the Younger Dryas "slow-down or shut-down". It is also incumbent upon us to ^{14}C date all *A. palmata* in Abdul (2016) for which we have U-Th ages and SST estimates so one can generate $\Delta^{14}C$ and SST estimates from the same samples.

Intervals of lower reservoir age should also be confirmed at other S. Atlantic and Pacific sites. Although we have exhausted our collection of Younger Dryas age samples from Kiritimati, we have Tahiti coral samples from IODP Expedition 310 drill cores that can provide a second Pacific Younger Dryas $\Delta^{14}C$ record. We also have coral samples from Puerto Rico, US Virgin Islands and several other Western Atlantic and Caribbean sites, courtesy of Dennis Hubbard (Oberlin College). Preliminary ^{14}C and U-Th dating (J. Rubenstone; unpublished data) suggests some of the corals potentially date to the Younger Dryas (12.9 to 11.6 kyr BP). Most of the samples are the species *Acropora palmata*, the gold standard for estimating past sea level (Abdul et al., 2016; Fairbanks, 1989). Therefore, paired U-Th and ^{14}C dating of samples from the collection not only has the potential for investigating MRA variability and $\Delta^{14}C$ independent of Barbados but can also provide a Caribbean wide late deglacial Holocene sea level record to complement the Barbados *Acropora palmata* record (Abdul et al., 2016). Likewise, $\delta^{18}O$ obtained from the same *Acropora palmata* can be used to generate a Caribbean wide Holocene- late deglacial record of sea surface temperature (Abdul, 2016; Abdul et al., 2011).

Variability in $\Delta^{14}C$ between 20 and 18 kyr BP is much larger than expected considering the combined dating errors in U-Th and ^{14}C. Triplicate ^{14}C dating combined with SEM imaging of select samples is probably required to determine if there are unidentified dating artifacts from contamination of modern ^{14}C, either intrinsic to samples or acquired during graphitization. We should also consider the hypothesis that variability in $\Delta^{14}C$ during 20-18 kyr BP could be related to rapid production changes due to instability in the geomagnetic dipole, prior and during the Hilina Pali excursion. One test of the "dipole instability" theory would be to conduct high resolution ^{14}C dating in annually banded *Montastrea annularis* corals from BBDS 11, RGF 15, and RGF 9, in an attempt to splice together record of $\Delta^{14}C$ with decadal resolution. The approach would similarly be applied to *Montastrea annularis* corals that date to the time of the Mono Lake event. There are multiple candidates currently in the collection. BBDS 10-42 thru BBDS 10-45 include a dozen 10 to 20 cm oriented *Montastrea annularis* expected to date from 30 to 32 kyr BP, providing additional dating of the Mono Lake event as well as the potential for high resolution ^{14}C dating. Annually banded corals are the only archive that can yield high-resolution $\Delta^{14}C$ records, as demonstrated in both modern and Younger Dryas age samples (Burr et al., 2009; Guilderson et al., 2005; Nurhati et al., 2009). Speleothem $\Delta^{14}C$ records contain inherent smoothing due to their slow growth rates, low U content, and limited sample resolution.

Better dating of the Hilina Pali event is needed, as $^{40}Ar/^{39}Ar$ ages are not precise enough (± 1,000 years). We should involve a student to generate U-Th isochron ages from individual phases separated from Tabernacle Hill lavas.

More U-Th (and perhaps U-Pa) dating of Araki corals for potential calibration data points should be undertaken, particularly those in the 40 to 34 kyr age range or between the Laschamp and Mono Lake events. We have ~ 100 Araki corals that have not undergone any preliminary screening for calcite. Any new data could also be used to supplement existing compiled for our ongoing Marine Isotope Stage 3 and 4 sea level reconstruction using Araki Island corals (Mortlock et al., 2010).

Finally, I have been collaborating with R. Sherrell (Rutgers) and Dan Sinclair (University of Wellington) by providing U-Th dates from a number of speleothems, collected from island sites (e.g., Cook Islands, Tonga) in the Western Pacific. Several specimens may overlap in age with the Mono Lake and Hilina Pali events and with the Hulu Cave H82 speleothem record so they could be considered as "potential" archives for comparison to our coral records.

5.3 References

Abdul, N. A., 2016, Late Deglaciation (13.9 to 8 kyr BP) Tropical Atlantic Sea Surface Temperature recorded in Barbados reef crest coral *Acropora palmata* PhD]: Rutgers University.

Abdul, N. A., Mortlock, R. A., Wright, J. D., and Fairbanks, R. G., 2016, Younger Dryas sea level and meltwater pulse 1B recorded in Barbados reef crest coral *Acropora palmata*: Paleoceanography, v. 31, no. 2, p. 330-344.

Abdul, N. A., Mortlock, R. A., Wright, J. D., Fairbanks, R. G., and Teneva, L. T., 2011, Atlantic Warm Pool Trigger for the Younger Dryas Climate Event, AGU, San Francisco, Calif: Fall Meeting.

Bard, E., Hamelin, B., Fairbanks, R. G., and Zindler, A., 1990, Calibration of the ^{14}C timescale over the past 30,000 years using mass spectrometric U-Th ages from Barbados corals: Nature, v. 345, p. 405-410.

Burr, G. S., Beck, J. W., Corrège, T., Cabioch, G., Taylor, F. W., and Donahue, D. J., 2009, Modern and Pleistocene Reservoir Ages Inferred from South Pacific Corals: Radiocarbon, v. 51, no. 1, p. 319-335.

Charles, C. D., and Fairbanks, R. G., 1992, Evidence from Southern Ocean sediments for the effect of North Atlantic deep-water flux on climate: Nature, v. 355, no. 6359, p. 416-419.

Chiu, T.-C., Fairbanks, R. G., Cao, L., and Mortlock, R. A., 2007, Analysis of the atmospheric ^{14}C record spanning the past 50,000 years derived from high-precision $^{230}Th/^{234}U/^{238}U$, $^{231}Pa/^{235}U$ and ^{14}C dates on fossil corals: Quaternary Science Reviews, v. 26, no. 1-2, p. 18-36.

Deschamps, P., Durand, N., Bard, E., Hamelin, B., Camoin, G., Thomas, A. L., Henderson, G. M., Okuno, J., and Yokoyama, Y., 2012, Ice-sheet collapse and sea-level rise at the Bolling warming 14,600 years ago: Nature, v. 483, no. 7391, p. 559-564.

Durand, N., Deschamps, P., Bard, E., Hamelin, B., Camoin, G., Thomas, A. L., Henderson, G. M., Yokoyama, Y., and Matsuzaki, H., 2013, Comparison of ^{14}C and U-Th ages in corals form IODP #310 cores offshore Tahiti: Radiocarbon, v. 55, no. 2, p. 1-26.

Elsasser, W., Ney, E. P., and Winckler, J. R., 1956, Cosmic-ray intensity and geomagnetism: Nature, v. 178, p. 1226-1227.

Fairbanks, R. G., 1989, A 17,000-year glacio-eustatic sea level record: influence of glacial melting rates on the Younger Dryas event and deep-ocean circulation: Nature, v. 342, no. 6250, p. 637-642.

Guilderson, T. P., Cole, J. E., and Southon, J. R., 2005, Pre-bomb $\Delta^{14}C$ variability and the Suess effect in Cariaco Basin surface waters as recorded in hermatypic corals: Radiocarbon, v. 47, p. 57–65.

Hain, M. P., Sigman, D. M., and Haug, G. H., 2014, Distinct roles of the Southern Ocean and North Atlantic in the deglacial atmospheric radiocarbon decline: Earth and Planetary Science Letters, v. 394, p. 198-208.

Hoffmann, D. L., Beck, J. W., Richards, D. A., Smart, P. L., Singarayer, J. S., Ketchmark, T., and Hawkesworth, C. J., 2010, Towards radiocarbon calibration

beyond 28ka using speleothems from the Bahamas: Earth and Planetary Science Letters, v. 289, no. 1-2, p. 1-10.

Hughen, K., Southon, J., Lehman, S., Bertrand, C., and Turnbull, J., 2006, Marine-derived ^{14}C calibration and activity record for the past 50,000 years updated from the Cariaco Basin: Quaternary Science Reviews, v. 25, no. 23-24, p. 3216-3227.

Jenks, G. H., and Sweeton, F. H., 1952, Calorimetric Determination of the Relationship between the Half-Life and Average Beta-Energy of C^{14}: Physical Review v. 86, p. 803-804.

Lal, D., 1988, Theoretically expected variations in the terrestrial cosmicray production rates of isotope *in* Castagnoli, G. C., ed., Solar–Terrestrial Relationships and the Earth Environment in the Last Millennia: Amsterdam, NY, North-Holland.

McManus, J. F., Francois, R., Gherardi, J. M., Keigwin, L. D., and Brown-Leger, S., 2004, Collapse and rapid resumption of Atlantic meridional circulation linked to deglacial climate changes: Nature, v. 428, no. 6985, p. 834-837.

Mortlock, R. A., Fairbanks, R. F., Bloom, A., Cao, L., Wright, J. D., Abdul, N., Mey, J., Ellins, K., Teneva, L., and Brainard, C., 2010, Sea Level from 1,000 to 60,000 years BP: the fossil coral record from Barbados and Araki Island, ICP Meeting: La Jolla, CA.

Nurhati, I. S., Cobb, K. M., Charles, C. D., and Dunbar, R. B., 2009, Late 20th century warming and freshening in the central tropical Pacific: Geophysical Research Letters, v. 36, no. 21, p. L21606.

Ramsey, C. B., Staff, R. A., Bryant, C. L., Brock, F., Kitagawa, H., van der Plicht, J., Schlolaut, G., Marshall, M. H., Brauer, A., Lamb, H. F., Payne, R. L., Tarasov, P. E., Haraguchi, T., Gotanda, K., Yonenobu, H., Yokoyama, Y., Tada, R., and Nakagawa, T., 2012, A Complete Terrestrial Radiocarbon Record for 11.2 to 52.8 kyr B.P: Science, v. 338, no. 6105, p. 370-374.

Reimer, P. B., Baillie, M. G. L., Bard, E., Bayliss, A., Beck, J. W., Blackwell, P. G., Bronk Ramsey, C., Buck, C. E., Burr, G. S., Edwards, R. L., Friedrich, M., Grootes, P. M., Guilderson, T. P., Hajdas, I., Heaton, T., Hogg, A. G., Hughen, K., Kaiser, F., Kromer, B., McCormac, G., Manning, S., Reimer, R. W., Richards, D. A., Southon, J., Talamo, S., Turney, C., van der Plicht, J., and Weyhenmeyer, C. E., 2009, IntCal09 and Marine09 Radiocarbon Age Calibration Curves, 0–50,000 Years cal BP: Radiocarbon, v. 51, p. 1111-1150.

Reimer, P. B., Bard, E., Bayliss, A., Beck, J. W., Blackwell, P. G., Bronk Ramsey, C., Buck, C. E., Cheng, H., Edwards, R. L., Friedrich, M., Grootes, P. M., Guilderson, T. P., Haflidason, H., Hajdas, I., Hatte, C., Heaton, T., Hoffmann, D. L., Hogg, A. G., Hughen, K., Kaiser, F., Kromer, B., Manning, S., Niu, M., Reimer, R. W., Richards, D. A., Scott, E. M., Southon, J., Staff, R. A., Turney, C., and van der Plicht, J., 2013, IntCal13 and Marine13 Radiocarbon Age Calibration Curves 0-50,000 years Cal BP: Radiocarbon, v. 55, no. 4, p. 1869-1887.

Singarayer, J. S., Richards, D. A., Ridgwell, A., Valdes, P. J., Austin, W. E. N., and Beck, J. W., 2008, An oceanic origin for the increase of atmospheric radiocarbon during the Younger Dryas: Geophysical Research Letters, v. 35, no. 14.

Singer, B., Jicha, B., He, H., and Zhu, R., 40Ar/39Ar Evidence for a 17 ka Geomagnetic Field Excursion at Changbaishan Volcano, Northeastern China, *in* Proceedings AGU Fall Meeting Abstracts2011, Volume 1, p. 04.

Southon, J., Noronha, A. L., Cheng, H., Edwards, R. L., and Wang, Y., 2012, A high-resolution record of atmospheric ^{14}C based on Hulu Cave speleothem H82: Quaternary Science Reviews, v. 33, no. 0, p. 32-41.

Turrin, B., Champion, D. E., Mortlock, R. A., Fairbanks, R. G., and Swisher, C. C., 2013, $^{40}Ar/^{39}Ar$ and U-series ages of a Late Pleistocene geomagnetic excursion in Western North America: The Hilina Pali event in Western North America? , AGU, Fall 2013, Volume GP31A-06: San Francisco.

Chapter Six

Appendices

Sample	Species	U-series I.D.	^{232}Th (ppt)	^{238}U (ppm)	error	[^{234}U/^{238}U]	error	[^{230}Th]/[^{234}U]	error	[^{230}Th/^{238}U]	U-Th Age (yr)	Cal. Age (yr BP)	error (yr)	mean Cal age (yr BP)	error	2 error	Initial δ^{234}U	error	^{14}C age (years BP)	mean ^{14}C age	2 error	AMS ID	^{14}C age corr	Δ^{14}C (‰)	2 error	REF
BBDS 10-13-1	*A. palmata*	AN100823.004	547	3.150	0.001	1.1409	0.0007	0.1069	0.0002	0.1220	12323	12263	26	12263	26	52	145.9	1.1	10788	10788	100	OS-95653	10448	201	17	
BBDS 10-14-2	*A. palmata*	AN100811.002	162	2.945	0.001	1.1417	0.0005	0.1071	0.0002	0.1223	12344	12284	23	12284	23	46	146.8	0.8	10714	10714	70	OS-101784	10374	215	13	
BBDS 10-14-3	*A. palmata*	AN100811.003	250	3.242	0.001	1.1402	0.0006	0.1088	0.0002	0.1241	12550	12490	26	12407	9	18	145.3	0.8	10527	10527	110	OS-101783	10187	262	17	
BBDS 10-14-3.2	*A. palmata*	Neptune131101	511	3.379	0.000	1.1415	0.0002	0.1081	0.0001	0.1234	12460	12397	9				146.6	0.8								
BBDS 10-16-2	*A. palmata*	AN110601.001	321	3.268	0.001	1.1412	0.0006	0.1092	0.0002	0.1246	12598	12538	13	12538	13	26	146.4		10744	10744	70	OS-104683	10404	248	12	
BBDS 10-17-4	*A. palmata*	AN100819.003	1206	2.907	0.001	1.1401	0.0006	0.1096	0.0002	0.1250	12650	12590	30	12590	30	60	145.0	0.9	10781	10781	70	OS-101789	10441	250	14	
BBDS 10-18-1	*A. palmata*	AN100812.001	1262	3.164	0.001	1.1422	0.0005	0.1109	0.0002	0.1267	12804	12744	30	12778	16	32	147.5	0.7	10989	10989	80	OS-91635	10649	246	13	
BBDS 10-18-1.2	*A. palmata*	AN110607.003	1216	3.171	0.001	1.1402	0.0005	0.1113	0.0002	0.1269	12853	12790	18				145.4	0.8								
BBDS 10-18-2	*A. palmata*	AN100812.002	782	3.218	0.001	1.1424	0.0004	0.1101	0.0003	0.1258	12707	12647	37	12647	37	74	147.6	0.6	10960	10960	50	OS-101503	10620	231	13	
BBDS 10-20-2	*A. palmata*	AN100812.003	343	3.125	0.001	1.1405	0.0005	0.1097	0.0002	0.1251	12661	12601	19	12628	12	24	145.6	0.7	10997	10947	42	OS-95661	10607	230	7	
BBDS 10-20-2.2	*A. palmata*	Neptune130507	117	3.101	0.000	1.1412	0.0002	0.1101	0.0001	0.1257	12710	12647	16				146.4	0.4	10928			OS-101504				
BBDS 10-20-4	*A. palmata*	AN070615.004	100	3.227	0.001	1.1408	0.0004	0.1102	0.0002	0.1257	12722	12665	31	12749	13	26	146.0	0.6	10950	10946	51	OS-95654	10606	249	9	
BBDS 10-20-4.2	*A. palmata*	Neptune130507	116	3.279	0.000	1.1398	0.0002	0.1111	0.0001	0.1266	12831	12768	15				145.0	0.3	10944			OS-101502				
BBDS 10-20-9	*A. palmata*	AN100812.005	109	3.014	0.001	1.1410	0.0005	0.1117	0.0002	0.1274	12900	12840	19	12840	19	38	146.0	0.7	11069	11069	70	OS-101787	10729	243	12	
BBDS 10-23-3	*A. palmata*	AN100819.002	349	2.990	0.001	1.1405	0.0005	0.1158	0.0003	0.1321	13409	13349	36	13349	36	72	146.0	0.7	11790	11790	100	OS-95655	11450	209	18	
BBDS 10-24-3	*A. palmata*	AN100712.001	36	3.319	0.001	1.1408	0.0005	0.1180	0.0002	0.1346	13671	13611	28	13611	28	56	146.0	0.7	12279	12279	130	OS-104806	11939	174	21	
BBDS 10-25-4	*A. palmata*	AN100713.001	71	3.114	0.001	1.1428	0.0006	0.1191	0.0003	0.1361	13811	13751	32	13751	32	64	148.0	0.8	12234	12234	100	OS-95648	11894	201	18	
BBDS 10-26-1	*A. palmata*	AN100818.003	60	3.051	0.001	1.1368	0.0005	0.1179	0.0003	0.1341	13670	13610	38	13610	38	76	142.0	0.7	12230	12230	100	OS-95649	11890	181	18	
BBDS 10-26-4	*A. palmata*	AN100819.001	55	2.984	0.006	1.1399	0.0005	0.1201	0.0004	0.1369	13933	13873	52	13895	10	20	146.0	0.7	12331	12331	80	OS-104807	11991	207	12	
BBDS 10-26-4	*A. palmata*	Neptune150617	189	3.090	0.005	1.1442	0.0003	0.1203	0.0001	0.1377	13961	13896	10				150.1	0.4								
BBDS 10-27-1	*A. palmata*	AN100818.004	45	3.213	0.001	1.1397	0.0005	0.1203	0.0002	0.1371	13958	13898	30	13898	30	60	145.0	0.7	12500	12500	90	OS-104809	12160	182	16	
BBDS 10-28-4	*A. palmata*	Neptune130709	755	3.272	0.000	1.1289	0.0002	0.2333	0.0001	0.2634	28865	28802	17	28802	17	34	139.9	0.3	24831	24831	220	OS-104810	24491	546	42	
BBDS 10-28-5	*A. palmata*	AN070615.002	272	3.233	0.001	1.1289	0.0005	0.2311	0.0004	0.2609	28552	28495	58	28495	58	116	140.0	0.7	24731	24731	150	OS-91510	24391	508	35	
BBDS 10-31-2	*A. palmata*	AN070523.002	135	3.219	0.001	1.1287	0.0005	0.2347	0.0003	0.2649	29050	28993	49	28993	49	98	140.0	0.7	24890	24890	130	OS-91512	24550	570	31	
BBDS 10-37-4	*A. palmata*	AN070523.003	119	3.242	0.001	1.1328	0.0005	0.2513	0.0004	0.2846	31411	31354	53	31516	31	62	145.0	0.8	25475	25475	150	OS-101499	25135	981		
BBDS 10-37-4	*A. palmata*	Neptune1608	17	3.179	0.002	1.1353	0.0003	0.2531	0.0003	0.2873	31670	31605	39				147.9	0.5								
BBDS 10-7-2	*A. palmata*	AN070615.003	59	3.278	0.001	1.1421	0.0005	0.0978	0.0003	0.1117	11215	11158	33	11158	33	66	147.0	0.7	10350	10350	90	OS-104680	10010	109	15	
BBDS 10-8-3	*A. palmata*	AN100708.001	210	2.987	0.001	1.1429	0.0007	0.0991	0.0003	0.1132	11366	11306	35	11306	35	70	147.6	1.0	10368	10368	70	OS-104681	10028	127	14	
BBDS 11-17-7	*A. palmata*	AN100927.002	35	3.490	0.001	1.1392	0.0005	0.1439	0.0003	0.1639	16910	16850	40	16850	40	80	146.1	0.7	14605	14605	100	OS-91634	14265	300	20	
BBDS 11-18-11	*A. palmata*	AN100930.002	88	3.219	0.001	1.1355	0.0005	0.1570	0.0003	0.1783	18590	18530	39	18530	39	78	142.8	0.7	16036	16036	140	OS-104811	15696	333	26	
BBDS 11-18-2	*A. palmata*	AN100927.003	69	3.296	0.001	1.1342	0.0005	0.1561	0.0003	0.1770	18470	18410	32	18410	32	64	141.3	0.7	15540	15540	120	OS-95234	15200	398	23	

Sample	Species	U-series I.D.	^{232}Th (ppt)	^{238}U (ppm)	error	[^{234}U/^{238}U]	error	[^{230}Th]/[^{234}U]	error	[^{230}Th/^{238}U]	U-Th Age (yr)	Cal. Age (yr BP)	error (yr)	mean Cal age (yr BP)	error	2 error	Initial δ^{234}U	error	^{14}C age (years BP)	mean ^{14}C age	2 error	AMS ID	^{14}C age corr	Δ^{14}C (‰)	2 error	REF
BBDS 11-18-3	*A. palmata*	AN100928.001	77	3.182	0.001	1.1360	0.0005	0.1548	0.0004	0.1758	18300	18240	45	18240	45	90	143.2	0.7	15534	15534	90	OS-95235	15194	371	21	
BBDS 11-18-7	*A. palmata*	AN100928.002	101	3.257	0.001	1.1371	0.0006	0.1576	0.0008	0.1792	18659	18599	108	18478	15	30	144.5	0.9	15649	15649	100	OS-95445	15309	390	18	
BBDS 11-18-7.2	*A. palmata*	Neptune130507	566	3.370	0.001	1.1369	0.0002	0.1566	0.0001	0.1781	18539	18476	15				144.3	0.3								
BBDS 11-20-4	*A. palmata*	AN100628.005	195	3.444	0.001	1.1385	0.0007	0.1619	0.0003	0.1844	19222	19162	42	19162	42	84	146.0	1.1	16361	16361	110	OS-95442	16021	382	24	
BBDS 11-20-6	*A. palmata*	AN100629.004	79	3.086	0.001	1.1358	0.0005	0.1625	0.0003	0.1845	19291	19231	42	19231	42	84	143.0	0.7	16485	16485	70	OS-10497	16145	373	18	
BBDS 11-22-5.2	*A. palmata*	AN110610.002	107	3.155	0.001	1.1354	0.0005	0.1656	0.0002	0.1880	19694	19631	20	19631	20	40	143.2	0.7	16538	16538	80	OS-91509	16198	431	16	
BBDS 11-23-3	*A. palmata*	AN100706.001	90	3.558	0.001	1.1361	0.0007	0.1652	0.0007	0.1877	19651	19591	37	19591	37	74	144.0	1.0	16613	16613	80	OS-91521	16273	411	19	
BBDS 11-9-6	*A. palmata*		209	3.105	0.001	1.1389	0.0005	0.1239	0.0002	0.1411	14408	14348	27	14348	27	54	144.7	0.8	12877	12877	80	OS-101786	12537	191	14	
BBDS 14-11-1	*A. palmata*	AN070730.003	336	3.521	0.001	1.1420	0.0004	0.1353	0.0003	0.1545	15824	15767	34	15767	34	68	148.4	0.6	13779	13779	70	OS-91520	13439	264	15	
BBDS 14-11-6	*A. palmata*	AN100818.006	206	3.237	0.001	1.1415	0.0005	0.1393	0.0002	0.1590	16327	16267	30	16267	30	60	148.0	0.8	14073	14073	130	OS-95066	13733	295	23	
BBDS 14-12-2	*A. palmata*	AN100818.005	90	3.350	0.000	1.1402	0.0005	0.1384	0.0002	0.1578	16217	16157	30	16157	30	60	147.0	0.7	14000	14000	70	OS-91508	13660	289	15	
BBDS 14-13-4	*A. palmata*	AN100628.004	105	3.593	0.002	1.1405	0.0006	0.1448	0.0002	0.1652	17031	16971	30	16971	30	60	147.0	0.9	14618	14618	110	OS-95658	14278	317	20	
BBDS 14-14-1	*A. palmata*	AN070730.004	127	3.369	0.001	1.1386	0.0004	0.1465	0.0003	0.1668	17239	17182	39	17158	10	20	145.5	0.7	14481	14481	120	OS-95065	14141	371	21	
BBDS 14-14-1	*A. palmata*	Neptune130726	552	3.432	0.000	1.1414	0.0002	0.1463	0.0001	0.1670	17219	17156	11				148.5	0.2								
BBDS 14-15-3	*A. palmata*	AN100624.004	112	3.203	0.001	1.1368	0.0006	0.1524	0.0002	0.1733	18001	17941	26	17941	26	52	144.0	0.9	15253	15253	110	OS-95064	14913	369	21	
BBDS 14-16-10	*A. palmata*	AN100628.003	110	3.112	0.001	1.1405	0.0006	0.1510	0.0003	0.1722	17813	17753	41	17753	41	82	148.0	0.9	15145	15145	110	OS-95650	14805	356	23	
BBDS 14-16-6	*A. palmata*	AN100622.002	106	3.369	0.002	1.1408	0.0009	0.1542	0.0003	0.1759	18229	18169	37	18169	37	74	148.0	1.3	15184	15184	120	OS-95063	14844	419	19	
BBDS 14-16-8	*A. palmata*	AN110609.005	144	3.131	0.001	1.1361	0.0005	0.1539	0.0002	0.1749	18194	18131	21	18131	21	42	143.2	0.7	15145	15145	110	OS-95646	14805	420	21	
BBDS 14-17-3	*A. palmata*	AN100628.002	198	3.059	0.001	1.1354	0.0006	0.1541	0.0003	0.1749	18210	18150	40	18150	40	80	143.0	0.9	15345	15345	110	OS-95062	15005	388	16	
BBDS 14-3-4	*A. palmata*	AN100712.002	454	3.363	0.001	1.1378	0.0005	0.1238	0.0002	0.1408	14389	14329	23	14329	23	46	144.0	0.7	12623	12623	90	OS-95449	12283	227	15	
BBDS 14-3-6	*A. palmata*	AN100712.003	807	3.327	0.001	1.1395	0.0005	0.1238	0.0002	0.1411	14393	14333	26	14333	26	52	145.0	0.7	12762	12762	120	OS-95075	12422	206	19	
BBDS 14-4-3	*A. palmata*	AN070730.001	382	2.947	0.001	1.1386	0.0004	0.1248	0.0003	0.1421	14516	14459	33	14491	23	46	144.0	0.6	12823	12823	90	OS-95061	12483	220	15	
BBDS 14-4-3.2	*A. palmata*	AN100706.002	805	3.166	0.001	1.1393	0.0005	0.1253	0.0003	0.1428	14584	14524	33				145.0	0.8								
BBDS 14-5-2	*A. palmata*	AN100624.002	54	3.461	0.002	1.1424	0.0008	0.1268	0.0003	0.1449	14770	14710	41	14710	41	82	148.5	1.2	12847	12847	90	OS-95067	12507	249	19	
BBDS 5-4-5	*A. palmata*	AN070614.003	108	3.484	0.001	1.1390	0.0005	0.1392	0.0003	0.1586	16321	16264	36	16264	36	72	145.6	0.7	14045	14045	80	OS-94736	13705	299	17	
BBDS 11-23-3	*A. palmata*	AN100706.001	90	3.558	0.001	1.1361	0.0007	0.1652	0.0002	0.1877	19651	19591	37	19591	37	74	143.9	0.9	16613	16613	110	OS-91639	16273	411	19	
BBDS 10-41-1	*M. annularis*	AN110610.001	168	2.486	0.001	1.1288	0.0005	0.2498	0.0003	0.2819	31200	31137	46	31137	46	92	140.7	0.7	25753	25753	150	OS-91507	25413	828	40	
BBDS 10-45-1	*M. annularis*	AN070725.004	138	2.341	0.001	1.1276	0.0005	0.2521	0.0005	0.2843	31538	31481	75	31481	75	150	140.0	0.8								
BBDS 10-51-2	*M. annularis*	AN070524.001	52	2.634	0.001	1.1263	0.0005	0.2585	0.0004	0.2911	32465	32408	62	32363	16	32	138.0	0.7	29104	29104	220	OS-101785	28764	397	38	
BBDS 10-51-2	*M. annularis*	Neptune160411	341	2.608	0.000	1.3090	0.0002	0.2582	0.0001	0.2920	32425	32360	17				143.4	0.3								
BBDS 11-10-3	*M. annularis*	Neptune140610	142	2.126	0.000	1.1389	0.0002	0.1257	0.0002	0.1432	14635	14571	13	14571	13	26	144.8	0.4	12813	12813	150	OS-95229	12473	234	23	

Sample	Species	U-series I.D.	^{232}Th (ppt)	^{238}U (ppm)	error	[^{234}U/^{238}U]	error	[^{230}Th]/[^{234}U]	error	[^{230}Th/^{238}U]	U-Th Age (yr)	Cal. Age (yr BP)	error (yr)	mean Cal age (yr BP)	error	2 error	Initial δ^{234}U	error	^{14}C age (years BP)	mean ^{14}C age	2 error	AMS ID	^{14}C age corr	Δ^{14}C (‰)	2 error	REF
BBDS 11-11-4	*M. annularis*	AN100930.001	65	2.368	0.001	1.1393	0.0005	0.1252	0.0003	0.1426	14566	14506	66	14602	9	18	145.1	0.8	12805	12805	100	OS-95230	12465	240	16	
BBDS 11-11-4	*M. annularis*	Neptune150617	238	2.386	0.000	1.1403	0.0002	0.1260	0.0001	0.1437	14669	14604	9				146.3	0.3								
BBDS 11-11-6	*M. annularis*	AN101008.005	87	2.203	0.001	1.1366	0.0005	0.1259	0.0003	0.1431	14654	14594	63	14717	12	24	142.4	0.7	12878	12878	120	OS-95644	12538	246	19	
BBDS 11-11-6	*M. annularis*	Neptune150617	224	2.207	0.000	1.1406	0.0002	0.1270	0.0001	0.1448	14786	14721	12				146.6	0.3								
BBDS 11-12-1	*M. annularis*	AN101008.004	141	2.327	0.001	1.1396	0.0004	0.1259	0.0003	0.1435	14653	14593	79	14647	8	16	145.5	0.6	12945	12945	90	OS-95233	12605	225	14	
BBDS 11-12-1	*M. annularis*	Neptune150617	131	2.398	0.000	1.1405	0.0002	0.1264	0.0001	0.1441	14713	14648	8				146.5	0.3								
BBDS 11-1-3	*M. annularis*	AN070726.001	227	2.674	0.001	1.1405	0.0006	0.1001	0.0003	0.1141	11491	11434	34	11434	34	68	145.1	0.9								
BBDS 11-13-1	*M. annularis*	AN101005.001	76	2.469	0.001	1.1412	0.0005	0.1262	0.0004	0.1440	14694	14634	105	14665	22	44	147.2	0.7	12837	12837	100	OS-95232	12497	244	17	
BBDS 11-13-1.2	*M. annularis*	Neptune130507	143	2.450	0.000	1.1383	0.0002	0.1265	0.0002	0.1440	14729	14666	22				144.2	0.3								
BBDS 11-24-1	*M. annularis*	AN110610.004	227	2.411	0.001	1.1355	0.0004	0.1692	0.0002	0.1921	20165	20102	27	20102	27	54	143.4	0.7	17096	17096	120	OS-95443	16756	413	23	
BBDS 11-24-3	*M. annularis*	AN110610.005	74	2.497	0.001	1.1342	0.0005	0.1676	0.0002	0.1901	19961	19898	26	19898	26	52	142.0	0.7	17246	17246	120	OS-95444	16906	353	22	
BBDS 11-24-7	*M. annularis*	Neptune130516	184	2.503	0.000	1.1340	0.0003	0.1669	0.0001	0.1892	19864	19801	19	19801	19	38	141.7	0.4	17277	17277	120	OS-95656	16937	332	21	
BBDS 11-32-4	*M. annularis*	AN070727.003	35	3.892	0.002	1.1296	0.0009	0.2026	0.0004	0.2289	24618	24561	49	24561	49	98	139.0	1.3	21175	21175	160	OS-95448	20835	459	34	
BBDS 11-34-2	*M. annularis*	AN070727.004	85	2.365	0.000	1.1291	0.0004	0.2104	0.0004	0.2376	25683	25626	53	25655	41	82	138.8	0.7	21565	21565	240	OS-101498	21225	586	49	
BBDS 11-34-2.2	*M. annularis*	AN100706.003	93	2.394	0.001	1.1282	0.0006	0.2110	0.0005	0.2380	25756	25696	64				137.9	0.9								
BBDS 14-1-7	*M. annularis*	AN110609.002	204	2.322	0.001	1.1412	0.0006	0.1083	0.0001	0.1236	12492	12429	12	12476	7	14	146.3	0.8	11505	11505	90	OS-95647	11165	127	14	
BBDS 14-1-7.2	*M. annularis*	Neptune131101	359	2.368	0.001	1.1415	0.0003	0.1089	0.0003	0.1243	12559	12496	8				146.5	0.3								
BBDS 14-8-6.2	*M. annularis*	Neptune130709	399	2.750	0.000	1.1425	0.0003	0.1328	0.0002	0.1517	15513	15450	22	15450	22	44	152.3	0.3	13458	13458	80	OS-94733	13118	266	14	
BBDS 5-3-10	*M. annularis*	AN101005.002	72	2.643	0.001	1.1429	0.0006	0.1334	0.0002	0.1525	15591	15531	31	15531	31	62	149.3	0.8	13734	13734	100	OS-91633	13394	236	18	
BBDS 5-3-2	*M. annularis*	AN101007.007	241	2.656	0.001	1.1418	0.0005	0.1289	0.0002	0.1472	15032	14972	30	14972	30	60	148.0	0.7	13165	13165	90	OS-101788	12825	239	17	
BBDS 5-3-5	*M. annularis*	AN070731.004	267	2.799	0.001	1.1414	0.0004	0.1317	0.0003	0.1503	15375	15318	32	15318	32	64	148.0	0.6	13588	13588	90	OS-94729	13248	226	17	
BBDS 5-3-7	*M. annularis*	AN101008.001	106	2.956	0.001	1.1410	0.0006	0.1331	0.0003	0.1518	15546	15486	39	15486	39	78	147.3	0.8	13680	13680	90	OS-94730	13340	237	18	
BBDS 5-3-8	*M. annularis*	AN101008.002	107	2.837	0.001	1.1413	0.0005	0.1333	0.0004	0.1522	15582	15522	46	15578	13	26	147.7	0.7	13930	13930	110	OS-94731	13590	213	17	
BBDS 5-3-8.2	*M. annularis*	Neptune130507	145	2.887	0.000	1.1415	0.0002	0.1341	0.0002	0.1531	15675	15612	20				147.9	0.3								
BBDS 5-3-8.3	*M. annularis*	Neptune130726	134	2.843	0.000	1.1434	0.0002	0.1337	0.0001	0.1528	15623	15560	17				149.9	0.3								
BBDS 5-3-9	*M. annularis*	AN101008.003	266	3.161	0.001	1.1422	0.0005	0.1330	0.0003	0.1519	15542	15482	40	15482	40	80	148.6	0.8	13706	13706	80	OS-94732	13366	233	17	
BBDS 6-4-5	*M. annularis*	Neptune130726	175	2.595	0.000	1.1464	0.0002	0.1056	0.0001	0.1211	12160	12097	9	12097	9	18	151.5	0.3	10732	10732	90	OS-104677	10392	185	14	
BBDS 6-4-6	*M. annularis*	Neptune130709	380	2.538	0.000	1.1420	0.0002	0.1125	0.0001	0.1284	12997	12934	18	12934	18	36	147.4	0.2	11236	11236	80	OS-104678	10896	232	13	
BBDS 6-5-1	*M. annularis*	Neptune130516	406	2.491	0.000	1.1433	0.0003	0.1130	0.0001	0.1292	13061	12998	17	12998	17	34	148.7	0.4	11221	11221	110	OS-95645	10881	244	18	
BBDS 6-5-3	*M. annularis*	Neptune150617	182	2.278	0.000	1.1455	0.0003	0.1153	0.0001	0.1321	13347	13282	9	13282	9	18	151.1	0.3	11592	11592	70	OS-104679	11252	229	11	
BBDS 11-25-4	*Porites sp.*	Neptune130516	198	3.037	0.000	1.1338	0.0002	0.1737	0.0001	0.1969	20751	20688	16	20688	16	32	141.9	0.3	17878	17878	130	OS-95657	17538	376	23	
BBDS 11-19-3	*Porites sp.*	AN100629.005	311	2.632	0.001	1.1349	0.0006	0.1572	0.0004	0.1784	18611	18551	46	18551	46	92	142.2	0.8	15941	15941	110	OS-95447	15601	353	24	
RGF 12-14-2	*A. palmata*	AN050408.001	582	3.301	0.001	1.1405	0.0006	0.1114	0.0003	0.1270	12866	12816	37	12925	23	46	145.7	1.0	11265	11265	50	CAM 99009	10925	226	10	1

Sample	Species	U-series I.D.	^{232}Th (ppt)	^{238}U (ppm)	error	[^{234}U/^{238}U]	error	[^{230}Th]/[^{234}U]	error	[^{230}Th/^{238}U]	U-Th Age (yr)	Cal. Age (yr BP)	error (yr)	mean Cal age (yr BP)	error	2 error	Initial δ^{234}U	error	^{14}C age (years BP)	mean ^{14}C age	2 error	AMS ID	^{14}C age corr	Δ^{14}C (‰)	2 error	REF
RGF 12-14-2.2	*A. palmata*	081904LC1	652	3.046	0.001	1.1399	0.0006	0.1129	0.0003	0.1286	13046	12996	30				145.1	1.0	11265				10925			3
RGF 12-15-4	*A. palmata*	AN031107.002	127	3.141	0.001	1.1397	0.0005	0.1122	0.0001	0.1279	12969	12919	17	12990	12	24	145.0	0.5	11447	11447	38	WHOI N=3	11107	208	7	1,2
RGF 12-15-4.2	*A. palmata*	AN031110.003	153	3.146	0.001	1.1384	0.0005	0.1134	0.0001	0.1291	13116	13066	17				143.7	1.0	11447				11107			1
RGF 12-16-5.2	*A. palmata*	AN040528.001	39	3.024	0.001	1.1407	0.0005	0.1148	0.0002	0.1310	13288	13238	56	13214	10	20	146.1	0.7	11523	11490	43	KIA 27093	11183	229	7	3
RGF 12-16-5	*A. palmata*	Neptune151215	127	2.963	0.000	1.1423	0.0002	0.1148	0.0001	0.1311	13278	13213	10				147.7	0.3	11471			KIA 27093	11131			
RGF 12-17-2.2	*A. palmata*	AN031105.005	43	3.104	0.001	1.1381	0.0005	0.1144	0.0001	0.1301	13229	13179	16	13157	14	28	143.3	0.7	11502	11502	38	OS-605,5643, 5853, CAMS 99626	11162	224	7	2,3
RGF 12-17-2.3	*A. palmata*	AN061705.004		3.136	0.001						13161	13105	25				146.9	0.7	11502				11162			
RGF 12-17-3	*A. palmata*	AN060531.004	337	3.115	0.001	1.1402	0.0005	0.1139	0.0002	0.1299	13177	13121	28	13121	28	56	145.5	0.8	11710	11710	80	KIA 30192	11370	188	14	3
RGF 12-17-4	*A. palmata*	AN060601.001	243	3.125	0.001	1.1397	0.0005	0.1135	0.0002	0.1294	13123	13067	26	13067	26	52	145.0	0.8	11610	11610	90	KIA 30193	11270	195	15	3
RGF 12-17-6	*A. palmata*	AN060626.003	33	3.092	0.001	1.1409	0.0006	0.1134	0.0003	0.1293	13106	13050	34	13050	34	68	146.2	0.8	11705	11705	100	KIA 30194	11365	178	18	3
RGF 12-18-2 ǂ	*A. palmata*	AN060717.001	44	2.991	0.001	1.1418	0.0004	0.1138	0.0003	0.1299	13156	13100	42	13086	25	50	147.1	0.6	11710	11710	100	KIA 30195	11370	183	16	3
RGF 12-18-2.2 ǂ	*A. palmata*	AN100708.004	45	3.201	0.001	1.1405	0.0004	0.1136	0.0003	0.1296	13138	13078	32				145.8	0.6	11710				11370			
RGF 12-18-3	*A. palmata*	AN060628.005	42	3.279	0.001	1.1410	0.0005	0.1132	0.0002	0.1291	13082	13026	30	13026	30	60	146.3	0.7	11655	11655	90	KIA 30196	11315	182	16	3
RGF 12-19-3	*A. palmata*	AN060627.001	203	3.071	0.001	1.1426	0.0005	0.1140	0.0002	0.1302	13182	13126	24	13126	24	48	148.0	0.7	11715	11715	80	KIA 30197	11375	188	14	3
RGF 12-19-5	*A. palmata*	AN060629.001	543	3.022	0.001	1.1418	0.0004	0.1146	0.0002	0.1308	13258	13202	25	13202	25	50	147.2	0.6	11775	11775	80	KIA 30198	11435	190	14	3
RGF 12-21-10	*A. palmata*	AN031111.002	186	3.476	0.001	1.1385	0.0005	0.1180	0.0001	0.1344	13682	13632	16	13632	16	32	144.0	0.8	12075	12075	60	CAMS 99630	11735	207	10	1
RGF 12-21-2	*A. palmata*	AN031110.004	184	3.040	0.001	1.1374	0.0006	0.1174	0.0002	0.1335	13605	13555	19	13555	19	38	142.8	0.8	11898	11898	38	CAMS 99627, 99631	11558	223	8	1
RGF 12-21-6	*A. palmata*	AN031111.001	107	3.021	0.001	1.1374	0.0005	0.1176	0.0002	0.1337	13624	13574	26	13574	26	52	142.8	0.7	11945	11945	70	CAMS 99628	11605	218	13	1
RGF 12-21-7	*A. palmata*	AN040528.003	65	2.897	0.001	1.1386	0.0007	0.1176	0.0002	0.1339	13628	13578	26	13578	26	52	144.1	1.0	11922	11922	40	CAMS WHOI	11582	222	10	1
RGF 12-22-2	*A. palmata*	AN060628.001	53	2.906	0.001	1.1407	0.0004	0.1176	0.0002	0.1341	13623	13567	29	13567	29	58	146.2	0.6	12215	12215	80	KIA 30200	11875	177	14	3
RGF 12-23-2	*A. palmata*	AN060601.002	23	3.006	0.001	1.1387	0.0005	0.1187	0.0002	0.1352	13764	13708	31	13708	31	62	144.2	0.7	12280	12280	90	KIA 30201	11940	188	16	3
RGF 12-26-3	*S. radians*	AN061306LC2		3.198	0.001	1.1431	0.0008				14085	14029	39	14029	39	78	143.1	0.5	12845	12845	110	KIA 30202	12505	151	19	3
RGF 12-28-6	*A. palmata*	021301RM1	245	3.191	0.001	1.1257	0.0004	0.2385	0.0003	0.2684	29640	29590	41	29590	41	82	136.6	0.5	25311	25311	92	CAMS 73953, 73919	24971	602	24	1
RGF 12-28-7	*A. palmata*	021301RM2	482	2.982	0.001	1.1274	0.0004	0.2432	0.0004	0.2742	30264	30214	56	30150	40	80	138.7	0.5	25248	25248	70	CAMS N=4	24908	728	22	1
RGF 12-28-7 rep	*A. palmata*	073101RM2	863	3.216	0.001	1.1284	0.0005	0.2423	0.0004	0.2734	30130	30080	58				139.9	0.5	25248				24908			1
RGF 12-29-2	*A. palmata*	021401RM2	84	3.247	0.001	1.1261	0.0003	0.2410	0.0005	0.2714	29948	29898	75	30152	35	70	137.3	0.5	25300	25300	98	CAMS 73921, 73946	24960	717	25	1
RGF 12-29-2 rep	*A. palmata*	080201RM2	68	3.241	0.001	1.1269	0.0004	0.2433	0.0003	0.2742	30275	30225	40				138.3	0.5	25300				24960			1

Sample	Species	U-series I.D.	^{232}Th (ppt)	^{238}U (ppm)	error	[^{234}U/^{238}U]	error	[^{230}Th]/[^{234}U]	error	[^{230}Th/^{238}U]	U-Th Age (yr)	Cal. Age (yr BP)	error (yr)	mean Cal age (yr BP)	error	2 error	Initial δ^{234}U	error	^{14}C age (years BP)	mean ^{14}C age	2 error	AMS ID	^{14}C age corr	Δ^{14}C (‰)	2 error	REF
RGF 12-30-3	*A. palmata*	021401RM1		3.037	0.001						30292	30242	48	30242	48	95	140.0		25225	25225	60	CAMS 73922, 73951	24885	752	33	
RGF 12-5-2.A	*A. palmata*	AN031021.003	596	3.515	0.001	1.1407	0.0006	0.0997	0.0002	0.1137	11443	11393	30	11390	12	24	145.4	0.8	10270	10270	50	CAMS 99004	9930	152	8	1
RGF 12-5-2.B	*A. palmata*	AN031022.001	382	3.553	0.001	1.1411	0.0005	0.0997	0.0001	0.1137	11440	11390	14				145.8	0.7	10270				9930			1
RGF 12-9-3	*P. asteroides*	P54/Chiu/050103TC1	266	2.685	0.001	1.1364	0.0005	0.1047	0.0002	0.1190	12052	12002	25	12002	25	50	141.1	1.0	10540	10540	50	CAMS 99005	10200	200	10	1
RGF 12-9-5	*A. palmata*	050103TC3	349	2.798	0.001	1.1383	0.0005	0.1064	0.0003	0.1211	12253	12203	38	12203	38	76	143.1	0.5	10485	10485	70	CAMS 99006	10145	238	16	1
RGF 12-9-6	*A. palmata*	AN031107.001	1726	3.273	0.001	1.1387	0.0005	0.1061	0.0001	0.1208	12220	12170	15	12170	15	30	143.5	0.5	10505	10505	50	CAMS 99007	10165	230	9	1
RGF 13-1-11	*M. annularis*	AN040529.001	54	2.547	0.001	1.1377	0.0007	0.1432		0.1258	14646	14596	26	14596	26	52	143.5	1.0	12838	12838	60	WHOI 3	12498	234	12	1
RGF 13-1-2	*M. annularis*	AN050825.003	48	2.604	0.001	1.1456	0.0006				14598	14548	40	14548	40	80	146.0	0.5	12810	12810	88	KIA 27094	12470	231	18	3
RGF 13-2-4	*M. annularis*	AN060222.001	120	2.580	0.001	1.1408	0.0004	0.1243	0.0004	0.1418	14458	14408	45	14408	45	90	146.7	0.5	12865	12865	80	KIA 28711	12525	202	18	3
RGF 13-4-2	*P. asteroides?*	AN060222.003	246	3.005	0.001	1.1388	0.0005	0.1414	0.0003	0.1610	16596	16546	37	16546	37	74	145.4	0.7	14350	14350	90	KIA 28712	14010	294	19	3
RGF 13-4-3	*P. asteroides?*										16548	16498	38	16498	38	76	147.2	0.7	14290	14290	90	KIA 28713	13950	296	19	3
RGF 13-4-4	*P. asteroides*	AN050621.002 (No U ID. This is Th ID)	394	3.075	0.001	1.1404	0.0005	0.1409	0.0002	0.1606	16583	16528	30	16528	30	60	147.1	0.7	14436	14436	98	KIA 27349	14096	277	18	3
RGF 13-5-1A	*M. annularis*	P54/Cao/021606LC2		2.616	0.001	1.1471	0.0007				16468	16418	40	16606	26	52	147.1		14485	14504	54	KIA 28714	14164	279	12	3
RGF 13-5-1B	*M. annularis*	AN060316.006	4092	2.286	0.001	1.1405	0.0005	0.1416	0.0003	0.1616	16628	16578	36				147.3	0.7	14525			KIA 28715	14185			3
RGF 13-5-1C	*M. annularis*	P54/Cao/012506LC3		2.534	0.001	1.1477	0.0008				16687	16637	38				147.7		14505			KIA 28716	14165			3
RGF 13-6-4	*M. annularis*	AN050824.003	74	2.655	0.001	1.1405	0.0005	0.1447	0.0004	0.1651	17018	16968	55	16897	11	22	147.5	0.8	14633	14633	98	KIA 27343	14293	303	16	3
RGF 13-6-4.2	*M. annularis*	Neptune151215	98	2.622	0.000	1.1406	0.0002	0.1443	0.0001	0.1646	16966	16901	12				147.5	0.3								
RGF 13-6-6	*M. annularis*	AN060227.002	405	2.530	0.001	1.1404	0.0005	0.1438	0.0003	0.1640	16906	16856	39	16856	39	78	147.3	0.8	14641	14641	98	KIA 27344	14301	296	20	3
RGF 13-6-7	*M. annularis*	AN060301.002	132	2.364	0.001	1.1399	0.0005	0.1434	0.0004	0.1635	16849	16799	45	16799	45	90	146.7	0.7	14868	14868	98	KIA 27345	14528	251	20	3
RGF 13-6-8	*M. annularis*	AN060301.003	458	2.350	0.001	1.1380	0.0005	0.1459	0.0004	0.1661	17173	17123	45	16934	11	22	144.9	0.7	14855	14855	98	KIA 27346	14515	273	16	3
RGF 13-6-8	*M. annularis*	Neptune130726	1398	2.444	0.000	1.1388	0.0002	0.1445	0.0001	0.1645	16985	16922	12				145.6	0.3	14855				14515			
RGF 13-7-1	*M. annularis*	AN060531.001	840	3.089	0.001	1.1392	0.0004	0.1390	0.0003	0.1583	16287	16237	37	16237	37	74	145.8	0.6	14555	14616	78	KIA 27347	14276	206	16	3
RGF 13-7-1	*M. annularis*																		14700			BETA 321514	14360			
RGF 13-7-3	*P. asteroides*	AN050510.004	375	2.818	0.001	1.1381	0.0005	0.1476	0.0005		17384	17334	66	17334	66	132	145.1	0.7	14950	14950	100	KIA 30203	14610	321	27	
RGF 13-7-6	*A. palmata*	AN050510.003	449	2.740	0.001	1.1379	0.0005	0.1492	0.0004	0.1698	17586	17536	57	17417	37	74	144.9	0.8	15155	15155	68	KIA 27105	14815	300		
RGF 13-7-6	*A. palmata*	AN060927.004	338	2.753	0.001	1.1355	0.0005	0.1476	0.0004	0.1676	17389	17333	48				142.3	0.7	15155				14815			
RGF 13-8-2	*M. annularis*	AN060601.004	59	2.552	0.001	1.1351	0.0007	0.1477	0.0003	0.1677	17401	17351	38	17351	38	76	141.9	1.0	15080	15080	100	KIA 30204	14740	302	20	3
RGF 13-8-9	*A. palmata*	082801RM2	120	3.369	0.001	1.1322	0.0004	0.1495	0.0005	0.1693	17630	17580	69	17373	10	20	138.9	0.5	14840	14840	46	CAMS 81539, 88790	14500	345	8	1
RGF 13-8-9	*A. palmata*	Neptune130726	262	3.622	0.001	1.1375	0.0002	0.1480	0.0001	0.1683	17431	17368	10				144.4	0.2	14840				14500			1

Sample	Species	U-series I.D.	^{232}Th (ppt)	^{238}U (ppm)	error	[^{234}U/^{238}U]	error	[^{230}Th]/[^{234}U]	error	[^{230}Th/^{238}U]	U-Th Age (yr)	Cal. Age (yr BP)	error (yr)	mean Cal age (yr BP)	error	2 error	Initial δ^{234}U	error	^{14}C age (years BP)	mean ^{14}C age	2 error	AMS ID	^{14}C age corr	Δ^{14}C (‰)	2 error	REF
RGF 14-2-3	*M. annularis*	AN060626.002	301	2.511	0.001	1.1402	0.0006	0.1382	0.0002	0.1575	16189	16139	28	16139	28	56	146.8	0.8	14240	14240	100	KIA 30243	13900	249	18	3
RGF 14-3-5	*M. annularis*	AN060628.004	122	2.672	0.001	1.1352	0.0005	0.1516	0.0003	0.1721	17893	17843	42	18059	12	24	142.3	0.7	15610	15610	110	KIA 30244	15270	328	19	3
RGF 14-3-5	*M. annularis*	Neptune130726	105	2.494	0.000	1.1370	0.0002	0.1535	0.0001	0.1746	18141	18078	12				144.2	0.3	15610				15270			
RGF 15-10-1	*A. palmata*	110601RM2	111	2.977	0.001	1.1320	0.0004	0.1640	0.0002	0.1856	19488	19438	25	19421	23	46	139.5	0.5	16160	16160	56	CAMS 88770, 88784	15820	462	13	1
RGF 15-10-1	*A. palmata*	AN041222.001	87	3.082	0.001	1.1385	0.0005	0.1633	0.0004	0.1859	19395	19345	53				146.3	0.5	16160				15820			1
																			16110			OS-105002	15770			
RGF 15-10-2	*A. palmata*	AN050204.002	80	3.167	0.001	1.1367	0.0006	0.1641	0.0003	0.1865	19500	19450	36	19450	36	72	144.4	0.8	16479	16479	56	CAMS 88771, 88792	16139	410	16	3
RGF 15-10-3	*A. palmata*	AN050204.003	128	3.497	0.001	1.1378	0.0005	0.1622	0.0003	0.1845	19253	19203	37	19203	37	74	145.5	0.7	16198	16198	46	3 CAMS	15858	418	15	3
RGF 15-10-4	*A. palmata*	AN050204.004	115	3.330	0.001	1.1395	0.0005	0.1576	0.0002	0.1796	18667	18617	21	18617	21	42	147.1	0.7	15765	15765	70	CAMS 88773	15425	394	14	3
RGF 15-10-6	*A. palmata*	082001RM2	73	3.221	0.001	1.1339	0.0004	0.1528	0.0003	0.1732	18046	17996	35	17996	35	70	140.9	0.5	15015	15015	80	CAMS 86505, 99025	14675	419	19	3
RGF 15-12-2	*A. palmata*	082101RM1	115	3.108	0.001	1.1321	0.0006	0.1651	0.0002	0.1869	19631	19581	26	19544	15	30	139.6	1.0	16475	16475	90	CAMS 86521	16135	427	17	1
RGF 15-12-2	*A. palmata*	AN050406.004	75	3.296	0.001	1.1356	0.0005	0.1641	0.0003	0.1864	19505	19455	40				143.3	0.7	16475				16135			1
RGF 15-12-2	*A. palmata*	P54/mortlock/082101RM1		3.108	0.001	1.1396	0.0010				19595	19545	22				139.6	1.0	16475				16135			3
RGF 15-12-4	*A. palmata*	082101RM2	139	3.233	0.001	1.1311	0.0004	0.1632	0.0002	0.1846	19387	19337	23	19337	23	46	138.5	0.5	16465	16465	80	CAMS 88774	16125	394	16	3
RGF 15-13-4	*M. annularis*	082101RM4	620	2.176	0.000	1.1334	0.0004	0.1665	0.0003	0.1887	19820	19770	31	19736	24	48	141.0	0.5	16725	16734	67	CAMS 86519	16385	416	14	1
RGF 15-13-4	*M. annularis*	AN050207.001	74	2.205	0.001	1.1367	0.0006	0.1659	0.0003	0.1886	19734	19684	38				144.5	0.8	16745			CAMS 86510	16405			1
RGF 15-13-6	*Diploria sp.*			2.823	0.001						19484	19429	30	19429	30	60	139.4	0.5	16840	16840	56		16500	345	14	1
RGF 15-14-3	*M. annularis*	082201RM2	69	2.481	0.001	1.1325	0.0004	0.1643	0.0002	0.1861	19533	19483	27	19483	27	54	140.0	0.5	16975	16975	90	CAMS 86511	16635	331	17	1
RGF 15-14-4	*M. annularis*	082201RM3	71	2.334	0.001	1.1334	0.0005	0.1655	0.0002	0.1876	19688	19638	25	19638	25	50	141.0	1.0	16939	16939	52	CAMS AND WHOI	16599	363	12	1
RGF 15-14-7	*Diploria sp.*	AN050207.002	88	2.432	0.001	1.1375	0.0007	0.1658	0.0003	0.1886	19728	19673	33	19673	33	66	145.3	1.0	16615	16615	90	CAMS 88779	16275	425	20	1
RGF 15-15-2	*Diploria sp.*			2.396	0.001						19727	19672	64	19543	12	24	143.4	0.5	17073	17073	66	CAMS 86512, 86522	16733	325	12	1
RGF 15-15-2.2	*Diploria sp.*		123	2.591	0.000	1.1347	0.0003	0.1649	0.0001	0.1871	19603	19538	12				142.3	0.4								
RGF 15-15-3	*Diploria sp.*			2.685	0.001						19645	19590	44	19590	44	88	143.1	0.9	17070	17070	56	CAMS 88780, 88793	16730	333	17	1
RGF 15-15-5	*Diploria sp.*			2.505	0.001						19677	19622	34	19622	34	68	143.1	0.9	17150	17150	90	CAMS 86513	16810	325	18	1
RGF 15-15-7	*M. annularis*	AN050207.003	106	2.325	0.001	1.1367	0.0005	0.1690	0.0003	0.1921	20135	20085	33	20085	33	66	144.7	0.8	17125	17125	80	CAMS 88781	16785	405	18	1
RGF 15-15-8	*M. annularis*	110101RM3	57	2.330	0.001	1.1310	0.0004	0.1676	0.0003	0.1896	19963	19913	34	19913	34	68	138.6	0.5	17218	17218	56	CAMS AND WHOI	16878	361	15	1

Sample	Species	U-series I.D.	^{232}Th (ppt)	^{238}U (ppm)	error	[^{234}U/^{238}U]	error	[^{230}Th]/[^{234}U]	error	[^{230}Th/^{238}U]	U-Th Age (yr)	Cal. Age (yr BP)	error (yr)	mean Cal age (yr BP)	error	2 error	Initial δ^{234}U	error	^{14}C age (years BP)	mean ^{14}C age	2 error	AMS ID	^{14}C age corr	Δ^{14}C (‰)	2 error	REF
RGF 15-15-9	*M. annularis*	AN050207.004	56	2.415	0.001	1.1364	0.0005	0.1689	0.0002	0.1920	20132	20082	27	20082	27	54	144.4	1.0	17203	17203	56	CAMS 88783, 88789	16863	391	13	1
RGF 15-17-2	*M. annularis*	AN041222.004	296	2.494	0.001	1.1387	0.0005	0.1732	0.0003	0.1972	20684	20634	39	20634	39	78	147.0	0.7	17745	17745	120	KIA 25004	17405	390	24	1
RGF 15-17-3	*M. annularis*	AN031107.003	60	2.414	0.001	1.1318	0.0004	0.1727	0.0002	0.1954	20625	20575	31	20575	31	62	139.7	0.7	17825	17825	110	KIA 25003	17485	367	21	1
RGF 15-18-1	*M. annularis*	AN040106.004	47	2.329	0.000	1.1359	0.0004	0.1719	0.0002	0.1953	20519	20469	32	20469	32	64	144.1	0.7	17670	17670	100	KIA 25002	17330	376	20	1
RGF 15-18-2	*M. annularis*	AN041223.001	112	2.461	0.001	1.1382	0.0006	0.1730	0.0007	0.1969	20664	20614	89	20582	12	24	146.5	0.9	17800	17800	110	KIA 25001	17460	372	19	1
RGF 15-18-2	*M. annularis*	Neptune150617	193	2.375	0.000	1.1357	0.0002	0.1729	0.0001	0.1963	20646	20581	12				143.8	0.3								
RGF 15-18-3	*M. annularis*	AN050207.005	60	2.245	0.001	1.1358	0.0005	0.1739	0.0002	0.1975	20784	20734	31	20734	31	62	144.0	0.8	17740	17740	140	KIA 25000	17400	408	27	1
RGF 15-18-4	*M. annularis*	AN050210.002	37	2.450	0.001	1.1356	0.0005	0.1738	0.0003	0.1973	20764	20714	43	20714	43	86	143.8	0.7	17860	17860	120	KIA 24999	17520	384	25	1
RGF 15-19-2	*M. annularis*	AN050413.005	76	2.472	0.001	1.1341	0.0007	0.1772	0.0003	0.1952	20554	20504	39	20504	39	78	142.1	1.0	17980	17881	85	KIA 24998	17541	346	19	1
RGF 15-19-2	*M. annularis*																		17782			OS-105003	17442			
RGF 15-19-3	*M. annularis*	AN031110.002	65	2.550	0.001	1.1314	0.0005	0.1731	0.0002	0.1959	20682	20632	30	20632	30	60	139.3	0.8	18110	18110	120	KIA 24997	17770	328	22	1
RGF 15-19-5	*M. annularis*	AN060928.001	179	2.218	0.001	1.1325	0.0006	0.1741	0.0006	0.1971	20806	20756	79	20874	17	34	140.6	0.9	18030	18030	140	KIA 24996	17690	381	25	
RGF 15-19-5	*M. annularis*	Neptune150617	454	2.314	0.000	1.1349	0.0002	0.1751	0.0002	0.1988	20944	20879	17				143.2	0.3								
RGF 15-20-6	*M. annularis*	AN060713.005	71	2.458	0.001	1.1335	0.0005	0.1759	0.0004	0.1994	21047	20997	54	21128	22	44	141.7	0.8	18270	18270	180	KIA 30205	17930	383	32	3
RGF 15-20-6.2	*M. annularis*	Neptune151215	156	2.477	0.000	1.1350	0.0002	0.1772	0.0002	0.2011	21218	21154	24				143.3	0.3								
RGF 15-22-7	*M. annularis*	P54/Cao/083006LC1									21729	21679	60	21679	60	120			18660	18660	160	KIA 30206	18320	408	35	3
RGF 15-2-4	*M. annularis*	082001RM1	60	2.269	0.000	1.1393	0.0004	0.1091	0.0002	0.1243	12583	12533	26	12533	26	56	144.4	0.5	10843	10843	38	CAMS and WHOI	10503	232	10	1
RGF 15-4-1	*M. annularis*	081904LC2	124	2.224	0.001	1.1397	0.0006	0.1123	0.0004	0.1280	12976	12926	49	12865	25	50	145.0	1.0	11020	11033	35	CAMS 81551	10680	255	9	1
RGF 15-4-1	*M. annularis*	AN050413.003	299	2.365	0.001	1.1419	0.0006	0.1116	0.0003	0.1275	12894	12844	29				147.1	1.0	11045			CAMS 82279	10705			1
RGF 15-5-1	*M. annularis*	081904LC3	18	2.409	0.001	1.1405	0.0006	0.1121	0.0004	0.1279	12957	12907	54	12885	18	36	145.7	1.0	11465	11465	70	CAMS 81552	11125	190	12	1
RGF 15-5-1	*M. annularis*	AN040529.002	30	2.642	0.001	1.1413	0.0005	0.1119	0.0002	0.1278	12933	12883	19				146.6	0.8	11465				11125			1
RGF 15-5-2	*M. annularis*	AN040529.003	25	2.467	0.001	1.1410	0.0006	0.1130	0.0002	0.1289	13063	13013	22	13013	22	44	146.3	0.8	11505	11505	50	CAMS 82283	11165	202	10	1
RGF 15-5-3	*A. palmata*	AN031106.003	48	3.003	0.001	1.1385	0.0005	0.1256	0.0001	0.1431	14623	14573	15	14573	15	30	144.4	0.7	12730	12730	70	CAMS 81553	12390	247	12	1
RGF 15-7-1	*M. annularis*	AN041220.003	69	2.544	0.001	1.1420	0.0006	0.1266	0.0002	0.1445	14735	14685	22	14685	22	44	148.0	0.8	12880	12880	38	CAMS 81554, 82284	12540	241	9	1
RGF 15-8-1	*A. palmata*	110501RM2	232	3.246	0.001	1.1328	0.0005	0.1567	0.0003	0.1775	18544	18494	36	18494	36	72	140.0	0.5	15307	15307	40	CAMS 81555, 82285	14967	454	15	1
RGF 15-9-5	*A. palmata*	121702TC3	50	2.963	0.001	1.1367	0.0004	0.1560	0.0002	0.1773	18458	18408	26	18408	26	52	144.0	0.5	15188	15188	80	CAMS 86508, 86518	14848	460	17	1
RGF 16-12-6	*A. palmata*	082801RM1	75	2.991	0.001	1.1374	0.0004	0.1007	0.0001	0.1145	11562	11512	17	11512	17	34	141.9	0.5	10335	10335	60	CAMS 86514	9995	160	10	1

Sample	Species	U-series I.D.	^{232}Th (ppt)	^{238}U (ppm)	error	[^{234}U/^{238}U]	error	[^{230}Th]/[^{234}U]	error	[^{230}Th/^{238}U]	U-Th Age (yr)	Cal. Age (yr BP)	error (yr)	mean Cal age (yr BP)	error	2 error	Initial δ^{234}U	error	^{14}C age (years BP)	mean ^{14}C age	2 error	AMS ID	^{14}C age corr	Δ^{14}C (‰)	2 error	REF
RGF 16-12-7	*A. palmata*	AN041202.006	37	3.168	0.001	1.1461	0.0005	0.1000	0.0001	0.1146	11479	11429	16	11429	16	32	151.0	0.7	10215	10215	70	CAMS 112216	9875	166	11	3
RGF 7-10-2	*A. palmata*	AN040901.005	92	2.878	0.001	1.1448	0.0006	0.0791	0.0003	0.0906	8984	8934	30	8934	30	60	148.5	0.9	8320	8320	40	CAMS 106527, CAMS 106888	7980	91	10	1
RGF 7-12-2	*A. palmata*	AN040902.002	66	3.207	0.001	1.1455	0.0006	0.0810	0.0002	0.0928	9205	9155	18	9155	18	36	149.4	0.8	8595	8595	34	CAMS 106528,106889,106907	8255	83	7	1
RGF 7-16-2	*A. palmata*	AN040903.003	49	3.104	0.001	1.1457	0.0005	0.0849	0.0002	0.0972	9668	9618	23	9675	15	30	149.7	0.7	9005	9005	50	CAMS 106529	8665	96	8	1
RGF 7-16-2.2	*A. palmata*	AN100707.001	74	3.240	0.001	1.1433	0.0005	0.0858	0.0002	0.0981	9782	9722	21				147.4	0.8	9005				8665			
RGF 7-16-6	*A. palmata*	AN040903.001	198	3.068	0.001	1.1452	0.0005	0.0874	0.0002	0.1001	9972	9922	21	9922	21	42	149.3	0.8	9160	9160	70	CAMS 106530	8820	108	11	1
RGF 7-19-3	*P. asteroides*	AN040903.002	251	2.990	0.001	1.1446	0.0006	0.0876	0.0003	0.1003	9991	9941	33	9941	33	66	148.8	0.8	9275	9275	60	CAMS and WHOI	8935	95	12	1
RGF 7-26-2	*A. palmata*	AN050406.003	120	2.983	0.001	1.4150	0.0005	0.0946	0.0002	0.1080	10832	10782	22	10804	16	32	145.8	0.5	9706	9706	38	WHOI	9366	152	7	1
RGF 7-26-2.2	*A. palmata*	AN050511.004	35	3.025	0.001	1.1429	0.0005	0.0950	0.0002	0.1086	10880	10830	24				147.4	0.7	9706				9366			
RGF 7-4-2	*P. asteroides*	AN040901.002	212	2.623	0.001	1.1467	0.0005	0.0651	0.0002	0.0746	7339	7289	19	7289	19	38	149.8	0.8	6865	6865	50	CAMS 106524	6525	72	8	1
RGF 7-9-6	*A. palmata*	AN040901.004	404	3.363	0.001	1.1459	0.0006	0.0791	0.0002	0.0907	8986	8936	22	8936	22	44	149.6	0.8	8325	8325	50	CAMS 106526	7985	91	9	1
RGF 8-20-4	*A. palmata*	AN050127.002	81	3.061	0.001	1.1439	0.0006	0.0921	0.0002	0.1053	10529	10479	19	10479	19	38	148.3	1.0	9650	9650	70	KIA 28718	9310	115	11	3
RGF 8-22-1.A	*A. palmata*	AN061012.002	539	3.279	0.001	1.1411	0.0005	0.0948	0.0003	0.1082	10860	10804	35	10838	24	48	145.0	0.5	10044	10044	70	OS-105008	9704	109	12	
RGF 8-22-1.B	*A. palmata*	AN061016.001	219	3.195	0.001	1.1404	0.0005	0.0954	0.0003	0.1088	10923	10867	32				145.0	1.0	10044				9704			
RGF 9-11-2	*A. palmata*	AN030618.001	43	3.101	0.001	1.1409	0.0004	0.1233	0.0002	0.1407	14333	14283	22	14251	11	22	146.7	0.6	12735	12735	80	CAMS 96029	12395	198	12	1
RGF 9-11-2A	*A. palmata*	AN031021.001	74	3.261	0.001	1.1380	0.0005	0.1228	0.0001	0.1398	14272	14222	18				143.7	0.8	12735				12395			1
RGF 9-11-2B	*A. palmata*	AN031022.002	53	3.131	0.001	1.1378	0.0005	0.1231	0.0002	0.1401	14309	14259	20				143.5	0.7	12735				12395			1
RGF 9-1-2	*M. annularis*	042401KS2	75	2.232	0.001	1.1379	0.0004	0.1062	0.0003	0.1208	12229	12179	33	12179	33	66	142.7	0.5	10565	10565	48	CAMS 77013, 77026	10225	222	12	1
RGF 9-12-5	*A. palmata*	AN031106.002	1790	3.293	0.001	1.1369	0.0005	0.1243	0.0002	0.1413	14458	14408	20	14408	20	40	142.6	0.8	12780	12780	56	CAMS 96030, 96032	12440	215	10	1
RGF 9-12-7A	*A. palmata*	AN031021.002	137	3.273	0.002	1.1397	0.0005	0.1242	0.0001	0.1416	14444	14394	19	14396	12	24	145.5	0.8	12780	12780	38	CAMS 99002, 99011	12440	213	7	1
RGF 9-12-7B	*A. palmata*	AN031022.003	320	3.339	0.001	1.1382	0.0005	0.1242	0.0001	0.1414	14447	14397	17				144.0	0.7	12780				12440			1
RGF 9-13-3	*A. palmata*	AN040528.002	46	3.000	0.001	1.1391	0.0005	0.1254	0.0002	0.1428	14589	14539	23	14539	23	46	144.9	0.8	12680	12680	60	CAMS 99003	12340	249	12	1
RGF 9-14-2	*M. annularis*	AN060627.003	828	2.572	0.001	1.1400	0.0005	0.1249	0.0004	0.1424	14527	14477	47	14477	47	94	145.8	0.8	12895	12895	90	KIA 30189	12555	207	19	3
RGF 9-15-2	*A. palmata*	AN060628.002	1264	3.116	0.001	1.1397	0.0005	0.1258	0.0003	0.1434	14639	14583	35	14583	35	70	145.6	0.7	12815	12815	90	KIA 30190	12475	235	17	3
RGF 9-15-3	*M. annularis*	AN060628.003	142	2.337	0.000	1.1413	0.0006	0.1260	0.0003	0.1439	14672	14622	40	14622	40	80	147.3	0.8	13080	13080	100	KIA 30191	12740	201	19	3
RGF 9-1-6	*M. annularis*	042001DP3	89	2.434	0.001	1.1391	0.0004	0.1049	0.0002	0.1195	12079	12029	30	12029	30	60	144.0	0.5	10600	10600	60	CAMS 77008	10260	195	12	1
RGF 9-1-7	*M. annularis*	042301JS1	78	2.418	0.001	1.1361	0.0005	0.1027	0.0004	0.1166	11806	11756	53	11783	25	50	140.7	0.5	10590	10590	60	CAMS 77018	10250	161	11	1

Sample	Species	U-series I.D.	^{232}Th (ppt)	^{238}U (ppm)	error	[^{234}U/^{238}U]	error	[^{230}Th]/[^{234}U]	error	[^{230}Th/^{238}U]	U-Th Age (yr)	Cal. Age (yr BP)	error (yr)	mean Cal age (yr BP)	error	2 error	Initial δ^{234}U	error	^{14}C age (years BP)	mean ^{14}C age	2 error	AMS ID	^{14}C age corr	Δ^{14}C (‰)	2 error	REF
RGF 9-1-7	*M. annularis*	110101RM1	61	2.459	0.001	1.1408	0.0006	0.1030	0.0002	0.1175	11841	11791	29				145.6	1.0	10590				10250			1
RGF 9-17-1	*M. annularis*	AN061031.004	365	2.272	0.001	1.1394	0.0005	0.1280	0.0003	0.1458	14913	14857	42	14936	24	48	145.4	0.8	13005	13005	90	OS-105009	12665	259	16	
RGF 9-17-1.2	*M. annualris*	Neptune130709	2338	2.481	0.000	1.1425	0.0003	0.1290	0.0001	0.1474	15036	14973	29				148.7	0.5								
RGF 9-1-8	*M. annularis*	042301AC2	60	2.254	0.000	1.1394	0.0003	0.1067	0.0007	0.1215	12289	12239	87	12118	17	34	144.3	0.5	10580	10656	46	CAMS 77021	10316	199	8	1
RGF 9-1-8	*M. annularis*	050103TC5	76	2.263	0.001	1.1369	0.0007	0.1062	0.0003	0.1208	12236	12186	42				141.7	1.0	10760			CAMS 96023	10420			1
RGF 9-1-8	*M. annularis*	AN030606.002	59	2.380	0.001	1.1411	0.0004	0.1055	0.0002	0.1204	12147	12097	20				146.0	0.6								
RGF 9-18-2	*M. annularis*	AN061031.002	84	2.518	0.001	1.1387	0.0004	0.1416	0.0003	0.1613	16628	16572	37	16793	15	30	145.3	0.6	14423	14423	110	OS-104814	14083	321	19	
RGF 9-18-2.2	*M. annualris*	Neptune130709	118	2.540	0.000	1.1408	0.0003	0.1418	0.0001	0.1617	16643	16580	16				147.6	0.4								
RGF 9-20-2	*A. palmata*	082801RM3	144	3.495	0.001	1.1368	0.0005	0.1537	0.0003	0.1748	18166	18116	37	18116	37	74	144.0	0.5	15313	15313	60	CAMS AND WHOI	14973	388	16	1
RGF 9-21-10	*A. palmata*	AN050413.002	78	3.364	0.001	1.1375	0.0006	0.1545	0.0004	0.1758	18268	18218	44	18218	44	88	144.8	0.8	15400	15400	70	CAMS 81542	15060	390	19	1
RGF 9-21-11	*A. palmata*	AN050408.002	76	3.545	0.001	1.1376	0.0005	0.1542	0.0005	0.1754	18226	18176	56	18219	9	18	144.9	0.8	15405	15405	60	CAMS 81543	15065	389	11	1
RGF 9-21-11.2	*A. palmata*		98	3.538	0.000	1.1371	0.0002	0.1548	0.0001	0.1761	18309	18224	9				144.4	0.2								
RGF 9-21-6	*A. palmata*	081804LC1	42	3.431	0.001	1.1350	0.0004	0.1542	0.0003	0.1750	18224	18174	33	18174	33	66	142.2	0.5	15295	15295	60	WHOI	14955	401	15	1
RGF 9-2-3	*M. annularis*	042401SG1	122	2.384	0.001	1.1373	0.0004	0.1048	0.0003	0.1192	12067	12017	32	12016	19	38	142.1	0.5	10715	10703	42	CAMS 86523	10363	178	8	1
RGF 9-2-3	*M. annularis*	110701RM1	84	2.328	0.001	1.1396	0.0005	0.1048	0.0002	0.1195	12065	12015	24				144.5	0.5	10690			CAMS 77019	10350			1
RGF 9-24-2	*A. palmata*	081804LC3	59	3.250	0.001	1.1360	0.0005	0.1584	0.0002	0.1799	18766	18716	28	18716	28	56	143.4	1.0	15928	15928	60	CAMS 81544, 82276	15588	382	14	1
RGF 9-24-4	*A. palmata*	081804LC5	84	2.981	0.001	1.1356	0.0005	0.1591	0.0003	0.1807	18856	18806	33	18806	33	66	143.0	1.0	15830	15830	70	CAMS 81545	15490	415	17	1
RGF 9-2-5	*M. annularis*	050203LC1	122	2.228	0.001	1.1387	0.0005	0.1055	0.0003	0.1202	12153	12103	39	12095	23	46	143.5	0.5	10850	10878	49	CAMS 96024	10538	164	10	1
RGF 9-2-5	*M. annularis*	AN050411.002	187	2.383	0.000	1.1431	0.0004	0.1054	0.0003	0.1205	12141	12091	28				148.1	0.6	10905			CAMS 96031	10565			1
RGF 9-2-7	*M. annularis*	042001TC1	105	2.281	0.001	1.1382	0.0007	0.1074	0.0004	0.1222	12377	12327	45	12300	23	46	143.1	1.0	10770	10770	60	CAMS 77011	10430	209	11	1
RGF 9-2-7 rep	*M. annularis*	110701RM2	88	2.225	0.001	1.1389	0.0004	0.1071	0.0002	0.1220	12340	12290	28				143.8	0.5	10770				10430			1
RGF 9-27-5 rep	*A. palmata*	120902TC1	74	3.157	0.001	1.1344	0.0005	0.1612	0.0004	0.1828	19125	19075	55	19075	55	110	141.8	1.0	16376	16376	56	CAMS 86516, 81547	16036	365	21	1
RGF 9-3-2	*M. annularis*	110501RM1	95	2.231	0.001	1.1413	0.0005	0.1072	0.0001	0.1223	12353	12303	14	12303	14	28	146.3	0.5	10775	10775	38	CAMS 77015, 82280	10435	208	7	1
RGF 9-3-4	*M. annularis*	050203LC2	133	2.456	0.001	1.1381	0.0006	0.1103	0.0006	0.1255	12730	12680	75	12465	15	30	143.2	1.0	10952	10952	52	CAMS 77012, 96025	10612	206	9	1
RGF 9-3-4.2	*M. annularis*	Neptune150617	205	2.495	0.001	1.1435	0.0003	0.1086	0.0001	0.1242	12521	12456	15				148.6	0.4								
RGF 9-34-10	*P. asteroides*	020901RM2	205	2.925	0.001	1.1309	0.0005	0.1824	0.0003	0.2063	21908	21858	41	21858	41	82	139.3	0.5	18590	18590	80	CAMS 73924	18250	451	20	1
RGF 9-34-7	*P. asteroides*	020901RM1	470	2.893	0.001	1.1316	0.0005	0.1813	0.0003	0.2052	21764	21714	41	21714	41	82	140.0	0.5	18550	18550	56	CAMS 73923, 73952	18210	433	17	1
RGF 9-34-8	*P. asteroides*	121802TC4	221	2.849	0.001	1.1362	0.0005	0.1820	0.0003	0.2068	21852	21802	41	21802	41	82	144.8	0.5	18585	18585	80	CAMS 82275	18245	442	20	1

Sample	Species	U-series I.D.	^{232}Th (ppt)	^{238}U (ppm)	error	[^{234}U/^{238}U]	error	[^{230}Th]/[^{234}U]	error	[^{230}Th/^{238}U]	U-Th Age (yr)	Cal. Age (yr BP)	error (yr)	mean Cal age (yr BP)	error	2 error	Initial δ^{234}U	error	^{14}C age (years BP)	mean ^{14}C age	2 error	AMS ID	^{14}C age corr	Δ^{14}C (‰)	2 error	REF
RGF 9-35-2	*P. asteroides*	020901RM3	176	2.960	0.001	1.1316	0.0005	0.1829	0.0003	0.2070	21972	21922	41	21972	27	54	140.0	0.5	18670	18670	56	CAMS 73925, 73950	18330	457	14	1
RGF 9-35-2.2	*P. asteroides*	080201RM3	189	2.981	0.001	1.1310	0.0006	0.1836	0.0003	0.2076	22060	22010	36				139.5	1.0	18670				18330			1
RGF 9-35-6	*M. annularis*	020901RM4	88	2.262	0.001	1.1325	0.0005	0.1847	0.0005	0.2092	22210	22160	62	22160	62	124	141.1	0.5	18750	18750	80	CAMS 73926	18410	476	27	1
RGF 9-3-6	*P. asteroides*	AN030606.003	593	2.769	0.001	1.1404	0.0004	0.1119	0.0002	0.1276	12923	12873	24	12873	24	48	145.6	0.5	11395	11395	70	CAMS 96026	11055	199	13	3
RGF 9-37-2	*M. annularis*	121902TC1	93	2.161	0.001	1.1317	0.0005	0.1875	0.0003	0.2122	22586	22536	46	22521	32	64	140.4	0.5	19460	19460	82	CAMS 86507, 86517	19120	411	18	1
RGF 9-37-2.2	*M. annularis*	AN100709.001	126	2.346	0.002	1.1300	0.0009	0.1874	0.0003	0.2117	22565	22505	46				138.5	1.4								
RGF 9-37-3	*M. annularis*	021201RM2	91	2.189	0.001	1.1317	0.0004	0.1878	0.0004	0.2125	22624	22574	48	22574	48	96	140.4	0.5	19360	19360	80	CAMS 73927	19020	438	22	1
RGF 9-38-1	*M. annularis*	121100RM4	73	2.349	0.001	1.1315	0.0005	0.1913	0.0003	0.2165	23094	23044	37	23044	37	74	140.4	1.0	19820	19820	80	CAMS 73928	19480	437	19	1
RGF 9-38-2	*M. annularis*	102400RM1	96	2.331	0.001	1.1292	0.0006	0.1932	0.0005	0.2182	23346	23296	61	23296	61	122	138.0	1.0	19720	19720	80	CAMS 73925	19380	500	27	1
RGF 9-38-3	*M. annularis*	102400RM2	76	2.316	0.001	1.1293	0.0007	0.1913	0.0003	0.2160	23089	23039	38	23039	38	76	138.0	1.0	19750	19750	80	CAMS 73930	19410	449	20	1
RGF 9-39-2	*M. annularis*	102400RM3	98	2.573	0.001	1.1289	0.0005	0.1974	0.0003	0.2229	23917	23867	44	23867	44	88	137.9	0.5	20310	20310	100	CAMS 73931	19970	494	24	1
RGF 9-39-3	*M. annularis*	102500RM1	140	2.402	0.003	1.1307	0.0011	0.1974	0.0005	0.2232	23908	23858	69	23858	69	138	139.9	1.5	20260	20260	80	CAMS 73932	19920	502	29	1
RGF 9-39-4	*Diploria sp.*		113	2.501	0.001	1.1287	0.0006	0.2049	0.0004	0.2313	24933	24883	55	24883	55	110	138.1	1.0	21080	21080	80	CAMS 73933	20740	535	26	1
RGF 9-39-5A/B	*Diploria sp.*	102600RM1	1296	2.238	0.001	1.1302	0.0004	0.2027	0.0003	0.2291	24629	24579	41	24579	41	82	139.5	0.5	21016	21016	48	3 CAMS	20676	491	17	1
RGF 9-40-4	*Diploria sp.*	110201RM1	318	2.695	0.001	1.1266	0.0004	0.2061	0.0002	0.2322	25095	25045	30	25045	30	60	135.9	0.5	21380	21380	100	CAMS 73937	21040	508	22	
RGF 9-41-10	*M. annularis*	011701RM2	78	2.272	0.001	1.1300	0.0006	0.2121	0.0004	0.2397	25916	25866	53	25866	53	106	139.9	1.0	21790	21790	100	CAMS 73942	21450	582	28	1
RGF 9-41-13	*M. annularis*	011701RM3	164	2.251	0.001	1.1285	0.0004	0.2151	0.0004	0.2428	26328	26278	50	26136	31	62	138.4	0.5	22070	22070	100	CAMS 73944	21730	579	23	1
RGF 9-41-13	*M. annularis*	080801RM1	281	2.394	0.001	1.1283	0.0005	0.2134	0.0003	0.2408	26094	26044	40				138.1	0.5	22070				21730			1
RGF 9-41-3	*M. annularis*	102600RM2	166	2.301	0.001	1.1293	0.0005	0.2105	0.0003	0.2378	25695	25645	40	25645	40	80	139.0	1.0	21670	21670	100	CAMS 73938	21330	564	25	1
RGF 9-41-6	*M. annularis*	110101RM2	76	2.119	0.001	1.1281	0.0005	0.2112	0.0004	0.2383	25793	25743	61	25743	61	122	137.8	1.0	21760	21760	100	WHOI	21420	565	30	1
RGF 9-41-8	*M. annularis*	011601RM3	58	2.147	0.000	1.1287	0.0004	0.2105	0.0003	0.2376	25689	25639	45	25639	45	90	138.4	0.5	21740	21740	58	CAMS	21400	549	20	1
RGF 9-41-9	*M. annularis*	011701RM1	68	2.418	0.001	1.1299	0.0004	0.2112	0.0004	0.2387	25791	25741	53	25741	53	106	139.7	0.5	21760	21760	100	CAMS 73941	21420	565	28	1
RGF 9-7-2	*P. asteroides*	AN060914.007	240	2.900	0.001	1.1385	0.0004	0.1200	0.0003	0.1366	13927	13877	35	13877	35	70	144.0	0.6	12635	12635	100	KIA 30187	12295	160	17	
RGF 9-8-2	*A. palmata*	AN030606.004	1124	3.197	0.001	1.1396	0.0005	0.1218	0.0002	0.1388	14150	14100	27	14083	20	40	145.3	0.7	12615	12615	80	CAMS 96027	12275	192	13	1
RGF 9-8-2	*A. palmata*	AN040527.012	1978	3.228	0.001	1.1405	0.0005	0.1215	0.0002	0.1386	14114	14064	29				146.2	0.8	12615				12275			1
RGF 9-9-4	*A. palmata*	AN060531.003	640	3.130	0.001	1.1386	0.0005	0.1226	0.0003	0.1396	14243	14187	40	14187	40	80	144.3	0.7	12755	12755	90	KIA 30188	12415	186	18	3
RGF 9-9-7	*A. palmata*	AN030619.004	3441	3.162	0.001	1.1409	0.0006	0.1233	0.0002	0.1407	14332	14282	26	14288	19	38	146.8	0.9	12795	12795	80		12455	195	13	3
RGF 9-9-7	*A. palmata*	AN031106.001	2923	3.083	0.001	1.1361	0.0005	0.1234	0.0002	0.1402	14345	14295	29				141.7	0.8	12795			CAMS 96028	12455			1
RGF 7-5-5*	*A. palmata*	AN040901.003	54	3.240	0.001	1.1446	0.0005	0.0824	0.0001	0.0944	9380	9330	17	9330	17	34	146.4	0.7	8705	8705	38	CAMS 106525, 106887, 106891	8365	91	7	1

Sample	Species	U-series I.D.	^{232}Th (ppt)	^{238}U (ppm)	error	[^{234}U/^{238}U]	error	[^{230}Th]/[^{234}U]	error	[^{230}Th/^{238}U]	U-Th Age (yr)	Cal. Age (yr BP)	error (yr)	mean Cal age (yr BP)	error	2 error	Initial δ^{234}U	error	^{14}C age (years BP)	mean ^{14}C age	2 error	AMS ID	^{14}C age corr	Δ^{14}C (‰)	2 error	REF
RGF04 1-5-3	*A. palmata*	AN050203.003	5742	3.606	0.001	1.1439	0.0004	0.0886	0.0001	0.1014	10109	10054	17	10054	17	34	148.1	0.5	9305	9305	70	KIA28720	8965	106	11	3
RGF04 1-6-7	*A. palmata*	AN050203.004	1718	2.997	0.001	1.1459	0.0005	0.1062	0.0003	0.1217	12229	12174	35	12174	35	70	151.0	1.0	10745	10745	80	KIA28721	10405	194	16	3

Araki ID	Terrace	Species	U series ID	^{232}Th (ppt)	^{238}U (ppm)	error	[^{234}U/^{238}U]	error	[^{230}Th/^{234}U]	error	[^{230}Th/^{238}U]	Cal Age (yr BP)	error (yr)	2 error (yr)	Initial δ^{234}U	error	[^{231}Pa]/[^{235}U]	2 error	U/Pa age (yr BP)	error (yr)	2 error (yr)	Concordant	^{14}C age uncorr (yr)	^{14}C age corr (yr)	2 sig error (yr)	AMS ID	Δ^{14}C (‰)	2 error (‰)	Ref
AK-BD-2	D		102803TC5	10	1.995	0.001	1.1263	0.0006	0.2829	0.0003	0.3186	36014	43	86	139.9	0.9							30547	30182	316		821	19	1
AK-BD-3	D	P	102903TC1	8	3.903	0.001	1.1268	0.0005	0.2725	0.0003	0.3071	34467	39	78	139.8	0.8	0.5233	0.0060	35020	300	600	Y	29351	28986	288		753	17	1
AK-BD-4	D	P	102903TC2	29	2.723	0.001	1.1274	0.0005	0.2796	0.0003	0.3152	35518	43	86	140.9	0.8	0.5219	0.0043	34880	215	430	Y	31110	30745	440		599	17	4
AK-BD-5	D	P	062603TC2	13	2.636	0.001	1.1264	0.0005	0.2844	0.0005	0.3204	36247	74	148	140.1	0.8	0.5470	0.0065	37430	340	680	Y	31670	31305	520		629	29	1
AK-BD-9	D	Pl	102903TC6	734	2.826	0.001	1.1249	0.0005	0.3074	0.0003	0.3458	39759	42	84	139.8	0.8	0.5695	0.0039	39830	215	430	Y	35090	34725	800		628	17	1,4
AK-BD-10	D	Fs	010803RM1	12	2.579	0.001	1.1263	0.0004	0.3069	0.0003	0.3457	39684	50	100	141.3	0.6							35274	34909	560		576	19	1
AK-BD-11	D	Pl	063003TC3	299	2.691	0.001	1.1256	0.0004	0.2986	0.0004	0.3361	38401	58	116	140.0	0.8	0.5611	0.0036	38920	195	390	Y	33108	32743	456		768	25	1,4
AK-L-1	D			16	2.129	0.000	1.1310	0.0004	0.2672	0.0003	0.2672	33677	39	78	144.1	1.1													1
AK-K-1	D	P	112504TC2	27	3.804	0.001	1.1273	0.0007	0.2844	0.0003	0.3206	36240	46	92	141.0	1.1							32137	31772	512		536	17	1
AK-K-2	D	Plla	042203TC2	24	2.454	0.001	1.1279	0.0005	0.2842	0.0003	0.3206	36216	49	98	141.7	1.5	0.5425	0.0056	36960	290	580	Y	30980	30615	300		769	21	1
AK-AB-1	E	P.l.	30423.001	57	2.516	0.001	1.1231	0.0005	0.3602	0.0003	0.4045	48273	49	98	141.1	0.7	0.6368	0.0095	47870	630	1260	Y	44410	44045	1060		429	17	1
ARA04-2D	D	G	112304RM1	29	2.334	0.000	1.1299	0.0005	0.3077	0.0009	0.3477	39799	140	280	145.3	0.8							35050	34685	460		644	56	1
ARA04-10D	D	F	112304TC2	9	2.452	0.000	1.1299	0.0005	0.3085	0.0004	0.3486	39930	58	116	145.4	0.7	0.5415	0.0091	36850	470	940	N	34570	34205	420		773	25	1
ARA04-11D	D	G	102604LC5	36	2.441	0.000	1.1280	0.0005	0.3149	0.0003	0.3552	40923	54	108	143.7	0.8	0.5820	0.0072	41200	410	820	Y	35640	35275	400		750	23	1
ARA04-17D	D		011805TC1	6	3.101	0.001	1.1289	0.0005	0.2863	0.0003	0.3232	36521	44	88	142.9	0.8							31710	31345	300		676	18	1
ARA04-19D	D	P	011805TC2	94	3.374	0.001	1.1307	0.0005	0.2830	0.0003	0.3200	36031	44	88	144.7	0.8							32070	31705	300		510	16	1
ARA04-22D	D	P	112304RM4	44	2.951	0.001	1.1323	0.0005	0.2829	0.0004	0.3203	36008	64	128	146.5	0.7							31220	30855	280		674	26	1
ARA04-40E	E	Plla	102604RM4	10	2.493	0.001	1.1236	0.0005	0.3658	0.0003	0.4110	49203	45	90	142.1	0.7	0.6499	0.0034	49600	230	460	Y	45160	44795	1140		457	16	1,4
ARA04-43E	E	P	092204LC2	17	2.837	0.001	1.1252	0.0005	0.3597	0.0006	0.4048	48183	102	204	143.5	0.7	0.6413	0.0109	48460	730	1460	Y	46060	45695	1260		151	28	1
ARA04-44E	E	P	092204LC3	69	3.144	0.001	1.1262	0.0005	0.3609	0.0007	0.4064	48378	112	224	144.7	0.9	0.6403	0.0110	48330	735	1470	Y	44750	44385	1100		387	38	1
ARA04-71E	E	F	092304LC1	27	2.223	0.001	1.1258	0.0005	0.3312	0.0005	0.3729	43519	82	164	142.2	0.8							38860	38495	760		604	32	1
ARA04-73E	E		092304LC2	14	2.145	0.001	1.1270	0.0005	0.3348	0.0005	0.3774	44098	83	166	143.9	0.8	0.6084	0.0040	44310	245	490	Y	39710	39345	620		548	31	4
ARA04-75E	E	P	092304LC2	27	2.947	0.001	1.1254	0.0005	0.3395	0.0006	0.3820	44850	90	180	142.3	0.7	0.6151	0.0047	45120	290	580	Y	41710	41345	780		322	29	4
ARA04-77E	E	F	092304LC4	8	2.608	0.001	1.1280	0.0005	0.3333	0.0005	0.3759	43840	86	172	144.9	0.8							39700	39335	640		502	31	1
ARA04-85E	E	G	092304LC5	4	2.562	0.000	1.1262	0.0004	0.3310	0.0004	0.3727	43474	72	144	142.8	0.7	0.5864	0.0080	41720	460	920	N	40460	40095	660		307	23	1
ARA04-93D	D		010906RM1	23	2.697	0.001	1.1272	0.0005	0.2842	0.0007	0.3204	36196	75	150	139.9	0.7	0.5331	0.0083	36010	425	850	Y	31250	30885	340		706	31	
ARA04-94D	D		051305RM1	13	2.162	0.001	1.1272	0.0005	0.3104	0.0007	0.3499	40144	63	126	142.6	0.7	0.5718	0.0107	40090	595	1190	Y	33520	33155	400		1073	32	
ARA04-95D	D		082806RM3	27	2.791	0.001	1.1256	0.0005	0.2798	0.0007	0.3149	35322	75	150	138.9	0.7	0.5346	0.0070	36150	355	710	Y	29790	29425	300		841	33	
AK-M-1	F	P.l.b.	060706RM2	272	3.205	0.001	1.1241	0.0005	0.3618	0.0007	0.4067	48535	114	228	142.3	1.0	0.6415	0.0088	48480	585	1170	Y	43210	42845	1160		713	47	
ARA04-34E	E		060105RM1	26	2.373	0.000	1.1238	0.0004	0.3642	0.0006	0.4093	48938	100	200	142.2	0.6	0.6521	0.0097	49900	670	1340	Y	43320	42955	1180		774	43	
ARA04-32E	E		051205RM2	24	2.337	0.000	1.1240	0.0007	0.3629	0.0008	0.4080	48743	125	250	142.3	1.0	0.6930	0.0102	55810	800	1600	N	44530	44165	1340		490	45	
AK-BC-2	C	F.s.	40524.004	9	2.437	0.001	1.1410	0.0006	0.0671	0.0002	0.0765	7518	17	34	144.0	1.5							6895	6530	60		101	5	1
AK-F-2	D	Fp	082504TC3	9	2.555	0.001	1.1287	0.0006	0.2831	0.0006	0.3195	36047	96	192	142.5	0.9							31610	31245	920		602	37	1
AK-AA-1	D	Fs	082504TC4	15	2.271	0.001	1.1280	0.0004	0.2942	0.0004	0.3319	37724	68	136	142.5	0.7	0.5590	0.0071	38690	385	770	Y	34090	33725	1260		441	24	1
AK-BE-1b	E	P.l.	051205RM4	337	2.705	0.001	1.1228	0.0005	0.3446	0.0006	0.3869	45689	93	186	139.7	0.7	0.6329	0.0060	47360	390	780	Y	42310	41945	1920		358	31	1,4
ARA05 718 D17	D		Neptune13	221	2.716	0.001	1.1236	0.0005	0.2918	0.0002	0.3278	37354	32	64	137.4	0.8							32407	32042	460	OS-105004	699	13	
ARA05 718 D19	D		Neptune13	36	2.582	0.001	1.1258	0.0008	0.3197	0.0005	0.3599	41672	73	146	141.5	1.3							34464	34099	320	OS-105005	1218	39	
ARA05 718 D60	D		Neptune13	50	2.650	0.001	1.1258	0.0006	0.2703	0.0002	0.3043	34128	32	64	138.6	0.9							30096	29731	240	OS-105007	534	12	
ARA05 B6	B	P	070315LC4	1602	2.640	0.001	1.1462	0.0006	0.0424	0.0002	0.0486	4668	22	44	146.7	0.6							4753	4388	70	OS-86199	19	5	
ARA05 B12	B	P	061228LC1	14	2.469	0.001	1.1436	0.0007	0.0592	0.0002	0.0677	6594	22	44	146.3	0.7							6597	6232	60	OS-86200	22	5	
ARA05 C5	C	P	061228LC2	32	2.264	0.001	1.1429	0.0007	0.0616	0.0002	0.0704	6876	30	60	145.5	0.7							7243	6878	70	OS-86201	-24	7	
ARA05 C8	C	P	061228LC4	463	2.348	0.001	1.1438	0.0008	0.0633	0.0002	0.0724	7077	30	60	145.8	0.8							7305	6940	120	OS-86202	-8	7	
S-C-4			082304RM5	17	2.904	0.001	1.1490	0.0004	0.0118	0.0001	0.0136	1249	10	20	149.5	0.6							1885	1520	60		-37	2	1
S-T-2			082704RM3	42	2.586	0.001	1.1479	0.0005	0.0307	0.0002	0.0352	3352	17	34	149.4	0.8							3490	3125	70		17	4	1
S-W-2			083004RM1	72	2.454	0.001	1.1473	0.0007	0.0410	0.0003	0.0471	4521	29	58	149.2	1.0							4315	3950	60		57	7	1
S-X-1			082704RM4	91	2.562	0.001	1.1472	0.0006	0.0468	0.0002	0.0537	5182	21	42	149.4	0.8							4775	4410	70		81	5	1

Fp- Favia pallida
P- Porites sp
G-Goniastrea
F- Favia sp
Plla-Platygyra
P.l.b.-Porites lobata
F.s.- Favia stelligera
"S" samples: Santo Island

Sample	Species	U-series I.D.	^{232}Th (ppt)	^{238}U (ppm)	error	[^{234}U/^{238}U]	error	[^{230}Th]/[^{234}U]	error	[^{230}Th/^{238}U]	U-Th Age (yr)	Cal. Age (yr BP)	error (yr)	Mean Cal age (yr BP)	error (yr)	2 error	Initial δ^{234}U	error	^{14}C age (years BP)	Mean ^{14}C age	2 error	AMS ID	^{14}C age corr	Δ^{14}C (‰)	2 error
CHR 8-1-2	A. hyacinthus	AN050825.001	8	3.207	0.001	1.1439	0.0005	0.0786	0.0002	0.0899	8927	8877	17	8877	17	34	148.0	0.5	8375	8375	42	CAMS 75377	8061	73	7
CHR 4-1-9	A. hyacinthus	AN991029.005	35	3.677	0.001	1.1389	0.0004	0.1055	0.0002	0.1201	12146	12096	24	12096	24	48	143.7	0.5	10500	10500	60	CAMS 77444	10186	216	10
CHR 4-2-5	A. hyacinthus	AN991101.003	29	3.650	0.001	1.1408	0.0005	0.1105	0.0002	0.1261	12759	12709	26	12709	26	52	146.0	0.7	11050	11050	60	CAMS 75371	10736	223	11
CHR 5-2-5	A. hyacinthus	AN010618.002	41	3.506	0.001	1.1387	0.0005	0.1043	0.0002	0.1188	12003	11953	16	11953	16	32	143.5	0.7	10587	10587	32	CAMS 82282	10273	182	10
CHR 4-2-7	A. hyacinthus	Neptune160416	179	3.811	0.001	1.1420	0.0002	0.1109	0.0001	0.1267	12807	12742	5	12742	5	10	147.2	0.3	11280	11280	60	CAMS75372	10966	193	12
CHR 4-2-9	A. hyacinthus	Neptune160416	287	3.901	0.000	1.1340	0.0002	0.1122	0.0001	0.1277	12964	12899	9	12899	8	17	143.6	0.3	11290	11290	60	CAMS75376	10976	214	10
CHR 7-4-5	A. hyacinthus	Neptune160416	411	3.940	0.001	1.1415	0.0002	0.1112	0.0001	0.1270	12846	12781	7	12781	7	13	146.8	0.3	11300	11300	60	CAMS75380	10986	196	11
CHR 7-5-2	A. hyacinthus	Neptune160416	111	3.968	0.001	1.1368	0.0002	0.1115	0.0001	0.1268	12884	12819	9	12819	9	17	141.8	0.3	11300	11357	60	CAMS76138	11043	193	15
CHR 7-5-2																			11420			CAMS76151			
CHR 7-5-2																			11350			CAMS77447			

Appendix Table 1: Activity ratios, concentration data, U-Th, U-Pa, and ^{14}C ages for samples dated in this study. Data separated according to location. All uncertainties are listed at 1 sigma unless otherwise noted. Age equations are as reported Mortlock et al. (2005) using the decay constants and half-lives reported in Cheng et al. (2000). Calendar ages are reported as years BP (relative to 1950). Previously published data and other sources of data are referenced as follows: 1. (Fairbanks et al., 2005) 2. (Mortlock et al., 2005) 3. (unpublished data; Cao, 2010) 4. (Chiu et al., 2006). AMS ^{14}C ID's refer to the following dating facilities: CAMS (Lawrence Livermore National Laboratories), OS (NOSAMS), KIA (Leibniz Laboratory for Radiometric Age Determination and Isotope Research). "AK" Araki coral species and terrace designations are from Urmos (1985).

AGU PUBLICATIONS

234

Paleoceanography

REPLY

10.1002/2016PA003047

This article is a reply to a comment by *Bard et al.* [2016] doi:10.1002/2016PA002979.

Key Points:
- Evidence supports that Younger Dryas sea level slow stand and MWP-1B are reliably recorded by reef-crest coral Acropora palmata at Barbados
- Results indicate that Tahiti reefs reported in Bard et al. (2010) were unable to keep up with rapidly rising sea level during MWP-1B
- Tahiti SL error bars are greater than reported; a full error analysis shows Tahiti overlaps with the Barbados SL curve

Correspondence to:
R. A. Mortlock,
rmortloc@rci.rutgers.edu

Citation:
Mortlock, R. A., N. A. Abdul, J. D. Wright, and R. G. Fairbanks (2016), Reply to comment by E. Bard et al. on "Younger Dryas sea level and meltwater pulse 1B recorded in Barbados reef crest coral *Acropora palmata*" by N. A. Abdul et al., *Paleoceanography*, *31*, 1609–1616, doi:10.1002/2016PA003047.

Received 12 OCT 2016
Accepted 20 NOV 2016
Accepted article online 1 DEC 2016
Published online 20 DEC 2016

Reply to comment by E. Bard et al. on "Younger Dryas sea level and meltwater pulse 1B recorded in Barbados reef crest coral *Acropora palmata*" by N. A. Abdul et al.

Richard A. Mortlock[1], Nicole A. Abdul[1], James D. Wright[1], and Richard G. Fairbanks[2]

[1]Earth and Planetary Sciences, Rutgers, State University of New Jersey, Piscataway, New Jersey, USA, [2]Earth and Environmental Sciences, Columbia University, New York, New York, USA

Abstract Abdul et al. (2016) presented a detailed record of sea level at Barbados (13.9–9 kyr B.P.) tightly constraining the timing and amplitude during the Younger Dryas and Meltwater Pulse 1B (MWP-1B) based on U-Th dated reef crest coral species *Acropora palmata*. The Younger Dryas slow stand and the large (14 m) rapid sea level jump are not resolved in the Tahiti record. Tahiti sea level estimates are remarkably close to the Barbados sea level curve between 13.9 and 11.6 kyr but fall below the Barbados sea level curve for a few thousand years following MWP-1B. By 9 kyr the Tahiti sea level estimates again converge with the Barbados sea level curve. Abdul et al. (2016) concluded that Tahiti reefs at the core sites did not keep up with intervals of rapidly rising sea level during MWP-1B. We counter Bard et al. (2016) by showing (1) that there is no evidence for a hypothetical fault in Oistins Bay affecting one of the Barbados coring locations, (2) that the authors confuse the rare occurrences of *A. palmata* at depths >5 m with the "thickets" of *A. palmata* fronds representing the reef-crest facies, and (3) that uncertainties in depth habitat proxies largely account for differences in Barbados and Tahiti sea level differences curves with *A. palmata* providing the most faithful proxy. Given the range in Tahiti paleodepth uncertainties at the cored sites, the most parsimonious explanation remains that Tahiti coralgal ridges did not keep up with the sea level rise of MWP-1B.

1. MWP-1B—Not an Artifact of Local Tectonics

The basis for *Bard et al.*'s [2010] rejection of MWP 1B recorded at Barbados is its absence at Tahiti. *Bard et al.* [2010] proposed a tectonic explanation for MWP-1B, and *Bard et al.* [2016] further expanded on *Carlson and Clark* [2012] to argue that the MWP-1B sea level jump in Barbados is an artifact of an earthquake or variable uplift rates affecting coring location RGF 7 and 8 [*Abdul et al.*, 2016; *Peltier and Fairbanks*, 2006]. *Carlson and Clark* [2012] base their tectonic argument on an older section of the Barbados sea level curve presented in *Peltier and Fairbanks* [2006], noting a discrepancy or offset in sea level estimates between core RGF 9 and four dated samples from core RGF 15. *Carlson and Clark* [2012] attributed the apparent offset between core sites to higher uplift rates, more than twice the estimated rate [*Fairbanks*, 1989; *Peltier and Fairbanks*, 2006].

Our primary reason for dismissing the tectonic argument for MWP-1B is that we have determined that the water depth at coring location RGF 15 was incorrectly reported for the four RGF 15 *Acropora palmata* published in *Peltier and Fairbanks* [2006]. Core RGF 15 was drilled at the exact same coring stations as Cores RGF 13 and RGF 14 and at the same GPS coordinates and in the same four-point mooring spread. Based on the ship's location, the entry log for Core RGF 15 water depth should have been recorded as 269 ft (81.8 m) below mean sea level, exactly as the station entry entered for Cores RGF 13 and RGF 14. Instead, the Core RGF 15 Cruise Report lists the water depth as 248 ft (75.4 m) or 6.38 m, shallower, which we now believe to be in error. We apologize for the confusion caused by this logging error [*Peltier and Fairbanks*, 2006]. The corrected results (+6.38 m water depth correction) for the four RGF 15 sea level estimates reported in *Peltier and Fairbanks* [2006] overlap the published data from cores RGF 13 and RGF 9 [*Peltier and Fairbanks*, 2006]. Furthermore, in our forthcoming publication, we show that depth-corrected RGF 15 data overlap and are redundant with abundant *A. palmata* data obtained from two new drill cores (BBDS 11 and BBDS 14) both from the coring location corresponding to RGF 9. Therefore, there is no basis for the offsets between coring locations being caused by earthquakes or variable uplift rates. We consider replotting of Barbados sea level data with higher uplift rates [*Bard et al.*, 2016, Figure 1] to be unjustified.

One simple argument to be made against a hypothetical fault drawn in *Bard et al.* [2010] that extends offshore and through our array of drilling sites is that the supposed fault would cut through the prominent First High Cliff, a feature that has been extensively mapped and dated as the last interglacial reef [*Taylor*, 1974]. There are no significant changes in the elevation of the First High Cliff above present-day sea level in the area of Oistins Bay. The exposed reef terraces to the east of the Christ Church standard traverse are not affected by the Christ Church anticline, suggesting that uplift can be assumed to be small and relatively uniform to the west of South Point [*Radke and Schellmann*, 2006].

1.1. Coring Reef Strategy for Sea Level Reconstruction at Barbados and Tahiti: Sequence Stratigraphy Versus Lithostratigraphy

The different coring strategies employed at Barbados and Tahiti provide the clearest explanation as to why MWP-1B is recorded at Barbados but not at Tahiti. At Barbados, we targeted a series of parallel, submerged offshore constructional reefs, based on detailed bathymetry [*Macintyre*, 1967; *Macintyre et al*., 1991] and previous coring results [*Fairbanks*, 1989; *Peltier and Fairbanks*, 2006] for the sole purpose of extracting a deglacial sea level curve. The Oistins Bay region was selected for coring the deglacial sea level sequence based on the optimum growth conditions for the reef-crest coral, *A. palmata*, observed from kilometers of exposed uplifted Pleistocene reefs and dozens of onshore cores.

Previously, sea level studies in Barbados [*Fairbanks*, 1989] indicated that sea level jumped during MWP-1A and MWP-1B causing the keep-up reef in Barbados to drown and a new shallow water *A. palmata* reef-crest facies reestablished a coral reef landward of the drowned reef. A deep to shallow coring transect is required and predicted for melt water pulses and is the only way one can reconstruct the deglacial sea level curve at Barbados. This sequence stratigraphic strategy guided our core selection sites.

The "keep-up" *A. palmata* reef that recorded the Younger Dryas segment of the Barbados sea level curve became a "give-up" reef during MWP-1B. At those same drilling locations, the drowning event is documented by the *A. palmata* facies being replaced by deeper dwelling *Acropora cervicornis* fragments and cemented reef sands indicating that the sea level recorder is lost. A post-MWP-1B record can only be obtained from the dating of a new keep-up reef that established shoreward and in shallower water (and where we drilled), but only when sea level rise had slowed so that vertical accumulation of *A. palmata* was able to match sea level rise. We note that similar to MWP-1B, MWP-1A is also bracketed by *A. palmata* records obtained from deeper and shallower cores. We contend that no coral reef in the world can keep up with the +30 mm yr^{-1} sea level rise during MWP-1A and MWP-1B. To our knowledge, there is no radiometrically dated record of a coral reef that shows sustained vertical growth rates greater than 25 mm yr^{-1} [*Montaggioni*, 2005].

The coring strategy employed at Tahiti failed to recover MWP-1B because the redundant coring was conducted on the outer edge of the modern barrier reef flat for a variety of geologic purposes. Unlike Barbados, on Tahiti there is no opportunity for a coring sequence of younger reefs transgressing shoreward with rising sea level. The Tahiti coring strategy is classic lithostratigraphy (Figure 1). The dated material in Tahiti cores provides overlapping sea level estimates and suggests a reef that was largely keeping up with sea level rise up until the end of the Younger Dryas (Figure 2). After the Younger Dryas and through MWP-1B, Tahiti reefs accumulated close to the same rate as during the 14–12 kyr B.P. interval (Table S2 in supporting information) [*Bard et al*., 2010]. As shown at Barbados, a MWP greater than 30 mm yr^{-1} requires shoreward migration of the reef-crest facies and establishment of a new reef. One cannot record a MWP by dating coralgal assemblages at the same location, and thus, the Holocene Tahiti reef gives way to a "catch-up" reef as sea level data plot deeper compared to same age *A. palmata*. Evidence for MWP-1B at Tahiti can only come from drilling shoreward, but unfortunately, dating of material from the back reef zone indicates material that is of much younger (6 kyr) age [*Cabioch et al*., 1999]. We note that a core jumping approach was adopted at Tahiti where MWP-1A was captured only by coring in a shallower location [*Deschamps et al*., 2012].

2. *Acropora Palmata*, When Sampled From the Reef-Crest Facies—An Excellent Sea Level Proxy

In section 2, *Bard et al.* [2016] argues that *A. palmata* may have occupied water depths of 10–15 m during the last deglaciation. Figures 2 and S2 in *Abdul et al.* [2016] demonstrate that all *A. palmata* plot either with Tahiti

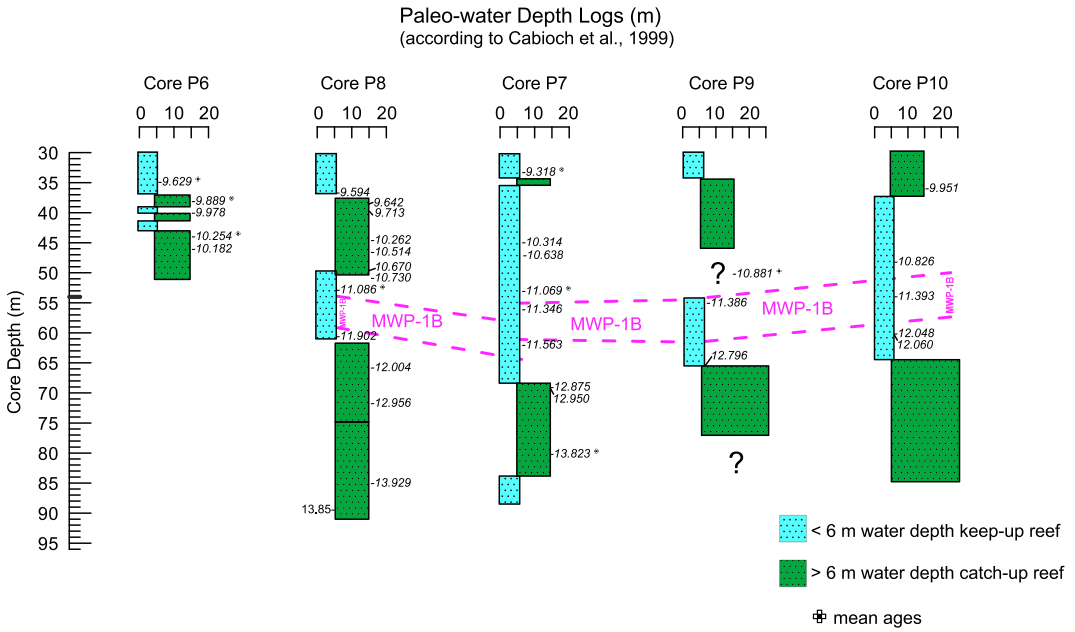

Figure 1. Core logs of estimated paleo-water depth for Tahiti drill cores (horizontal axis in meters) plotted against core depth (vertical axis in meters) reproduced from *Cabioch et al.* [1999]. Blue stippling illustrates shallow water coralgal communities (<6 m). Green stippling are deeper water communities (6–25 m paleo-water depth). The Younger Dryas and early to mid-Holocene interval is mostly represented by deeper water communities (green). Ages are from *Bard et al.* [2010] with crosses denoting mean ages of replicates. Pink dashed lines indicate the interpolated intervals that bracket MWP-1B as identified in the Barbados *Acropora palmata* sea level record [*Abdul et al.*, 2016]. The interval is mostly represented by the shallow water community (blue stippling) but yielded only three dated samples that fall within MWP-1B. Cores P6, P8, and P9 were drilled at an angle between 30 and 33° from vertical adding to the uncertainty in depth assignments.

corals or at shallower depth and within the depth uncertainties assigned to corals in both records. At no time from 13.9 to 9 kyr B.P. is *A. palmata* found deeper than Tahiti corals. Therefore, a discussion of *A. palmata* depth habitat is irrelevant to the time interval and sea level curve presented in *Abdul et al.* [2016]. However, a reviewer and editor require that we address this point and thus the ensuing discussion.

Bard et al. [2016] identify a melt water pulse at Tahiti (14.65–14.31 kyr B.P) [*Deschamps et al.*, 2012] that they claim is 500 years older than MWP-1A (14.04–13.63 kyr B.P.), the type section first defined at Barbados. *Bard et al.* [2016] and *Deschamps et al.* [2012] argue that these are the same global sea level event and that they should have the same ages and that Tahiti is correct. Therefore, *A. palmata* facies at Barbados must have been living deeper than its modern depth habitat of 0 to 5 m.

The *Abdul et al.* [2016] record has added nine new *A. palmata* data points spanning 13.9–13.6 kyr B.P. from drill cores BBDS 10 and RGF 12 that fill a 300 year and 7 m gap in the deglacial sea level record of *Peltier and Fairbanks* [2006]. The more detailed record now demonstrates, unequivocally, the "keep-up" reef reestablished at Barbados by 13.9 kyr B.P. at 81 m below sea level (bsl) and not 13.63 kyr B.P. and 74.5 m bsl as previously constrained by lower resolution records of *Fairbanks* [1989], *Bard et al.* [1990a, 1990b], and *Peltier and Fairbanks* [2006]. The update to the Barbados sea level record is important. Combining the revised post-MWP-1A record [*Abdul et al.*, 2016] with *A. palmata* data recording the onset of MWP-1A [*Peltier and Fairbanks*, 2006] generates a sea level jump with a timing and amplitude more or less consistent with the Tahiti reconstruction. Therefore, in light of the new data published in *Abdul et al.* [2016] and our sea level curve in Figure 2, it can no longer be argued that differences between the Tahiti and Barbados record of MWP-1A are evidence of deeper living *A. palmata* facies [*Bard et al.*, 2016; *Deschamps et al.*, 2012].

While there are multiple assertions to modern *A. palmata* occupying water depths of up to 17 m [*Bard et al.*, 2010; *Carlson and Clark*, 2012; *Deschamps et al.*, 2012], the thick successions of U-Th dated reef crest facies *A. palmata* that plot with remarkable fidelity and redundancy [*Abdul et al.*, 2016] should not be confused with isolated colonies, living depths in excess of 20 m, such as those reported in the Gulf of Mexico [*Zimmer et al.*, 2006]. Based on the location, water depth, and photographs, the two coral specimens reported in *Zimmer*

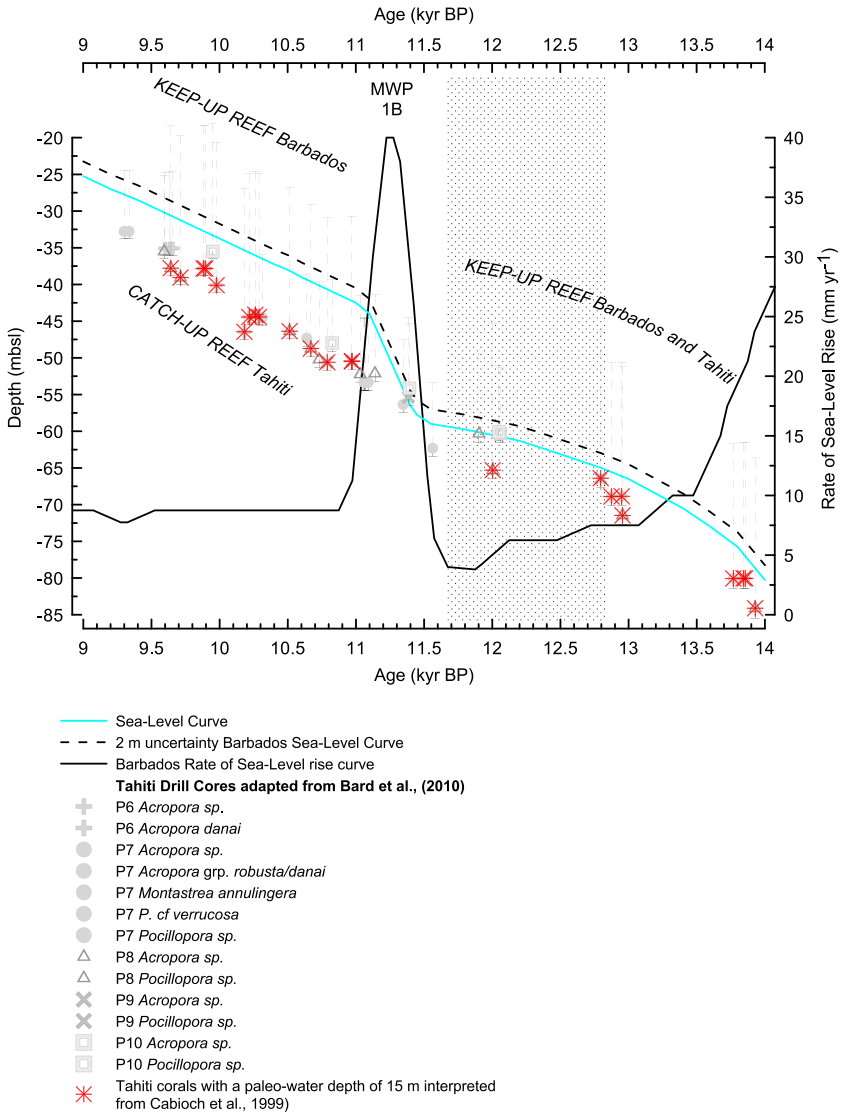

Figure 2. Tahiti data from *Bard et al.* [2010] plotted with the Barbados sea level curve. Cyan line is the Barbados sea level curve constructed from *Acropora palmata* corals with "best estimate "(dashed line) of its uncertainty [*Abdul et al.*, 2016]. Rate of sea level rise (black line) in mm yr^{-1} (right vertical axis) computed from the Barbados sea level curve. Tahiti data from *Bard et al.* [2010] (grayscale symbols) generated from coralgal assemblages *Acropora danai*, *A. gpe robusta*/danai, *Acropora* sp., *Montastrea annuligera*, *P. cf verrucosa*, and *Pocillopora* sp. and associated red algae encruster *Hydrolithon onkodes*. Red stars indicate coralgal samples in *Bard et al.* [2010] and interpreted by *Cabioch et al.* [1999] to have paleo-water depth >6 m bsl and up to 25 m bsl (see Figure 2). We estimate the paleodepth uncertainty for Tahiti data as the combined uncertainty due to paleo-water depth according to *Cabioch et al.* [1999], uncertainty due to estimates in subsidence rates (0.15 to 0.5 mm yr^{-1}), and uncertainty from inclined drilling for angles ranging from 30 to 33° from vertical (~2 m in P6, P8, and P9). Inclusion of the paleodepth uncertainty illustrates that there is complete overlap between the Tahiti data and the Barbados sea level curve.

et al. [2006] are more likely *Acropora prolifera*, a genetic hybrid between *A. palmata* and *Acropora cervicornis*. Only genetic testing can resolve the species identity of the isolated specimens at the remote Flower Garden Reef [*Zimmer et al.*, 2006]. There is no *A. palmata* facies (thickets) observed on Flower Garden Reef because the water depths are too deep.

Bard et al. [2016] take the argument further and suggest that the combined asexual and sexual reproductive strategies employed by *A. palmata* "lend it to being an unreliable indictor of extreme sea level change" because the fragmenting asexual strategy relies on transport of *A. palmata* fragments that could be transported downslope during rapid sea level rise. This is a moot point because all of the Barbados *A. palmata*

Table 1. Comparison of Tahiti Subsidence Rate Estimates From Radiometric Dating, Geodetic Measurements, and Coral Reef Stratigraphy[a]

Tahiti Subsidence Rate Estimates		
Rate (mm yr^{-1})	Method	Reference[b]
0.21 to 0.25	K-Ar dating of subaerial lava in P7	1,2
0.15	Height and age of Holocene reefs	3
0.39	Open-system MIS 9 corals	4
0.5	Geodetic (GPS)	5

[a]The subsidence rate calculated based on the depth and age of a basalt layer subject to several critical variables: unknown elevation or water depth at time of basalt emplacement, erosion prior to coralgal colonization, and decreasing subsidence rates postbasalt emplacement. Using limited measurements on Holocene reefs to compute subsidence rates has its own particular sources of error. These include uncertainties in the paleowater depth of the Holocene coralgal ridges, the ages of the geomorphic features, and the true paleo-sea level at the age of the elevated Holocene coralgal ridges, and confusion with storm deposits due to the poor species identification success. The short time interval over which the Holocene reef has been subsiding also leads to larger uncertainties. Subsidence rate based on the open-system Uranium series dates for MIS 9 corals incorporate modeled ages and extrapolation of water depth from an imported sea level curve. Modern geodetic estimates using a variety of techniques including GPS, DORIS, and combined satellite altimetry and tide gauge sea level records led *Fadil et al.* [2011] to conclude that 0.5 ± 0.5 mm yr^{-1} is the best estimate, and therefore, Tahiti may be tectonically stable. We conclude that the best available estimates for Tahiti subsidence range from 0.15 to 0.5 mm yr^{-1} with a large uncertainty and include this source of uncertainty in the Tahiti data plotted in Figure 2.

[b]References: 1, *Le Roy* [1994]; 2, K-Ar age of 549 ± 11 ka (unpublished data, as referenced in *Bard et al.* [1996]); 3, *Pirazzoli et al.* [1985]; 4, *Thomas et al.* [2012]; 5, *Fadil et al.* [2011].

sea level data reported in *Abdul et al.* [2016] are either shallower or at the same paleo-sea level as the Tahiti sea level estimates. To the contrary, the fragmenting of massive *A. palmata* fronds is exactly what leads to massive, monospecific *A. palmata* fossil beds occupying acres of surface area in the modern Caribbean reefs and Pleistocene reefs of Barbados.

3. Barbados Corals Track Regional Sea Level

Geophysical models of the glacio-isostatic adjustment (GIA) predict that the sea level response at Barbados is reasonably close to the global sea level record [*Peltier and Fairbanks*, 2006]. Other models disagree; however, suggesting sea level at Barbados may be sensitive to local differences in mantle viscosity and mantle structure stemming from its location proximate to a subduction zone [*Austermann et al.*, 2013; *Lambeck et al.*, 2014]. *Clark et al.* [2002] argued that there should be a fast regional response due to gravitational changes between ice and water masses, the magnitude and timing of which will depend on the source of melting. Although *Abdul et al.* [2016] did not incorporate GIA corrections into the high-resolution Barbados sea level curve spanning 13.9–9 kyr B.P., data from our previous studies have been incorporated into numerous GIA models to reconstruct both the global (eustatic) and local responses to sea level [*Clark et al.*, 2002; *Lambeck et al.*, 2014; *Milne and Mitrovica*, 2008; *Peltier*, 2002, 2005; *Peltier and Fairbanks*, 2006]. While it might be tempting to ascribe differences between the Barbados and Tahiti sea level during melt water events to GIA or the gravitational response [*Bard et al.*, 2010; *Clark et al.*, 2002], the various sources of error and uncertainty in their respective sea level reconstructions must be considered. Collectively the sources of error in sea level reconstructions at Barbados and Tahiti include subsidence or uplift corrections, depth of habitat, and drill depth, among others.

Admittedly, the modeling results of *Austermann et al.* [2013] imply that the proximity to a subduction zone may complicate the Barbados estimate of the Last Glacial Maximum low stand. However, isostatic adjustments associated with deglaciation occur on much longer timescales (5–7 kyr postglacial decay times) [*Mitrovica et al.*, 2000] and cannot generate the magnitude or rapidity in the centennial-scale accelerations in the Barbados sea level record. Unfortunately, the sources of model error are highly controversial within the modeling community and cannot be rigorously evaluated at this time.

3.1. Subsidence Corrections

Tahiti subsidence rates are not well constrained with estimates ranging from 0.15 to 0.5 mm yr^{-1} with no published consensus within this range (Table 1). The uncertainties on these published subsidence rate estimates are very high. *Bard et al.* [1996, 2010] and *Deschamps et al.* [2012] chose 0.25 mm yr^{-1}, but the justification is not well explained, based on *Pirazzoli and Montaggioni* [1988], *Le Roy* [1994], and elsewhere (unpublished data, as referenced in *Bard et al.* [1996]). Applying the subsidence rate published by *Fadil et al.* [2011] and *Pirazzoli and Montaggioni* [1988], a 12 kyr B.P. sample could have a subsidence correction ranging from 2 m to 6 m.

Barbados is not immune from uncertainties in uplift rate corrections [*Bender et al*., 1979; *Matthews*, 1973]. Our study area has a relatively low uplift rate, and the continuity and exposure of dated onshore and offshore Pleistocene reefs is the best evidence for relative constancy. Importantly, application of a ±50% uncertainty to a uniform correction of 0.34 mm kyr^{-1} would add just ±2 m uncertainty to our paleodepth estimates and would not change our interpretation of the Barbados sea level record including MWP 1B.

3.2. Depth Assignments

Cabioch et al. [1999] identify "four distinct but poorly diversified coralgal communities that can be delineated in the Tahiti postglacial reef succession and can be classified according to their depth range." They are described as "robust-branching *Acropora*" (0–6 m water depth), "tabular *Acropora*" (6–15 m), "domal *Porites*" (6–15 m), and "branching *Porites*" (5–30 m). However, the paleo-water depths of Tahiti dated coralgal assemblages as defined by *Cabioch et al.* [1999] are not used in *Bard et al.* [2010]. The deeper depth habitats can explain why the Tahiti coral data from cores P6–P10 fall on or below the Barbados sea level curve (Figure 2).

In comparison, the Barbados sea level record presented in *Abdul et al.* [2016] is based on 90 samples of a single species, *A. palmata*, a species that can generally be assigned a depth habitat of 5 m or less and which dominates the Caribbean reef crest community forming dense, high-relief monospecific thickets [*Goreau*, 1959; *Lighty et al*., 1982; *Morelock et al*., 2001; *Weil et al*., 2002]. *A. palmata* is one of the fastest growing corals, and its massive size and density minimizes postdepositional transport. We obtained several hundred *A. palmata* samples from multiple coring locations with redundant drill cores, and many of the individually dated samples range between 10 and 20 cm in length. The Barbados offshore cores were obtained during three cruises using different drilling ships, drilling rigs, crews, and ship positioning systems. That adjacent, and often massive, *A. palmata* plot to within 1–5 m paleodepth of each other in the record presented in *Abdul et al.* [2016] is evidence that our drilling program captured *A. palmata* "thickets" that dominated the reef-crest zone and supports our assertion that the sea level curve in *Abdul et al.* [2016] has not been corrupted with data associated with allegedly deeper living *A. palmata*. We emphasize that though isolated specimens of *A. palmata* have been reported from deeper water, framework producing, reef crest faunas dominated almost exclusively by *A. palmata* must reflect water depths <5 m.

In summary, the collective sources of error in (i) subsidence corrections, (ii) water depth habitat of the dated specimens or surrounding sediments, and (iii) sample depth will lead to sea level error bars that are considerably greater than those reported by *Bard et al.* [2010, 1996]. Paleodepth error bars acknowledging any source of uncertainty are conspicuously absent in Figure 1 in *Bard et al.* [2016].

3.3. Meltwater Sourcing and GIA

Bard et al. [2016] are critical of the conclusion of *Abdul et al.* [2016] that MWP-1B was linked to the melting of the Laurentide (LIS) and Fennoscandian (FIS) ice sheets since it ignores GIA and that the conclusions conflict with recent reconstructions of ice sheet retreat [*Stroeven et al*., 2016]. Multiple ice sheets of varying proportion contributed to deglacial sea level rise and to melt water pulses. Our hypothesis that melting of the LIS and FIS contributed to MWP 1B was based on the available marine and terrestrial physical evidence while *Bard et al.* [2016] choose to place more credence on model results. These most recent reconstructions of the FIS for the Younger Dryas and published subsequent to *Abdul et al.* [2016] suggest slow or no retreat with some readvancement along most of the ice sheets margins during the Younger Dryas and much faster retreat after the Younger Dryas [*Cuzzone et al*., 2016; *Stroeven et al*., 2016]. This is consistent with the observation of a slowdown or near-still stand in Barbados sea level curve [*Abdul et al*., 2016]. In contrast, excluding lower rates of sea level rise during the Younger Dryas [*Bard et al*., 2010], Tahiti corals show a relatively constant rate of sea level rise from 14 to 9 kyr B.P. which seems somewhat remarkable given the insolation and pCO_2 changes and evidence for uneven retreat in the large ice sheets [*Cuzzone et al*., 2016; *Gowan et al*., 2016; *Stroeven et al*., 2016]. That MWP-1B is an anomaly from the trend line in sea level rise is as much defined by the Younger Dryas slow stand as by a sea level jump. The slow stand is now resolved with remarkable clarity in the high-resolution *A. palmata* record [*Abdul et al*., 2016] and generates a sea level deficit that distorts the sea level curve.

Barbados and Tahiti sea level reconstructions display remarkable overlap, except for the discrepancy during MWP-1B, when the combined uncertainties in paleodepth estimates are considered. That the records are so

similar contradicts modeling simulations that predict large differences in the GIA response between Barbados and Tahiti during deglaciation.

4. Conclusion

The Tahiti coral data overlap the Barbados sea level curve when the assigned paleo-water depth uncertainty of the Tahiti coral specimens and additional uncertainties discussed above are plotted and taken into consideration (Figure 2). Honoring the blanket multispecies depth uncertainty assigned to their samples by *Bard et al.* [2010] and their colleagues *Cabioch et al.* [1999], there is virtually no basis for claiming a mismatch between the Barbados sea level record and the Tahiti coralgal data. Having determined that there was an error in reporting the water depth for four *A. palmata* samples from drill core RGF 15 [*Peltier and Fairbanks*, 2006], the discrepancies between paleodepths in RGF 15 and RGF 9 have been resolved. Therefore, there is no justification to call upon a hypothetical fault to explain the offset of Tahiti data from the Barbados sea level curve [*Bard et al.*, 2010] during MWP-1B.

Acknowledgments
We thank K. Miller, two anonymous referees, and Editor E. Thomas for providing constructive comments that greatly assisted in preparing a more focused reply to the concerns and criticisms raised in the comment.

References

Abdul, N. A., R. A. Mortlock, J. D. Wright, and R. G. Fairbanks (2016), Younger Dryas sea level and meltwater pulse 1B recorded in Barbados reef crest coral *Acropora palmata*, *Paleoceanography*, *31*, 330–344, doi:10.1002/2015PA002847.

Austermann, J., J. X. Mitrovica, K. Latychev, and G. A. Milne (2013), Barbados-based estimate of ice volume at Last Glacial Maximum affected by subducted plate, *Nat. Geosci.*, *6*(7), 553–557.

Bard, E., B. Hamelin, and R. G. Fairbanks (1990a), U-Th ages obtained by mass spectrometry in corals from Barbados: Sea level during the past 130,000 years, *Nature*, *346*(6283), 456–458.

Bard, E., B. Hamelin, R. G. Fairbanks, and A. Zindler (1990b), Calibration of the ^{14}C timescale over the past 30,000 years using mass spectrometric U-Th ages from Barbados corals, *Nature*, *345*, 405–410.

Bard, E., B. Hamelin, M. Arnold, L. Montaggioni, G. Cabioch, G. Faure, and F. Rougerie (1996), Deglacial sea-level record from Tahiti corals and the timing of global meltwater discharge, *Nature*, *382*(6588), 241–244.

Bard, E., B. Hamelin, and D. Delanghe-Sabatier (2010), Deglacial meltwater pulse 1B and Younger Dryas sea levels revisited with boreholes at Tahiti, *Science*, *327*(5970), 1235–1237.

Bard, E., B. Hamelin, P. Deschamps, and G. Camoin (2016), Comment on "Younger Dryas sea level and meltwater pulse 1B recorded in Barbados reef crest coral Acropora palmata" by N. A. Abdul et al., *Paleoceanography*, *31*, 1603–1608, doi:10.1002/2016PA002979.

Bender, M., R. G. Fairbanks, F. W. Taylor, R. K. Matthews, J. G. Goddard, and W. S. Broecker (1979), Uranium-series dating of the Pleistocene reef tracts of Barbados, West Indies, *Geol. Soc. Am. Bull.*, *90*(6), 577–594.

Cabioch, Camoin, and Montaggioni (1999), Postglacial growth history of a French Polynesian barrier reef tract, Tahiti, central Pacific, *Sedimentology*, *46*(6), 985–1000.

Carlson, A. E., and P. U. Clark (2012), Ice sheet sources of sea level rise and freshwater discharge during the last deglaciation, *Rev. Geophys.*, *50*, RG4007, doi:10.1029/2011RG000371.

Clark, P. U., J. X. Mitrovica, G. A. Milne, and M. E. Tamisiea (2002), Sea-level fingerprinting as a direct test for the source of global meltwater pulse IA, *Science*, *295*(5564), 2438–2441.

Cuzzone, J. K., P. U. Clark, A. E. Carlson, D. J. Ullman, V. R. Rinterknecht, G. A. Milne, J.-P. Lunkka, B. Wohlfarth, S. A. Marcott, and M. Caffee (2016), Final deglaciation of the Scandinavian Ice Sheet and implications for the Holocene global sea-level budget, *Earth Planet. Sci. Lett.*, *448*, 34–41.

Deschamps, P., N. Durand, E. Bard, B. Hamelin, G. Camoin, A. L. Thomas, G. M. Henderson, J. Okuno, and Y. Yokoyama (2012), Ice-sheet collapse and sea-level rise at the Bolling warming 14,600 years ago, *Nature*, *483*(7391), 559–564.

Fadil, A., L. Sichoix, J.-P. Barriot, P. Ortéga, and P. Willis (2011), Evidence for a slow subsidence of the Tahiti Island from GPS, DORIS, and combined satellite altimetry and tide gauge sea level records, *C. R. Geosci.*, *343*(5), 331–341.

Fairbanks, R. G. (1989), A 17,000-year glacio-eustatic sea level record: Influence of glacial melting rates on the Younger Dryas event and deep-ocean circulation, *Nature*, *342*(6250), 637–642.

Goreau, T. F. (1959), The ecology of Jamaican coral reefs I. Species composition and zonation, *Ecology*, *40*(1), 67–90.

Gowan, E. J., P. Tregoning, A. Purcell, J.-P. Montillet, and S. McClusky (2016), A model of the western Laurentide Ice Sheet, using observations of glacial isostatic adjustment, *Quat. Sci. Rev.*, *139*, 1–16.

Lambeck, K., H. Rouby, A. Purcell, Y. Sun, and M. Sambridge (2014), Sea level and global ice volumes from the Last Glacial Maximum to the Holocene, *Proc. Natl. Acad. Sci. U. S. A.*, *111*(43), 15,296–15,303.

Le Roy, I. (1994), Evolution des volcans en système de point chaud: île de Tahiti, Archipel de la Société (Polynésie Française): Université de Paris 11, Orsay, France, p. 272.

Lighty, R. G., I. G. Macintyre, and R. Stuckenrath (1982), *Acropora palmata* reef framework: A reliable indicator of sea level in the Western Atlantic for the past 10,000 years, *Coral Reefs*, *1*(2), 125–130.

Macintyre, I. G. (1967), Submerged coral reefs, west coast of Barbados, West Indies, *Can. J. Earth Sci.*, *4*(3), 461–474.

Macintyre, I. G., K. Rützler, J. N. Norris, K. P. Smith, S. D. Cairns, K. E. Bucher, and R. S. Steneck (1991), An early Holocene reef in the western Atlantic: Submersible investigations of a deep relict reef off the west coast of Barbados, W.I, *Coral Reefs*, *10*(3), 167–174.

Matthews, R. K. (1973), Relative elevation of late Pleistocene high sea level stands: Barbados uplift rates and their implications, *Quat. Res.*, *3*(1), 147–153.

Milne, G. A., and J. X. Mitrovica (2008), Searching for eustasy in deglacial sea-level histories, *Quat. Sci. Rev.*, *27*(25–26), 2292–2302.

Mitrovica, J. X., A. M. Forte, and M. Simons (2000), A reappraisal of postglacial decay times from Richmond Gulf and James Bay, Canada, *Geophys. J. Int.*, *142*(3), 783–800.

Montaggioni, L. F. (2005), History of Indo-Pacific coral reef systems since the last glaciation: Development patterns and controlling factors, *Earth Sci. Rev.*, *71*(1–2), 1–75.

Morelock, J., W. Ramírez, A. Bruckner, and M. Carlo (2001), Status of coral reefs southwest Puerto Rico, *Caribbean J. Sci.*, *4*, 1–57.
Peltier, W. R. (2002), On eustatic sea level history: Last Glacial Maximum to Holocene, *Quat. Sci. Rev.*, *21*(1–3), 377–396.
Peltier, W. R. (2005), On the hemispheric origins of meltwater pulse 1a, *Quat. Sci. Rev.*, *24*(14-15), 1655–1671.
Peltier, W. R., and R. G. Fairbanks (2006), Global glacial ice volume and Last Glacial Maximum duration from an extended Barbados sea level record, *Quat. Sci. Rev.*, *25*(23-24), 3322–3337.
Pirazzoli, P. A., and L. F. Montaggioni (1988), Quaternary coastal changes Holocene sea-level changes in French Polynesia, *Palaeogeogr. Palaeoclimatol. Palaeoecol.*, *68*(2), 153–175.
Pirazzoli, P. A., L. F. Montaggioni, G. Delibrias, G. Faure, and B. Salvat (1985), Late Holocene sea-level changes in the Society Islands and in the northwest Tuamotu Atolls: Proceedings of the Fifth International Coral Reef Congress, v. Vol. 3: Symposia and Seminars (A). p. 131-136.
Radke, U., and G. Schellmann (2006), Uplift history along the Clermont Nose traverse on the west coast of Barbados during the last 500,000 years—Implications for paleo-sea level reconstructions, *J. Coast. Res.*, *22*(2), 350–356.
Stroeven, A. P., et al. (2016), Deglaciation of Fennoscandia, *Quat. Sci. Rev.*, *147*, 91–121.
Taylor, F. W. (1974), The uplifted reef tracts of Barbados, West Indies: Detailed mapping and radiometric dating of selected areas [M.Sc. dissert.]: Brown University, Providence, R.I., 235 p.
Thomas, A. L., et al. (2012), Assessing subsidence rates and paleo water-depths for Tahiti reefs using U-Th chronology of altered corals, *Mar. Geol.*, *295-298*, 86–94.
Weil, E., E. A. Hernández-Delgado, A. Bruckner, L. Ortoz, O. Nemeth, and H. Ruiz (2002), Distribution and status of Acroporid coral (Scleractinia) populations in Puerto Rico, Conference: NOAA-NMFS and NCORE Potential Application of the US Endangered Species Act (ESA) as a Conservation Strategy, Volume 1: RSMAS, Miami, Fla. USA, p. 71-92.
Zimmer, B., W. Precht, E. Hickerson, and J. Sinclair (2006), Discovery of *Acropora palmata* at the Flower Garden Banks National Marine Sanctuary, northwestern Gulf of Mexico, *Coral Reefs*, *25*(2), 192–192.